Copyright Warning & Restrictions

The copyright law of the United States (Title 17, United States Code) governs the making of photocopies or other reproductions of copyrighted material.

Under certain conditions specified in the law, libraries and archives are authorized to furnish a photocopy or other reproduction. One of these specified conditions is that the photocopy or reproduction is not to be "used for any purpose other than private study, scholarship, or research." If a, user makes a request for, or later uses, a photocopy or reproduction for purposes in excess of "fair use" that user may be liable for copyright infringement,

This institution reserves the right to refuse to accept a copying order if, in its judgment, fulfillment of the order would involve violation of copyright law.

Please Note: The author retains the copyright while the New Jersey Institute of Technology reserves the right to distribute this thesis or dissertation

Printing note: If you do not wish to print this page, then select "Pages from: first page # to: last page #" on the print dialog screen

Order Number 9107149

Computer modeling and analysis of biological rhythms

Yang, Shi Xiong, D.Eng.Sc.

New Jersey Institute of Technology, 1990

U·M·I

300 N. Zeeb Rd.
Ann Arbor, MI 48106

Computer Modeling and Analysis of Biological Rhythms

by

Shi Xiong Yang

Dissertation submitted to the Faculty of the Graduate School
of the New Jersey Institute of Technology in partial fulfillment
of the requirements for the degree of
Doctor of Engineering Science
1990

Approval Sheet

Title of Thesis: Computer Modeling and Analysis of Biological Rhythms

Name of Candidate: Shi Xiong Yang
Doctor of Engineering Science, 1990

Thesis Approved:

Dr. Stanley S. Reisman — Date
Professor, Dept. of Electrical Engineering

Dr. Walter N. Tapp — Date
Research Physiologist, VA Medical Ctr., E. Orange, NJ.

Dr. Peter Engler — Date
Associate Professor, Dept. of Electrical Engineering

Dr. Joseph Frank — Date
Associate Professor, Dept. of Electrical Engineering

Dr. Dennis Blackmore — Date
Professor, Dept. of Mathematics

VITA

Name: Shi Xiong Yang

Degree and date to be conferred: D.Eng.Sc., 1990.

Place of birth: NanJing, China.

Secondary education: High School of Shanghai Normal University.

Collegiate institutions attended	Year	Degree	Date of Degree
Dalian Marine Institute	1978-82	B.S.E.E.	Jan., 1982
New Jersey Institute of Technology	1984-86	M.S.E.E.	May, 1986
New Jersey Institute of Technology	1986-90	D.Eng.Sc.	May, 1990

Major: Electrical Engineering

Minor: Bioengineering

Abstract

Title of Thesis: Computer Modeling and Analysis of Biological Rhythms

Shi Xiong Yang, Doctor of Engineering Science, 1990

Thesis directed by: Dr. Stanley S. Reisman and Dr. Walter N. Tapp

Biological rhythms are an important phenomenon and feature of physiologic systems. Indirect means have to be employed for their description and exploration due to the unclear internal nature of the system. This study analyzed and developed several possible mathematical models using single or multidimensional nonlinear differential equations to approach the experimental circadian data. The numerical solutions of the models were obtained by computer simulation and the simulated and experimental acquired circadian data were analyzed in both the time and frequency domains. Phase plane plots, phase response curves and power spectrum analysis were employed to determine the nonlinearity of the system and its relation to the harmonic structure while bispectrum analysis showed the relation between the harmonics. Dynamic spectrum and frequency demodulation techniques were used to explore the dynamic transient process of the circadian rhythms when a stimulus is applied. The coherence function was examined to explore the frequency correlation between two different circadian rhythms: temperature and activity of the same subject. The study showed that a two dimen-

sional coupled nonlinear oscillator model can be used to describe the circadian rhythm better and a model with relatively large nonlinearity closely approximated the experimental data. The research revealed the harmonic structure of circadian rhythms. This structure related to the nonlinearity of the system with the 2nd harmonic of experimental data representing bimodality in the time series. All the models developed in this research reflected this important feature. The effects of a nonperiodic stimulus to the circadian system were simulated in the model and an "overshoot" phenomenon was found during the frequency transient process. High values of coherence were found at the fundamental and third harmonics while no phase relation was found between harmonics of the experimental data using the bispectrum method.

Contents

Abstract

Dedication ii

Acknowledgements vi

1 Introduction 1

1.1 Introduction to the Mechanism of Biological Oscillators 1

1.2 Circadian Rhythms 5

1.3 Past and Current Research Trends 9

1.4 Scope of the Research 13

2 Experimental Circadian Data Acquisition, Pre-Processing and General Appearance 18

2.1 Introduction 18

2.2 Experimental Data Acquisition System 19

2.3 Preprocessing of Experimental Data 21

2.4 General Appearance of Real Circadian Data 24

2.4.1 Time Series of Circadian Rhythms 25

2.4.2 Frequency Characteristics of Circadian Data 28

3 Classical Mathematical Tools for Analysis of Nonlinear Oscilla-

tion **30**

3.1 Introduction 30

3.2 Analysis of Linear Oscillation 32

3.3 Linear Model for Circadian Rhythms: Its simulation and Limitation 34

3.4 Analytical Methods for Nonlinear Oscillator Analysis 39

3.4.1 Introduction 39

3.4.2 Asymptotic Method 41

3.4.3 Perturbation Method 45

4 Mathematical Modeling and Computer Simulation **51**

4.1 Introduction 51

4.2 Application of Computer Simulation Program 54

4.3 CSMP Computer Simulation Program and the Effects of Integration Methods 56

4.4 Computer Simulation of Van der Pol Type Model: Comparison of Simulation Results and Analytic Results 60

4.5 Modified Van der Pol Oscillator Model 68

4.6 Simulation and Analysis of Coupled Oscillator Models 74

4.6.1 Kronauer Coupled Oscillator Model 75

4.6.2 Pavlidis's Biological Oscillator Model. 81

4.7 Our Two Dimensional Coupled Van der Pol Oscillator Model: Simulation and Analysis 84

4.7.1 Direct Coupling System 88

4.7.2 Velocity Coupling System 95

4.8 Three Dimensional Coupled Oscillator Model 99

5 Analysis of Circadian Rhythms Using Topological Methods **105**

5.1 Introduction 105

5.2 Phase Space and Phase Plane Method 107
5.3 Phase Response Curve Method and its Application 115
5.4 Raster Plotting and Its Application 119

6 Spectral Analysis of Circadian Rhythms 126

6.1 Introduction 126
6.2 Fourier Analysis: Principles and Techniques 129
6.3 Data Pre–Processing: Zero Padding, Windowing and Segmentation 133
6.3.1 Zero padding 133
6.3.2 Windowing 134
6.3.3 Data Segmentation 137
6.4 Spectra of the Experimental Data 138
6.5 Spectral Approach in Modeling 146

7 Effects of Stimulus on Circadian Rhythms 151

7.1 Introduction 151
7.2 Frequency Entrainment Analysis 154
7.3 Phase Shift by Nonperiodic Stimulus 162
7.4 Analysis of Dynamic Process with Nonperiodic Stimulus 165
7.4.1 Dynamic Spectral Analysis 165
7.4.2 Frequency Demodulation Analysis 168
7.5 Stopping the Oscillation in Van der Pol oscillator 173

8 High Order Spectral Analysis on Circadian Rhythms 178

8.1 Theory of Coherence Function 178
8.1.1 Introduction 178
8.1.2 Importance of Smoothing in Cross Spectrum Estimation . . 181

8.2 Computing of Coherence and Experimental Results 182
8.3 The Bispectrum 186
8.3.1 Introduction 186
8.3.2 Bispectrum Computation and Smoothing 190
8.4 Phase Coupling Detection Using Bispectrum Method 192

9 Conclusions **197**
9.1 Summary of the Research 197
9.2 Summary of Nonlinearity Analysis on the Models 202
9.3 Conclusions 204
9.4 Further Development of the Study 206

Bibliography **209**

Appendix **212**

A CSMP Simulation Programs

B FFT and other programs

C MACRO Programs

List of Tables

4.1 *Summary of fixed step integration methods.* 57

4.2 *Execution times of each integration step for 7 different integration methods.* 59

4.3 *The period of biological oscillator model with different d and b.* 84

5.1 *Configuration of equilibrium points.* 110

List of Figures

1.1 *EKG Waveform, high frequency biological oscillator.* 3

1.2 *EKG waveform with arrhythmias, a biological oscillator possibly coupled or excited by another oscillator.* 4

1.3 *Circadian temperature time series recorded from a "free running" Rhesus monkey. x-axis: sampling points (144 points a day). y-axis: amplitude.* 5

1.4 *Computer predicted biorhythm of the author in May, 1990. S-the physical cycle, K-the emotional cycle, C-the intellectual cycle.* 6

1.5 *Entrainment of the locomotor activity of a cockroach.* 8

1.6 *Bimodal distribution of unintended sleep episodes during the last 22 hour of a 40 hour constant routine. N=278 sleep episodes, 16 subjects.* 12

2.1 *Circadian temperature data acquisition system.* 20

2.2 *(a) Received data by original antenna. (b) Received data by improved antenna.* 22

2.3 *Time series of monkey's temperature circadian rhythm. x-axis: sample points (144 sample points a day). y-axis: temperature in centigrade degree. a) 7 days data of Monkey 10. b) 7 days data of Monkey 21. c) 7 days data of Monkey 34. d) 7 days data of Monkey 41.* 26

2.4 *Time series of rat's temperature circadian rhythm. x-axis: sample points (96 sample points a day). y-axis: temperature in centigrade degree. a) 10 days data of Rat 2. b) 10 days data of Rat 4.* 27

2.5 *The power spectrum from one of the experimental circadian data. The data was sampled at 6 samples/hour and the spectrum was computed by 16384 FFT point. x-axis: FFT point. y-axis: amplitude. The period is 24.38hr at FFT point 113. The period is 12.19hr at FFT point 226. The period is 8.13hr at FFT point 339.* 29

3.1 *Damped linear oscillation.* 34

3.2 *BEATS model of circadian rhythms of activity (A) and temperature (T).* 36

3.3 *Simulated time series waveform of "BEAT" model.* 37

3.4 *Angular threshold on the phase plane for BEAT model. Shaded region: sleep region. Unshaded region: wake region.* 38

4.1 *Comparison of 5 integration methods in CSMP: average absolute error as a function of step size and integration method. The step-size ranged from 10 to 10,000 integration steps per cycle of the cosine function (cosine function is the solution of this linear differential equation).* 58

4.2 *Time series of Van der Pol oscillator model with different μs. (a) μ=0.2. (b) μ=0.8. (c) μ=1.6 (d)μ=3.2.* 63

4.3 *Spectral function of Van der Pol oscillator model with different μs. (a) μ=0.2. (b) μ=0.8. (c) μ=1.6 (d) μ=3.2.* 65

4.4 *Comparison of simulation results and analytic solution: on frequencies of Van der Pol type model with different nonlinearity. a) On the frequency of fundamental frequency component. b) On the frequency of 3rd frequency component.* 67

4.5 *Comparison of simulation results and analytic results: on amplitudes of Van der Pol type model with different nonlinearity. a) The amplitude of three main frequency components of analytic solution. b) The amplitude of three main frequency components of computer simulation results.* 69

4.6 *Simulation results of modified Van der Pol oscillator with $A = 0.0001, 0.001, 0.01$ and $0.1, (\mu = 0.02)$. a) Time series. b) spectral function.* 70

4.7 *The frequency of two main frequency components in modified Van der Pol oscillator as A changes.* 72

4.8 *The amplitude of two main frequency components in modified Van der Pol oscillator as A changes.* 72

4.9 *The interaction of two nonlinear items in modified Van der Pol oscillator: the fundamental frequency and the first two harmonics of the system with* $A = 0.01$, $\mu = 0.2$ *to* $\mu = 3.0$. 73

4.10 *The interaction of two nonlinear items in modified Van der Pol oscillator: the fundamental frequency and the first harmonic of the system with* $A = 0.1$, $\mu = 0.2$ *to* $\mu = 3.0$. 74

4.11 *(a) Stimulus* $z(t)$ *in the model. (b)Designed characteristic frequency* ω_y. 78

4.12 *Time series of (a)* y *oscillator. (b)* x *oscillator.* 79

4.13 *(a) Detected period of the* y *oscillator. (b) Detected period of the* x *oscillator.* 80

4.14 *Phase response curve of a circadian system.* 82

4.15 *Phase plane plot of trajectories of the biological oscillator model.* . 83

4.16 *The statistics of car accidents from 6052 samples.* 86

4.17 *Our coupled oscillator model: two oscillators serve for one circadian rhythm.* 87

4.18 *Time series of direct coupling model with different* μ*s.a)* μ*=0.2. b)*μ*=0.8, c)*μ*=1.6, d)*μ*=3.2.* 90

4.19 *Spectral function of direct coupling model with different* μ*s. a)*μ*=0.2. b)*μ*=0.8, c)*μ*=1.6, d)*μ*=3.2.* 91

4.20 *Main frequency components of direct coupling model with different* μ*s. a)* $\mu = 0.2$. *b)*$\mu = 0.8$, *c)*$\mu = 1.6$, *d)*$\mu = 3.2$. 91

4.21 *3 main frequency components of coupled system with* $F_{xy} = 0.05$, *and* $\mu = 0.2$ *to* $\mu = 3.2$. 94

4.22 *3 main frequency components of coupled system with* $\mu_x = 0.1$, *and* $\mu_y = 0.2$ *to* $\mu_y = 3.2$. 95

4.23 *Subharmonic entrainment in velocity coupled system* 97

4.24 *Raster plotting of* x *period. (a) with* y *period of 28 hr.,* $F_{xy} = 0$ *and (b) with* y *period of 28 hr.,* $F_{xy} = 0.2$. 98

4.25 *Comparison of velocity coupling system with the experimental data. (a) Experimental results from one of the monkey subject. (b) Coupled oscillator model results.* 100

4.26 *a)Spectrum of a rat temperature data. b) Spectrum of a monkey temperature data.* 102

4.27 *3 dimensional coupled oscillator model.* 103

4.28 *The spectra of 3 dimensional coupled oscillator model. a) Coupling coefficient* $F_{zy} = 0.1$. *b).Coupling coefficient* $F_{zy} = 0.4$ 103

5.1 *Phase plane plot of spring system.* 108

5.2 *Phase plane portraits of different equilibrium points. (a) and (b): the trajectories move toward the equilibrium of the system, they are stable. (c), (d) and (e): the trajectories move away from the equilibrium of the system, they are unstable. (f) the trajectories share the equilibrium of the system and remain there, they are stable.* 109

5.3 *Phase plan plots of a Van der Pol oscillator with different values of* μ. 112

5.4 *Phase plane plot of a quasiperiodic oscillator.* 114

5.5 *Phase plane plot of the coupled oscillator model.* 116

5.6 *Phase response curve of circadian pacemaker by light stimulus.* 118

5.7 *Stimulus applied and the time series. a)The first time derivative of light pulse causing the phase of the model delay shifted. b)The first time derivative of light pulse causing the phase of the model advance shifted.* 120

5.8 *Examples of raster plots (x axis is scaled at 24 hours). a)The system is oscillating at the period of 24 hr. b)The system is oscillating at the period higher than 24 hr. The period in (b) could be found by finding the time difference between each horizontal line. This difference in (b) is 1 hour toward the delay (right) direction therefore the period is 25 hour.* 121

5.9 *Raster plot of circadian rhythm data obtained from experiment.* . . . 123

5.10 *Raster plotting of periods of the coupled oscillator model. (a) The 28 hr oscillator is entrained to 24 hr. (b) The 22 hr oscillator is entrained to 24 hr.* 124

5.11 *Raster plotting of periods of the coupled* ($F_{xy} = 0.6$) *oscillator model. (a) The 28 hr oscillator is entrained to 24 hr unstably. (b) The 22 hr oscillator is entrained to 24 hr unstably.* 125

6.1 *Spectral function of real circadian rhythms.a) Spectral function of a monkey temperature data. b) spectral function of a rat temperature data.* 128

6.2 Decibel amplitude responses of four different windows. 136

6.3 *Spectral functions of monkey 10.* 140

6.4 *Spectral functions of monkey 21.* 141

6.5 *Spectral functions of monkey 50.* 142

6.6 *Spectral functions of monkey 41.* 143

6.7 *Spectral functions of rat1.* 144

6.8 *Spectral functions of rat2.* 145

6.9 *The spectrum of single Van der Pol oscillator model.* 147

6.10 *Spectra of velocity coupled oscillator model with different coupling coefficient. a)* $F_{xy} = 0.04$, *b)* $F_{xy} = 0.4$. 148

6.11 The spectrum of a 3 dimensional coupled oscillator model. 149

7.1 *Entrainment range in a Van der Pol oscillator (with* $\mu = 0.1$*)* 156

7.2 *Fundamental frequency of the system with the stimulus of two different amplitude.* 157

7.3 *The period difference of the Van der Pol type model with the stimulus of varying frequency.* 158

7.4 *Spectra of Van der Pol type model with different* μ *under external stimulus. a)* $\mu = 0.01$. *b)* $\mu = 0.1$. *c)*$\mu = 0.8$. *d)*$\mu = 1.6$. 161

7.5 *Time series of Van der Pol type model. a) Phase delay-shifted by the stimulus. b) Phase advance-shifted by the stimulus.* 163

7.6 *Periods of Van der Pol type model. a) Phase delay-shifted by the stimulus. b) Phase advance-shifted by the stimulus.* 164

7.7 *Sequential spectra of Van der Pol type models. a) Spectra of the model with phase delay-shifted by the stimulus. b) Spectra of the model with phase advance-shifted by the stimulus.* 167

7.8 *Flowchart of frequency demodulation method.* 171

7.9 *Frequency demodulation results on a phase delay shifted model. a) After limiting. b) After differentiating. c) After detector. d) Frequency demodulation results.* 172

7.10 *The time series of stopped oscillation in Van der Pol oscillator model.*175

7.11 *phase plane of stopped oscillation. (a) Full plot of phase plane. (b)Detailed plot near the singularity.* 176

7.12 *Stopped the oscillation of the biological oscillator model.* 177

8.1 *Coherence of circadian temperature and activity of subject41. a) The coherence function between points 1 and 2048. b) The coherence function between points 1 and 200.* 184

8.2 *Power spectrum of the model with 3 harmonic-related frequencies.* . 192

8.3 *The bispectrum and bicoherence function results of the model with related phase. a) Bispectrum. b) Bicoherence.* 193

8.4 *The bispectrum and bicoherence function results of the model with unrelated phase. a) Bispectrum. b) Bicoherence.* 194

8.5 *(a)Smoothed spectrum of a experimental data. (b) Bispectrum result. (c) Bicoherence result.* 196

Acknowledgements

Mere words are not enough to express my gratitude to my advisor, Dr. Stanley Reisman, and Dr. Walter N. Tapp. Their mastery of the subject matter combined with a great deal of sincerity, enthusiasm and dynamism, have made working on this dissertation a valuable experience. Additional thanks need to be expressed to Dr. Benjamin H. Natelson for his personal and sincere care.

Special thanks are due to Mr. Tom Pritzel for his assistance in computer software.

Many thanks are due to the distinguished members of my committee: Dr. Peter Engler, Dr. Joseph Frank of Electrical Engineering, and Dr. Dennis Blackmore of Mathematics. Their valuable suggestions and stimulating discussions during the whole period of this research have considerably improved the quality of the dissertation.

I am really thankful to all the professors and staff of the Department of Electrical Engineering who have been helpful and supportive throughout the years I have spent at NJIT. Special thanks are due to Dr. Edwin Cohen, Dr. J.J. Strano, Dr. Kenneth Sohn and Ms. Brenda Walker.

Chapter 1

Introduction

1.1 Introduction to the Mechanism of Biological Oscillators

Biological oscillators are the "oscillators" existing in living organisms. The oscillating waveform in living beings have many different features which include distinct shapes, amplitudes, frequencies, phases, etc. [29, pages 29-48] Although the existence of biological rhythms has been well known since antiquity, the existence of biological oscillators has been accepted only in the past 20 years. A prominent view was that the rhythms were due to external periodic effects like the daily changes of light and dark or similar changes in temperature, etc.

It has been very difficult to prove physically the existence of biological oscillators, but recently there has been some significant progress. Scientists have for the first time altered the basic biological rhythms of animals by transplanting a small area of brain tissue believed to serve as the body's master "clock". [35] The experiments involved transplanting brain tissue between hamsters with fundamentally different biological rhythms, which confirmed the hypothesis that a small area of

the brain called the suprachiasmatic nucleus serves as the master clock. When animals are kept in the dark, their sleep-wake cycle is set by a master biological clock, which coordinates the release of various hormones, changes in temperature and other daily rhythms. Normally a hamster has a free-running period of about 24 hours. That is, they wake up and start running approximately every 24 hours, based on this internal clock. It was believed that most animals set their clock according to the amount of daylight and darkness.

In the experiments the suprachiasmatic nucleus, which is located above where the two optic nerves cross in the brain, were removed from the hamsters. These hamsters then ran randomly at any time of the day or night. Further experiments were done by implanting fetal tissue believed to contain the nucleus back into the animals and the rhythms were restored. When different fetal cells from hamsters with different free running periods were implanted, the free running period of the donor was exhibited. This experiment gave the idea of the existing organ with the function of circadian rhythm, but it was still not sure whether this organ controlled the rhythm or merely allowed the rhythm to be expressed.[35] This interesting experiment, along with other new discoveries in recent years, have pushed the research in biological oscillators to a new level.

Biological oscillators, if divided into categories by their free running period, may include the following types:

1. Short period oscillations.

   These oscillators generate high frequency oscillations, such as heartbeats. Due to the high oscillating frequency, this type of biological oscillator shows more obviously endogenous nature. The heartbeat waveform (measured as

Figure 1.1: *EKG Waveform, high frequency biological oscillator.*

EKG) has an oscillation period between 0.1 seconds and 5 seconds. Normally the shape and period are kept almost constant as shown in Fig.1.1. Much research was done to explore the mechanism of the heartbeat. Some phenomena could be possibly explained from the point of view of biological oscillators. For example, the baseline drift of EKG waveforms implies coupling from other oscillators with lower oscillating frequency, e.g., respiration. The arrhythmias observed in an EKG waveform imply the possibilities of either coupling or excitation by another abnormal oscillator with different characteristics (e.g., amplitude, frequency or shape, depending on the type of arrhythmias). Fig. 1.2 shows an EKG signal with periodic arrhythmias.

2. Long period oscillations.

   These oscillations are usually on the order of 24 hours and have received considerable attention, especially in the past 20 years. It is obvious that they are of major importance in many biological functions: for example, the treatment of circadian sleep disorders, such as the rapid time zone change (jet–lag) syndrome, delayed sleep phase syndrome, shift work dyssomnia and

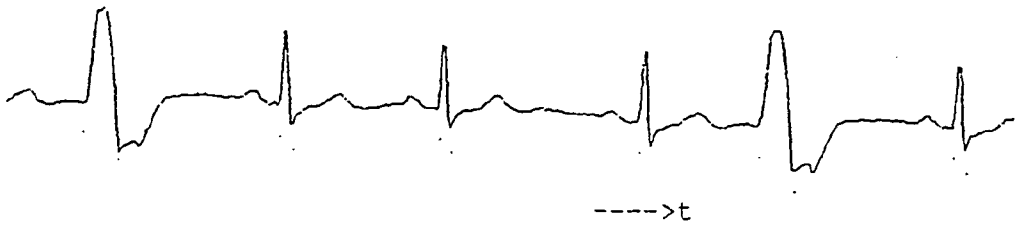

Figure 1.2: *EKG waveform with arrhythmias, a biological oscillator possibly coupled or excited by another oscillator.*

disrupted sleep in the elderly, the daily rhythms of susceptibility to drugs, etc.

Fig.1.3 shows an example of recorded circadian temperature data from a "free running" Rhesus monkey, which has a period of 24.17 hours. The biological mechanism responsible for the circadian rhythms is still unclear. Therefore exploration in this field has some special difficulties. Our research on biological oscillators were concentrated mainly in the field of circadian rhythms.

3. Very long period oscillations.

   The biorhythm cycle is a very long period oscillation, with period around 30 days[3]. It is believed that these very long period oscillations start from the date of birth and that these very long period oscillators have different periods for three biorhythms:

   Physical cycle, about 23 days.

   Emotional cycle, about 28 days.

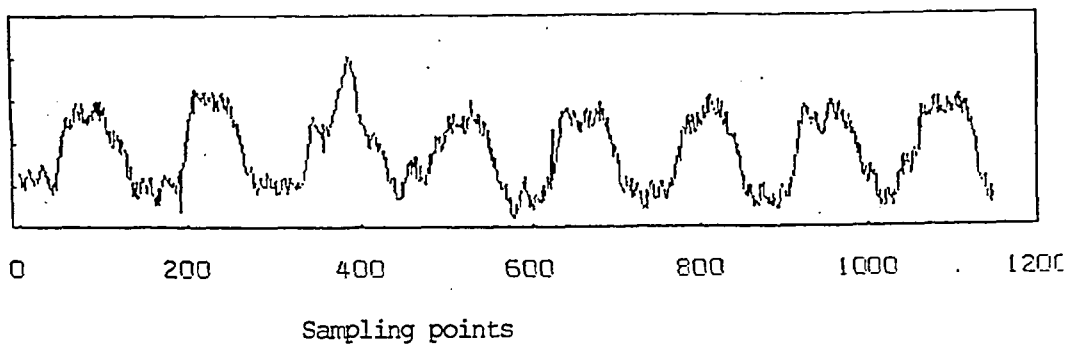

Figure 1.3: *Circadian temperature time series recorded from a "free running" Rhesus monkey. x-axis: sampling points (144 points a day). y-axis: amplitude.*

Intellectual cycle, about 33 days.

It was reported that the research results of biorhythms have been applied to practice in some countries. For example, in China, the assignment of workers in some positions where high levels of concentrations are needed (e.g., on duty in a power plant; air plane pilots, etc) were made according to their biorhythm cycles [13]. Fig.1.4 shows the computer predicted biorhythm of the author during one month.

1.2 Circadian Rhythms

Circadian rhythms are biological oscillations with a period of around 24 hours. The work of researchers, especially during this century, has resulted in much impressive evidence that the daily cycle of biological phenomena are controlled by internal oscillators rather than by the alternation of light and darkness in their environment[29, pages 29–30].

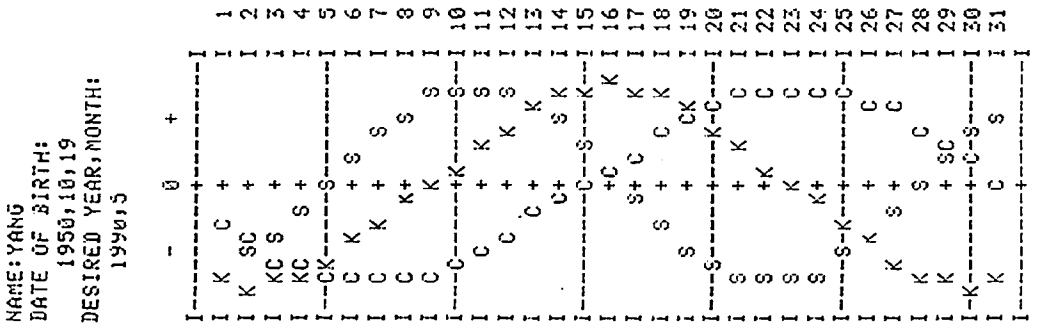

Figure 1.4: *Computer predicted biorhythm of the author in May, 1990. S–the physical cycle, K–the emotional cycle, C–the intellectual cycle.*

Many experiments were performed by keeping the subjects in carefully controlled environments (so called "free-running " noncyclic experimental conditions): the subjects were kept in isolation, with constant temperature and constant light (or darkness), and with food and water continuously available in excess. Outside stimuli, such as noise which might disturb the subjects, were kept to a minimum. All the factors which might inform the subjects "about time of day" were eliminated. Under such circumstances, the subjects typically show a well organized wake–sleep cycle, which consists of a several–hour stage during which gross motor activity is concentrated, followed by a sustained block of rest or sleep. This cycle repeats itself, with a period on the order of 24 hour. Most such rhythms are "self-sustained", in the sense that they persist, without evidence of damping, for as long as the recording is continued.[19] The experimental results exhibit a periodicity in subjects' behavior. The periods of such rhythms varied between 22 and 26 hours. For example, the core temperature, continuously measured with a rectal

thermometer, tended to rise during the day, and fall to a minimum just before wake-up time. Some literature states that the circadian period is almost always different from 24 hours [14] which strongly suggests the existence of endogenous oscillators in living systems. Because the period of the rhythms is rarely exactly 24 hours, Halberg suggested the term circadian (from the Latin "circa diem"; i.e., about a day) for such phenomena [29, page 31].

Although the internal mechanism of circadian rhythms is unclear, it is obvious that this endogenous oscillator has exhibited similar dynamics to some nonlinear oscillators:

1. The oscillator is self sustained. It has almost constant period, but it may vary or be modulated depending on different nonlinear properties, e.g., the oscillator with a large nonlinear portion will exhibit relatively high harmonic components which affect its constant period.

2. The behavior of the oscillator can be made to follow periodic changes of light and/or temperature. This is commonly referred to as entrainment or synchronization by external stimulation. Entrainment is possible only if the period of the external cycle is close to the endogenous period or an integer multiple or submultiple of it. Fig.1.5 is a raster plot from an experimental record which shows the locomotor activity of a cockroach[36]. Raster plotting is a graphic form specially used in circadian research. Each horizontal line of this plot represents an estimated period (a day) and different symbols represent the amplitude of oscillation. If the real oscillation period is exactly the same as estimated, the symbols in each line will keep the same position. Otherwise the variation of oscillation can be seen directly from the raster

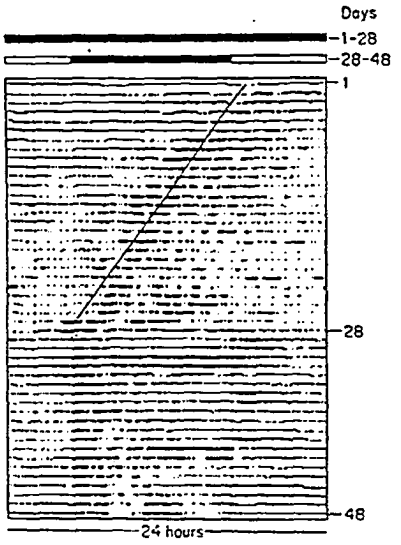

Figure 1.5: *Entrainment of the locomotor activity of a cockroach.*

plot. We will discuss the detailed application of this method in chapter 5. In fig.1.5, the start of the activity has a period of less than 24 hours while at the twelfth day a photo-periodic regime is applied, and its period is entrained to 24 hours at 28th day. The details of the analysis of entrainment will be discussed in chapter 7.

3. The phase of the oscillator can be shifted by nonrepetitive stimuli. It can be shifted by one or several stimuii but not by a periodic stimulus. The amount of the phase shift depends on both the stimulus itself and its timing with respect to the endogenous rhythm. The latter relationship is of great importance in the study of biological oscillators. [22]

4. The rhythm of an oscillator can be totally disrupted by applying a specially designed stimulus, i.e., if a stimulus is applied at the right time with proper amplitude and width, it may possibly disrupt the oscillation or even stop the oscillation. The relationship of the circadian rhythms to the stimulus will

also be discussed extensively in Chapter 7.

1.3 Past and Current Research Trends

Research in the field of circadian rhythms has received considerable attention during the past 20 years. As we mentioned earlier, when considering biological oscillators, one has to deduce its structure from experimentally obtained behavior where the nature of the behavior is usually unclear. Therefore effective mathematical tools and other techniques were sought.

Aschoff and Wever used their specially designed, fully equipped laboratory as a time-isolation environment to obtain their circadian data. This enabled them to acquire an early understanding of internal desychronization and the human circadian system in general. A circadian pacemaker was assumed to underlie the stable oscillation of core body temperature. They proposed a mathematical model showing the internal desynchronization of two different circadian rhythms: body temperature and activity. [45]. They pointed out that these two circadian clocks had different properties. After desynchronization, these two rhythms do not keep the same oscillation period. The temperature period shortens by much less than the activity period lengthens - hence the temperature pacemaker is "stronger" (in addition to being more "stable" in its period). Even though the different circadian rhythms couple internally to each other, the temperature rhythm has relatively more "strength". The temperature pacemaker thus acts like an "internal zeitgeber (stimulus)". Their work has played an important role in clarifying many aspects of the circadian system in animals and humans.

Colin S. Pittendrigh did much research in this field. He presented experimental

results of daily rhythms as a coupled oscillator system and introduced the principle of entrainment in circadian rhythms. [30]

Theodosios Pavlidis studied the dynamic properties of biological oscillators and the mathematical techniques necessary for their investigation [29]. He developed a biological oscillator model from the phase characteristics of the oscillation responding to the stimulus, i.e., *phase response curves*. He used this model to study the relationship between the PRC (phase response curve) and the circadian rule. The model results showed different phase response charactertics in different time periods. We will discuss this model in chapter 4.

Richard E. Kronauer and his colleagues presented several mathematical models of the human circadian system. One of his models contains two interacting oscillators where temperature and rest-activity are each governed by an oscillator of the Van der Pol type[23]. A van der Pol type oscillator is a self-sustained nonlinear oscillator which has a simple mathematical form. Therefore much investigation has been done on this type of oscillator.

In their model, the two oscillators, "x" and "y" refer to two circadian pacemakers; x dominates the core body temperature rhythm, and y regulates the sleep-wake cycle. The oscillators affect one another through "velocity" coupling. The periodic zeitgeber is modeled as forcing on one of the oscillators. This model was used to reveal the dynamics of synchronization and desynchronization between two coupled oscillators. Our simulation of this coupled oscillator model will be introduced in chapter 4. Our circadian rhythm model is also based on the modification of this Kronauer's model.

Borbely [7] has proposed a model of sleep regulation which unifies findings

from classical sleep research with those of the more recent circadian studies. In Borbely's model, sleep is regulated by two processes, S and C. The S variable corresponds loosely to "fatigue", and may actually represent a neurochemical sleep promoting factor. It builds up during waking hours and decays during sleep. Borbely also postulated the C process, a circadian component of sleep regulation. C is taken to be independent of either sleep or waking. The Sum of S and C represents the total sleep propensity. A sleep episode ends when this sum falls below a certain threshold.

Borbley's model has intuitive and physiological appeal, and it has inspired the quantitative work of Daan and Beersma. They formalized and extended this conceptual model. In their model, S and C regulate the sleep-wake cycle. Sleep onset occurs when S crosses a high threshold H and wake-up occurs when S falls below a low threshold L. H and L are slightly noisy. Process C is generated by a single circadian pacemaker which imposes an approximately sinusoidal modulation on the thresholds. Hence there are circadian influences on the sleep-wake fluctuations: Process C strongly synchronizes S if the threshold oscillations have large amplitude A; otherwise S adopts a periodicity governed mainly by the separation of the thresholds H and L.

Mary Carskadon has studied subjects on a 40 hour constant routine. [24] During this sleep deprivation protocol, subjects are supposed to stay awake for 40 hour in a constant posture. She found that the subjects occasionally drop off into a "microsleep." For a few seconds the brain falls asleep and the EEG pattern changes suddenly. What Carskadon has found is that these unintended sleep episodes are most likely to occur at certain times of day. The histogram of microsleeps has local maxima at the temperature trough and nap phase, and local minima at the two

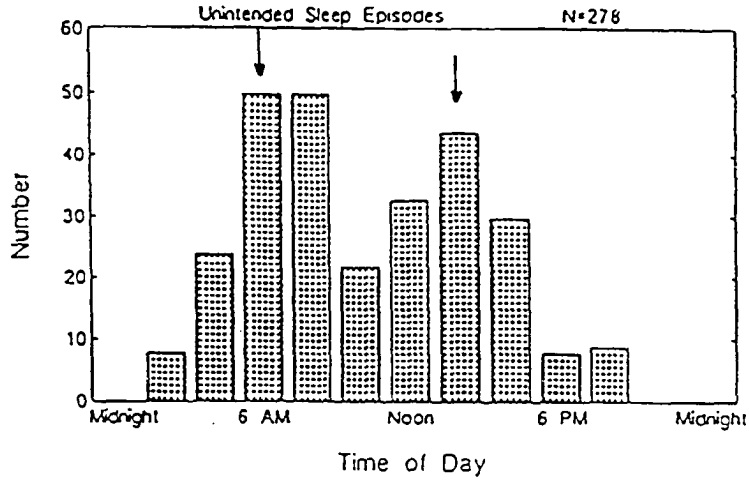

Figure 1.6: *Bimodal distribution of unintended sleep episodes during the last 22 hour of a 40 hour constant routine. N=278 sleep episodes, 16 subjects.*

wake-maintenance zones. This bimodal rhythm phenomenon is shown in figure 1.6. The bimodal rhythm was also found in our experiment data and therefore was one of the important consideration for our model.

In 1989, Charles A. Czeisler, R. Kronauer and their colleagues, announced their research results from 45 human circadian rhythm resetting trials [14]. Each trial consisted of an initial endogenous circadian phase assessment, a three cycle stimulus (each cycle included 5 hours of bright light, an ordinary indoor room light and darkness), and a final phase assessment. The data indicate that the sensitivity of the human circadian pacemaker to light is far greater than previously recognized. The magnitude and direction of the phase shifts induced by the three cycle light stimulus were primarily dependent on the timing of exposure to bright light, as well as the initial circadian phase at which the light exposure occurred. The largest phase shifts caused by exposure to the three light cycle stimuli was

greater than 8 hours. The experiment showed that the light probably exerts its action on the human circadian pacemaker via nerves connecting the retina and the hypothalamus. Two types of responses have been described in their experiment, type 0 and type 1. Type 1 is a weak or incremental resetting in which the maximal shift is only a few hours. In type 0 resetting, on the other hand, the biological clock can be reset by up to 12 hours, regardless of the initial circadian rhythm or sleep-wake cycle. These results have implied a therapeutic use of light in the management of disorders of circadian regulation.

Dr.Czeisler and his team did a study with a 66-year-old woman whose biological clock was phase-advanced by about 6 hours.[15] They reset the woman's circadian pacemaker by exposing her to 4 hours of bright light each evening, even though her sleep-wake cycle was held constant. In the first 1 to 2 days her system had already shifted 6 hours. This study showed the practical application for the light treatments of circadian sleep disorder and other problems.

1.4 Scope of the Research

This research concentrates on circadian rhythms which are biological oscillations having a period of around 24 hours. These types of biological oscillators, as mentioned before, play an important role in physiologic systems. Our emphasis in this field was on modeling and analysis of the circadian rhythms in both time and frequency domains.

It is important to first investigate and gather experimental circadian data. Our experimental circadian data acquisition system was built at the VA Medical Center, East Orange, New Jersey. This system was built to continuously monitor

and record long term circadian data from animal subjects. The experimental data we obtained include temperature, activity and feeding frequency from monkeys and rats. **Temperature** data are of special interest for the following reasons:

1. Temperature has often been regarded as the most stable, and best regulated circadian rhythm;
2. The phase of the temperature cycle is an important determinant of sleep onset and sleep length.
3. The phase of the temperature cycle has been linked to circadian performance effects.

In chapter 2, we will introduce our data acquisition system and the general characteristics of the acquired circadian temperature data which will give us the basic understanding for further modeling and analysis.

Due to the unknown internal nature of the system, indirect means have to be employed for the description and exploration of biological oscillators. Most of the biological oscillators belong to the nonlinear oscillator category, which complicates the analysis. Computer modeling and simulation is one of the most effective indirect methods. In chapter 3, we will first introduce the basic mathematical theory and classical mathematical tools for linear and nonlinear oscillation analysis. Our simulation results on a linear model will be presented and the limitation of this model will be discussed. Classical analytic methods are effective methods to solve some "weak" nonlinear systems but errors will be generated with an increase in the system nonlinearity, and the algorithm will become very complicated for the multi-dimensional nonlinear system. We will discuss our result on one of model

using the analytic method and in chapter 4 we will present a comparison of the analytical method and computer simulation method of a one-dimensional Van der Pol oscillator with varying degree of nonlinearity.

In chapter 4, modeling circadian rhythms by single or multi-dimensional nonlinear differential equations will be discussed. We will first discuss our simulation results of two previous models which are Pavlidis's biological oscillator model and Kronauer's coupled oscillator model. Then we will introduce the development and the analysis of our models which include a modified Van der Pol oscillator model, and a two and a three dimensional coupled oscillator model. The two dimensional coupled oscillator model has been presented in the literature to describe the circadian system [23] while our modeling emphasized the bimodality, which is a prominent feature of many circadian rhythms. Circadian activity rhythms in rats, hamsters, birds, and many other animals exhibit two prominent peaks, with one peak at the beginning of activity followed by a second peak late in activity [31]. In addition, humans exhibit a strong bimodal distribution of daily sleep latency, an objective measure of sleepiness. Such observations suggest that the source of the bimodal patterns is an eminent characteristic of the circadian system. Therefore our model attempts to present this feature. This idea is also substantiated from the analysis of the frequency spectrum which will be introduced in chapter 6.

The experimentally acquired data and model data are compared and analyzed using topological methods. In chapter 5, we will introduce the phase plane method and phase response curve method for nonlinear analysis. The phase plane results of our Van der Pol oscillator model with different degrees of nonlinearity will be presented. We have effectively determined the nonlinearity of our models by this technique. Raster plotting is a graphic method especially useful for circadian

rhythm research which was used in our experimental data recording.

The simulated and experimental data are then further analyzed in the frequency domain. The spectral function is a powerful tool to determine the structure of a system. In our case, it was used in determining the general and dynamic characteristics of experimental and simulated circadian data. In chapter 6, we will first review the general principles of the Fourier transform and spectral function. The data pre-processing and the spectral analysis of circadian rhythms will then be discussed. The spectral functions obtained from our experimental subjects will be presented in section 6.4. They have common structures while each one also has distinct features. We related the spectral structure of experimental data to our models. Especially, we explored the relations between harmonic structure and nonlinearity of the system which will be introduced in section 6.5.

The dynamic process of circadian rhythm is an important issue which will be introduced in chapter 7. A biological oscillator could be stimulated by a periodic or nonperiodic external force. The periodic stimulus may cause the oscillator either to be entrained or to be in an "almost periodic mode". The entrainment that occurs at the natural frequency of the external stimulus is near that of the biological oscillator, while in the "almost periodic mode" both the excited frequency and original frequency of the biological oscillator co-exist in the system. We applied periodic stimuli with different amplitude and frequency range to our models to determine the entrainment range. Then, the transient process due to a nonperiodic stimulus was examined. Under certain circumstances, the circadian oscillator can be exposed to abrupt changes in the phase of the entraining stimulus. The most familiar example is air travel across time zones. This phase shift produced by traveling to a new local time is often accompanied by "jet lag." Formally, the

change to a new environmental time represents a *nonperiodic* stimulus to the circadian system which can lead to temporary changes in the amplitude, frequency or the phase of the oscillator [22]. The processes during phase shifts have often shown complicated patterns of transient behavior. Our investigation into the transient behavior of our model following nonperiodic stimuli is discussed in sections 7.3 and 7.4. Using the dynamic spectrum and frequency demodulation methods respectively, we found the "overshot" phenomenon during the transient process. If the nonperiodic stimulus is applied at the proper time, with proper amplitude and pulse width, the transient process can even cause a "temporary stopping" of the oscillation. This process was also simulated using our model and will be introduced in section 7.5.

The use of the bispectrum and coherence for the analysis of circadian rhythms will be discussed in chapter 8. The bispectrum method was applied to determine the relations between harmonic components of the circadian rhythms while the coherence function was used to examine the frequency correlations between two different circadian rhythms (e.g., temperature and activity) of the same subject. We applied the coherence function to our experimental data and found that correlation occurred at the fundermental and 3rd harmonic in one of our subjects.

Chapter 2

Experimental Circadian Data Acquisition, Pre-Processing and General Appearance

2.1 Introduction

The circadian rhythm is a long period oscillation phenomenon. The period of this type of rhythm is around 24 hours. The experimental circadian data, including core-temperature, and sleep-wake cycle, can be acquired from monitoring long term experiments. The "length" of recording for analysis should be at least 240 hours (10 cycles) and usually several "sections of data" are needed. This long term data recording results in the following special considerations for the design of a data acquisition system and the pre-processing of the acquired data.

1. Our experimental data are mainly acquired from monkeys and other animals which are free ranging, and any form of restrictive wired system would be unsuitable. The transducers (sensors) attached to the subjects should not restrict their activities, or the transducer will be damaged. Therefore, special

design of transducers of light weight and small size should be considered, and the transducers should be wireless.

2. The A/D sampling rate for data acquisition should be considered to meet both accuracy and storage capacity requirements. Accuracy means that the circadian data acquired should have enough information to determine its characteristics. For example, if a rate of 14 samples/24hrs is used for the A/D convertor, we can, in theory, get information up to the 7th harmonic of a 24hr circadian cycle. In practice, up to 10 times this rate, i.e., 140 samples/24 hours is used to enhance accuracy. On the other hand, if the sampling rate is too high, a large storage capacity is required for long term recording. Therefore we should select the sampling rate to compromise for both accuracy and storage consideration. In our system, a rate of 144 samples/24hr is used;

3. The acquired raw data may be accompanied by noise, baseline drift and some temporary interruption. These unwanted signals should be filtered out, or smoothed (pre-processed), before doing further processing. The preprocessing should be considered on both the raw analog data and the digital data.

2.2 Experimental Data Acquisition System

Most of our experimental circadian rhythm data were taken from six Rhesus monkeys. These monkeys were kept in cages under carefully controlled light, temperature and noise conditions. The lights in these cages could be controlled either by a timer or computer controlled switches which determined whether the experiment was under"free running" or entrainment conditions. The circadian data we collected included daily temperature data, sleep-activity data and feeding data.

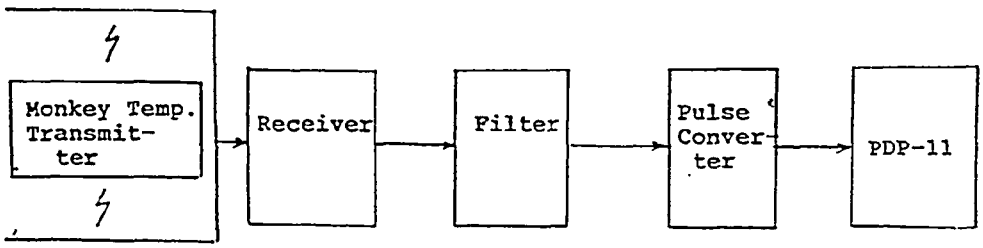

Figure 2.1: *Circadian temperature data acquisition system.*

Temperature and activity data were mainly used in this research.

Fig 2.1 shows a diagram of our monkey temperature data acquisition system at the VA Medical Center, East Orange, New Jersey. We used a telemetry system where the wireless temperature transducer and transmitter module (Mini-Mitter) were implanted into the monkey's body by simple surgery. This module continuously transmitted the pulses whose rate was proportional to the temperature. The modules were calibrated before being implanted to obtain the temperature–pulse rate conversion curve. The pulse rate is usually in the range between 100/min and 200/min at room temperature. The carrier frequency of the transmitter was selected between 27.0 MHz and 28.0 MHz. The module contained a lithium battery designed to last about 1 year.

The receivers used in the system were the SONY ICE-2010 PLL synthesized high sensitivity receivers. Each receiver monitored two transmitters selected by a computer controlled station selection switch. The received signal was then sent to

an analog low-pass filter; with 3dB cut off at 1 kHz for noise filtering. The signal was then interfaced to the computer. The computer was programmed to accept and count the pulses from each I/O channel for 2 minutes out of every 10 minutes for a sampling rate 144 samples/24hr. This sampling rate ensures the detection of several tens of harmonics of the 24 hour circadian cycle. The acquired raw temperature data (144 points for each subject per day) were stored in the PDP-11 computer and then transferred to the VAX 11-750 computer once a day.

The sleep-activity data was recorded by monitoring the movement within the cage. These cages were specially designed to be "floating" such that the sensors mounted on the corners of the floating cages recorded the movement of the monkey in the cage. The data sampling and processing are basically the same as for the temperature data.

The monkey feeding data were monitored with a microswitch mounted on the food pipe. The switch was triggered each time the subject took food.

2.3 Preprocessing of Experimental Data

The long term circadian data is easily subject to interference and interruption, due to a number of possible causes. For example, the 27 MHz shortwave signals could be contaminated by noise interference generated by the computer equipment. Occasionally this interference could be transmitted over the power line from a remote location. This noise from the power line may be eliminated by a line filter, while the interference transmitted by the electromagnetic fields is more difficult to remove. In order to provide an acceptable acquisition system, we concentrated on optimizing:

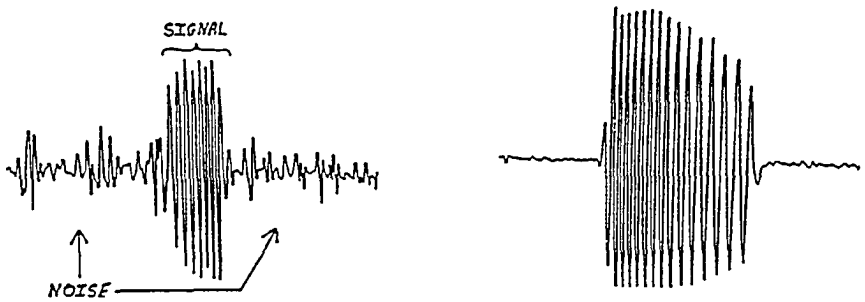

Figure 2.2: *(a) Received data by original antenna. (b) Received data by improved antenna.*

1. The receiver antenna design. A specially designed antenna is installed in the cage which greatly improves the S/N ratio over previous designs.[6] This multi–functional antenna is insulated from the metal of the cage and the cage is grounded to help shield the antenna against outside RF interference. Fig.2.2 shows the comparison of the reception between original and improved antennas.

2. Selection of the proper AM band gain and attenuation of the receiver. The AM band gain of the receiver is continuously adjustable. The proper AM band gain occurs when the S/N ratio is maximized.

3. Selection of a different AM band mode (wide band or narrow band) of the receiver. In the case of heavy noise interruption, a narrow band reception is selected.

The preprocessing of the experimental data includes the following steps:

1. Removing very corrupted data which may be blank or seriously distorted. If these portions are used for further processing, the rest of the good data could be possibly affected. These portions of data could be removed by carefully examining the entire data. Due to the varying forms of the interference, it is difficult to automate this procedure. This procedure was therefore done manually. The pre-processing program can readily handle the data if the interference does not exceed 10% of the record.

2. Scaling. The normal circadian rhythm signal should be in a given amplitude range. A signal that in out of this range may be caused by a fault of the system or by interference. The scaling procedure works like a limiter, that is, it eliminates the signal out of the normal range. For example, the normal temperature range for a monkey should be between $36°C$ to $40°C$. Our scaling procedure eliminates signals below $34°C$ and above $42°C$, which ensures the obtaining of a meaningful signal.

3. Detrending. Very low frequency components contained in a circadian signal (frequencies in the range 0 to $2.5^{-6}Hz$) are usually caused either by the instruments used to acquire the signal or by such effects as the long term trend of monkey circadian rhythms. Those components smear the power spectrum of the signal at low frequencies. They also smear the result of the processing of the low frequency components by techniques such as complex demodulation. These trends can even dominate the spectrum. Therefore, the very low frequency component in the signal should be removed (detrended) before the signal is further processed. This detrending procedure is done by a robust local regression procedure. [9]. The low trend is first extracted from relatively long term data (e.g., 10 days) and then this trend is subtracted

from the original data. The detrending work is done by a Macro subroutine written in S language (S is a programming environment for data analysis and graphics from AT &T Bell Laboratories) using a function *Lowess*. The function *Lowess* is used to smooth data in n (user defined parameter) points while we use it to extract very low frequency components (periods of around 7 days or more). This low frequency component is then subtracted from the time series, thus accomplishing detrending. The Macro subroutine *Detrend* is listed in the Appendix.

4. Smoothing. Data smoothing refers to the measures which are introduced into a data processing scheme in order to reduce the effects of observational errors (commonly called noise). Since data smoothing generally also has a mutilative effect on the signal component, it presents a need for careful analysis to achieve desirable results. The smoothing of data should exclude the noise but the signal should not be distorted. The smoothing algorithms was tested on several data sets. This was done by use of a Macro *Lwclean*.

In summary, the preprocessing algorithm includes removing interrupted sections, scaling, detrending and smoothing the data. All the preprocessing is written in S language which simplifies the process algorithm. All the functions and Macros as mentioned above are combined in a Macro *Pre*, which is listed in the Appendix.

2.4 General Appearance of Real Circadian Data

To model and analyze circadian rhythms it is important to understand the general appearance of real circadian rhythms in both the time and frequency domains.

2.4.1 Time Series of Circadian Rhythms

Fig 2.3 and Fig 2.4 show the waveforms of circadian temperature time series obtained from several subjects under test. Fig.2.3(a)-(d) show 7 days of temperature circadian rhythm data from four different monkeys. Fig.2.4 (a) and (b) show 7 days of temperature circadian rhythm data from 2 different rats. All of these data were previously preprocessed.

These waveforms give us the following basic insights into practical circadian time series:

1. The waveforms are distorted cosine-like waveforms. The highest peak of the waveform is at around 11 am and the valley is around 11 pm. The period of the waveforms can be detected by zero crossing detection or peak detection. The results show that the period is around 24 hrs. The distortion is probably caused by nonlinearity, but the nonlinearity could not be found from the time series directly.

2. Some of the circadian time series show a second or third small peak during one cycle. This implies that these waveforms contain some high harmonic frequency components.

3. The waveforms are noisy and not smooth.

To address the above characteristics more directly, we must look at the signals in the frequency domain.

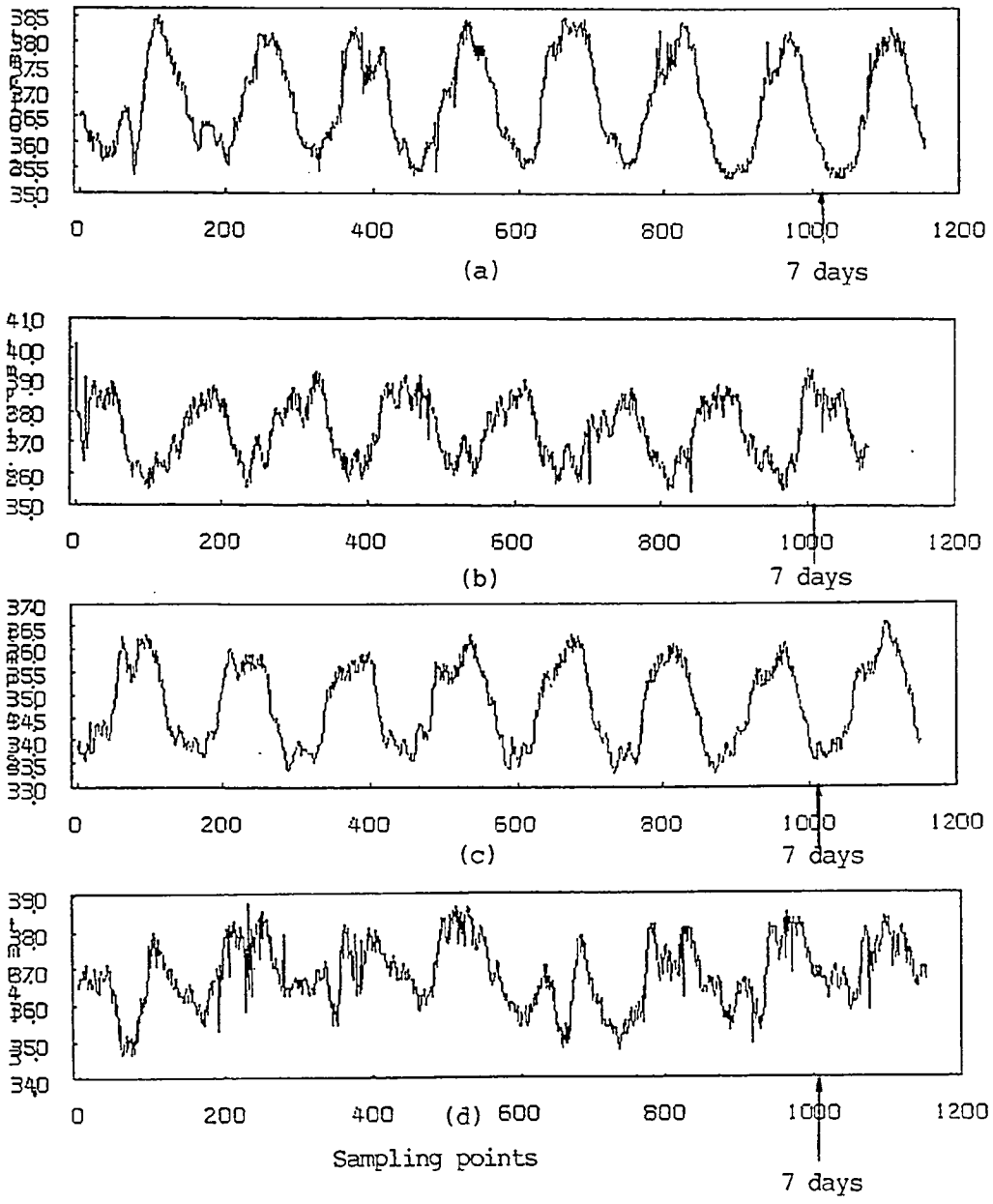

Figure 2.3: *Time series of monkey's temperature circadian rhythm. x-axis: sample points (144 sample points a day). y-axis: temperature in centigrade degree. a) 7 days data of Monkey 10. b) 7 days data of Monkey 21. c) 7 days data of Monkey 34. d) 7 days data of Monkey 41.*

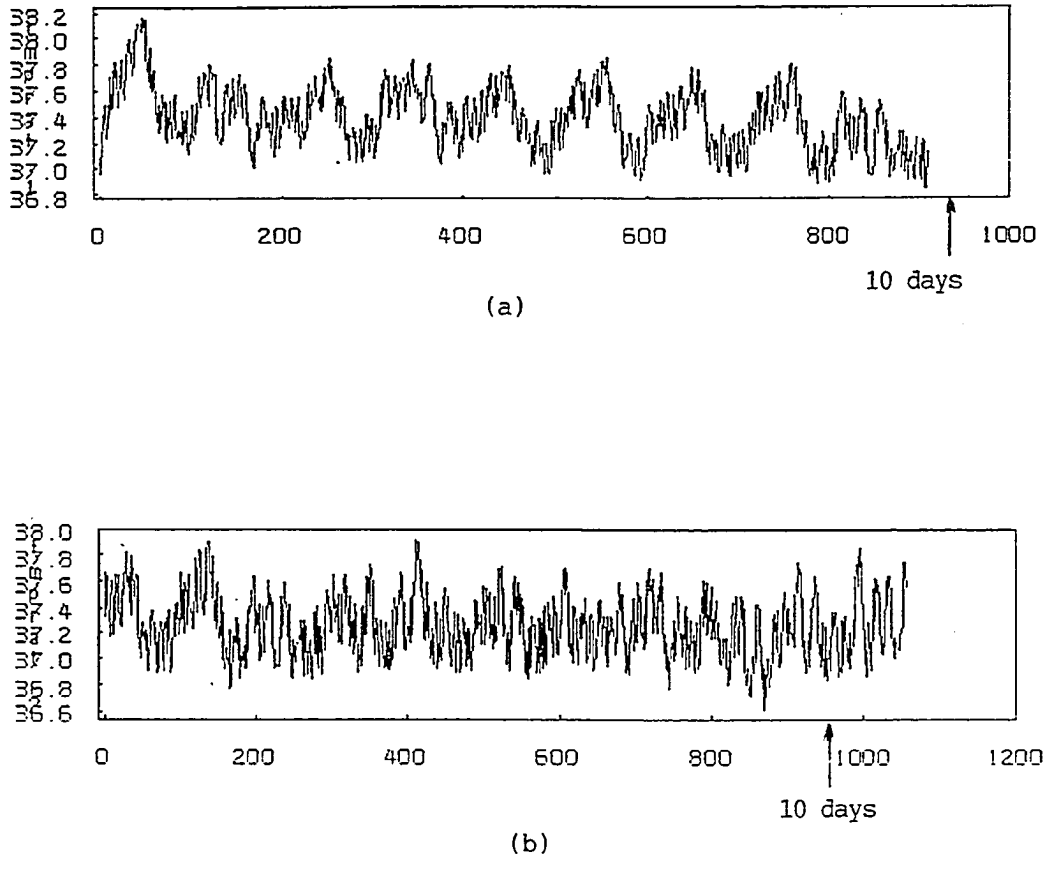

Figure 2.4: *Time series of rat's temperature circadian rhythm. x-axis: sample points (96 sample points a day). y-axis: temperature in centigrade degree. a) 10 days data of Rat 2. b) 10 days data of Rat 4.*

2.4.2 Frequency Characteristics of Circadian Data

To further understand the obtained circadian data, we need to explore the general aspect of their spectral functions. The spectral function shows the detection and measurement of the frequencies, amplitudes, phases of decomposed sinusoids in a time series which is especially helpful for exploring a system whose characteristics are unclear like the circadian rhythms. The principles and techniques of spectral analysis will be discussed in chapter 6. In section 6.4, several sets of spectral functions obtained from our experimental data will be presented. Figure 2.5 shows one of the spectra from the experimental data where we can see the main frequency component is at FFT point 113. Since we transformed 16384 points and the sampling rate was 6 samples/hour, the period of point 113 is

$$\frac{16384}{6(113-1)} = 24.38 hours$$

The spectrum also shows the 2nd, 3rd and higher harmonic components. The analysis of these harmonics will be discussed out in chapter 6, where we will show how these harmonics relate to the nonlinearity of the system.

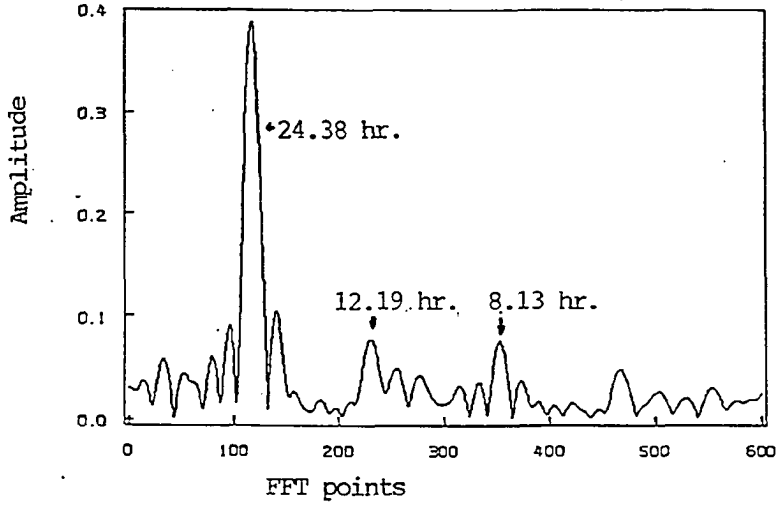

Figure 2.5: *The power spectrum from one of the experimental circadian data. The data was sampled at 6 samples/hour and the spectrum was computed by 16384 FFT point. x-axis: FFT point. y-axis: amplitude. The period is 24.38hr at FFT point 113. The period is 12.19hr at FFT point 226. The period is 8.13hr at FFT point 339.*

Chapter 3

Classical Mathematical Tools for Analysis of Nonlinear Oscillation

3.1 Introduction

Many of today's most interesting problems in the physical and life sciences concern the behavior of nonlinear systems, especially the onset of chaotic behavior under deterministic conditions. Biological oscillators are basically all nonlinear. The linearization commonly practiced are good for approximate analysis. However, for certain cases the linear treatment may not be applicable at all. Many complicated phenomena occur in the systems because of their nonlinearity which can not, in principle, occur in linear systems.

Although the phenomena of nonlinear oscillations have been recognized by many scientists for a number of years, developments in the theory and methods of nonlinear analysis have been stimulated in recent years by the application of digital computers. Among the major trends in modern developments of nonlinear analysis are: the study of *the analytical method* (including computer application)

for obtaining the complete solution of the system; the *topological method* of graphic solution and the *computer simulation method* for numerical solution of complicated, multidimensional nonlinear systems.

In this chapter we will first introduce the general analysis of *linear oscillators*. This analysis helps us to understand the properties of linear oscillation which can also be used for approximate analysis of nonlinear systems. In section 3.2.1, we will introduce a linear model of circadian rhythms as well as the computer simulation results, from which we can see the differences between the linear model and the real circadian rhythm data as we presented in chapter 2. We will therefore understand the limitation of the linear model and the necessity of using a nonlinear model to describe the biological oscillators.

The **analytical methods** we will describe in section 3.2 include the asymptotic method and the perturbation method. These two methods are the traditional mathematical tools for an analytical solution of nonlinear systems. They were developed to find the periodic analytical solutions of nonlinear differential equations. The advantage of the analytic method is that it can be used to find the complete solution of the system thereby allowing knowledge of the general aspect of the system at any time. Recently, some computer programs were designed for obtaining the analytical solutions of linear or nonlinear differential equations but they were limited to some simple typical nonlinear systems. In our applications, it was found that the traditional analytic method applied only to the "weakly" nonlinear systems and the error became larger as the nonlinearity increased.

The **computer simulation method** is based on mathematical or mechanical models. With successive iteration, the computer simulation can generate the

numerical solution of the system for the time length defined. By selecting proper integration algorithms, the numerical solution obtained by the computer simulation can yield high accuracy. The disadvantage is that the computer simulation method can not generate the complete description of the nonlinear system simulated. In section 3.4, after our introduction of two analytic methods, the computer simulation results of a single Van der Pol type model with different nonlinearity will be presented. The results will also be compared to those obtained using the analytical method.

In this research, we formulated and tested several nonlinear mathematical models to simulate circadian rhythms. The solution of these models were obtained through computer simulation which turned out to be a very powerful method, and in some cases, possibly the only method. The computer modeling and simulation will be discussed in chapter 4.

3.2 Analysis of Linear Oscillation

For the simple types of nonlinear differential equations, it is possible to find their properties by the study of the approximate linear system. For example, the appearance of the trajectories of the given nonlinear system near the equilibrium point is generally the same as for the approximating linear system. In order to take full advantage of this principle, we have to know the configurations of linear systems which can be used to approximate the nonlinear system. The mathematical models of circadian rhythms are usually *nonlinear* but the analysis of linear oscillators will help us to understand the basic mathematical methodology, and is also helpful to see why linear models can not be applied in nonlinear analysis. In this section we

will first discuss the properties of linear oscillation systems.

Generally, a linear oscillation can be described by *second order, ordinary differential equations* of the form:

$$a(x)y'' + b(x)y' + c(x)y = f(x) \tag{3.1}$$

The typical homogeneous differential equation of a linear oscillator with constant coefficients is

$$m\frac{d^2y}{dt^2} + h\frac{dy}{dt} + ky = 0 \tag{3.2}$$

where m,h and k are real constants.

The characteristic equation is

$$m\tau^2 + h\tau + k = 0 \tag{3.3}$$

Its roots are

$$\tau = -\frac{h}{2m} \pm \frac{\sqrt{h^2 - 4km}}{2m} \tag{3.4}$$

or

$$\tau = -\frac{h}{2m} \pm i\frac{\sqrt{4km - h^2}}{2m} \tag{3.5}$$

The solution will depend on whether $h^2 - 4km$ is positive or negative. In the case of complex roots $\alpha + i\beta$ where $\alpha < 0$ the solutions is

$$y = e^{\alpha t}(c_1 cos\alpha t + c_2 sin\alpha t) = Ae^{\alpha t}sin(\beta t + \phi) \tag{3.6}$$

This solution represents a damped oscillation as shown in fig.3.1.

If we fix m and vary h, then we observe the following:

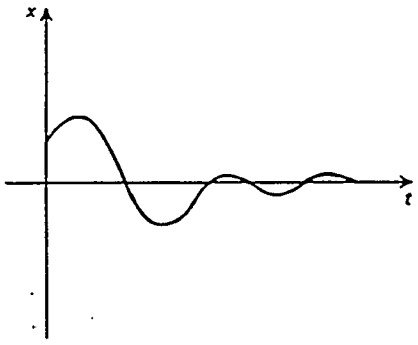

Figure 3.1: *Damped linear oscillation.*

For $h = 0$, the equation represents a simple sinusoidal oscillation (simple harmonic motion).

$$y = (c_1 cos\beta t + c_2 sin\beta t) = Asin(\beta t + \phi) \tag{3.7}$$

In a physical system, it describes the motion of a mass-spring system without friction.

As h increases from 0, the oscillation is increasingly damped.

For $h^2 = 4km$, we have a critically damped oscillation, and the discriminant is 0. Beyond this value, we have overdamped motion.

The oscillation described above in the case without friction could be used to approximately describe the circadian rhythms as we will see in the next section.

3.3 Linear Model for Circadian Rhythms: Its simulation and Limitation

A linear model "BEATS" was created by Wever [39]. This is a coupled oscillator model but each oscillator is based on linear oscillation. In this model,

the type I - x oscillator is

$$x = sin\omega_x t$$

and type II - y oscillator is

$$y = sin(\omega_y t + \phi)$$

respectively. The temperature rhythm is principally controlled by a type I oscillator, with some small "masking" contribution from the type II oscillator which dominates the activity cycle.

In practice, the temperature rhythm is always more stable than the other rhythms. Therefore, in the model, type I oscillators are "stronger" than type II oscillators, and also more "stable".

Wever's interesting point is that a mere superposition of such oscillations in many ways resembles the observed data. In other words, the output of the oscillators are summed but do not interact dynamically. Therefore the structure of this model includes two superposed oscillators as shown in Fig.3.2. The activity-rest rhythm A and the temperature rhythm T are then modeled as a superposition of x and y:

$$A = ay + (1 - a)x \tag{3.8}$$

$$T = bx + (1 - b)y \tag{3.9}$$

where $(1 - a)$ and $(1 - b)$ are the coupling coefficients between A and T. a and b are in the range between 0 and 1, which we chose to be > 0.5 in this model. In the model the angular frequency of circadian rhythm x is selected as one unit, i.e., $\omega_x = 1$ while $\omega_y \leq 1$.

The linear type equation is the first important feature of the model. The author was trying to reduce the complication of the model to better understand

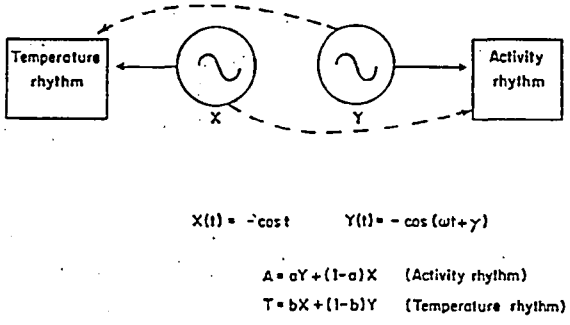

Figure 3.2: *BEATS model of circadian rhythms of activity (A) and temperature (T).*

the relations in the model. Fig.3.3 shows the simulated activity waveform. The variation of amplitude is caused by the T oscillator. The amplitude decreased every 5 cycles periodically which is called a "beat".

Comparing the output time series with the real experimental circadian data (see Fig.2.4), it can be seen that the linear waveform of the time series is very different from the real data. This is because only a single frequency component exists in this model while "rich" harmonic components exist in the real data. These harmonics generate "multi-pattern" complicated time series and the harmonics of the system are related to the nonlinearity of the system which we will show in the next section.

Therefore, as we pointed out at the beginning of the chapter, although the linear approximation model is easy to understand and to program and simulate, it can not reflect the characteristics of the circadian system.

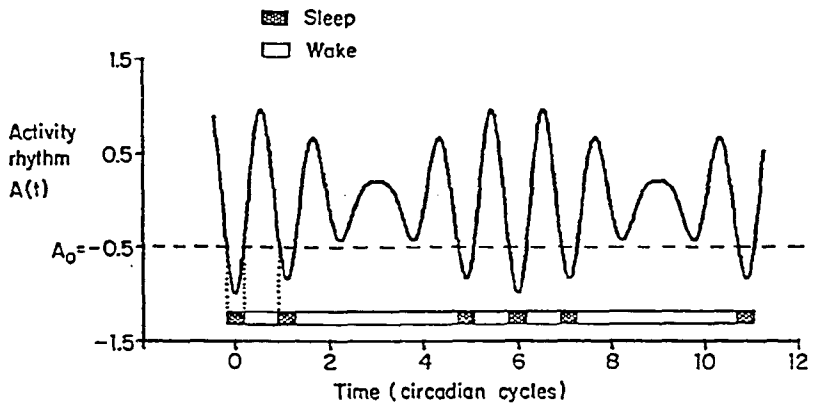

Figure 3.3: *Simulated time series waveform of "BEAT" model.*

The angular threshold used in this model was another important difference from the other models. The sleep–wake period was usually determined by a level threshold. As we can see in Fig.3.3, $A = -0.5$ is used as a level threshold in the model, and the outputs of the system above this threshold represent the wake cycles while the ones below the threshold represent the sleep cycles. Since the "beating" of two oscillators in this model generated relatively large changes of the amplitude, the level threshold criterion, if used in this model, generates unrealistically long wake episodes. The angular threshold was designed to solve this problem. The angular threshold is shown on the phase plane by the angle as we can see in Fig 3.4. The trajectories in the shaded region represent the sleep region while the ones in the unshaded region represent the wake region. They are distinguished by the angle on the phase plane instead of by the level on the time series.

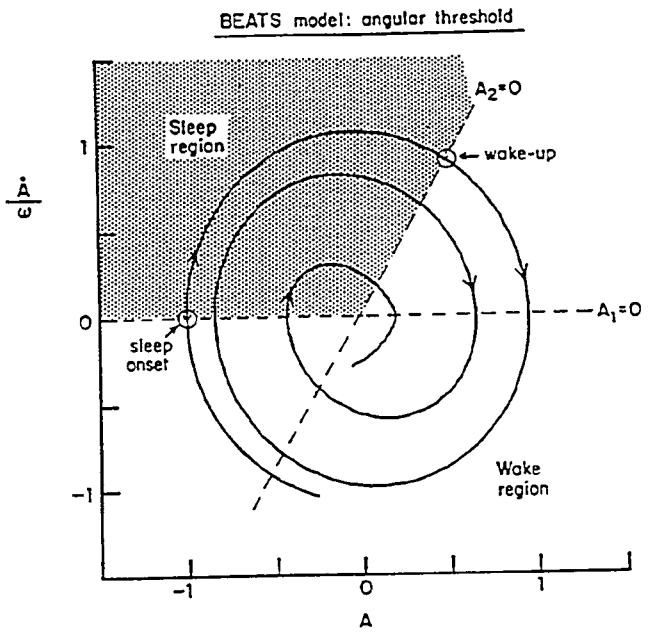

Figure 3.4: *Angular threshold on the phase plane for BEAT model. Shaded region: sleep region. Unshaded region: wake region.*

3.4 Analytical Methods for Nonlinear Oscillator Analysis

3.4.1 Introduction

There is considerable advantage in finding an analytical solution for a differential equation when that is possible. The analytical solution may be obtained in algebraic form without the necessity of introducing numerical values for parameters or initial conditions during the process. Once the solution is obtained, any desired range of possible solutions can be explored.

It should be recognized that explicit solutions are generally impossible to obtain for nonlinear systems. The practical methods used to solve these systems are topological methods and numerical methods which will be discussed in chapter 4 and chapter 5. Only a few nonlinear equations from actual physical systems are simple enough to allow exact solution. There are generally no methods capable of yielding an exact solution of an arbitrarily selected nonlinear differential equation.

Let us consider a system of n 1st order differential equations:

$$dx_i/dt = X_i(t), \qquad i = 1, 2, \cdots, n \tag{3.10}$$

Where $X_1, \cdots, X_n$ are analytical functions of the unknown variables $x_1, \cdots, x_n$ and the time t. If $x_1, \cdots, x_n$ are components of an n vector x and, $X_1, \cdots, X_n$ are components of an n vector X, the above system equations may be written in the simpler form

$$dx/dt = X(x, t) \tag{3.11}$$

It may happen that X depends upon x alone and not upon t. The above equation

then becomes

$$dx/dt = X(x) \tag{3.12}$$

A system of this type is said to be *autonomous*. Alternatively, the system function depending on time t is said to be nonautonomous. Most of the biological oscillators are autonomous systems. [29, page 13]

To use analytic methods to solve the nonlinear differential equation, we have to first understand the *uncertain properties* of the oscillating frequency in a nonlinear system. This principle states that the natural frequency of a nonlinear system is not a certain value for all different nonlinearity, i.e., the oscillating frequency varies with the nonlinearity. To understand this principle, let us consider the following example of a nonlinear differential equation:

$$\frac{d^2x}{dt^2} + x + \mu x^3 = 0 \tag{3.13}$$

If we assume the power series solution

$$x(t) = x_0(t) + \mu x_1(t) + \mu^2 x_2(t) + \cdots \tag{3.14}$$

and substitute Eq.3.14 into the original differential Eq.3.13, the μ terms must be equated to zero separately, i.e., the sums of the terms with μ, the sums of the terms with μ^2, $\cdots$, etc, should each be equal to zero respectively. Equating these coefficients separately to zero gives the following sequence of linear equations:

$$\frac{d^2x_0}{dt^2} + x_0 = 0 \tag{3.15}$$

$$\frac{d^2x_1}{dt^2} + x_1 = -x_0^3 \tag{3.16}$$

With the initial conditions given, we can solve each linear differential equation to get x_0, x_1, x_2, etc. We find

$$x_0(t) = A\cos t \tag{3.17}$$

$$x_1(t) = (-3/8)A^3 t sint - (1/32)A^3(cost - cos3t) \qquad (3.18)$$

$\cdots$, etc.

where A is a constant determined by the initial conditions.

A serious difficulty may often be encountered in the form of the so-called "secular terms". The secular terms are the terms in equations which will grow indefinitely when t tends to infinity, and thus destroy the *convergence* of the series solution. For example, the first term of $x_1(t)$ in Eq.3.18, $-3/8 \cdot A^3 t sint$, which will grow indefinitely as t goes to infinity, has this property.

To solve this problem, we have to realize that in a nonlinear oscillator system, the solution may not be necessarily *periodic with constant period.* In this example, since the x_0 term above is fixed as a periodic function, the remaining terms must account for the variation of the period, thus resulting in the appearance of *secular terms.* For the elimination of secular terms, precaution must be taken so that the unknown frequency of a free oscillation and the amplitude of a self excited oscillation should **not be fixed** in a nonlinear system. Therefore the solution we assume for a nonlinear system should not have a constant frequency and amplitude, and instead should be assumed to be functions of the nonlinearity. Next, we will discuss two methods of solving nonlinear differential equations with small nonlinear parameters by considering the problems mentioned above.

3.4.2 Asymptotic Method

The asymptotic method is the first analytic method which we used to solve the nonlinear differential equations in our circadian models. It can be used for

oscillating systems with weakly nonlinear parameters, namely those where the nonlinear term depends on a "small" parameter μ, and for $\mu = 0$, the system becomes linear. One of the advantages of this method is that it can be used to solve the nonlinear systems of higher than second order. There are several methods which could possibly be applied for second order systems with fewer applied to systems of higher order. As we shall introduce in section 5.2, the phase plane techniques could be used for second order systems but not for higher order systems.

A weakly nonlinear second order system which is likely to present sustained oscillations has the following general form:

$$d^2x/dt^2 - \mu f(x, dx/dt) + \omega^2 x = 0 \tag{3.19}$$

When $\mu = 0$, the system becomes a harmonic oscillator.

It is reasonable to assume that when μ is sufficiently small the solution for the system should be close to the solution of the original linear system. It is plausible [29, pages 16] that if self sustained oscillations exist, (trajectory of the limit cycle form) then the solution can be assumed to be a form containing linear oscillation ($cos\phi$) plus a series of unknown μ terms,

$$x = \alpha cos\phi + \mu u_1(\alpha, \phi) + \mu^2 u_2(\alpha, \phi) + \cdots \tag{3.20}$$

$$d\alpha/dt = \mu A_1(\alpha) + \mu^2 A_2(\alpha) + \cdots \tag{3.21}$$

$$d\phi/dt = \omega + \mu B_1(\alpha) + \mu^2 B_2(\alpha) + \cdots \tag{3.22}$$

For $\mu = 0$, the solution becomes $x = cos\phi$ with α a constant and $\phi = \omega t + \phi_0$, which is indeed the solution of the linear oscillator.

If we assume that,

1. μ is sufficiently small, the convergence of the series can be guaranteed;

2. As μ tends to zero, the truncated forms of the series converges to the true solution;

3. Only $A_1(\alpha)$ and $B_1(\alpha)$ will be significant, i.e., higher order μ terms are not considered;

Then

$$d\alpha/dt = \mu A_1(\alpha) \tag{3.23}$$

$$d\phi/dt = \omega + \mu B_1(\alpha) \tag{3.24}$$

This result is a sufficiently good approximation in many practical problems. Computing the derivatives of x using Eq.3.20 Eq.3.23 and Eq.3.24 while ignoring terms which are multiplied by powers of μ, we obtain:

$$dx/dt = -\alpha\omega sin\phi + \mu(A_1 cos\phi - \alpha B_1 sin\phi) \tag{3.25}$$

$$d^2x/dt^2 = -\alpha\omega^2 cos\phi - 2\omega\mu(A_1 sin\phi + \alpha B_1 cos\phi) \tag{3.26}$$

Replacing $x, dx/dt$ and d^2x/dt^2 in the original differential equation and expanding $\mu f(x, dx/dt)$ in a Taylor series, A_1 and B_1 can be determined, where

$$A_1(\alpha) = -1/2\pi\omega \int_0^{2\pi} f(\alpha cos\phi, -\alpha\omega sin\phi) sin\phi d\phi \tag{3.27}$$

$$B_1(\alpha) = -1/2\pi\omega\alpha \int_0^{2\pi} f(\alpha cos\phi, -a\omega sin\phi) cos\phi d\phi \tag{3.28}$$

Thus $A_1(\alpha)$ and $B_1(\alpha)$ are nothing more than the fundamental terms of the Fourier series expansion of $f(\alpha cos\phi, -\alpha\omega sin\phi)$.

It can be easily verified that if f is an even function of its first argument, i.e.,

$$f(\alpha cos\phi, -\alpha\omega sin\phi) = f(-\alpha cos\phi, -\alpha\omega sin\phi) \tag{3.29}$$

then $B_1(\alpha) = 0$ and $d\phi/dt = \omega$. In this case, the frequency of the system is independent of μ and equal to ω.

If f is an even function of its second argument, i.e.,

$$f(\alpha cos\phi, -\alpha\omega sin\phi) = f(\alpha cos\phi, \alpha\omega sin\phi) \tag{3.30}$$

then $A_1(\alpha) = 0$ and $d\alpha/dt = 0$. In this case, the amplitude is independent of μ and equal to a constant.

$d\phi/dt$ and $d\alpha/dt$ give us the most important information about which we are concerned: the frequency variation and amplitude variation of the oscillation. In the first case, where the nonlinear portion μ is an even function of its first argument, the oscillations are approximately isoperiodic, i.e., the frequency does not depend on μ or other parameters except through higher-order terms. The Van der Pol oscillator used in our model is an example where the nonlinear term

$$f(x, dx/dt) = (1 - x^2)dx/dt$$

is an even function of x ($x = \alpha cos\phi$). Therefore,

$$\begin{aligned} B_1(\alpha) &= 0 \\ d\phi/dt &= \omega \end{aligned}$$

and

$$\begin{aligned} A_1(\alpha) &= \alpha\omega/\pi\omega \int_0^{\pi} (1 - \alpha^2 cos^2\phi) sin^2\phi d\phi \\ &= (\alpha/2)(1 - \alpha^2/4) \qquad (3.31) \\ d\alpha/dt &= (\mu\alpha/2)(1 - \alpha^2/4) \qquad (3.32) \end{aligned}$$

When $\alpha = 2$, $d\alpha/dt = 0$. The system is expected to have a stable oscillation if μ is sufficiently small

$$x(t) = 2cos(\omega t + \phi_0) \tag{3.33}$$

The asymptotic technique is an effective method for one to explore the amplitude and frequency variation information of a nonlinear system. However, this method can be only applied in a system with a"weak" nonlinear parameter. Since the biological oscillator models usually contain large nonlinear parameters, this method cannot be generally applied.

3.4.3 Perturbation Method

Another powerful analytic method we tried for solving nonlinear differential equations in our models is the perturbation method. The use of this method began with astronomical calculations. But important contributions of Poincare and later mathematicians have extended the applicability of this method to include the more general field of nonlinear mechanics.[32] The perturbation method is also applicable to equations in which a small parameter is associated with the nonlinear terms. In applications, the method can be summarized in the following steps:

1. Assume that the desired solution can be expanded in a power series of the small parameter multiplied by coefficients which are functions of the independent variable. It is advantageous to replace the independent variable t by $\tau = \omega t$, where ω is the unknown frequency of the periodic solution.

$$x(\tau) = x_0(\tau) + \mu x_1(\tau) + \mu^2 x_2(\tau) + \cdots \tag{3.34}$$

and

$$dx/dt = \omega dx/d\tau \tag{3.35}$$

$$d^2x/dt^2 = \omega^2 d^2x/d\tau^2 \tag{3.36}$$

Because ω is not a fixed constant, it is necessary to develop the unknown quantity ω in a series with respect to μ, the coefficients in the series being periodic functions of τ. Therefore we have,

$$\omega = \omega_0 + \mu x_1(\tau) + \mu^2 x_2(\tau) + \cdots \tag{3.37}$$

2. Substitute the assumed power series solution (both x and ω) into the differential equation and determine the coefficients of the like powers of μ, one by one, usually by solving a sequence of second order linear equations in $x_i(\tau)$, which also involve the unknown frequency quantities w_i.

3. Since only the periodic solution is under consideration, the initial condition of τ may be chosen arbitrarily. We so choose it so that $x'(\tau) = 0$, at $\tau = 0$.

As an example, we consider Van der Pol's equation again

$$\ddot{x}/dt^2 - \mu(1 - x^2)dx/dt + x = 0 \tag{3.38}$$

where μ is a small positive quantity. Replacing the independent variable t by $\tau = \omega t$ as before:

$$\omega^2 x'' - \mu\omega(1 - x^2)x' + x = 0 \tag{3.39}$$

Insertion of the x series (Eq.3.34) and ω (Eq.3.37) series results in a sequence of linear equations:

$$\mu^0 : \qquad \omega_0^2 x_0'' + x_0 = 0 \tag{3.40}$$

$$\mu^1: \quad \omega_0^2 x_1'' + x_1 = -2\omega_0\omega_1 x_0'' + \omega_0(1 - x_0^2)x_0' \tag{3.41}$$

$$\mu^2: \quad \omega_0^2 x_2'' + x_2 = -(2\omega_0\omega_2 + \omega_1^2)x_0''$$
$$-2\omega_0\omega_1 x_1'' + \omega_1(1 - x_0^2)x_0'$$
$$-2\omega_0 x_0 x_1 x_0' + \omega_0(1 - x_0^2)x_1' \tag{3.42}$$

$\cdots$, etc.

We will now look at each power of μ separately.

For μ^0:

To solve $\omega_0^2 x_0'' + x_0 = 0$, utilizing $x(\tau + 2\pi) = x(\tau)$ and $x'(0) = 0$, we will have

$$x_0 = A_0 cos\tau \tag{3.43}$$

$$\omega_0 = 1 \tag{3.44}$$

where the constant A_0, not yet determined, is fixed in the next step. The zero-order solution given by Eq.3.43 is the generating solution.

For μ^1:

By substituting the solution of x_0 into Eq.3.41, we obtain

$$x_1'' + x_1 = 2\omega_1 A_0 cos\tau + A_0(\frac{A_0^2}{4} - 1)sin\tau + \frac{A_0^3}{4}sin3\tau \tag{3.45}$$

This differential equation can be solved by superposition, i.e., solve the following equations:

$$x_1'' + x_1 = 2\omega_1 A_0 cos\tau$$
$$x_1'' + x_1 = A_0(\frac{A_0^2}{4} - 1)sin\tau$$
$$x_1'' + x_1 = \frac{A_0^3}{4}sin3\tau$$

The special solution from the $cos\tau$ and $sin\tau$ terms of the above equation would contain terms of the type $\tau cos\tau$ and $\tau sin\tau$. These terms, as we mentioned in section 3.1, are the secular terms, which will cause problems as t approaches infinity.

The periodicity condition for $x_1(\tau)$, therefore, requires that the coefficients of $cos\tau$ and $sin\tau$ be zero, that is,

$$2\omega_1 A_0 cos\tau = 0$$

and

$$A_0(\frac{A_0^2}{4} - 1)sin\tau = 0$$

which will require $A_0 = 0$, or $\frac{A_0^2}{4} - 1 = 0$ and $\omega_1 = 0$. We note that $A_0 = 0$ provides a solution of zero amplitude, so the possible solution of A_0 is $A_0 = 2$. To take $A_0 = -2$ gives only a solution of opposite phase, that is, π radians out of phase with the solution in the equation. The general solution of x_1 may now be written as:

$$x_1 = A_1 cos\tau + B_1 sin\tau - (1/4)sin3\tau \tag{3.46}$$

The constant B_1 is solved by the requirement that $x_1'(0) = 0$; thus

$$B_1 = 3/4$$

The constant A_1 is determined in the next step.

For μ^2 order,

the equations lead to

$$\begin{aligned} x_2'' + x_2 &= (4\omega_2 + \frac{1}{4})cos\tau \\ &\quad +2A_1 sin\tau - \frac{3}{2}cos3\tau + 3A_1 sin3\tau + \frac{5}{4}cos5\tau \end{aligned} \tag{3.47}$$

The periodicity condition for $x_2(\tau)$ yields the following relations:

$$\omega_2 = -1/16$$

$$A_1 = 0$$

Hence,

$$x_1 = \frac{3}{4}sin\tau - \frac{1}{4}sin3\tau \tag{3.48}$$

Using the partial results from μ^1 and μ^2 terms, the general solution of Eq.3.47 becomes

$$x_2 = A_2cos\tau + B_2sin\tau + \frac{3}{16}cos3\tau - \frac{5}{96}cos5\tau \tag{3.49}$$

The constant B_2 is determined by using the requirement that $x_2'(0) = 0$; thereby we obtain $B_2 = 0$. By proceeding analogously, we can determine the unknown quantities in the right-hand members of the equation. After some calculation it is found that the periodicity condition for $x_3(\tau)$ yields

$$A_2 = -1/8$$

Hence,

$$x_2 = -\frac{1}{8}cos\tau + \frac{3}{16}cos3\tau - \frac{5}{96}cos5\tau \tag{3.50}$$

Including the terms of the second order in μ, we have

$$\begin{aligned} x &= (2 - \frac{1}{8}\mu^2)cos\omega t + \frac{3}{4}\mu sin\omega t + \frac{3}{16}\mu^2 cos3\omega t \\ &\quad -\frac{1}{4}\mu sin3\omega t - \frac{5}{96}\mu^2 cos5\omega t \end{aligned} \tag{3.51}$$

and, the frequency ω is given by

$$\omega = 1 - \frac{1}{16}\mu^2 \tag{3.52}$$

It can be seen now that the perturbation method gives more accurate solution than the asymptotic method which only gives the variation information of the amplitude and the frequency as we have seen in Eq.3.32 and Eq.3.33. The procedures of this method are also more complicated. In the next chapter, we will introduce the Van der Pol oscillator as a model for circadian rhythms. The computer simulation results of the model will be compared with the solution obtained using the perturbation method.

Chapter 4

Mathematical Modeling and Computer Simulation

4.1 Introduction

Modeling serves to develop mathematical equations for describing the system studied. In many situations the whole or part of the internal structure of these systems are unknown. The modeling process includes tests of the assurance of the model, to modify the equations established and discover the optimal parameters of the models. The circadian rhythm is a complicated biological oscillator system. Because of its unknown internal structure, indirect means have to be developed for its exploration. Mathematical modeling is one of the useful methods. The following questions now arise at this point:

1. What kind of mathematical equations should be selected to describe the biological oscillator?

2. How can we use the model to investigate the general and special (under some special conditions) properties of the system?

3. How can we determine if the modeling and the simulation results indeed represent the real biological oscillator?

4. How should the model be improved to approach the real world?

The studies of time series and frequency spectrum charactertics of biological oscillators, first discussed in chapter 2, tells us that these systems may be possibly described by nonlinear mathematical oscillator models. The numerical solutions of the models, usually from nonlinear differential equations, can be obtained by computer simulation no matter how complicated the system. Therefore, as pointed out in previous chapters, it is important to understand and investigate various possible mathematical models by using techniques such as the analytical method, topological method, spectral analysis, etc. Computer simulation will help us to obtain iteration results for further exploration of the mechanism of the model and testing parameters of the models.

To model circadian rhythms or other biologic oscillators, we should have the knowledge of existing biological oscillators and existing models. As discussed in chapter 2 we have obtained several long period records of circadian temperature data from Rhesus monkeys and rats. The analysis already completed helped us to understand the substantial features of the system and develop the models. The process of improving the model helps us to more deeply understand the system. To make the model approach the real circadian oscillator data, we should compare the computer simulation solution of the model with the experimental circadian data in both the time and frequency domain. We will then adjust the parameters repeatedly. Different initial conditions and stimuli may be applied to the model and the response of the model will be compared with the real data and analyzed.

Several mathematical models exist for circadian rhythms. These models have the following common features:

1. Self-sustainment is realized in most species. The biological oscillators are endogenous. This property will probably be lost when some special external stimuli are applied;

2. The external stimulus will synchronize the system in a certain range; i.e., the biological oscillators could be entrained by an external zeitgeber but they may have different internal stiffness which would cause different response range to the stimulus;

3. The oscillator is nonlinear with varying levels of nonlinearity. The nonlinearity alters the oscillating frequency and harmonic structure;

4. The circadian rhythms may be caused by one oscillator coupled to other oscillators. The models should reflect these connections.

These common features should be included in our model. However, we place our main emphasis on building a model to approach the real experimental circadian data in both time and frequency domains. The frequency analysis will help more precisely to reveal the nature of the system, and it should be consistent with the model.

In this chapter we will introduce several mathematical models we studied and then discuss the simulation results in detail. Our development and analysis of a single Van der Pol oscillator model and modified Van der Pol oscillator model for circadian rhythms will be first introduced. The latter helps us to explore the possibility of expanding harmonic structure of the model. Then we will go to the area of

coupled oscillator models. This type of model gives more freedom to approach the real physiological phenomena of circadian rhythms. Our simulation and analysis results of two existing models will be discussed. Then the detailed analysis of our two dimensional Van der Pol coupled oscillator models will be presented. Models with different types of nonlinearity and coupling will be explored. The analytic results include both time and frequency domains.

4.2 Application of Computer Simulation Program

After the mathematical model is established, computer simulation is employed to obtain the solutions. In the years before the development and wide acceptance of the digital computer, solutions for system simulations and differential equations were commonly programmed on the analog computer. The problem with the analog computer was the necessity for the user to give careful consideration to both magnitude and time scaling of the problem variables. Complex operations usually required special purpose hardware and complicated panel wiring. In digital computers, high level computer languages such as C, FORTRAN, BASIC have provided users with a convenient method for system simulation and in the solution of nontrivial mathematical equations. In many cases, specialized computer programs have been developed that are directly tailored to a particular class of problems. A notable example is in the area of modeling physical systems. Several software packages are available in this area. The numerical solution in these programs is usually computed by the iteration method. By substituting the given initial values into the equation, the program will readily solve the differential equation whether it is a linear or nonlinear equation. But if the error of the obtained solution ex-

ceeds the threshold, the differential equation will be solved again by reducing the computing time interval. The requirements for a simulation package generally are the following:

1. Simplified program statements;
2. The flexibility of program structure, i.e., no special restriction on parameters such as the order of the equations to be solved;
3. As most of the differential equations are solved by integration, the selection of integration method is important. There are several integration methods for discrete numerical calculation. Not all the methods are appropriate for different differential equations.
4. The speed of the program. This requirement is not only related to the hardware, but also related to the language, algorithm, the library of subroutines and functions included.

Several simulation packages for the IBM PC were tried in this research. They are DMSP [17], CSMP [38] and mathCAD [1]. DMSP is written in the BASIC language. It is easy to write the statements and run the program. DMSP is slow since it is written in an interpreter language. CSMP includes all the functions of DMSP, but CSMP has more functions and graphics capability, and since CSMP is written in FORTRAN, it is also much faster. MathCAD is a powerful package for solving general mathematical problems. The problem is that its integration routine is very slow, and therefore it is not suitable for simulation purposes.

4.3 CSMP Computer Simulation Program and the Effects of Integration Methods

The computer simulation work in this research is done by CSMP, (Continuous System Modeling Program adapted for the IBM PC and compatibles). CSMP is a scientific simulation program package, in which the mathematical model can be easily programmed. CSMP offers sophisticated solution possibility and flexible output forms. The output forms of CSMP which we used to analyze the simulation results include:

1. Waveform graphic output.
2. Data file numerical output.
3. Data file output with different parameters.

We will now discuss the integration methods used in the program, which is the most often used procedure and normally a pivotal point for solving nonlinear differential equations. There are five fixed step and two variable step integration methods available in CSMP. No strict rule is used to select the integration method but there are several factors which have to be considered, and the experience of simulating practical models will be helpful in choosing the proper integration method. Table 4.1 shows the summary of five fixed step methods available in CSMP.

Two variable step methods in CSMP are the variable step *Runge-Kutta* method (CSMP named RKS) and the fifth-order, predictor-corrector, *Milne* method (CSMP named MLINE). RKS is the method automatically used in the CSMP. MLINE is

Summary of Fixed-Step Integration Methods

CSMP Name	*Method*
RKSFX	Fourth-order Runge-Kutta with fixed interval
SIMP	Simpson's Rule integration
TRAPZ	Trapezoidal integration
ADAMS	Adams-Second Order
RECT	Rectangular integration

Table 4.1: *Summary of fixed step integration methods.*

similar to the RKS integration technique in that it uses rather sophisticated numerical algorithms and adjusts the step-size to meet the changing conditions. In the variable step methods, it is not necessary to specify the integration step size. The absolute value of the estimated integration error (ABSERR) and the relative magnitude of the estimated error(RELERR) are compared with user-specified error bounds and step size is adjusted accordingly.

For certain types of problems, fixed-step integration methods must be employed. In some types of problems where sudden changes or discontinuity occur, e.g., an impulse passes the system, the variable-step methods may demand an integration step which is smaller than the minimum allowed. If this occurs the run is terminated at that point. The user then has to increase the error requirement and decrease the integration interval or, use one of the fixed-step methods. If the output interval is very small, the maximum step size is constrained by the output and there is no need to use a sophisticated, time-consuming integration technique. A simple fixed-step method may be used.

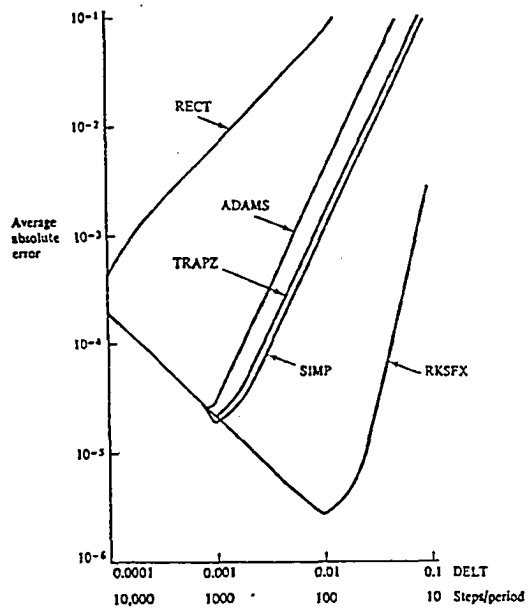

Figure 4.1: *Comparison of 5 integration methods in CSMP: average absolute error as a function of step size and integration method. The step-size ranged from 10 to 10,000 integration steps per cycle of the cosine function (cosine function is the solution of this linear differential equation).*

Fig 4.1 shows a comparison of five different fixed-step size integration methods used in solving a linear differential equation. The results shown in fig.4.1 are only intended to show the relative accuracy of the various methods as a function of step size. The curves also illustrate that a small integration interval does not necessarily give the greatest accuracy. If the frequency content of the solution can be estimated, Fig.4.1 can be helpful in estimating the appropriate step-size. As previously mentioned, the various integration methods are greatly different in complexity and consequently require different amounts of computing time.

The other fact that should be considered in selecting the integration method is that in many problems the most time-consuming portion of the simulation is not the numerical integration, but the calculation required at each integration

Integration Method	*Number of Times that all Statements in the Dynamic Segment are Executed for Each Integration Step*
RKSFX & RKS	4
SIMP	3
MILNE	2
TRAPZ	2
ADAMS	1
RECT	1

Table 4.2: *Execution times of each integration step for 7 different integration methods.*

step. The number of times that all statements in the Dynamic segment are executed for each integration step depends upon the method. Table 4.2 contains this information for all seven methods. If the problem requires a large number of calculations for each integration step, a savings in computer time may result if a smaller step–size is used in conjunction with a less sophisticated integration method.

We simulated all of our models of circadian rhythms using CSMP. The main rule to select an integration method in our simulation, as mentioned above, is the optimum choice of **obtaining sufficient accuracy and without using excessive computing time.** Therefore the simulation was usually started by using a variable step method. If the integration was not successful, then either the error bound was reduced or a fixed step method was employed. For example, in simulating the stopping of an oscillator, due to the sudden change of the time series, the fixed step method SIMP was used to get accurate results.

4.4 Computer Simulation of Van der Pol Type Model: Comparison of Simulation Results and Analytic Results

There are extensive analyses of the Van der Pol oscillator in the mathematical literature.[42] This type of oscillator has several advantages when used as a circadian rhythm model:

1. The solution of the Van der Pol oscillator is capable of describing features of self sustaining oscillation which corresponds to the endogenous characteristics of the circadian temperature or activity cycle;
2. The nonlinearity of the oscillator can be adjusted to reflect the nonlinearity of the circadian system;
3. The harmonic structure of the spectrum of the Van der Pol oscillator is similar to that of the circadian data.

The Van der Pol oscillator was introduced into several circadian rhythm models. However, the emphasis in our research was to explore:

1. the effects of the nonlinear portions of the system which include the effects of nonlinearity on the behavior of the system time series;
2. the relations between nonlinearity and the spectrum;
3. the selection of the non-linear parameter in the circadian rhythm model.
4. the effect of various parameters on the model's behavior in both the time and frequency domains.

5. the difference and limitation of using single and multi-dimensional Van der Pol type oscillators to describe the circadian rhythms and the possibility of using a modified type.

In this chapter, we will introduce several different circadian rhythm models based on the Van der Pol oscillator. The Van der Pol type oscillator is a simple representation of nonlinear oscillation which has an amplitude as well as a phase descriptor. We use a normalized parameter to simplify the basic Van der Pol oscillator equation as follows:

$$k^2\frac{d^2x}{dt^2} + \mu k(x^2 - 1)\frac{dx}{dt} + \omega^2 x = 0 \tag{4.1}$$

where k is a fixed time parameter, which is used to normalize the characteristic frequency of the system. k is selected such that, for $\omega = 1$ the system has a period of 24 hours,

$$k = \frac{24}{2\pi} \tag{4.2}$$

ω_x is the normalized frequency,

$$\omega_x = 24/T_x \tag{4.3}$$

For $T = 24hr$, $\omega_x = 1$, whereas for $T_x = 12.5hr$ (for example), $\omega_x = 24/12.5 = 1.92$.

μ is a parameter which represents the non-linearity of the system. If μ equals zero, the system becomes a linear system. The larger the value of μ, the stronger the nonlinearity.

The analysis of our experimentally acquired circadian rhythm data (as we discussed in chapter 2) and the comparison with the model data (as we shall discuss in the following chapters) suggests that a large value of μ should be used in the circadian model to approach the real circadian rhythm structure. Therefore the techniques for solving the Van der Pol type model with large μ should be considered.

The analytic solution of Van der Pol type oscillators, as we discussed in the previous sections, can be used to explore the complete behavior of the Van der Pol type equation but, as we will see here, this solution is restricted to small values of μ.

Computer simulation was used to obtain the numerical solution. Equation 4.1 was rewritten as the system

$$\frac{dx}{dt} = y \tag{4.4}$$

$$\frac{dy}{dt} = \frac{\mu}{k}(1-x^2)y - \frac{\omega^2}{k^2}x \tag{4.5}$$

Using the integration tools in the CSMP computer simulation package, Eq.4.4 and 4.5 can be solved for y and x. In general cases, if the nonlinear parameter μ is not too large (less than 10), Eq.4.4 and 4.5 can be solved by using a *variable step* integration method. The advantage of this method is that it saves simulation time and it is easy to obtain relatively accurate results. Fig.4.2 shows the plots of the time series obtained from the simulation with different μ. These plots give us the following information about the characteristics of Van der Pol type model in the time domain:

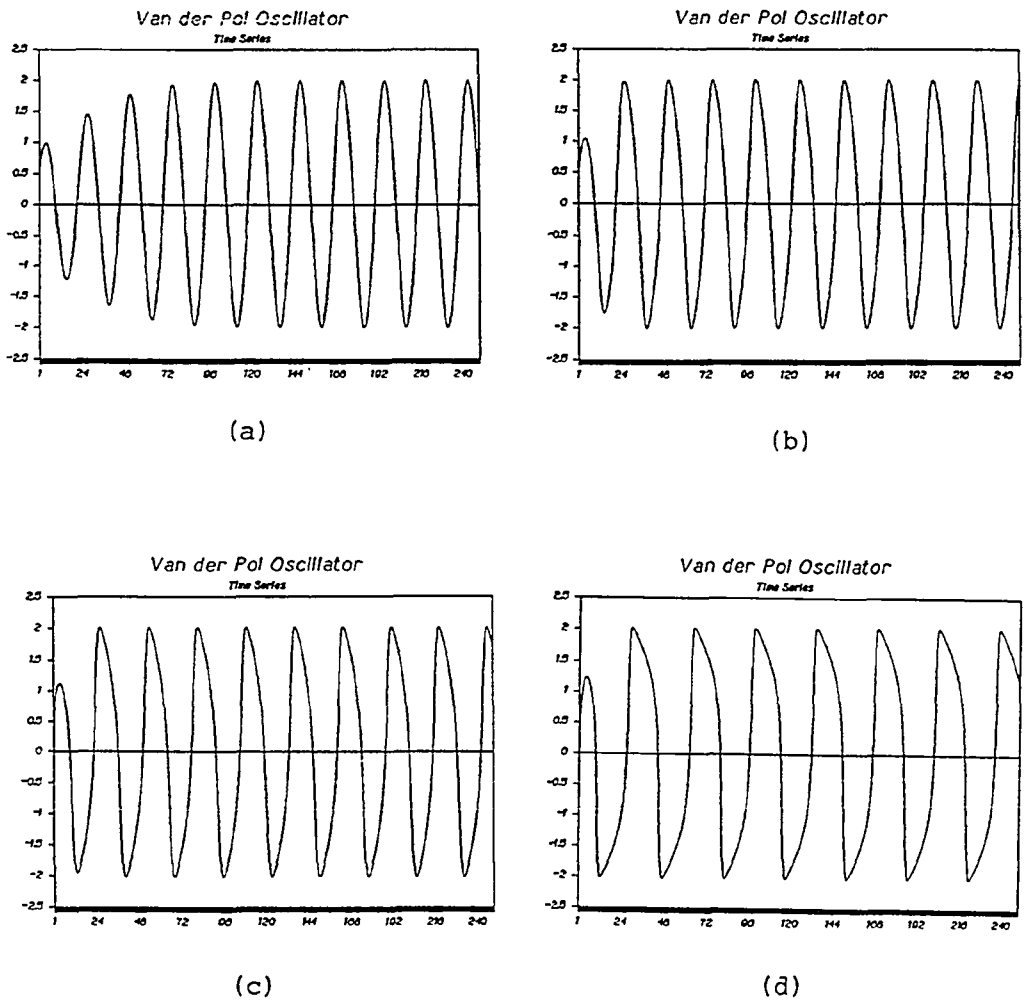

Figure 4.2: *Time series of Van der Pol oscillator model with different μs. (a) μ=0.2. (b) μ=0.8. (c) μ=1.6 (d)μ=3.2.*

1. The output waveforms of Van der Pol oscillators with small μ are cosine-like waveforms.

2. The waveforms are distorted from cosine-like waveforms as μ increases.

3. The zero-crossing detection results show that the period of the oscillation is very close to the period parameter we defined in Eq.4.3 ($\omega_x = 24/T_x$) when there exists a small μ in the system.

4. The period becomes longer as μ increases, which differs from the defined period in the equation.

The time series data were then transformed to the frequency domain using the FFT. Details about the FFT will be introduced in chapter 6. FFT results give us additional details of the Van der Pol oscillator model. Fig.4.3 shows the amplitude spectrum of the model corresponding to the same values of μ represented in fig 4.2. The spectral function also gives us the amplitude information of each frequency component which can be used to compare the computer simulation and analytic results.

The analysis of the spectral function yields the following results:

1. The spectra of Van der Pol oscillators consist of only the fundamental and odd harmonic frequency components.

   This is consistent with the result from the analytic solution which we obtained in the previous section using the *perturbation method*. The analytic solution of the Van der Pol type model is repeated in Eq.4.6. We can see from Eq.4.6 that only the ω, 3ω, 5ω, 7ω, $\cdots$ frequency components are included.

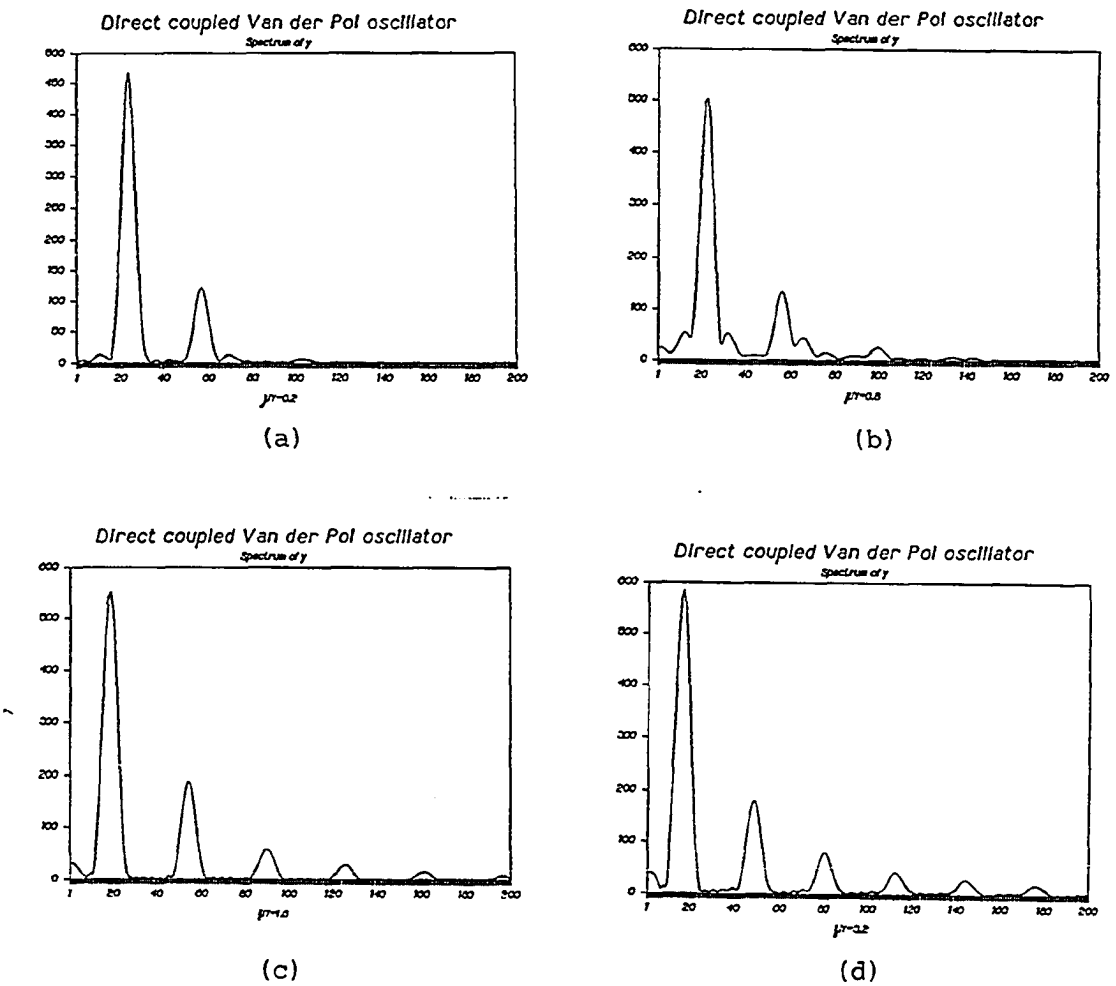

Figure 4.3: *Spectral function of Van der Pol oscillator model with different μs. (a) μ=0.2. (b) μ=0.8. (c) μ=1.6 (d) μ=3.2.*

$$x = (2 - \frac{1}{8}\mu^2)cos\omega t + frac34\mu sin\omega t + \frac{3}{16}\mu^2 cos3\omega t - \frac{1}{4}\mu sin3\omega t - \frac{5}{96}\mu^2 cos5\omega t + \cdots \quad (4.6)$$

2. The main frequency components (including the fundamental, third and fifth harmonics) were extracted from the spectral function of the computer simulation results using our program *Fextract* (see the program in the Appendix). The extracted components were then normalized and compared with the analytic results.

   We will first examine the *frequency* of the fundamental and harmonics in the case of different degree of nonlinearity of the system. The frequencies are decreased (the periods are increased) with the increase of the parameter μ. In our analytic solutions, we have

   $$\omega = \omega_{\mu=0}[1 - \frac{1}{16}\mu^2] \quad (4.7)$$

   This result is consistent with our simulation results, when μ is less than 1.6. But the error becomes larger as μ is increased. Figure 4.4 shows this comparison.

3. The *amplitudes* of the harmonic components become larger with increase of μ. This reveals the essentials of the nonlinearity in the Van der Pol models. Harmonic components in the spectrum correspond to the nonlinearity in the system. Due to the unnormalized magnitude of the power spectrum, the simulation data can only be compared with the analytic solution by the ratio of the amplitude of fundamental with harmonic component. The ratios in both the simulation and analytic results are very close for small μ. The

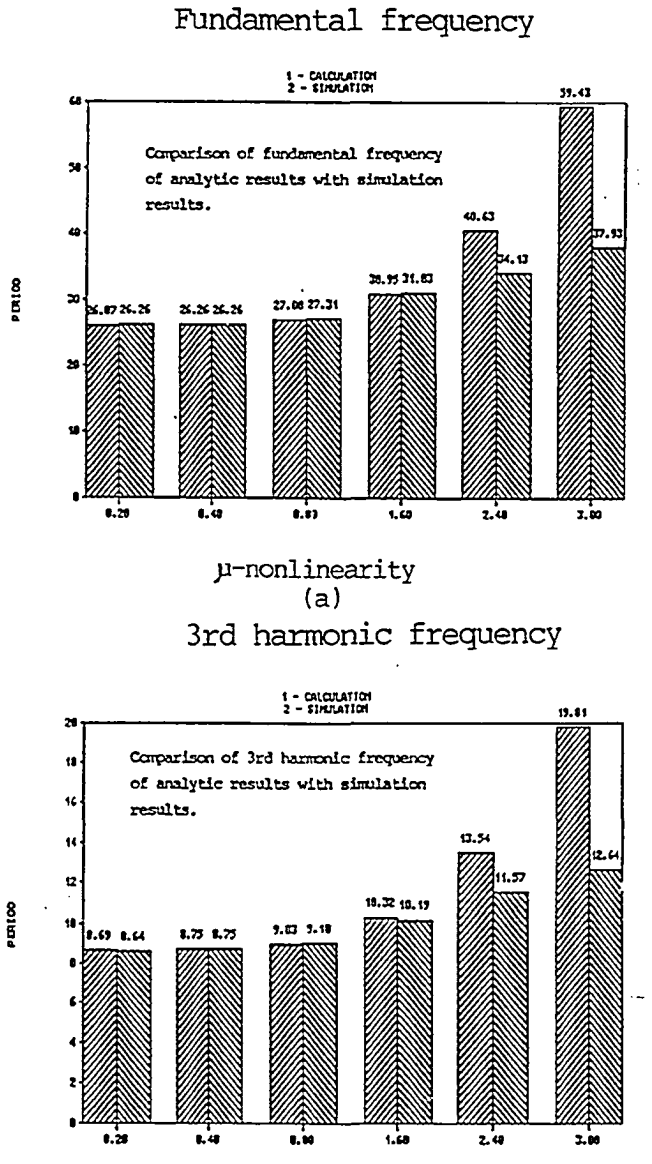

Figure 4.4: *Comparison of simulation results and analytic solution: on frequencies of Van der Pol type model with different nonlinearity. a) On the frequency of fundamental frequency component. b) On the frequency of 3rd frequency component.*

errors become large with the increase of μ. Figure 4.5 shows the amplitude comparison. These results show that the analytic method is not applicable for large μ ($\mu > 1.6$).

The analysis of the basic Van der Pol oscillator model gave us the understanding of the essentials of nonlinear oscillation – its time and frequency characteristics. The comparison of the numerical method and analytic method shows the latter develops larger errors with the increase of nonlinearity.

4.5 Modified Van der Pol Oscillator Model

The single Van der Pol type model in some way reflects the characteristics of real circadian rhythms but there are some major differences in both time and frequency domains. In this section, we will try to modify the single Van der Pol type model to approach the real data structure.

As shown in chapter 2, the frequency spectra of real circadian data consist of "rich" harmonic components. Therefore the time series show bimodal and other complicated waveforms. The one dimensional Van der Pol oscillator model however, shows small levels of harmonics.

To increase the "level" of harmonic terms which are lacking in this model, we modified the Van der Pol oscillator model by adding more nonlinear terms into the equation.

Consider the *Pendulum-type Oscillator* equation:

$$\frac{d^2x}{dt^2} + \mu\frac{dx}{dt} + Asinx = 0 \tag{4.8}$$

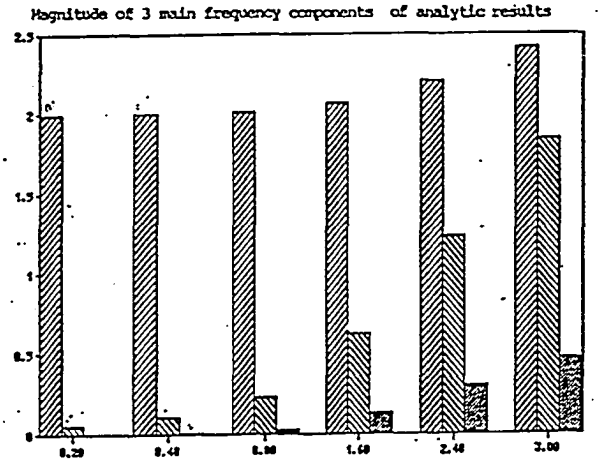

(a)

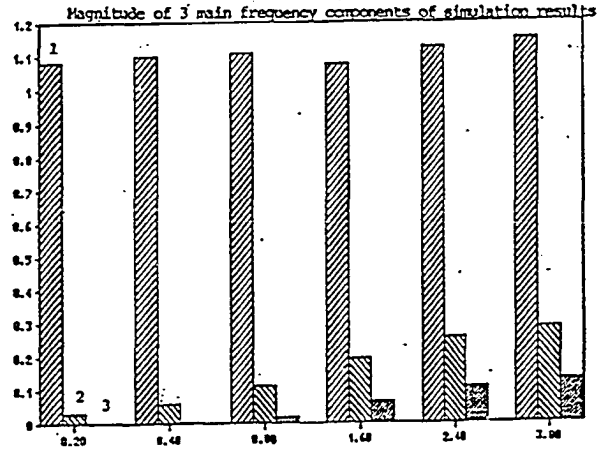

(b)

Figure 4.5: *Comparison of simulation results and analytic results: on amplitudes of Van der Pol type model with different nonlinearity. a) The amplitude of three main frequency components of analytic solution. b) The amplitude of three main frequency components of computer simulation results.*

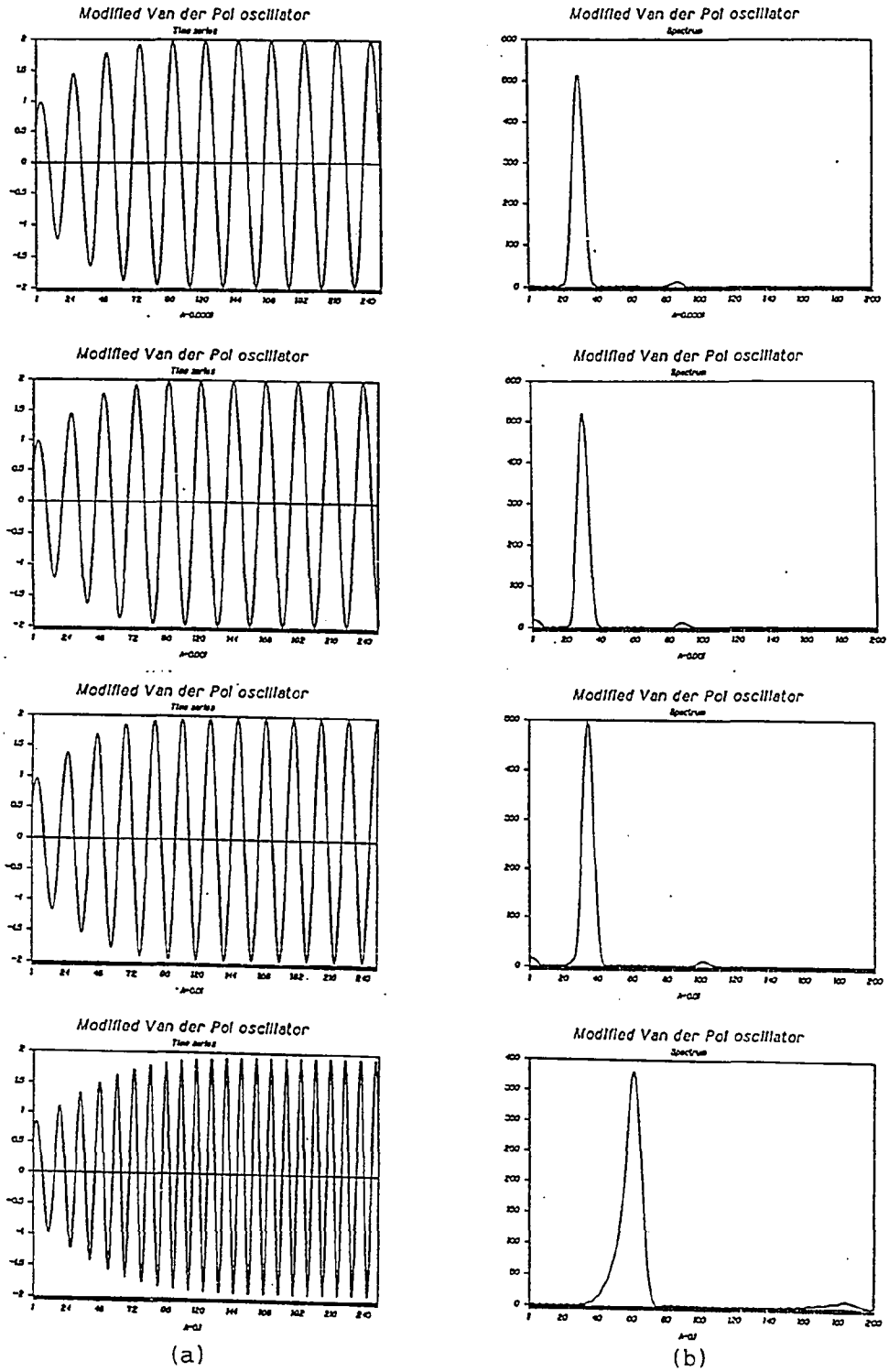

Figure 4.6: *Simulation results of modified Van der Pol oscillator with* $A = 0.0001, 0.001, 0.01$ *and* $0.1, (\mu = 0.02)$. *a) Time series. b) spectral function.*

Using Taylor series to expand the $Asinx$ term, taking only the first two terms of the expanded series, and substituting them into the Van der Pol oscillator model, we obtain what we call the *" modified Van der Pol oscillator model"*. The system equation now becomes

$$\frac{d^2x}{dt^2} + \frac{\mu}{k}(x^2 - 1)\frac{dx}{dt} + \frac{\omega^2}{k^2}x + Ax^3 = 0 \tag{4.9}$$

In Eq.4.9, A is the amplitude coefficient of the x^3 term; all the other parameters are the same as defined in the previous chapter.

To test the influence of the x^3 term in the model, we simulated this model by first selecting different values of A . Figure 4.6 shows the time series and spectra of the model ($\mu = 0.02$) for $A = 0.0001, 0.001, 0.01$ and 0.1. When A is small, the general structure of the spectrum is basically the same as the single Van der Pol type model. Increasing the level of the x^3 term causes the fundamental period to decrease (frequency to increase) rapidly. Fig.4.7 and fig.4.8 show respectively the frequency and amplitude of the two main (highest peak) frequency components extracted from the spectrum with different levels of the x^3 term. As we can see in Fig.4.7, the fundamental period of the model varies from 26.26 hr to 11.01 hr as A changes from 0.0001 to 0.1. However, the magnitude of the harmonic did not change much with the increase of A as we can see in fig.4.8. Therefore increasing the x^3 term cannot increase the harmonic levels as we expected.

We also tested the effects of interaction between the μ portion and the x^3 term in the system. These two nonlinear terms in the system have opposite effects on the fundamental frequency. As we discussed in the previous chapter, the characteristic frequency of a Van der Pol type oscillator decreases as μ increases. We have found that the frequency increases as A (the x^3 term) increases. In our simulation, the x^3

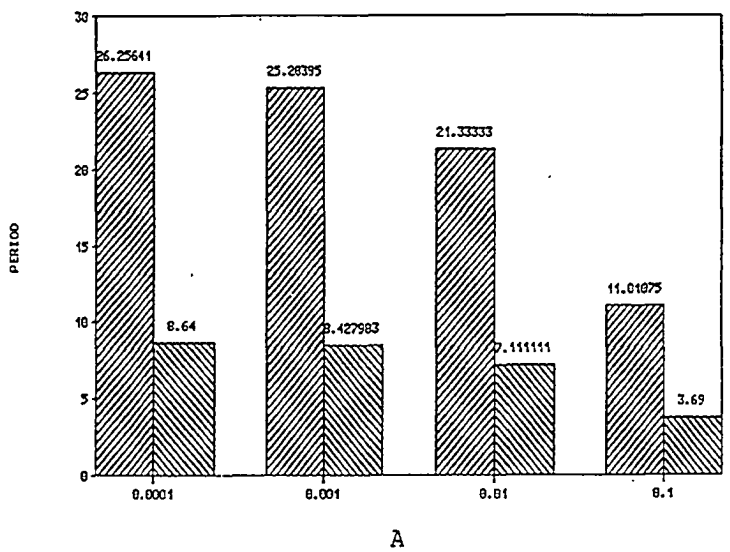

Figure 4.7: *The frequency of two main frequency components in modified Van der Pol oscillator as A changes.*

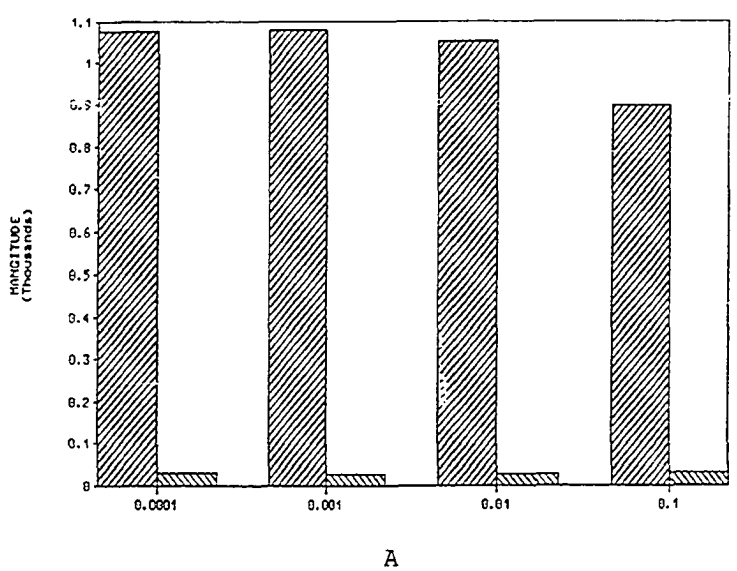

Figure 4.8: *The amplitude of two main frequency components in modified Van der Pol oscillator as A changes.*

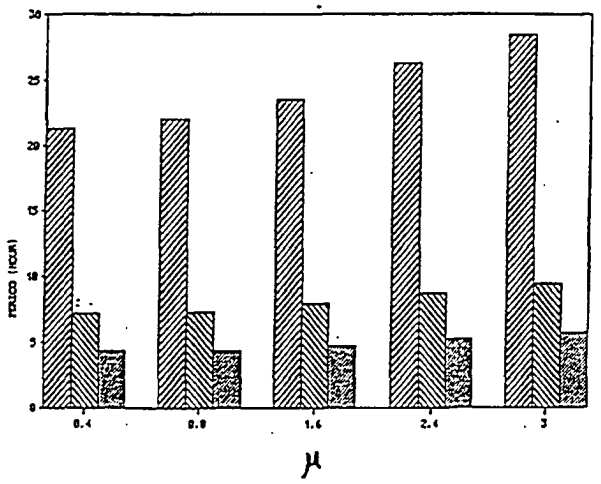

Figure 4.9: *The interaction of two nonlinear items in modified Van der Pol oscillator: the fundamental frequency and the first two harmonics of the system with* $A = 0.01$, $\mu = 0.2$ *to* $\mu = 3.0$.

term was first kept at a relatively small value of $A = 0.01$, which does not strongly affect the fundamental frequency. Then we increased the nonlinear parameter μ. This result is in Fig.4.9. It can be seen that the fundamental period increases as μ increases. Basically, this is very similar to the basic Van der Pol type model. Therefore, in the case of a relatively small x^3 term, A approximately 0.01, the final direction of the characteristic frequency shift is determined mainly by the μ term.

If the coefficient of the x^3 term, A, was maintained at 0.1, then it would strongly affect the fundamental frequency of the system. In this case, as we increased the value of μ to 3.0, the characteristic frequency changed very slightly. Thus the x^3 term dominates the system oscillating frequency. The fundamental period of the system remains at approximately 11 hr, and increases a small amount as $\mu becomes equal to 3.0$. This test result is shown in figure 4.10.

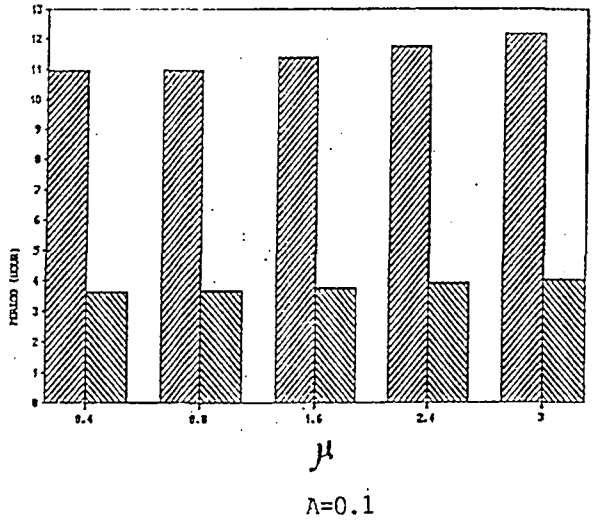

Figure 4.10: *The interaction of two nonlinear items in modified Van der Pol oscillator: the fundamental frequency and the first harmonic of the system with* $A = 0.1$, $\mu = 0.2$ *to* $\mu = 3.0$.

4.6 Simulation and Analysis of Coupled Oscillator Models

The one dimensional oscillator model has the limitations for the approximation of the real data that we discussed in the previous section. Using a coupled oscillator model will give us more degrees of freedom in the modeling. Therefore we have examined and compared several existing coupled oscillator models. These models use either linear or nonlinear mathematical equations to describe circadian rhythms. The study of these models helped us to understand the basic rules of modeling circadian rhythms. We include in our simulation results of two of these models. These are Kronauer's coupled Van der Pol oscillator model and Pavlidis's biological oscillator model.

4.6.1 Kronauer Coupled Oscillator Model

The Van der Pol oscillator model was introduced in section 4.4 for modeling circadian rhythms. A coupled oscillator model of the Van der Pol type equation was developed by Kronauer, et al(1982,1983) [23]. In his model, "x" and "y" refer to two circadian pacemakers. The"y" oscillator governed the timing of sleep and wakefulness and "x" oscillator dominated the temperature rhythm. These two oscillators affected one another by velocity coupling. Therefore the y oscillator is actually a sum of two components: the intrinsic y component and a significant circadian component due to coupling with the x oscillator. The explanation of spontaneous desynchronization was based on a hypothesized spontaneous lengthening of the original y oscillator frequency f_y. As the disparity between the original x oscillator frequency f_x and f_y increased, the x oscillator exerted less and less influence on the output of y. As Kronauer et al. explained, there was a dramatic change in the *timing* of sleep when desynchronization occurred, yet there was only a very small change in the y waveform. This was the crucial lesson learned from the model. In mathematical terms the distinction between phase trapping and desynchronization is that in phase-trapping the "x component of y" is larger than the "intrinsic component of y", while in desynchronization it is the intrinsic component which is larger. In other words, desynchrony is viewed by Kronauer et al. as a beat phenomenon, based on the summation of two waveforms to generate an admixture.

We simulated this model of the human circadian system with two interacting oscillators where,

x = Body temperature.

y = Rest–activity, sleep–wake cycle.

The x and y oscillator are coupled to each other through the derivative. In the solution,

$x < 0$ corresponds to the temperature below average temperature.

$y < 0$ corresponds to sleep.

The mathematical equations of this model are as follows:

$$k_y^2 \frac{d^2y}{dt^2} + \mu_y k(y^2 - 1)\frac{dy}{dt} + \omega_y^2 y + F_{xy}\frac{dx}{dt} = F_{zy}z(t) \tag{4.10}$$

$$k_x^2 \frac{d^2x}{dt^2} + \mu_x k(x^2 - 1)\frac{dx}{dt} + \omega_x^2 x + F_{yx}\frac{dy}{dt} = F_{zx}z(t) \tag{4.11}$$

here,

$k = \frac{24}{2\pi}$, which is the normalized time constant as we defined in the single Van der Pol type model;

μ_x is the nonlinear parameter of the x oscillator. In practice, it also represents the stiffness for the phase adjustment. In this model, $\mu_x = 0.1$.

μ_y is the nonlinear parameter of the y oscillator. μ_y was designed to characterize the transient property of the y oscillator.

The coupling coefficient, F_{yx} is the coupling from y to x and F_{xy} is the coupling from x to y. These two coupling coefficients are not necessarily equal. The ratio in this model $R = F_{xy}/F_{yx}$, was selected as 4; $F_{yx} = -0.04$ and $F_{xy} = -0.16$, which shows that the y oscillator had less influence on the x oscillator. In other words, the x oscillator is quite insulated from the y oscillator.

The frequency adopted for the oscillators in this model was normalized fre-

quency, i.e., the angular frequency $\omega = 1$ for the oscillator period is equal to 24 hours. Both oscillators represent different circadian rhythms; therefore ω_x and ω_y were in the range near 1. However, this model was mainly designed to simulate the synchronization and desynchronization process of two circadian rhythms. Therefore the natural frequencies of the two oscillators were selected as follows:

$\omega_x = 0.99$,

$\omega_y = 0.92$ for day 1–5. (The external stimuli were acting on the system in day 1–5.). Then ω_y decreases linearly from 0.92 to 0.78 between day 5 and day 100.

$\omega_x - \omega_y$, the frequency difference, often termed "detuning" between 2 oscillators, determined the absolute strength of the coupling at which the desynchronized stage "NS" occurs.

The "zeitgeber" $z(t)$ is the external stimulus acting on the "y" oscillator which simulates the light stimulus applied to the subject. The angular frequency of the stimulus is $\omega_z = 1$ (the period is 24 hour). A sinusoid is the simplest form of periodic stimulus. Due to the low internal stiffness of each oscillator, the oscillator responds strongly to a stimulus near the intrinsic period and much less to other periods (i.e, they are resonant). In this model, the zeitgeber was applied to the y oscillator from day 1 to 5 only. The effect of the zeitgeber drive on the two oscillators, F_{zx} and F_{zy}, is quite different. F_{zx} is taken to be zero and F_{zy} is made sufficiently strong (here $F_{zy} = 1$) to entrain the y oscillator to a 24hr period. The x oscillator was affected through the coupling. Therefore the y oscillator was driving the x oscillator. After day 5, since the natural frequency of oscillator y decreased, it finally caused the desynchronzation. Fig.4.11 to 4.13 show the simulation results. Fig.4.11 (a) shows the designed stimulus $z(t)$ and (b) shows

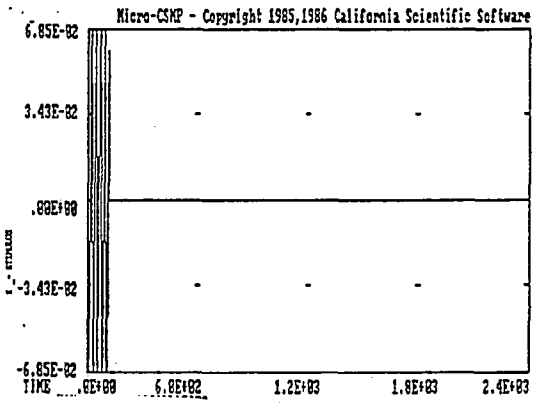

time (hours)

(a)

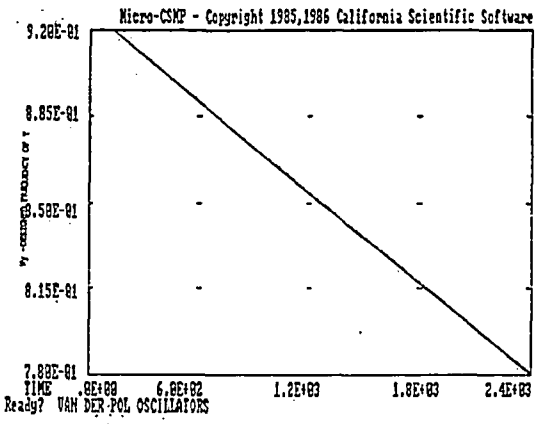

time(hours)

(b)

Figure 4.11: *(a) Stimulus $z(t)$ in the model. (b)Designed characteristic frequency ω_y.*

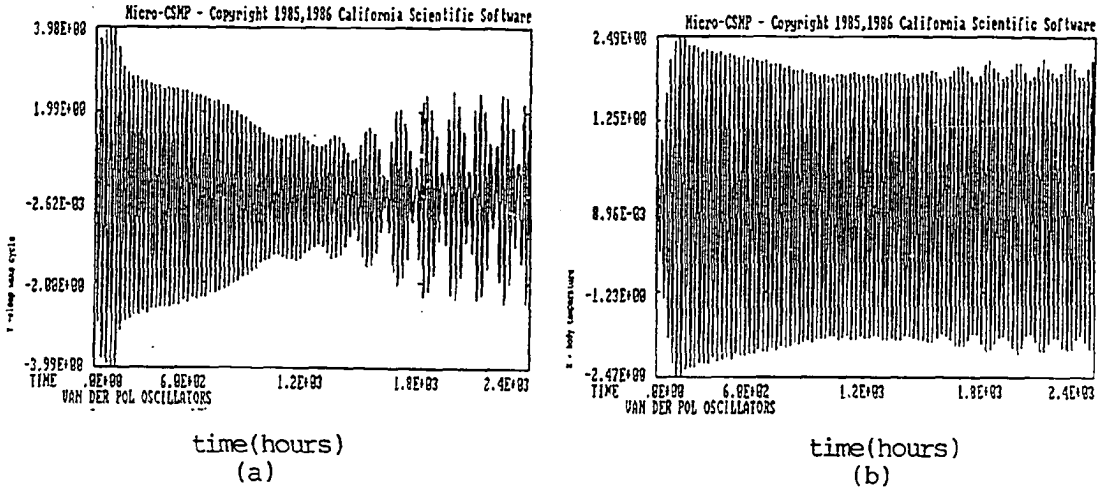

Figure 4.12: *Time series of (a) y oscillator. (b) x oscillator.*

the characteristic frequency ω_y. $z(t)$ was applied to the system for only 5 days and ω_y linearly decreased after day 5. These are two important facts causing the system desynchronization.

Fig.4.12 shows the time series of the x and y oscillations. The time series are recorded for 100 days while the zeitgeber is applied only during the first 5 days. Fig.4.13 shows the oscillation period of the x and y rhythms measured by the zero crossing detection method which shows the desychronization of these two circadian oscillators and which is the main feature of this model. The results of fig.4.13 show that in day 1 to 5 the system was synchronized by the zeitgeber. From day 5 to day 40, the two oscillators were almost synchronized which was the stage the author called the S stage. There were some significant quasirhythmic shifts of phase between the two oscillators starting from day 40. The author proposed the description "phase trapping" for this stage (P stage). After day 75 the two oscillators became totally desynchronized which was called the "NS" stage.

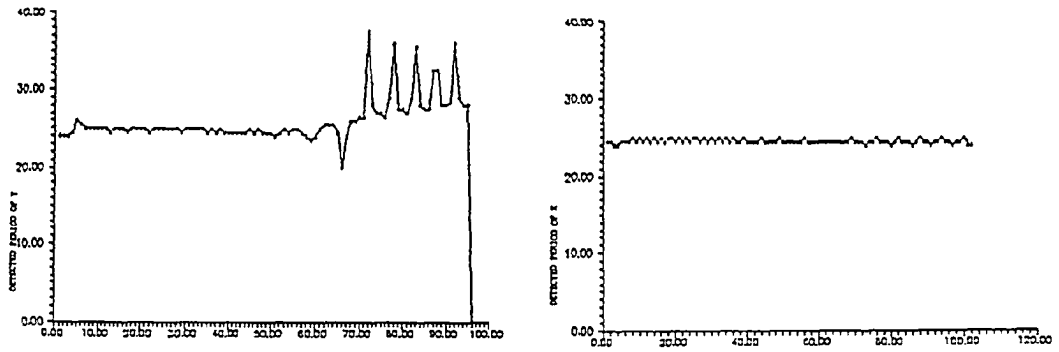

Figure 4.13: *(a) Detected period of the y oscillator. (b) Detected period of the x oscillator.*

The significance of this model is that it reveals the internal relations of desychronization. From the model described before we can see that three facts caused this deschronization:

1. The characteristic frequency of the y oscillator was designed to reduce linearly after day 5 in the model. As the frequency difference of the x and y oscillators became significantly large, they lose synchronization. Comparing fig.4.11 (b) with Fig.4.13 (a) we can see the deschronization started to occur at $\omega_y = 0.84$.

2. The nonlinearity of the y oscillator in the model decreased with the time, $\mu_y = 1/(2\pi D)$. Therefore the y oscillator stuck more strongly to its characteristic frequency as the time increases.

3. The external stimulus which synchronized the two oscillators was applied to the y oscillator only from day 1 to day 5.

4.6.2 Pavlidis's Biological Oscillator Model.

Pavlidis presented a biological oscillator model in 1973.[29, pages 102 - 107] The oscillator in his model has one degree of freedom described by the following (generic) pair of nonlinear differential equations.

$$dr/dt = f(r,s) \tag{4.12}$$

$$ds/dt = g(r,s) \tag{4.13}$$

where r and s are the two state variables and f and g are to be chosen so that the system of Eq.4.12 and Eq.4.13 exhibits a limit cycle. For a physical system it is reasonable to assume that the ranges of values taken by r and s are not unbounded , but between certain limits. The purpose here is to build a model having a phase response curve (PRC) similar to the real circadian system. We will discuss in more detail in chapter 5 the PRC which represents the system phase response characteristics with an external stimulus acting on it. Fig.4.14 is an experimental phase response curve, which shows that the circadian system has different phase shifts verse the phase of the stimulus applied. The phase may be advanced, delayed, or not changed. This model attempts to reflect these characteristics.

We simulated this model. The system equations of the model are the following:

$$dr/dt = r - cs - ds^2 + b - x, r \geq 0 \tag{4.14}$$

$$ds/dt = r - as \tag{4.15}$$

where r and s are two state variables and the system is designed to have a limit cycle. r is set to ≥ 0 which presents some important features. First, it causes r to be saturated at zero for part of cycle which corresponds to the PRC zone where

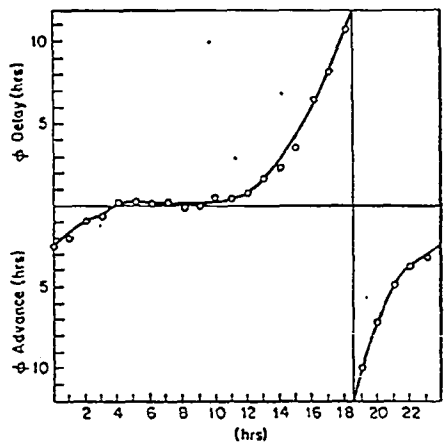

Figure 4.14: *Phase response curve of a circadian system.*

the phase response is near zero. (Circadian time 4–12 hour in fig.4.14). The phase response of the circadian system to the stimulus in other zones illustrates different effects. Also, the limit cycle includes a *segment of the axis* $r = 0$ as part of its trajectory. The system is designed in such a way so that the critical point is an unstable focus.[29, pages 103 – 107] All trajectories passing through the critical point eventually intersect the axis $r = 0$. Figure 4.15 shows the trajectories of the system.

The constants c and a determine the systems linear characteristics while d determine the systems nonlinear characteristics. b is a constant bias and x represents the stimuli. These parameters were tested in the simulation of this model. Following are some results.

a)Effects of b on a piecewise linear system.

(Note that d, the nonlinear parameter of the model was set to be zero which

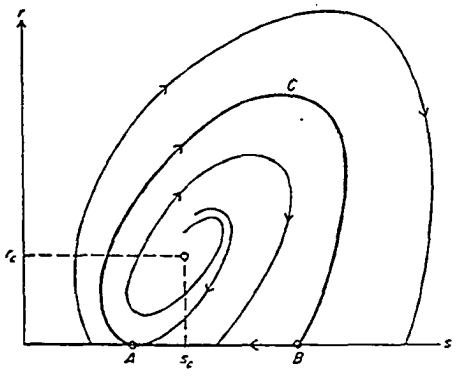

Figure 4.15: *Phase plane plot of trajectories of the biological oscillator model.*

made the system be a piecewise linear system.) For $a = 0.5$, $c = 0.6$, $d = 0$, $x = 0$, b, the constant bias on the system, was varied between 0.5 and 4.0. It was found that the oscillation period remained unchanged, which showed that the constant bias on the linear ($d = 0$) system will not change the oscillation period.

b)Effects of c on a piecewise linear system.

Again, the nonlinear parameter d was kept at zero. For $a = 0.5$, $b = 0.5$, $d = 0$, $x = 0$; c was varied from 0.6 to 0.8. It was found that c mainly determined the system period. The system period was reduced when c increased.

c)Effects of nonlinear portion.

Changing d, the parameter of the nonlinearity in the system equation, caused a change of amplitude and frequency of oscillation. In particular, b, the constant bias, had effects on the system period when d was not equal to 0. Table 4.3 shows this simulation result.

PERIODS OF OSCILLATION FOR VARIOUS VALUES OF b AND d

d	$b = 0.5$	$b = 4.0$	Ratio of periods
0.00	16.80	16.80	1.000
0.01	13.85	10.00	1.385
0.10	9.57	5.95	1.610
0.50	6.70	3.95	1.695

Table 4.3: *The period of biological oscillator model with different d and b.*

d)Effects of different initial conditions. Using the same parameters but with different initial conditions, we could set the starting point either inside or outside of the limit cycle. In both cases it finally approached the limit cycle. The modeled system is stable.

e)Effects of some specially designed stimuli on the system. There exists a value of the light intensity I' which, if applied for time interval T' at a point of the limit cycle C', will bring the state at or close to the singularity. The oscillation will then be completely damped out after the application of such an input. This issue will be further discussed in chapter 7.

4.7 Our Two Dimensional Coupled Van der Pol Oscillator Model: Simulation and Analysis

The simulation of the one dimensional nonlinear oscillator model gave us an understanding of the essentials of simple nonlinear oscillation. Due to the insufficiency of these one dimensional models, it seems that two or more interacting oscillators are needed to model the circadian rhythms for the following reasons:

1. The complicated time waveforms of the nonlinear circadian system suggest the possibility of the existence of two or more oscillators. For example, many circadian rhythms exhibit two peaks, i.e, "bimodality". These bimodal peaks with the secondary peak moving progressively through the main peak, and the low frequency trend, which causes very long period fluctuations, give evidence of the existing multi-oscillators in a circadian rhythm. Circadian activity rhythms in rats, hamsters, birds, and many other animals exhibit two prominent peaks, with one peak at the beginning of activity followed by a second peak late in activity. In human sleep-wake cycles, in addition to their nightly sleep, people have a second daily episode where sleepiness peaks in the early afternoon. Careful research has shown that this second dip in arousal is not due to a large lunch. Instead, both the nightly and the afternoon dips in arousal correspond to dips in body temperature. This bimodal substructure of our daily arousal and activities has practical everyday effects in areas such as performance and accident rates.[11] Fig.4.16 shows the statistics of the accidents from 6052 samples during a 24 hour interval. It shows two peaks of such accidents during a day, shortly after midnight and again shortly after noon.

   To examine the bimodal substructure of our biological data further, we attempted to develop a model of circadian temperature rhythms that would also account for the bimodal behavior temperature. In the one dimensional model simulation, we tried to enhance this phenomenon by changing the parameters or modifying the model as we did in section 4.5, but it was not successful. Therefore a two dimensional oscillator model should be developed. The bimodal pattern can be modeled by two coupled oscillators with a period ratio near 2:1. It should be emphasized that two oscillators in the

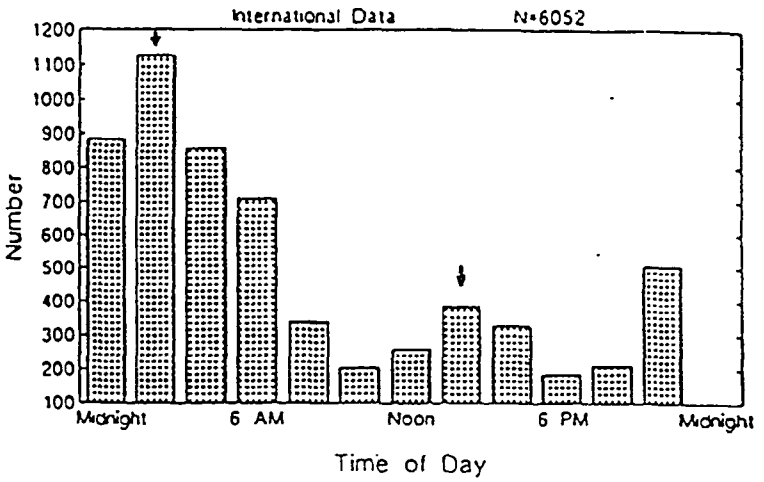

Figure 4.16: *The statistics of car accidents from 6052 samples.*

coupled oscillator model serve for one circadian rhythm with bimodality as shown in Fig.4.17.

2. The spectral analysis of the experimental circadian temperature and activity data showed that major frequency components of these data include fundamental, 2nd, 3rd and higher harmonics which are not in phase. The spectrum of the one dimensional Van der Pol type oscillator illustrates that this type of oscillator consists of only a fundamental and odd harmonics. Therefore the 2nd harmonic frequency can not be generated by a single Van der Pol oscillator model. From the viewpoint of spectral analysis, the coupled oscillator model is needed to account for the 2nd harmonic frequency component.

3. Different coupling modes and coupling intensities between the coupled oscillators may cause different spectral and time series structure. Therefore coupled oscillators give more degrees of freedom in the models.

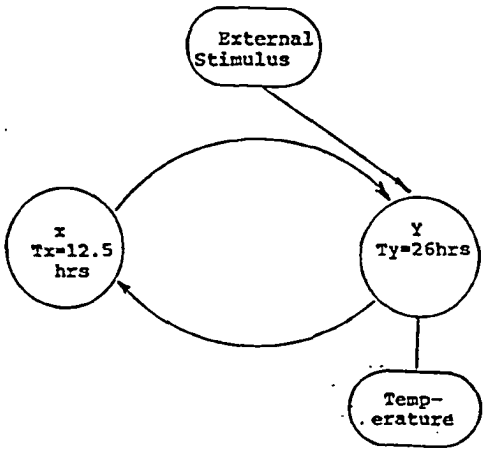

Figure 4.17: *Our coupled oscillator model: two oscillators serve for one circadian rhythm.*

It is difficult to obtain an analytic solution for coupled nonlinear oscillators. Therefore all the analysis presented here on coupled oscillators is based on results from numerical solution obtained from computer simulation.

Three different linear coupling methods were used to explore the coupling effects:

1. Direct coupling;
2. Derivative coupling;
3. Combination coupling.

"Linear" here means that the coupling terms are determined by the first power of x or y (method 1), or of their time derivatives, dx/dt and dy/dt (method 2), or both (method 3). Linear coupling has the property that no frequency components

are introduced into one oscillator from the other which are not already present in that other oscillator. These three coupling methods were simulated based on our two dimensional Van der Pol oscillator models.

4.7.1 Direct Coupling System

The direct coupling model use two oscillators which are coupled to each other directly through their output. This type of coupling has strong coupling effects between two oscillators. The direct coupling system was applied to a two dimensional Van der Pol oscillator model. As we mentioned before, to represent the bimodality of circadian rhythms, the characteristic frequencies of two coupled oscillators were selected as the fundamental and the second harmonic frequency in all of our two dimensional coupled oscillator models. The interacting coupling of these two oscillators was caused by direct coupling, i.e., position coupling. We defined the oscillator with the system fundamental frequency as the y oscillator and the one with the system second harmonic frequency as the x oscillator. The coupling of the y oscillator directly from the x oscillator is denoted by F_{xy} and vise versa. The coupling intensity determined by F_{xy} and F_{yx} between the two oscillators may not necessarily be equal. The selection of the remaining parameters is basically the same as we defined in the first order system. The direct coupling system is described by the following two dimensional nonlinear differential equations:

$$k_y^2\frac{d^2y}{dt^2} + \mu_y k(y^2-1)\frac{dy}{dt} + \omega_y^2 y + F_{xy}x = 0 \tag{4.16}$$

$$k_x^2\frac{d^2x}{dt^2} + \mu_x k(x^2-1)\frac{dx}{dt} + \omega_x^2 x + F_{yx}y = 0 \tag{4.17}$$

To represent the bimodality, the frequency of each oscillator should represent the frequency of a fundamental or 2nd harmonic respectively. When the nonlinearity

in either system is varied, the characteristic frequency in both oscillators of the system may change, which is also the case when the coupling coefficient varies. Therefore the fundamental frequency should be adjusted to meet different μ and F_{xy} (F_{yx}) selection in the system. To do this adjustment, we should first understand the mechanism of the frequency shift.

The effect of nonlinearity in the coupling system could be considered as the weighted sum of both oscillators in the system. For example, the nonlinear influence in the y oscillator should be considered not only from μ_y but also partially from μ_x. Recalling that increasing the strength of the nonlinearity in the single Van der Pol oscillator model caused the decrease of the system fundamental frequency and increase of the amplitude of the 3rd and 5th (and higher) harmonics, we would expect similar but stronger effects in the coupled system.

The simulation model is based on Eq.4.16 and Eq.4.17. The frequency parameters of the system were selected as: $T_y = 26hr$ and $T_x = 12.5hr$. The first trial examined the relations between the system frequency (real detected not defined) and the nonlinearity of both oscillators. Fig.4.18 shows the simulation results of the time series of a two dimensional model with equal coupling coefficients $F_{xy} = F_{yx} = 0.2$, and the nonlinear parameter μ varied from 0.2 to 3.0. Fig.4.19 shows the spectral functions. Comparing the result with the single Van der Pol oscillator model, we can see the second harmonic frequency component is inserted. The results also show that the effect of the nonlinearity on the system fundamental frequency in the coupled system is stronger than in the single system, because this effect is not only from the nonlinearity of one oscillator but also from the coupled oscillator.

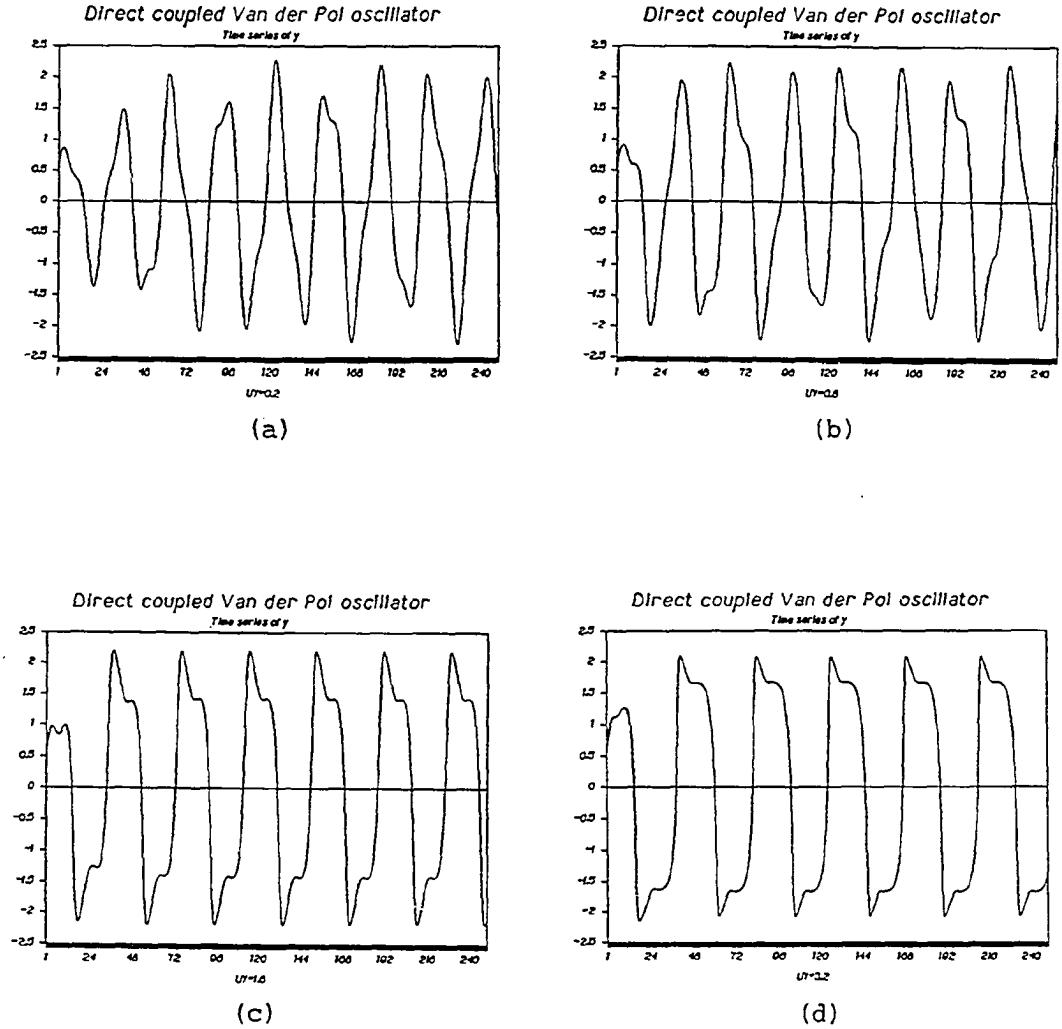

Figure 4.18: *Time series of direct coupling model with different* μ*s.a)* μ*=0.2. b)*μ*=0.8, c)*μ*=1.6, d)*μ*=3.2.*

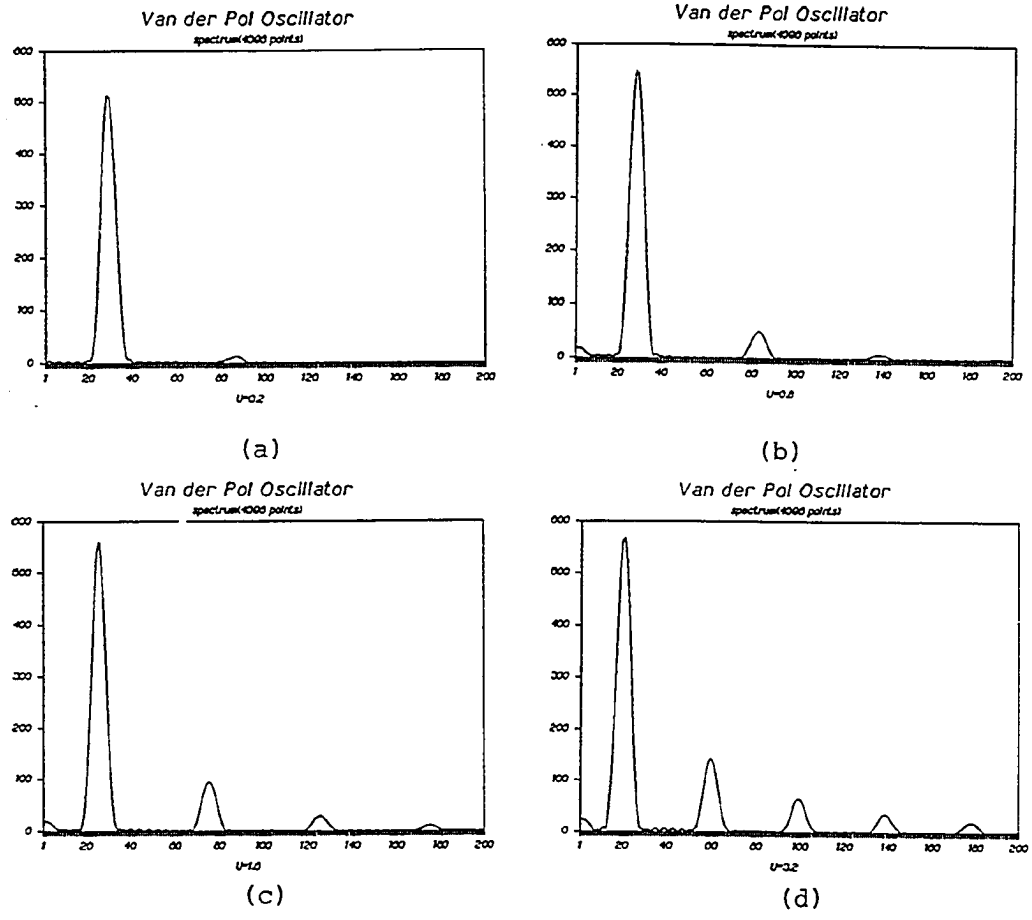

Figure 4.19: *Spectral function of direct coupling model with different μs. a)μ=0.2. b)μ=0.8, c)μ=1.6, d)μ=3.2.*

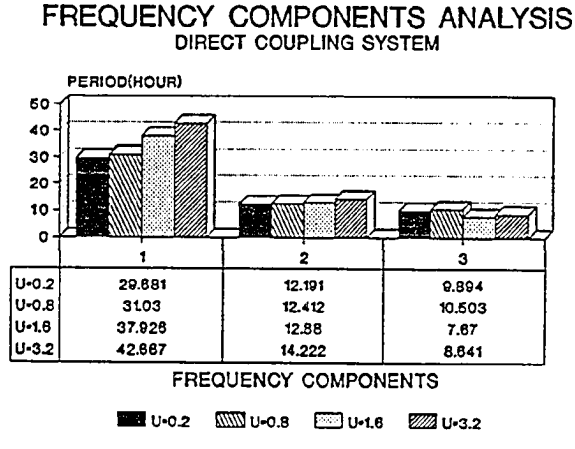

	1	2	3
U=0.2	29.681	12.191	9.894
U=0.8	31.03	12.412	10.503
U=1.6	37.926	12.88	7.67
U=3.2	42.867	14.222	8.641

Figure 4.20: *Main frequency components of direct coupling model with different μs. a) $\mu = 0.2$. b)$\mu = 0.8$, c)$\mu = 1.6$, d)$\mu = 3.2$.*

Fig.4.20 shows the main frequency components extracted from the spectral function. Carefully analyzing the varying trend of fig.4.20, we find there is a frequency transition process caused by μ_y and μ_x. We divide this frequency transition into 2 stages.

Stage one: μ_y and μ_x are in the range from 0.2 to 0.8. The fundamental period of the system varies from 29.68 hr. to 31.03 hr. This period deviates from its defined period (the characteristic frequency of y oscillator, 26 hour) by about 17%. The frequency of coupled oscillator x does not change significantly. The frequency of the 3rd, 5th and higher harmonics in the y oscillator follows the fundamental frequency changes, and the magnitude of the 3rd harmonic increases along with the increase of μ_y and μ_x.

Stage two: μ_y and μ_x are in the range equal to and greater than 1.6. The fundamental frequency of the y oscillator has a jump in this range. In stage one, the fundamental frequency was gradually pulled in the low frequency direction due to the nonlinearity, while this frequency jump is caused by the subharmonic entrainment. As we mentioned earlier, if the frequency of an oscillator is near an integer or sub-integer multiple of the forced oscillator, harmonic or subharmonic entrainment will occur. Here when the y oscillator is pulled near 1/3 of the frequency of the x oscillator, the y oscillator jumped to 1/3 of the frequency of the coupled oscillator x. As we can see in fig.4.20, the row 3 shows $\mu = 1.6$, the period of main frequency component is 37.93 hour which is about three times of that of the second frequency component (12.88 hour). This jump changes the whole structure of the spectral function. The three main frequency components after the jump become the fundamental, 3rd harmonic and 5th harmonic. The second harmonic inserted by the x oscillator no longer exists. The deviation of the real

frequency of oscillator y from its frequency defined in ω_y is now about

$$\frac{37.93 - 26.0}{26.0} = 53\%.$$

Examining the spectrum of y when $\mu = 0.8$ in fig.4.19, it can be seen that there are many small frequency components emerging up. These components were caused by the nonlinear portion of both y and x and they usually appear in the case that the system frequency is near entrainment. We will discuss this phenomenon in more detail in chapter 7. From the spectral function shown in fig.4.19 we can see the period of the y oscillator increases with the increase of μ_y and μ_x. As soon as the period of the y oscillator is near 3 times the period of the x oscillator, i.e., near the 1/3 entrainment range of the oscillator x, 1/3 subharmonic entrainment occurs. In what we called stage two, the "growing" frequency components were converted into pure harmonics and the spectrum becomes clear again.

Further exploration was done to explore various conditions which may cause 1/3 subharmonic entrainment. First we examined the effect of the coupling F_{xy} to y. The coupling coefficient F_{xy} was reduced from 0.2 to 0.05 which decreased the coupling from x to y about 75%. All the other parameters were kept the same values as above. The simulation was done by varying μ_x and μ_y. Fig 4.21 shows three main frequency components extracted from the spectral function. It was found that 1/3 harmonic entrainment occurred here when $\mu_y = \mu_x = 1.6$ instead of 0.8 when $F_{xy} = 0.2$. It also can be seen that the fundamental period is shorter than when the coupling coefficient was 0.2 as in fig.4.20. For example, the period of main frequency component when $\mu = 0.2$ is 29.68 hr as $F_{xy} = 0.2$ while it is 27.31 hr as $F_{xy} = 0.05$. The explanation for this case is that the nonlinear portion is weak due to the reduced coupling.

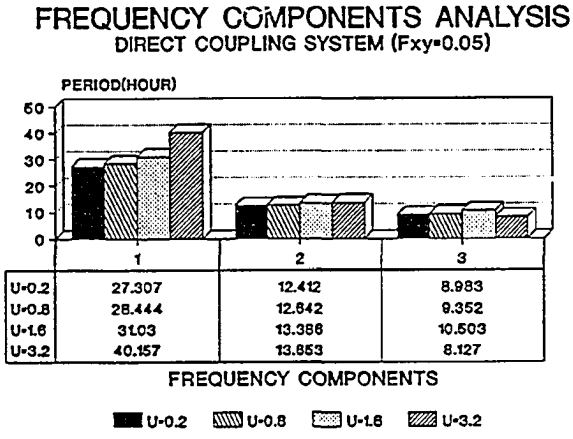

Figure 4.21: *3 main frequency components of coupled system with* $F_{xy} = 0.05$, *and* $\mu = 0.2$ *to* $\mu = 3.2$.

Second, we would like to see separately the influence of the nonlinearity of the x and y oscillators on this 1/3 entrainment. Instead of varying μ_x and μ_y simultaneously, we varied μ_y only while μ_x, the nonlinearity of the x oscillator, was kept at 0.1. Both the coupling coefficient F_{xy} and F_{yx} were set equal to 0.2 as in the previous model.

Fig 4.22 shows the result of this simulation where μ_y was varied from 0.2 to 3.2. The figure shows three main frequency components extracted from the spectral function. This result was compared with the result in Fig.4.20 where both μ_y and μ_x were varying from 0.2 to 3.2. We found the following:

1. When 1/3 subharmonic entrainment occurred, the fundamental frequency of the y oscillator was relatively higher (the period is shorter) than the case when μ_x and μ_y both increased.

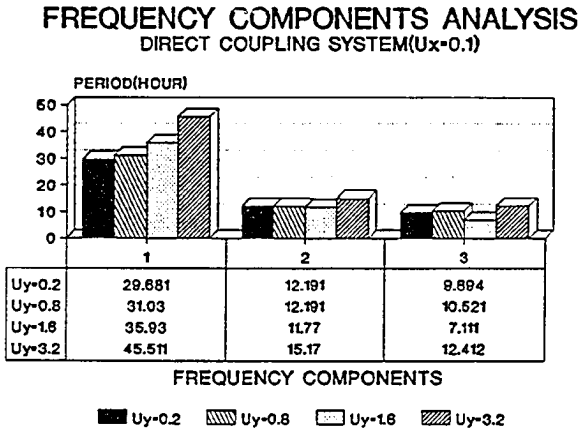

Figure 4.22: *3 main frequency components of coupled system with* $\mu_x = 0.1$, *and* $\mu_y = 0.2$ *to* $\mu_y = 3.2$.

2. The nonlinearity in both oscillators were acting on the system. However, the nonlinearity in the y oscillator had much more effect than the nonlinearity in the x oscillator.

3. The magnitude of the fundamental and harmonics of the x oscillator were relatively smaller than the case when μ_x and μ_y both increased.

4.7.2 Velocity Coupling System

The mathematical model of a velocity coupling system is based on the work by Kronauer.[23] In Kronauer et al's model, the two oscillators x and y drive two different activity rhythms – temperature and sleep wake. However, in our model, we assumed that both oscillators contributed to the same rhythm (e.g. temperature) but with different natural frequencies. Therefore two 2nd order Van der

Pol oscillators were used in our model to build an interacting system related by velocity-coupling as in the equations below:

$$k_y^2\frac{d^2y}{dt^2} + \mu_y k(y^2-1)\frac{dy}{dt} + \omega_y^2 y + F_{xy}\frac{dx}{dt} = 0 \tag{4.18}$$

$$k_x^2\frac{d^2x}{dt^2} + \mu_x k(x^2-1)\frac{dx}{dt} + \omega_x^2 x + F_{yx}\frac{dy}{dt} = 0 \tag{4.19}$$

Eq.4.18, Eq.4.19 differ from Eq.4.16 and 4.17 only in the coupling mode. T_y, the natural period of oscillator y, is equal to $24/\omega_y$, and is in the range between 22 to 24 hours while T_x (equals to $24/\omega_x$), the period of oscillator x, is approximately 12 hours. Two velocity-coupled oscillators could become mutually synchronized if their initial period difference $(T_y - T_x)$ is sufficiently small, typically in a range less than 4 hours. As expected under this condition, the simulation results showed that the synchronized pair adopts a period intermediate between T_x and T_y. One example of this is the simulation results of Kronauer's model as we introduced in section 4.6. Similarly, the two oscillators could also achieve subharmonic entrainment if the frequency of one oscillator was near an integer submultiple of the other oscillator's frequency $(T_y = nT_x)$. In the subharmonic entrainment case, the synchronized pair adopts a period intermediate between T_y and nT_x. Because the velocity coupling is weaker than the direct coupling mode, the effect of subharmonic entrainment is not so obvious as in the direct coupling case. Also high subharmonic (higher than 2) entrainment is relatively difficult, while in the direct coupling system, we see that 1/3 entrainment is not difficult to attain.

In contrast, if the frequency difference is outside the range of mutual entrainment frequency ratios, a velocity coupled oscillator can not achieve subharmonic entrainment. We examined the behavior of a coupled system where the free running period of the x oscillator was maintained at 12.5 hr. and the free running period of y was varied from 23 to 29 hr., with coupling from y to x, $F_{yx} = 0.1$ and

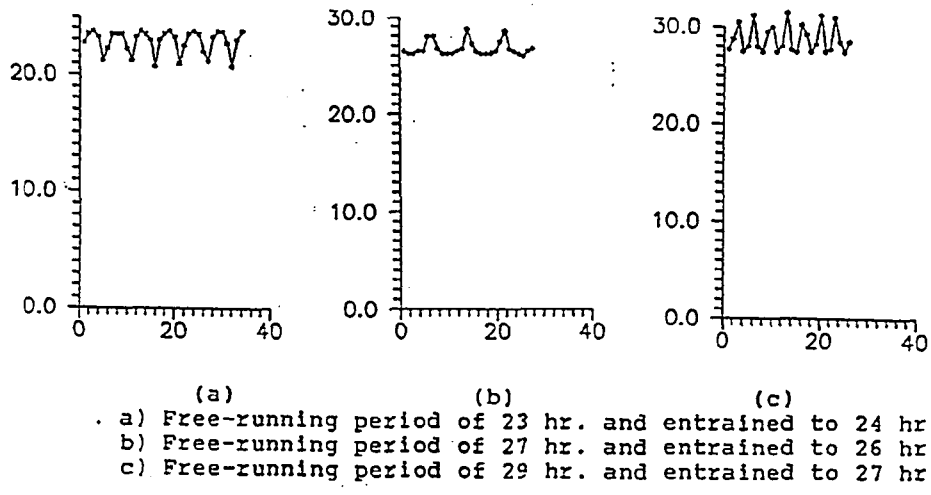

Figure 4.23: *Subharmonic entrainment in velocity coupled system*

coupling from x to y, $F_{xy} = 0.4$. Under these conditions, the two oscillators could achieve synchronization. The x oscillator pulled the period of y oscillator Ty, towards to $2T_x$, but the period of this coupled system was not very stable. Instead, the period fluctuated with complicated patterns. Fig.4.23 shows an example of these complicated fluctuations in period. Generally, subharmonic entrainment is much weaker than regular entrainment and velocity coupling is weaker than direct coupling. These two properties cause the instability here. However, the main purpose for us to build this coupled oscillator model is to insert the 2nd harmonic frequency component.

The y oscillator also shows weak influence on the frequency of the x oscillator. Fig.4.24 shows the period of the x oscillator (natural period = 12.5 hr.) in the velocity coupled system model where it is coupled with a y oscillator having a 28 hr period. The raster plotting scale is 12.5 hr. It can can be seen that the period of the x oscillator is increasing.

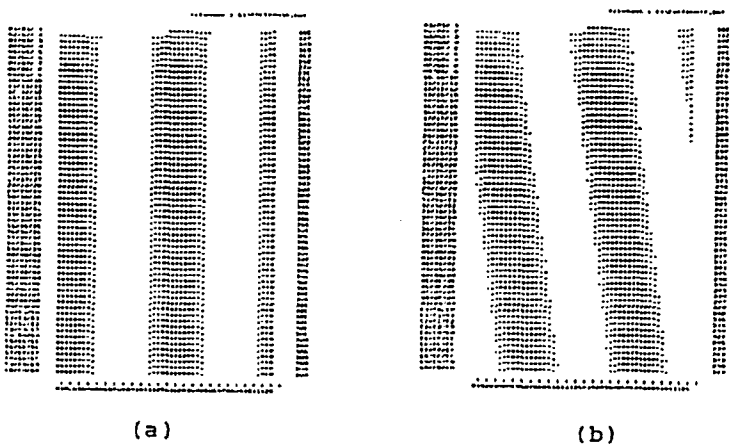

Figure 4.24: *Raster plotting of x period. (a) with y period of 28 hr., $F_{xy} = 0$ and (b) with y period of 28 hr., $F_{xy} = 0.2$.*

Velocity coupling has similar effects on the system as direct coupling, but it is much weaker. The selection of the frequency of the oscillators x and y in the velocity coupling system are basically the same as in the direct coupling system. ω_y and ω_x are the inherent normalized frequencies of oscillator x and y which represent the fundamental and 2nd harmonic frequency of the system. The fundamental frequency and harmonics of both the oscillators in the direct coupling system are easily influenced by the nonlinear portion in each oscillator. Therefore the natural frequency of both oscillators in the model should always be adjusted to match the frequency defined. In the velocity coupling system, the natural frequency is relatively stable.

Different velocity coupling coefficients were tested in our model to approach the experimental data. As we mentioned earlier, the coupling in the two dimensional system introduced the 2nd harmonic and higher harmonics as well as the

nonlinearity. Therefore the spectral function can help us to estimate the coupling coefficient. We compared the spectral function of our model with the experimental data, and found that in most cases strong coupling ($F_{xy} > 0.1$) in the velocity coupling model generated the required level of 2nd and higher harmonics. Therefore strong coupling should be applied in this model to approach the experimental data. Symmetric ($F_{xy} = F_{yx}$) and non-symmetric ($F_{xy} \neq F_{yx}$) coefficients were tested in the model and did not generate significant differences in the structure of the spectrum of the system, but symmetric coupling generates smaller high harmonic frequency components which is more like the real data.

The nonlinear parameter is also an important parameter being considered in the velocity coupling system. The main frequency components were extracted from the spectrum of the model with different μ_y and μ_x. The increase of μ_x and μ_y in the *direct coupling system* causes a frequency transition as we found and discussed in the previous section. This phenomenon did not appear in the velocity coupling system which shows that the direct coupling mode is much stronger than the velocity coupling mode. Fig.4.26 shows a comparison of our simulation results of the velocity coupling model with free running experimental data sets. It can be seen that the output of this model is very similar to the practical data, both in the time domain and in the the frequency domain.

4.8 Three Dimensional Coupled Oscillator Model

Practical circadian rhythms show varying and distinct features in both time and frequency domains. One important feature is the appearance of harmonics. According to the spectral analysis on the experimental data which is introduced

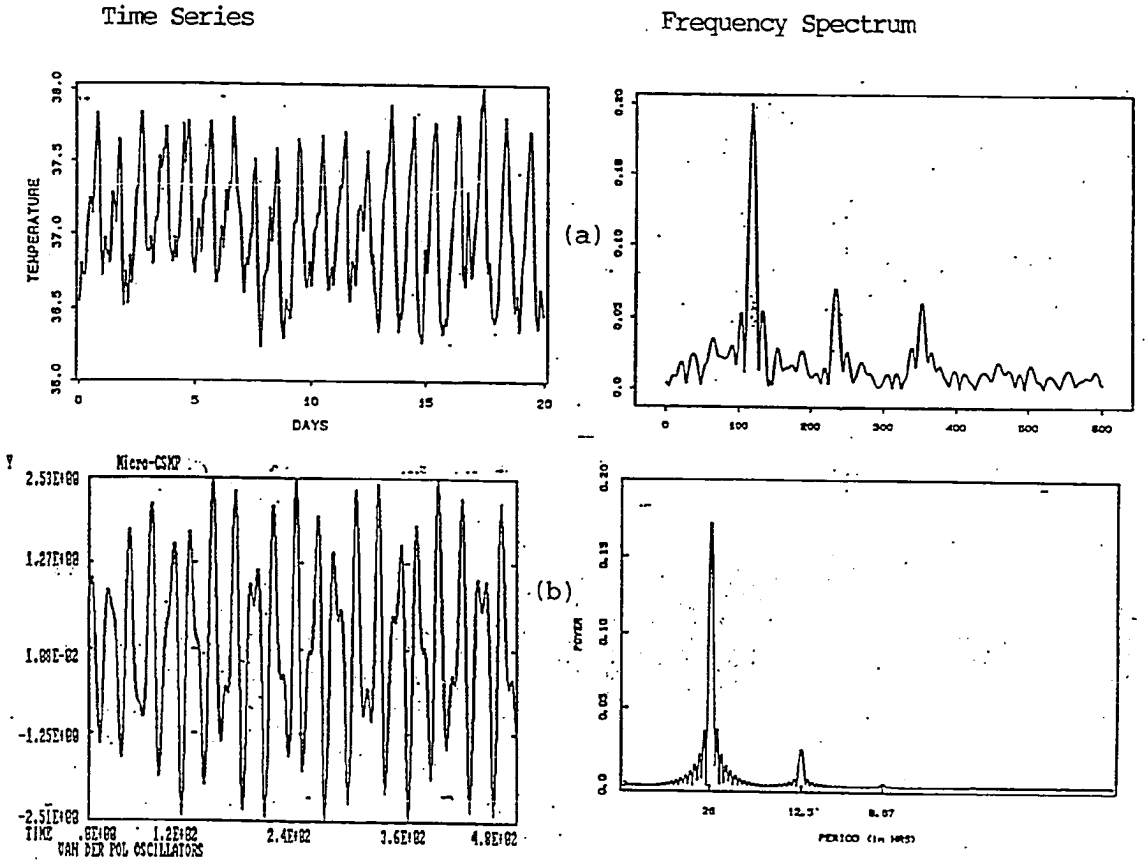

Figure 4.25: *Comparison of velocity coupling system with the experimental data. (a) Experimental results from one of the monkey subject. (b) Coupled oscillator model results.*

in chapters 2 and 6, the data of a free running circadian rhythm mainly consists of three distinct harmonic frequency components, i.e., fundamental, second and third harmonics. Usually, these three frequency components have different amplitudes and frequencies on different subjects under different conditions. In the time domain, these harmonics show "troughs" or "shoulders" as we have seen in chapter 2. To make our model approach the real data precisely, independent oscillators controlling these three harmonics separately should be considered in the model.

In section 4.7.1, we did a spectral analysis on the Van der Pol type oscillator. Fig.4.5 showed that a Van der Pol oscillator consisted of 3rd, 5th, $\cdots$, (odd) harmonic components. In our two dimensional coupled Van der Pol oscillator model discussed above, the fundamental and third harmonic frequency component were introduced by the main oscillator while the second harmonic was introduced by the coupled oscillator. The problem here is that the third harmonic component depends on the oscillator with the fundamental frequency and therefore, the level of this frequency component is not adjustable.

The experimental data always shows different harmonic structure for different species and subjects. Fig 4.26 (a) shows the spectrum from the temperature circadian data of a rat and (b) is from the temperature circadian data of a monkey. It can be seen that both spectral functions have similar structure but with different harmonic levels. It is difficult to use the same model to describe both circadian rhythms.

We designed a three dimensional model which consisted of three Van der Pol oscillators to simulate this complicated case. The three oscillators in the model were velocity-coupled to each other. Fig.4.27 shows the coupling structure diagram

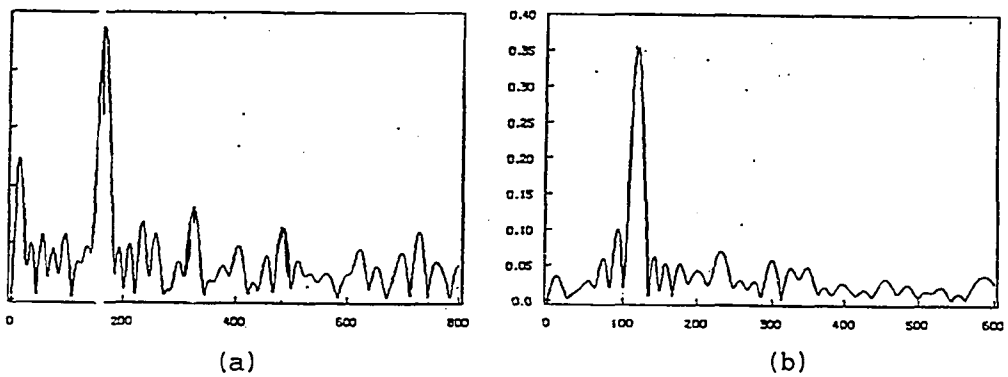

Figure 4.26: *a)Spectrum of a rat temperature data. b) Spectrum of a monkey temperature data.*

of this model. The three dimensional system is described by the following nonlinear differential equations:

$$k_y^2\frac{d^2y}{dt^2} + \mu_y k(y^2-1)\frac{dy}{dt} + \omega_y^2 y + F_{xy}\frac{dx}{dt} + F_{zy}\frac{dz}{dt} = 0 \qquad (4.20)$$

$$k_x^2\frac{d^2x}{dt^2} + \mu_x k(x^2-1)\frac{dx}{dt} + \omega_x^2 x + F_{yx}\frac{dy}{dt} + F_{zx}\frac{dz}{dt} = 0 \qquad (4.21)$$

$$k_z^2\frac{d^2z}{dt^2} + \mu_z k(y^2-1)\frac{dz}{dt} + \omega_z^2 y + F_{xz}\frac{dx}{dt} + F_{yz}\frac{dy}{dt} = 0 \qquad (4.22)$$

The basic parameters used in this model are similar to the two dimensional velocity coupling system. ω_y, ω_x, ω_z were defined as three main frequencies in the model. The coupling can be adjusted to simulate different experimental data. Fig 4.28 shows the spectra of two three-dimensional coupled oscillator models with different coupling. The idea of this model is to increase the degrees of freedom of the model. Fig 4.28 shows this flexibility. By adjusting the coupling coefficient among the three oscillators, we can get any desired harmonic structure. However,

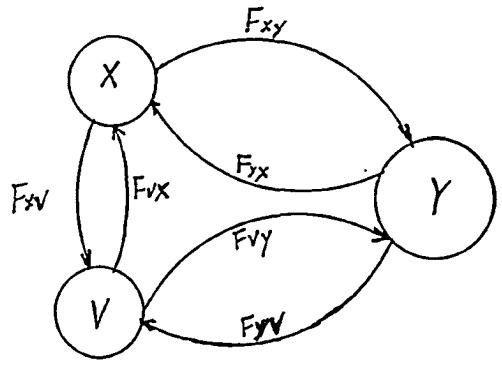

Figure 4.27: *3 dimensional coupled oscillator model.*

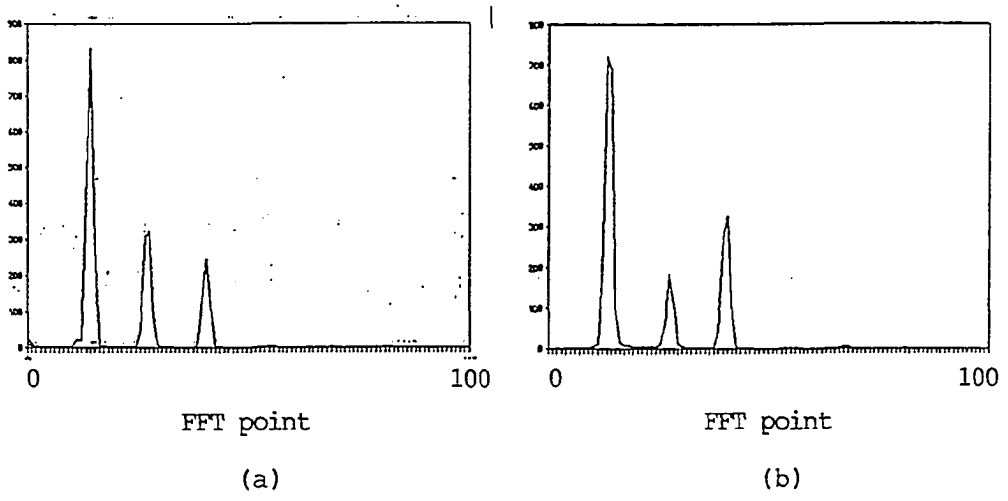

Figure 4.28: *The spectra of 3 dimensional coupled oscillator model. a) Coupling coefficient* $F_{zy} = 0.1$. *b). Coupling coefficient* $F_{zy} = 0.4$

this model also increases the complexity of the process. This model will be used to simulate the experimental data with unusual harmonic structures which the two dimensional oscillator model cannot generate.

Chapter 5

Analysis of Circadian Rhythms Using Topological Methods

5.1 Introduction

The topological analysis method is applicable to the study of autonomous(see section 3.4.1) systems and is widely utilized to investigate various phenomena of nonlinear oscillations. With this technique, the solutions of non-linear differential equations are obtained not as explicit functions of time but as solution curves in a phase plane, or, more generally, in a state space. In the study of biological oscillators, the topological method has its special importance.[20, pages 33-34]

The graphical solutions obtained for the biological system include phase response curves and raster plots which are very productive for the exploration of the system. The phase response curve method is based on the study of the representation of solutions of differential equations in the phase plane or phase space, i.e., phase response features. The raster plot is based on the periodic solution present in the nonlinear system. It can be used for long term data recording and trend

observation.

The study of biological oscillators presents a situation different from that in engineering and the physical sciences. There, oscillators could often be described by existing mathematical equations. The state variables are usually well defined and measurable. The study of most biological oscillators is subject to the following constraints:

1. The state variables are not known.
2. Even if they are known, they are not measurable.
3. The mathematical equations describing the dynamics are not available.

Therefore, the regular techniques in engineering can not be used in this case. Other techniques have to be considered for exploration of the properties of biological oscillators. For example, from the recorded circadian rhythm data, we could possibly find its time derivative. Then the phase plane curve could be possibly drawn with these two variables. The type of oscillation and stability could be further explored from the phase plane.

The other example is the application of the PRC – phase response curve. Even though the internal structure of the biological oscillator is unknown, we could apply some level of stimulus at different phases of the oscillation to observe the reaction of the system. The information obtained is called the Phase Response Curve(PRC), which will help our understanding of the system.

5.2 Phase Space and Phase Plane Method

The dynamic behavior of many physical systems can be described by a second-order differential equation or a system of two first-order differential equations. Such descriptions involve two variables which characterize the behavior of the system and are usually called the state of the system. They can be represented as coordinates in a plane. In this way the behavior of the system can be described in terms of plane curves. The general form of the mathematical equations describing a system which can be studied on the phase plane is,[21, pages 367]

$$dy/dt = f(x,y) \tag{5.1}$$

$$dx/dt = g(x,y) \tag{5.2}$$

We can eliminate t to obtain a first order equation in x and y:

$$dy/dx = f(x,y)/g(x,y) \tag{5.3}$$

The variable t can be interpreted as a reference parameter. Each solution curve with different t is a trajectory.

For example, the position and velocity of a mass m suspended from a spring with constant k has its motion determined by the equation

$$md^2y/dt^2 + ky = 0 \tag{5.4}$$

The solution of the above equation is

$$y(t) = Acos[(k/m)^{1/2}t + \phi] \tag{5.5}$$

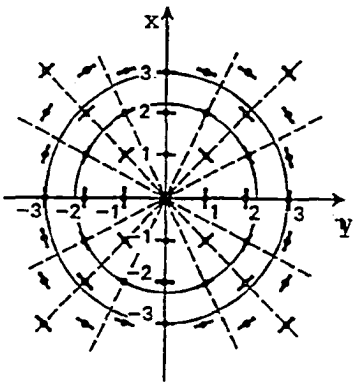

y	x	x'
1	0	∞
2	0	∞
0	1	0
1	1	−1
1	2	−2
−1	1	1
−2	1	2
0	2	0
1	2	−0.5
2	2	−1

Figure 5.1: *Phase plane plot of spring system.*

The derivative of $y(t)$ is:

$$x(t) = y'(t) = -(k/m)^{1/2} A sin[(k/m)^{1/2} t + \phi] \tag{5.6}$$

If the time dependence is eliminated in $x(t)$ and $y(t)$, we have

$$y^2 + (m/k)x^2 = A^2 \tag{5.7}$$

which represents ellipses in the xy plane. In the case where $m/k = 1$, the curves become circles as shown in fig.5.1, the figure shows a group of circles drawn by assuming different A values.

The points (x_e, y_e) for which *the derivative of y and x both take the value zero* are called points of *equilibrium, singularities, or critical points* of the system [21, pages 378–388]. The singularity of the system shown in fig.5.1 is the origin $(x = y = 0)$. If the initial point is exactly equal to such a point, it will remain unchanged since both the velocity (dy/dt) and the acceleration(dx/dt) are zero. If the initial point is close but not exactly equal to the critical point, there will be three possibilities:

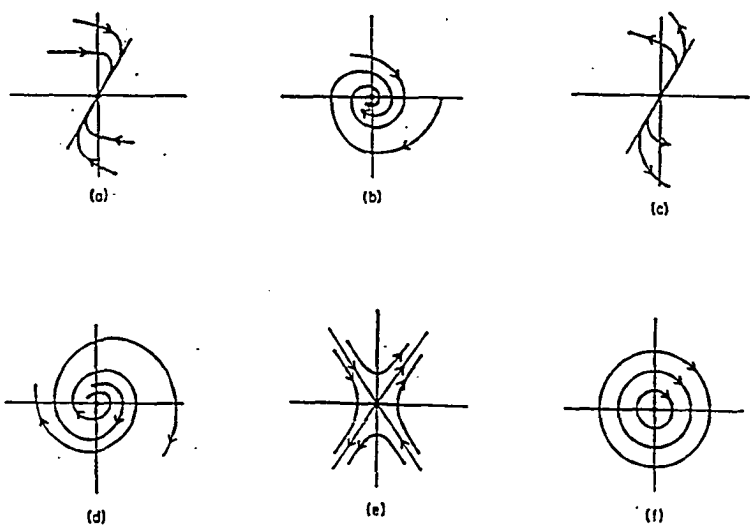

Figure 5.2: *Phase plane portraits of different equilibrium points. (a) and (b): the trajectories move toward the equilibrium of the system, they are stable. (c), (d) and (e): the trajectories move away from the equilibrium of the system, they are unstable. (f) the trajectories share the equilibrium of the system and remain there, they are stable.*

1. The distance between $(x(t), y(t))$ and (x_e, y_e) converges to zero with increasing t if $(x(t), y(t))$ are sufficiently close to (x_e, y_e) initially. In this case (x_e, y_e) is said to be asymptotically stable.

2. The distance between $(x(t), y(t))$ and (x_e, y_e) does not converge to zero, but it remains small if $(x(t), y(t))$ and (x_e, y_e) are close enough to begin with. We say in this case that (x_e, y_e) neutrally stable.

3. If the distance between $(x(t), y(t))$ and (x_e, y_e) eventually exceeds some positive value no matter how small it is initially, (x_e, y_e) is said to be unstable.

The analysis allows us to plot the trajectories of the system in the neighborhood of an equilibrium point. Fig.5.2 shows several phase plane portraits in the neighborhood of various types of critical points. Table 5.1 lists the configurations of these

Name	Stability	Real roots	In Fig.5.2 .
Stable node	Y	Y	a
Stable focus	Y	N	b
Unstable node	N	Y	c
Unstable focus	N	N	d
Saddle point	N	Y	e
Center	Y.	N	f

Table 5.1: *Configuration of equilibrium points.*

points. We are interested in the set of closed cycles which correspond to periodic biological oscillatory motion in our circadian rhythm system. These trajectories can be called periodic trajectories. They have the property that once the state of the system is in the closed cycle it will remain there for all times. Periodic trajectories which are asymptotically stable from both sides of the trajectory are called stable limit cycles or simply limit cycles. Those which are unstable from both sides are called unstable limit cycles or antilimit cycles.

Poincaré studied various properties of periodic trajectories. The following is a summary of his results: [33]

1. A periodic trajectory must surround at least one point of equilibrium.
2. If it surrounds exactly one point, then this can not be a saddle point; i.e., it is necessary that both roots have the same sign (stable).
3. If a surrounds more than one point, then there should be exactly one more focus, node, or center than saddle points.

The singularity of a linear oscillation is a center. The situation becomes more

complicated in the nonlinear oscillation case. The problem of establishing the existence of a limit cycle is generally very difficult. The method of contact curves introduced by Poincaré is sometimes useful in locating possible limit cycles. For this purpose we first consider a family of concentric circles with centers at the singular point and then determine on the xy plane the locus of the points where these circles are tangent to the integral curves. This locus is the contact curve. We assume that the contact loci lie in a bounded region of the xy plane. If a limit cycle occurs at all, it must of necessity lie in a ring domain with center at the singular point whose boundaries are the innermost and outermost circles of radii r_{max} and r_{min} respectively, which touch the contact curve.

Most of the solutions of our models are obtained through computer simulation, and therefore the phase plane plots could also be obtained from the numerical solution. The simulation time interval should be long enough to draw the complete motion of the system. In chapter 4, we introduced several models for circadian rhythms. We will now analyze their phase plane results.

Fig.5.3 shows the limit cycles of a single Van der Pol oscillator model with different values of μ. In section 4.4, we introduced and analyzed our simulation results of a single Van der Pol type model with different nonlinearity. Their time series and spectra were shown in Fig.4.4 and 4.5. The phase plane results shown here are based on the numerical solution of the same model, i.e., both the time series and the derivative of the time series were obtained from a long time simulation. In fig.5.3, we notice the following:

1. The limit cycle of this model are closed curves. Therefore the solution for $y(t)$, the time series of the system must be a periodic function of t, since $y(t)$

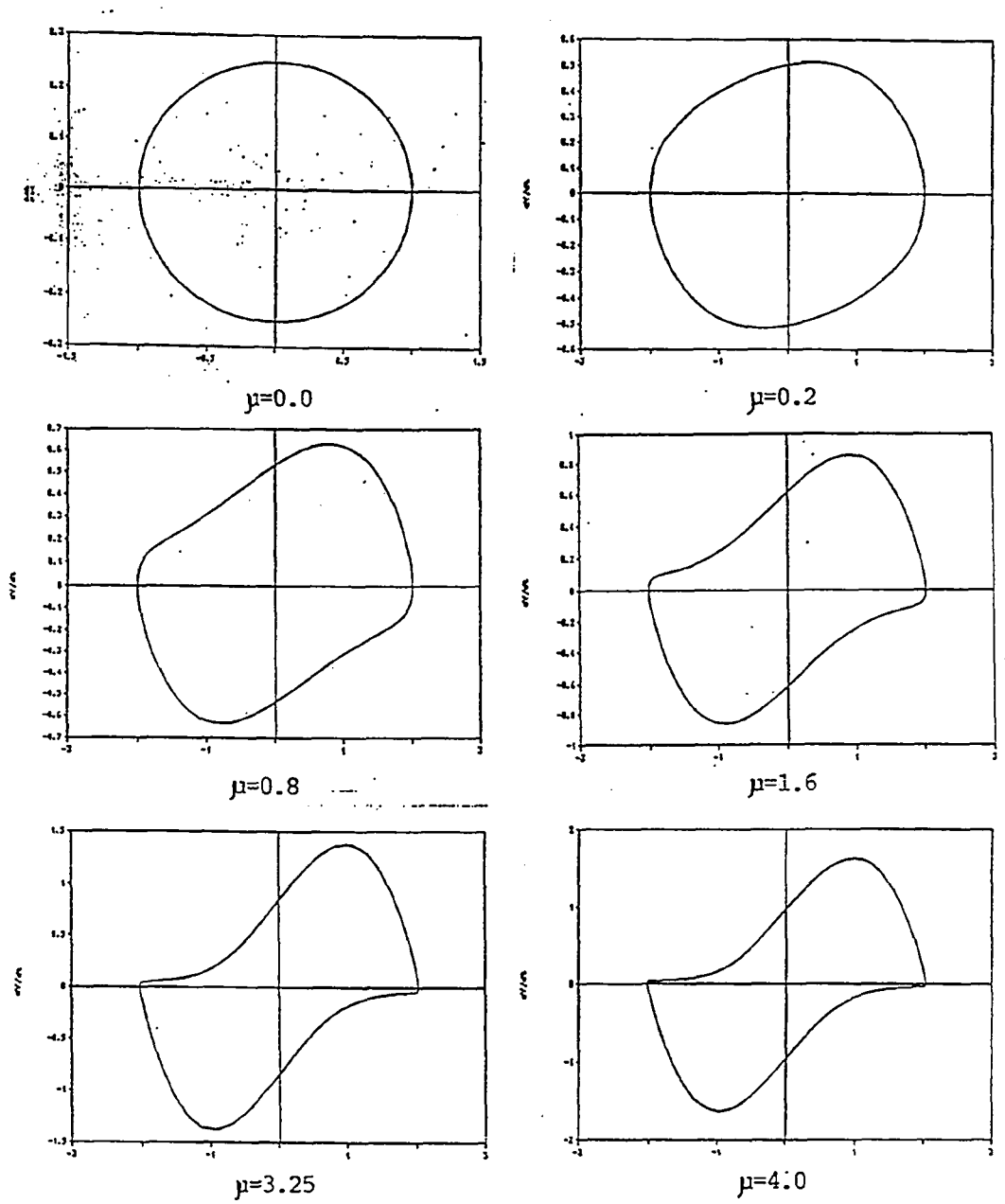

Figure 5.3: *Phase plan plots of a Van der Pol oscillator with different values of* μ.

must retrace the same pattern over and over again as we follow increasing t around the trajectory;

2. The equilibrium point is at the origin and is unstable for $\mu > 0$. More precisely if a small initial deviation from the equilibrium point is not corrected, then it leads to motion that converges to the limit cycle as t increases indefinitely. The trajectory of this type of model is a stable limit cycle. If the initial point is not at the origin, it will move toward the limit cycle;

3. In the case of $\mu = 0$, the model becomes a linear oscillator, and all the trajectories are circles with center at the origin. As μ increases, the nonlinearity causes a profound change in the trajectories.

More complex cases are the quasiperiodic or almost periodic motions. A quasiperiodic function f(t) is one which can be written as

$$f(t) = g(\omega_1 t, ..., \omega_m t) \tag{5.8}$$

where g is a continuous and periodic function with respect to each one of its arguments (with frequency ω_i). For example,

$$sin\omega_1 t + sin\omega_2 t$$

is a quasiperiodic function. It will be periodic only if ω_1 and ω_2 are in rational ratio. Fig.5.4 shows a phase plane plot of a quasiperiodic oscillator which was obtained from one of our simulation results. We simulated a single Van der Pol oscillator model twice with all the same parameters as in section 4.4 except $\mu = 0.1$ and $\mu = 0.2$ respectively. The time series from two simulation results were then subtracted. Fig.5.4 is the phase plane plot of this difference which shows that the

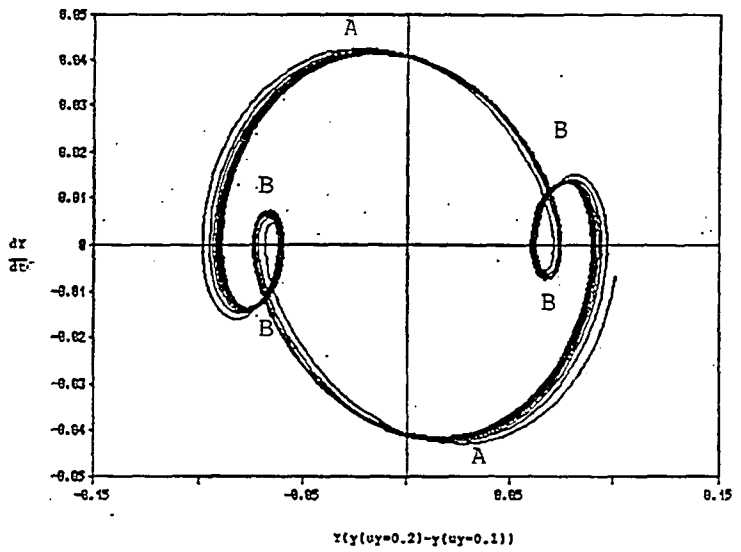

Figure 5.4: *Phase plane plot of a quasiperiodic oscillator.*

oscillator is in a "quasiperiodic" mode. It should be noticed that this quasiperiodic oscillation has very small amplitude according to the scale of the phase plane. Our understanding is that different nonlinearity cause the difference of oscillating frequency, therefore the difference of these two time series includes two different frequency oscillations as we can see in the phase plane. Points $A - A$ and $B - B$ on the phase plane demonstrate the two frequencies.

The phase plane technique for the analysis of quasiperiodic oscillators is very useful. The trajectory for this type of oscillator is a combination of two limit cycles. The movement will cross between these two cycles. In the biological oscillator case, due to different types of nonlinearity, different oscillation features will occur under different conditions. For example, an oscillator coupled with another oscillator having unequal frequency will either change its period and become "entrained" to a new period, or if it becomes "unentrained", and the two frequencies of oscillation will coexist in the system. The phase plane will show the quasiperiodicity in this

case.

Fig.5.5 shows the phase plane plot from a velocity coupled Van der Pol oscillator model for different degrees of nonlinearity. In this case, the situation becomes more complicated than the single Van der Pol type model. Comparing with the phase plane of the single Van der Pol type model in fig.5.3, we can see the basic shapes of these phase plane plots are similar to the single oscillator model case. But the important difference here is that the trajectory of a coupled oscillator is "multi-frequency mode" which is caused by the coupling of two oscillators with different natural frequencies. In chapter 4, we used other techniques to explore the coupled oscillator while the phase plane portraits give us more visible results about the nature of the system (oscillation or other type movement), its nonlinearity, coupling with another oscillator,etc. These are the important features of biological rhythms in our study. As we mentioned earlier, all of the outputs from our models were obtained through computer simulation. Therefore it was easy to get the phase plane plots by using the output variables from the simulation. In the simulation we use CSMP to output the variables and their derivatives to a data file. The program RWTP (listed in the Appendix) was written to convert the CSMP output to regular ASCII files. The phase plane plots were plotted by using LOTUS 123 graphic functions.

5.3 Phase Response Curve Method and its Application

The phase response curve (PRC) is defined as a plot of the phase shift of the oscillator verses the phase of the oscillator when a stimulus is applied. [2]

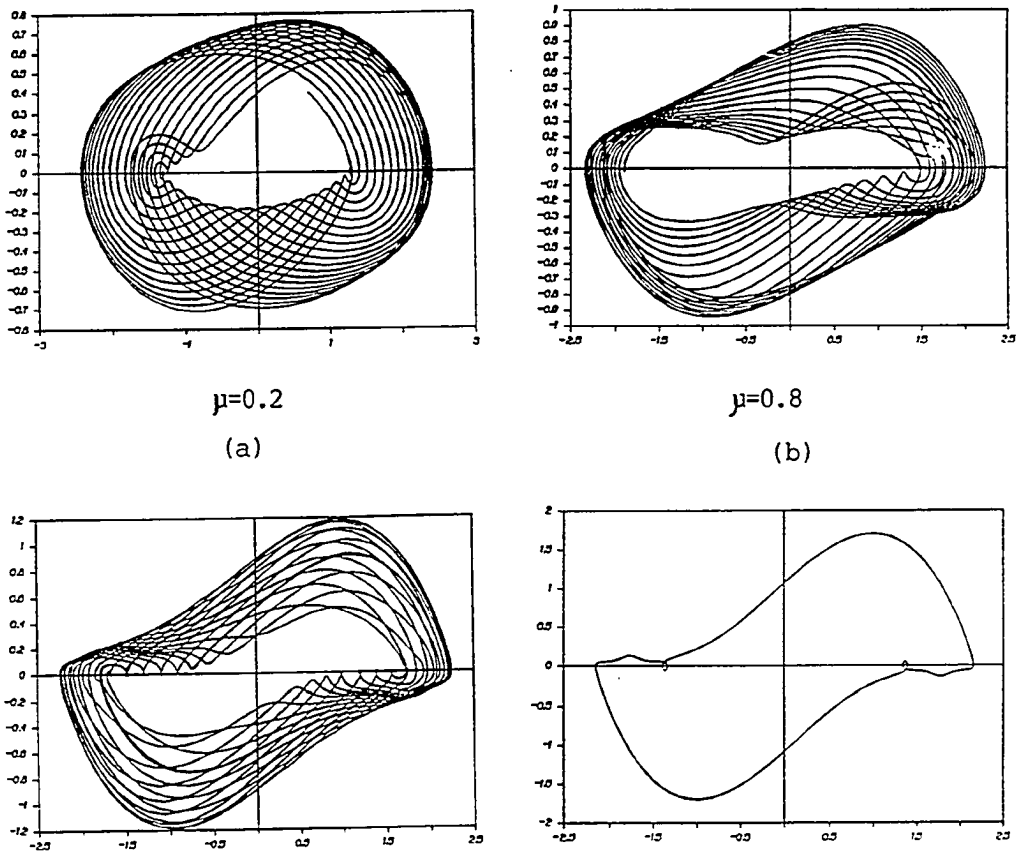

Figure 5.5: *Phase plane plot of the coupled oscillator model.*

Generally, nonlinear systems have dissimilar phase responses characteristics which is a very helpful feature in the study of biological oscillators. The phase response characteristics, including phase shift directions and amplitudes, to the stimulus applied at different timing positions reflect the system "entrainment" attributes. In practice, the phase response curve is usually obtained by a series of experiments, e.g., by applying a light stimulus to the subjects at different times during subjective day and night (subjective day is the await period for that subject, e.g., the time when the temperature rhythm is above the average). This type of experiment will give us the response information of a unknown biological oscillator, which is different for various subjects and species under different conditions.

Thirty years ago, a phase response curve of circadian rhythms to light stimuli was first described, revealing the mechanism by which pacemakers driving circadian rhythms are synchronized (entrained) to the 24 hour day. It was believed that social contacts, rather than the light dark cycle, synchronized the human circadian system to the 24 hour day. Subsequent studies demonstrated that the circadian clock of normal subjects could be entrained by a 24 hour cycle. It was found from the PRC that evening exposure to bright light rapidly shifted the phase of the endogenous component of the body temperature and cortisol cycles, even when the timing of the sleep-wake cycle was held constant.

Fig.5.6 shows an experimentally acquired phase response curve of circadian rhythms.[15] The figure shows three time zones A, B and C representing subjective day or night. In zone A, light exposure has no effect during the subjective daytime while the timing of behavior is delayed in zone B during the early hours of the subjective night and advanced in zone C late in the subjective night It can be seen that light exposure may advance, delay or have no effect on the phase of the

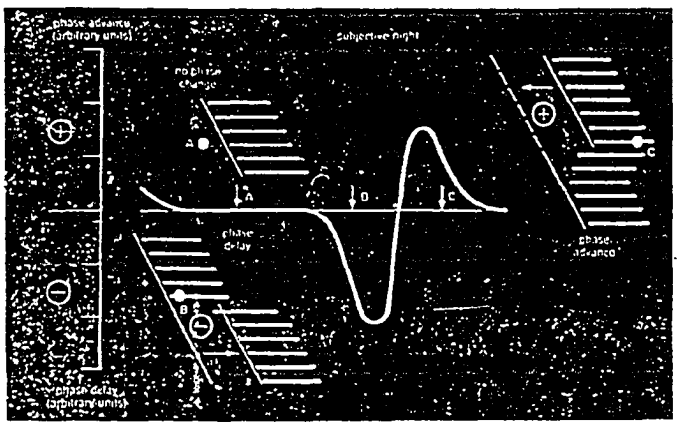

Figure 5.6: *Phase response curve of circadian pacemaker by light stimulus.*

circadian pacemaker. Some generalizations about the shape of the phase response curves can be stated.

1. Because of the continuity of dynamic systems they are expected to be continuous curves, except for jumps of size T (usually 2π).

2. There will be possible isolated zeros, or zero intervals on the PRC. The zero intervals have an infinite number of zeros in a region as in zone A of fig.5.6. If one plots a PRC then both its end points must have the same value. Therefore the total number of isolated zeros, zero intervals, and jumps of size T of a phase response curve must be even.

The PRC shows directly the system responses to a stimulus applied at different phases which is especially helpful in the design of experiments to explore the properties of unknown biological oscillators. PRCs to light exposure have recently been reported in some practical applications.[14]. Dr. Czeisler and his team

demonstrated that they could reset the circadian pacemaker of a sleep-disorder patient by exposing her to 4 hours of bright light each evening. The system had shifted 6 hours even though the period of the sleep-wake cycle was held constant. In their experiments, Dr. Czeisler and his team found that the timing of the light exposure was more critical than other factors

Fig.5.7 shows such stimuli applied in our single Van der Pol type model. We applied the light pulse stimulus by "velocity coupling" to the system, i.e., the first time derivative of the light pulse is applied to the model, which corresponds to the light pulse in real situation. Fig.5.7 a shows the time derivative of a light pulse which causes the phase of the model to be delay shifted and b shows the time derivative of a light pulse which causes the phase to be advance shifted. The amplitude of both light pulses are the same, the pulse durations of both are 1.5 hours wide while the timing at which the pulses are applied are different. The timing difference is 5 hours in our simulation program which is listed in the Appendix.

Therefore the timing of the stimulus applied either to the model or to the real subject has to be precisely controlled to get the expected phase shift direction and amplitude. Phase response curves give the complete phase response characteristics of the system. According to the PRC, we can design the experiment for phase delay-shift or advance-shift. It is also a good tool to design and test the models as in the case of the biological oscillator model we introduced in section 4.6.2.

5.4 Raster Plotting and Its Application

Raster plotting is a typical data record format in circadian rhythm research. This type of record shows the oscillation period of a circadian rhythm and its

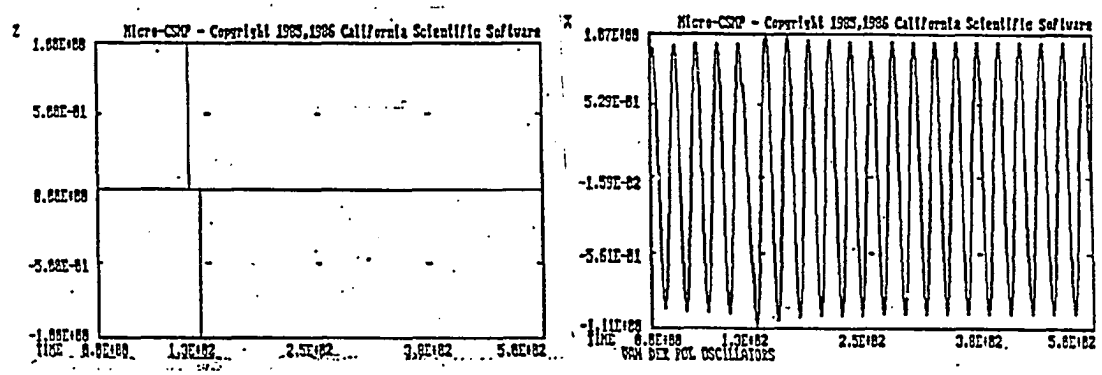

Single light pulse for phase delay shifting.

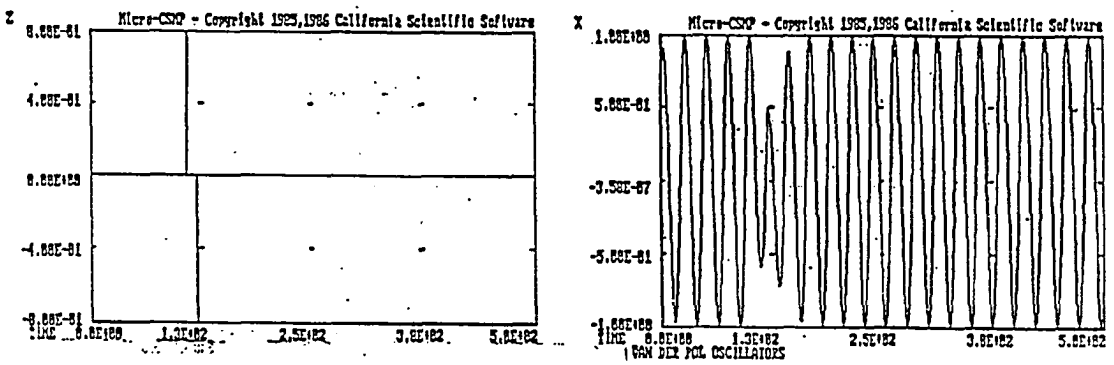

Single light pulse for phase advance shifting.

Figure 5.7: *Stimulus applied and the time series. a)The first time derivative of light pulse causing the phase of the model delay shifted. b)The first time derivative of light pulse causing the phase of the model advance shifted.*

varying trend directly. The full scale of the x axis of this plot is the estimated oscillation period. For example, we use 24 hours as the full scale of the x axis for circadian temperature rhythm data recording. Each horizontal line in the record is for a 24 hour interval, beginning from the topmost line and progressing down. The y axis of each line plots the intensity of the measured signal by different symbols, usually the darker symbol being used for higher intensity. If the same symbols in each horizontal line stay at the same horizontal position, the system is just oscillating at the assumed period. Otherwise we can find out the variation from the plot. Fig.5.8 shows two examples of raster plotting. The x scales on both a and b are 24 hours. Here (a) is the data from a model whose period is exactly at 24 hours while (b) is the data whose period is 25 hours. Raster plotting shows the difference clearly.

As mentioned in the first chapter, the researchers in the biological oscillator field have realized the existence of endogenous oscillators in living systems. One argument to support this theory is that if organisms are kept in carefully controlled environments, where the temperature and light intensity are kept constant, they still exhibit periodicities in their behavior. The experiments show such rhythms always being different from 24 hours - in general, varying between 22 and 24 hours. The raster plotting shows this trend very clearly in these experiments.

Raster plotting is used in recording almost all the circadian rhythm data. Another advantage of this type of plotting is that several months of data can be easily packed on to a single sheet, which is very convenient for long term data viewing. We used raster plotting mainly for two purposes:

1. It was used for our experimental data plotting. As introduced in chapter

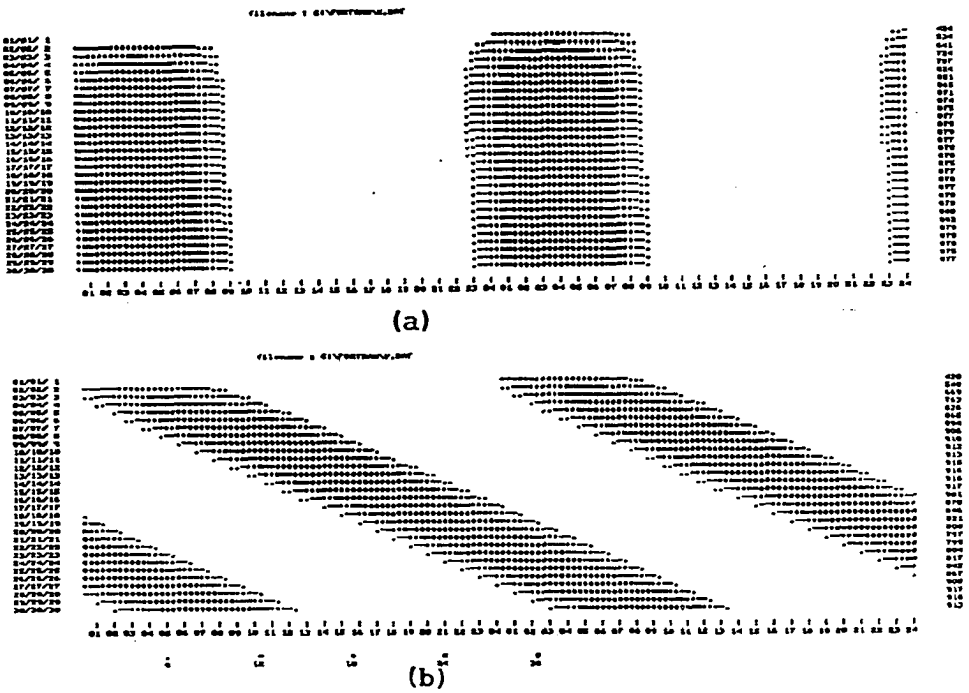

Figure 5.8: *Examples of raster plots (x axis is scaled at 24 hours). a)The system is oscillating at the period of 24 hr. b)The system is oscillating at the period higher than 24 hr. The period in (b) could be found by finding the time difference between each horizontal line. This difference in (b) is 1 hour toward the delay (right) direction therefore the period is 25 hour.*

2, we have built our data acquisition system for circadian rhythm data. It is very convenient to use raster plotting to view the trend and the possible interruption of the data. In the case of the phase shift experiment, this plot is very convenient for showing the experimental results. Figure 5.9 shows raster plots of our experimental activity, feeding and temperature data.

2. The raster plotting is used to explore the characteristics of our model. In chapter 4, we introduced its application in our coupled oscillator model where we would like to see if the period of one oscillator changed when the nonlinearity or coupling was changed due to the other oscillator. We will now show another interesting result using raster plotting. We addressed the question as to what would happen to the coupled oscillator model if we apply a periodic stimulus to it? The principles and detailed experimental results will be shown in chapter 7, but here are some results using raster plotting. Fig.5.10 (a) shows a coupled oscillator ($F_{xy} = F_{yx} = 0.2$) with 22 hr period entrained to 24 hr by a stimulus applied on day 10. and (b) shows a coupled oscillator ($F_{xy} = F_{yx} = 0.2$) with 28 hr period entrained to 24 hr also by a stimulus applied on day 10. The raster plot demonstrates that the "entrainment" is stable.

   Fig.5.11 is the same system except for a different coupling coefficient, ($F_{xy} = 0.6$, $F_{yx} = 0.2$). The raster plot shows the oscillator can not be stably "entrained" because the oscillation periods fluctuates.

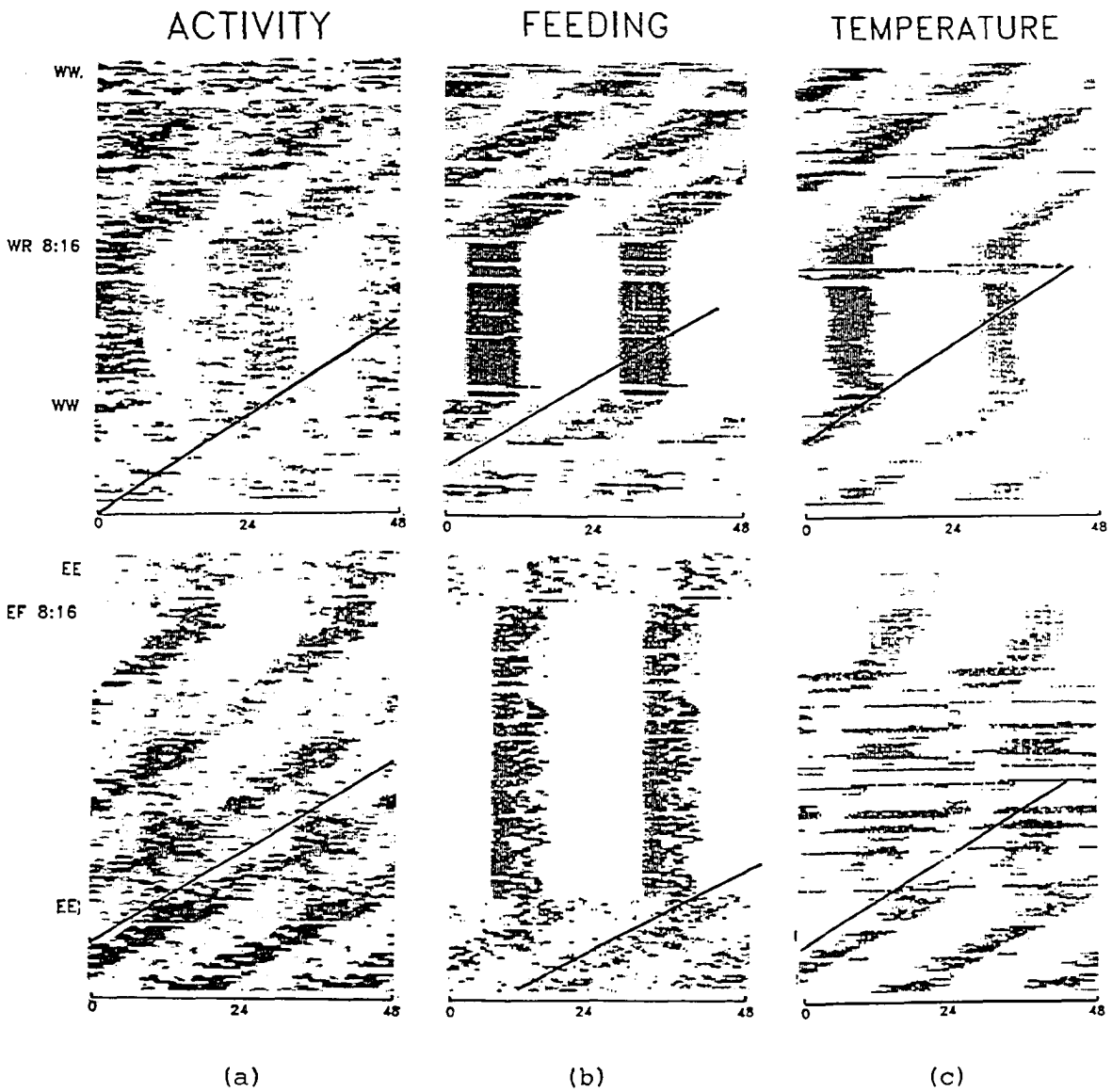

Figure 5.9: *Raster plot of circadian rhythm data obtained from experiment.*

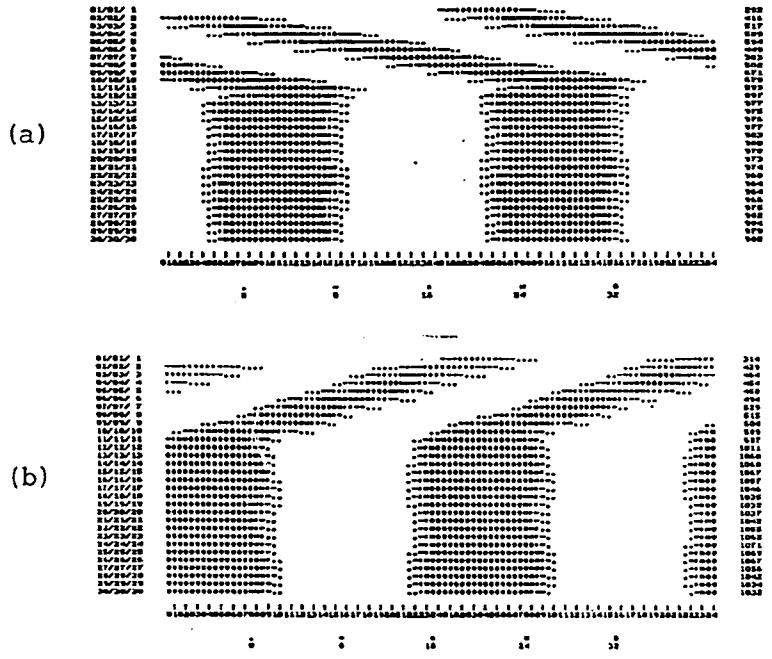

Figure 5.10: *Raster plotting of periods of the coupled oscillator model. (a) The 28 hr oscillator is entrained to 24 hr. (b) The 22 hr oscillator is entrained to 24 hr.*

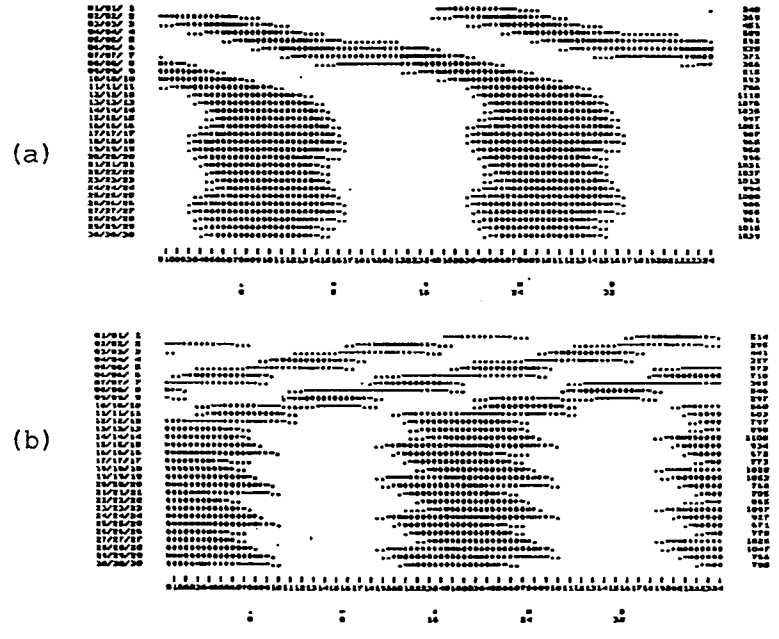

Figure 5.11: *Raster plotting of periods of the coupled ($F_{xy} = 0.6$) oscillator model. (a) The 28 hr oscillator is entrained to 24 hr unstably. (b) The 22 hr oscillator is entrained to 24 hr unstably.*

Chapter 6

Spectral Analysis of Circadian Rhythms

6.1 Introduction

The estimation of the spectral characteristics of a time series is of fundamental importance in the analysis of the natural properties of a system. It is widely employed in communication engineering, economics, physiology and many other areas. The spectral function is especially helpful for exploring the system whose characteristics are unclear. For example, the internal relationships of a circadian oscillator are very complicated. The oscillator may be coupled with, or affected by, another internal oscillator. Therefore the observed circadian data may be a combination of several time series. Spectral analysis will help us to discriminate different time series by identifying different frequency components, and to detect the characteristics of each of them.

Fourier analysis is a method for detection and measurement of the frequencies, amplitudes, phases and decay rates of decomposed sinusoids in a time series. Find-

ing the discrete sinusoidal components of a time series is a task in the province of harmonic analysis, a subfield of spectral estimation. In this research, the time series were either obtained from the model simulation or the experimentally collected data. The power spectral densities of both simulated and experimental data were computed, analyzed and compared. For example, it was found through spectral analysis that the circadian rhythms have harmonic and sub-harmonic structures. Experimental data from one "free running" monkey shows the power spectrum of circadian temperature has a main frequency peak at 24.17 hours as well as 2nd and 3rd harmonic peaks. Other experimental data obtained from a rat temperature record shows similar frequency peaks but with different intensity of the harmonics. Fig.6.1 shows the spectral function of two circadian rhythms, where (a) is the spectral function of monkey temperature data and (b) is the spectral function of rat temperature data. We can see clearly the difference in harmonic structure of these two spectra as we mentioned above; this information cannot be obtained from either the time series or other outputs directly from the system.

The following topics were studied in the frequency domain:

1. The frequency and amplitude as well as the ratio (to the main frequency component) of the harmonics and sub-harmonics were extracted from the processed experimental data. The underlying causes of these harmonics and subharmonics were explored.

2. The harmonic and subharmonic structure of different mathematical models were studied and compared with the results of step 1. Different modeling methods were used to obtain close agreement with the frequency structures found in the experimental data.

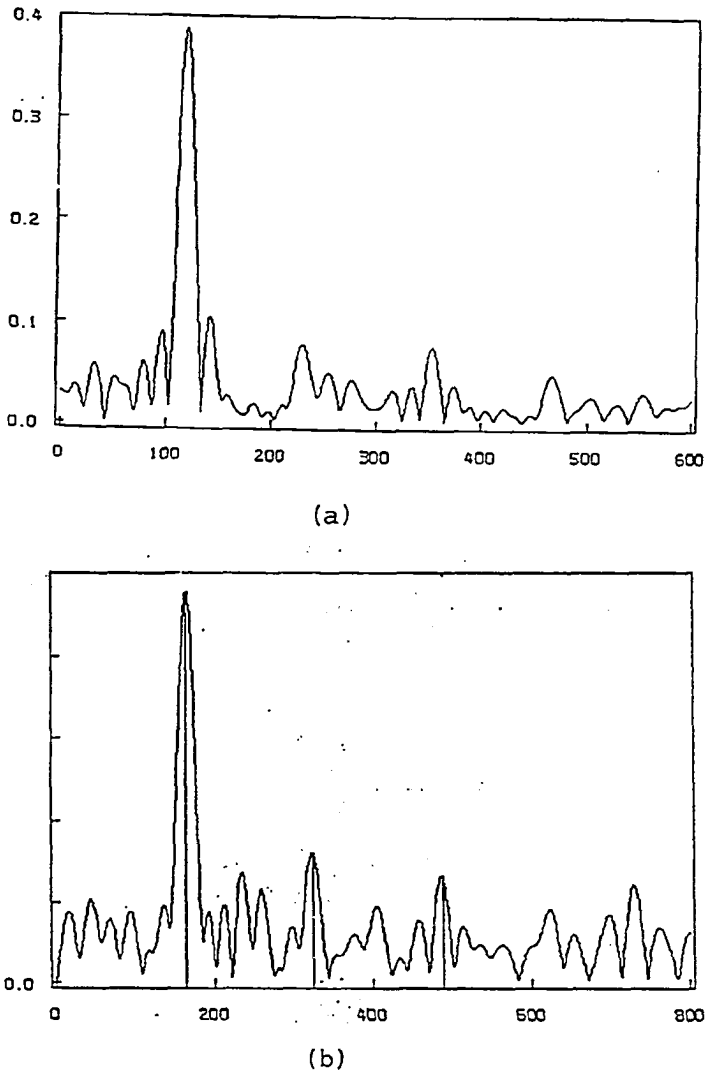

Figure 6.1: *Spectral function of real circadian rhythms.a) Spectral function of a monkey temperature data. b) spectral function of a rat temperature data.*

3. The relationships among different harmonics were studied using the bispectrum method. The bispectrum is a high order spectrum (the Fourier transform of the third order cumulant (TOC) sequence), and is generally used:

   a) To extract information in the signal of interest pertaining to deviations from Gaussianity;

   b) To detect the presence of nonlinear properties and quadratic phase coupling. The second application was examined in this research.

4. The cross correlation between two different circadian rhythms (e.g. temperature and activity) of the same experimental subject was explored in the frequency domain. The coherence function was computed using segmented and smoothed FFT data.

5. The dynamic spectrum (the spectrum of the system immediately following the application of a stimulus) was explored. The examination of this spectrum shows the transient dynamics of the system.

We are going to discuss topics 1 and 2 in this chapter while topics 3 and 4 will be discussed in chapter 8 and topic 5 will be discussed in chapter 7.

6.2 Fourier Analysis: Principles and Techniques

Fourier analysis can be treated as a decomposition of the time series in a sum of sinusoidal components (the coefficients of which are the discrete Fourier transform of the time series). It is the representation of a set of data in terms of sinusoidal functions. Here we will review some basic principles of Fourier analysis.

1. A periodic function can be expanded into a Fourier series.

The mathematical details of the derivations of the Fourier equations and additional properties can be found in various mathematical and engineering textbooks. [40, pages 80-84] It can be shown that a periodic function satisfying certain restrictions (usually causing no great limitations in engineering applications) can be expanded into the sum of an infinite number of harmonically related sine and cosine terms of the form,

$$x(t) = \frac{a_0}{2} + \sum_{m=1}^{\infty}(a_m cosm\omega_1 t + b_m sinm\omega_1 t) \tag{6.1}$$

Where

$$a_m = \frac{2}{T}\int_{-T/2}^{T/2} x(t) cosm\omega_1 t dt$$

and,

$$b_m = \frac{2}{T}\int_{-T/2}^{T/2} x(t) sinm\omega_1 t dt$$

Here, T = period of the waveform. ω_1 = fundamental radian frequency $= 2\pi\frac{1}{T}$. The development of many analytical and theoretical concepts can be simplified by use of the exponential Fourier series:

$$x(t) = \sum_{m=-\infty}^{\infty} C_m e^{jm\omega_1 t} \tag{6.2}$$

where

$$C_m = \frac{1}{T}\int_{-\infty}^{\infty} x(t) e^{-jm\omega_1 t} dt \tag{6.3}$$

The coefficients of these two forms can be related by

$$C_m = \frac{a_m - jb_m}{2} \tag{6.4}$$

$$a_m = 2R_e[C_m] = C_m + C_m^* \tag{6.5}$$

$$b_m = -2I_m[C_m] = j(C_m - C_m^*) \tag{6.6}$$

C_m, in general, is a complex number. C_m^* represents the complex conjugate. Therefore C_m can be rewritten as

$$C_m = |C_m|e^{j\phi_m} \tag{6.7}$$

and

$$|C_m| = \sqrt{\frac{a_m^2 + b_m^2}{2}} \tag{6.8}$$

For a given periodic signal, the complex set C_m is called the frequency spectrum of the signal. The set $|C_m|$ specifies the amplitude spectrum and the set ϕ_m specifies the phase spectrum.

2. A non periodic signal can be written as a Fourier Transform.

In the case of non–periodic signals, we may think of them as arising from a periodic signal in which the period is allowed to increase without limit. The difference between successive frequency components decreases as the period increases. In the limit the frequency difference approaches zero, and the curve becomes a continuous function of frequency. The Fourier transform pair is defined as

$$x(t) = \frac{1}{2\pi}\int_{-\infty}^{\infty} X(\omega)e^{j\omega t}d\omega \tag{6.9}$$

and

$$X(\omega) = \int_{-\infty}^{\infty} x(t)e^{-j\omega t}dt \tag{6.10}$$

where $X(\omega)$ is defined as the Fourier transform of $x(t)$. As in the case of a discrete spectrum (periodic case), the Fourier transform is a complex function and may also be expressed as:

$$X(\omega) = |X(\omega)|e^{j\phi(\omega)} \tag{6.11}$$

where $|X(\omega)|$ is the amplitude spectrum and $\phi(\omega)$ is the phase spectrum.

3. It should be noted that the spectrum is discrete for a periodic signal and is continuous for non-periodic signals.

4. The Fourier transform is periodic for a discrete time series.

   The discrete signal is sampled from a continuous signal. The spectrum of a sampled data signal consists of the original spectrum plus an infinite number of translated versions of the original spectrum. These various translated functions are shifted in frequency by amounts equal to the sampling frequency and its harmonics, i.e., the spectrum consists of the components located at $0, \pm f_s, \pm 2f_s, \pm 3f_s, \cdots$, etc., and is thus periodic in the frequency domain.

   According to Shannon's sampling theorem, f_s, the sampling frequency, must be greater or equal to $2f_h$, the highest signal frequency, otherwise the spectrum will be aliased. In practice, we usually use f_s much greater than $2f_h$ (e.g., 10 times of f_h) to ensure recovery of the original signal. In the study of biological oscillators, we should try to choose the sampling frequency as high as possible to avoid distortion of the unknown high frequency components by the sampling scheme employed. For example, in our data acquisition system, the basic circadian frequency is about 0.0000116 Hz but the data is sampled at 0.00167Hz. Therefore harmonics as high as 10th order can be acquired and not distorted.

5. The Fast Fourier Transform (FFT).

   The FFT is neither a variant of, nor an alternative to, the Discrete Fourier transform described above. It is an algorithm (or rather a related class of algorithms) for computing the discrete Fourier transform of a data series at all of the Fourier frequencies, using relatively few arithmetic operations. The background of the Fast Fourier Transform and its computational advantage

can be found in many books[40]. In the appendix we describe the algorithm used in this research to carry out harmonic analysis.

The Fourier analysis method, as discussed above, is basically used to decompose an arbitrary set of data points into periodic components whether or not the data appear periodic.

6.3 Data Pre–Processing: Zero Padding, Windowing and Segmentation

Experimental data, although they may appear to be non-periodic or almost periodic, do in fact contain interesting periodic components. The Fourier analysis method is the most practical method for detecting such components.

There are several important factors which have to be considered for performing Fourier analysis on practical data. First is the finite length of the data records. No estimation can be made for lags longer than the record. The finite length may not exactly fit the transforming length desired, and the short length of the transformation will cause the Fourier transform to produce unsmooth, imprecise data and frequency component leakage. The leakage effect is a spreading of the spectral components away from the correct frequency, resulting in an undesirable modification of the total spectrum.[40, pages 284–285]

6.3.1 Zero padding

The transformation length will determine the precision of the transformed frequency. For example, the sampling rate in collecting circadian temperature

data in our experimental system is 0.00167 Hz (6 samples/hour), so the transformed frequency is from 0 to 0.000833 Hz. If we use 1024 points for the Fourier transform, the frequency interval is 0.0000008134 Hz, but it will be reduced to 0.00000000509Hz if 16384 points are used. Usually the length of the data is less than the number of points required by the FFT. To meet the transformation length requirement, we can zero pad the data record, i.e., build an n (n=transformation point) dimensional data set with the first m points equal to the data and the remainder equal to zero. This procedure is called zero padding. [8]

6.3.2 Windowing

Before we transform the time series to the frequency domain, we have to first terminate the finite time series by multiplying it by a finite width "window". The selection of a proper window can result in the Fourier transform being smooth and having reduced leakage.

In the time domain, windowing is accomplished by multiplying the infinite time series $C_0(t)$ by a finite window function $w(t)$

$$c(t) = w(t)C_0(t) \tag{6.12}$$

We may regard $w(t)$ as a window of variable transmission which modifies the value of the infinite time series $C_0(t)$ differently for different lags. It is therefore natural to call $w(t)$ a lag window.

For any lag window which meets the conditions stated above, $c(t)$ is calculable from the data. Further, it is clear that $c(t) = 0$ for the data points outside of $C_0(t)$. Because $c(t)$ is defined for all values of t, it has a perfectly defined Fourier transform

$P(f)$. As pointed out before, we should pad zeros in the real data record to meet the requirement of transform length.

Different windows have different effects on the transform. However, all of the window functions are even functions of time when they are centered at the origin. We will now consider some common window functions.

1. **Rectangular Window.** The rectangular window is considered primarily as a basis for reference in studying other functions. The rectangular function is simply

$$\begin{aligned} w(t) &= 1 \qquad , for |t| < \tau/2 \\ w(t) &= 0 \qquad , elsewhere. \end{aligned} \tag{6.13}$$

The Fourier transform is

$$W(f) = \frac{\tau sin(\pi f \tau)}{\pi f \tau} \tag{6.14}$$

The window function here has a rectangular shape. τ is the window width, and $W(f)$ is the Fourier transform which is a sinc function. The rectangular window converges at a rate of $1/f$ for large f. This window has a simple form and realization in computing, but it has difficulties in leakage and convergence control which cause some large distortions of correct spectral function.

Since the problem mentioned above is caused by the abrupt termination of the time series, other windows with modified shapes have been developed.

2. **Hanning Window.** The Hanning, or cosine-squared window function is defined as

$$w(t) = cos^2\frac{\pi t}{\tau} = 0.5(1 + cos\frac{2\pi t}{\tau}) \quad , |t| \leq \tau/2$$

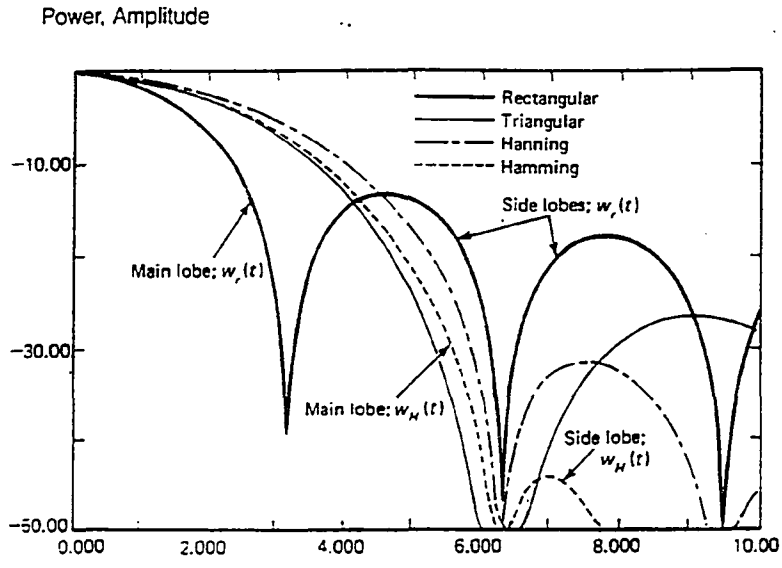

Figure 6.2: Decibel amplitude responses of four different windows.

$$w(t) = 0 \qquad ,elsewhere. \tag{6.15}$$

and its Fourier transform is

$$W(f) = \frac{\tau}{2}\frac{sin\pi f\tau}{\pi f\tau}[\frac{1}{1-(f\tau)^2}] \tag{6.16}$$

3. **Hamming Window.** The Hamming window function is a modification of the Hanning window which is defined as

$$\begin{aligned} w(t) &= 0.54 + 0.46cos\frac{2\pi t}{\tau} \quad ,|t| \leq \tau/2 \\ w(t) &= 0 \qquad ,elsewhere. \end{aligned} \tag{6.17}$$

and has Fourier transform:

$$W(f) = \frac{\tau sin\pi f\tau}{\pi f\tau}[\frac{0.54 - 0.08(f\tau)^2}{1-(f\tau)^2}] \tag{6.18}$$

Practically, Hanning and Hamming windows are two very widely used window functions, which round the data at the two ends using a cosine function. Fig.6.2

shows the amplitude responses in db of four different windows where we can see the effects of different windows on the main lobes and side lobes of the frequency responses. In general the spectrum of a window function should have a main lobe which is as narrow as possible and side lobes as small as possible relative to the main lobe. Fig.6.2 shows that the Hanning and Hamming windows have much better performance than the other two windows. In our Fourier analysis, the Hamming window is the most often used window for our experimental and model data transformation. This type of window gives satisfactory smoothing results as well as easy programming and acceptable computing time.

6.3.3 Data Segmentation

One of the techniques repeatedly suggested is to divide the time series $x(t)$ into segments, either overlapping or contiguous, and estimate features of the spectrum from the average spectra of the individual segments. Blackman and Tukey [41] suggested that the data be divided into several segments, and that direct spectral estimates be made using each of the short time series. A smoothed estimate can then be formed by averaging the individual spectral estimates. Davis [16] describes a commonly used method known as secondary analysis of the periodogram for improving the accuracy of frequency estimates of harmonics. The time series $x(t)$ is broken into M segments of equal length $T = (N-1)/M$ such that for each nonoverlapped segmentation $x_j(t)$

$$x_j(t)_{t=0}^{T} = x((j-1)T + t)_{t=0}^{T} \quad , j = 1, 2, \cdots, M \tag{6.19}$$

Each segmentation consists of M points of the original data set $x(t)$. The discrete Fourier transforms $X_j(w)$ of the segments $x_j(t)_{t=0}^{T}$ are computed at the estimated

frequency ω_0 of some harmonics in the data.

$$X_j(\omega_0) = \sum_{t=0}^{T} e^{-i\omega_0 t} x_j(t) \tag{6.20}$$

If the data $x(t)$ consists of a complex sinusoid of frequency ω_T plus noise $n(t)$, then

$$x(t) = Ae^{i\omega_T t} + n(t) \tag{6.21}$$

and

$$X_j(\omega_0) = Ae^{i\omega_T(j-1)T}[\sum_{t=0}^{T} e^{i(\omega_T-\omega_0)t}] + [\sum_{t=0}^{T} e^{i\omega_0 t} n(t)], j = 1, 2, \cdots, M \tag{6.22}$$

A least squares fit of a straight line to the phase of $X_j(\omega_0)$ as a function of j should have slope $T\omega_T$, allowing ω_T to be more accurately estimated. The average of M spectra will enhance the signal part in Eq.6.21 because they are correlated and reduce the noise part because they are uncorrelated.

We applied the segmentation method to spectral analyses as well as bispectrum analysis which will be discussed in chapter 8. This method indeed smooths and increases the degrees of freedom of the data. We will illustrate these effects in chapter 8.

6.4 Spectra of the Experimental Data

In chapter 2, we introduced the general aspects of circadian rhythm data in the time and frequency domains, which gave us information about experimental circadian data. In chapter 4, we introduced our models of circadian rhythms which were based on the understanding of these experimental data. In this section, we will further analyze the experimental data emphasizing their frequency characteristics.

As indicated in previous sections, the spectral function is a helpful tool for exploring the details of the circadian system and provides fundamental information from which to build the models. The Fourier transform of a signal can be expanded into the sum of an infinite number of harmonically related sine and cosine terms which enables us to see directly the frequency components present in circadian signals. The Fast Fourier transform used in this research implements the Sande-Turky radix-2 FFT algorithm. The computer program can be found in the Appendix. As we mentioned earlier, the spectra of circadian rhythms from different subjects or species, or from the same subject under different conditions, may have different structures. Therefore we need to individually examine the spectra of each subject or species carefully. A 16,384 point FFT was used in our Fourier transform program to yield the best smoothing results. The sampling frequency used in our data acquisition system is 6/hour. Therefore the frequency range of the resulting spectra is from 0 to $8.33 * 10^{-4} Hz$ (The maximum frequency equals 1/2 of the sampling frequency.) which corresponds to a minimum detectable harmonic period of 20 minutes.

Fig.6.3 to Fig.6.6 show the spectra transformed from circadian temperature rhythms of 4 monkeys under a free running condition. The results of each subject includes spectra from four different time episodes.

Fig.6.3 shows the spectra from Monkey 10 in a free running condition. All four sections show that the fundamental period is

$$\frac{16384}{6(111-1)} = 24.82 hours.$$

However the harmonic structure in these four time episodes are different. Fig.6.3(a) shows a relatively high 2nd harmonic, whose amplitude is about 31 percent of that

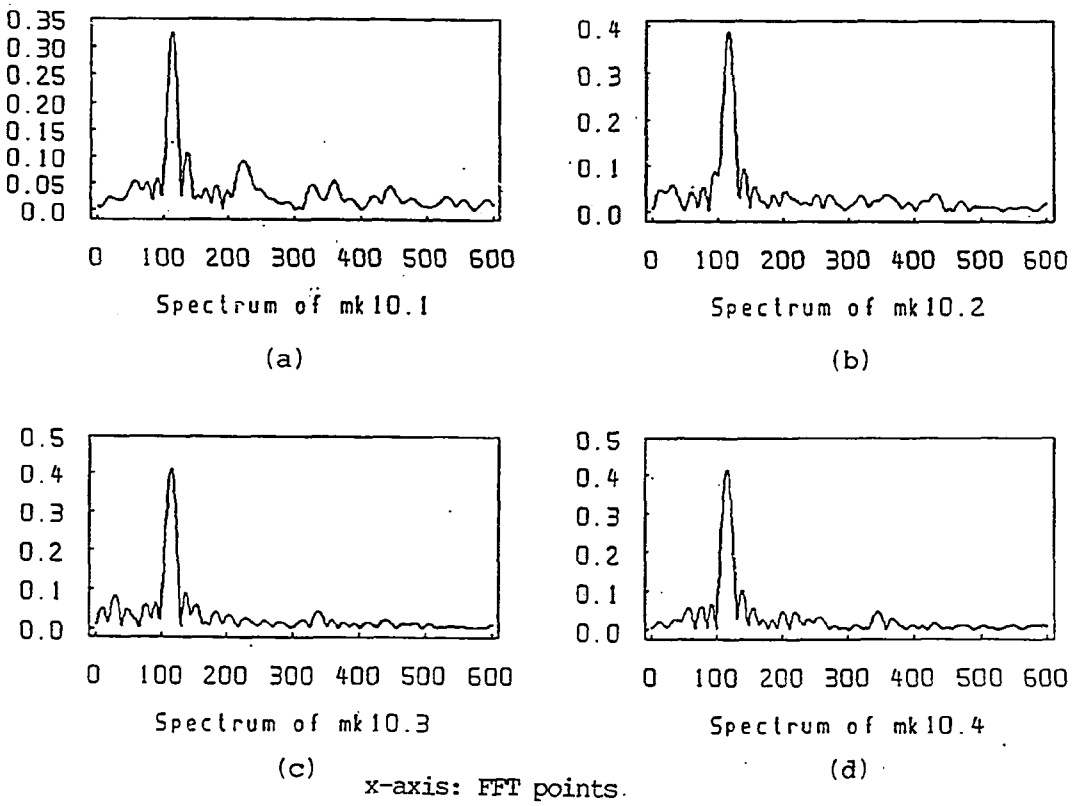

Figure 6.3: *Spectral functions of monkey 10.*

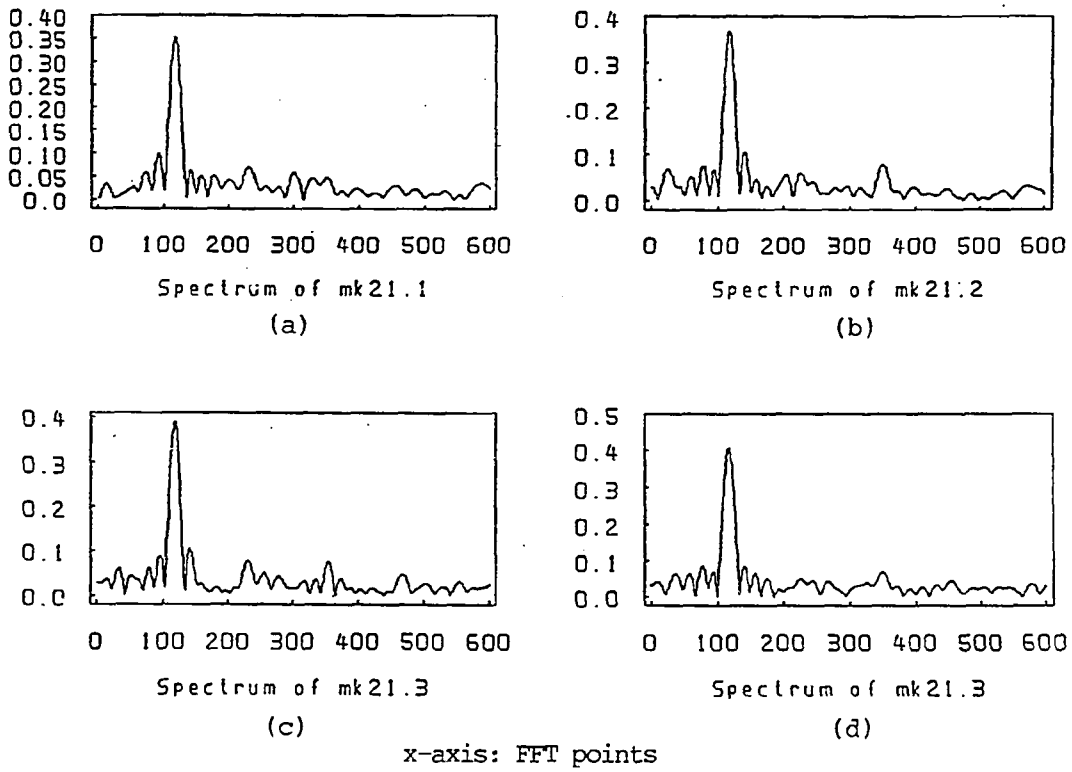

Figure 6.4: *Spectral functions of monkey 21.*

of the fundamental, while the 3rd harmonic is spread. The 2nd harmonic in (c) and (d) is not obvious, but the 3rd harmonic is quite evident.

Fig.6.4 shows the spectrum from Monkey 21, also in a free running condition. The fundamental period of Monkey 21 is at about

$$\frac{16384}{6(113-1)} = 24.32 hours.$$

(a) and (c) show almost the same amplitude level of 2nd and 3rd harmonics, while (b) and (d) shows a relatively clear 3rd harmonic.

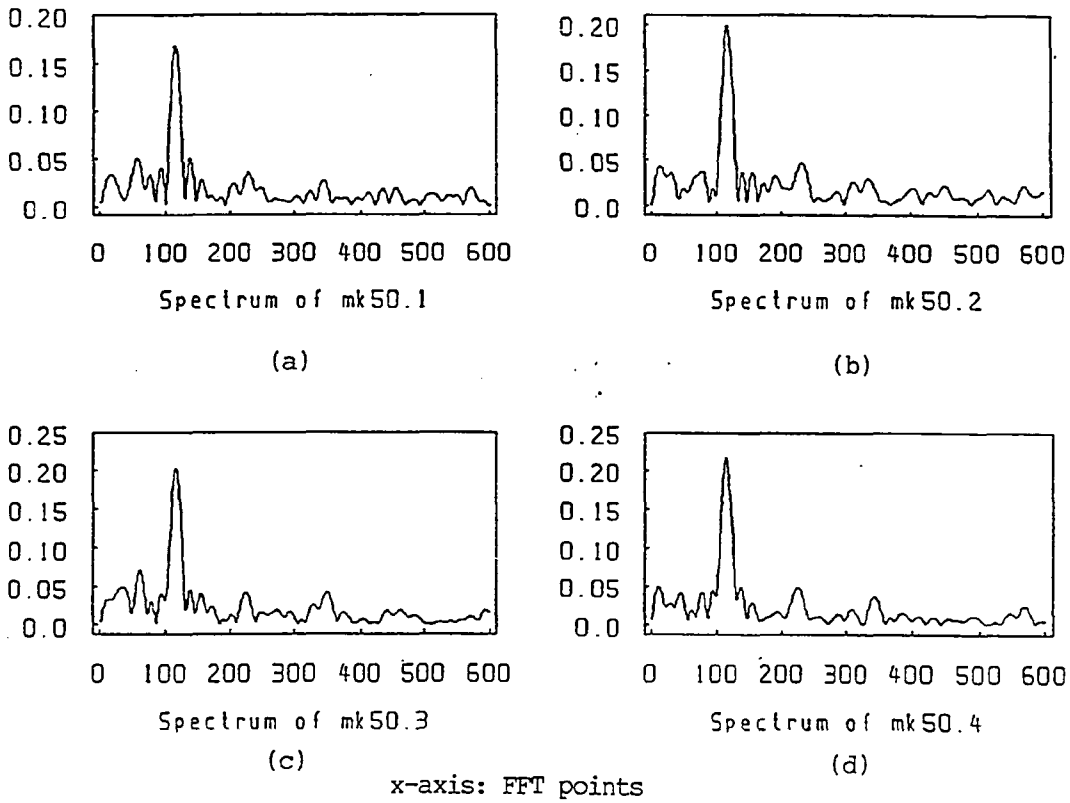

Figure 6.5: *Spectral functions of monkey 50.*

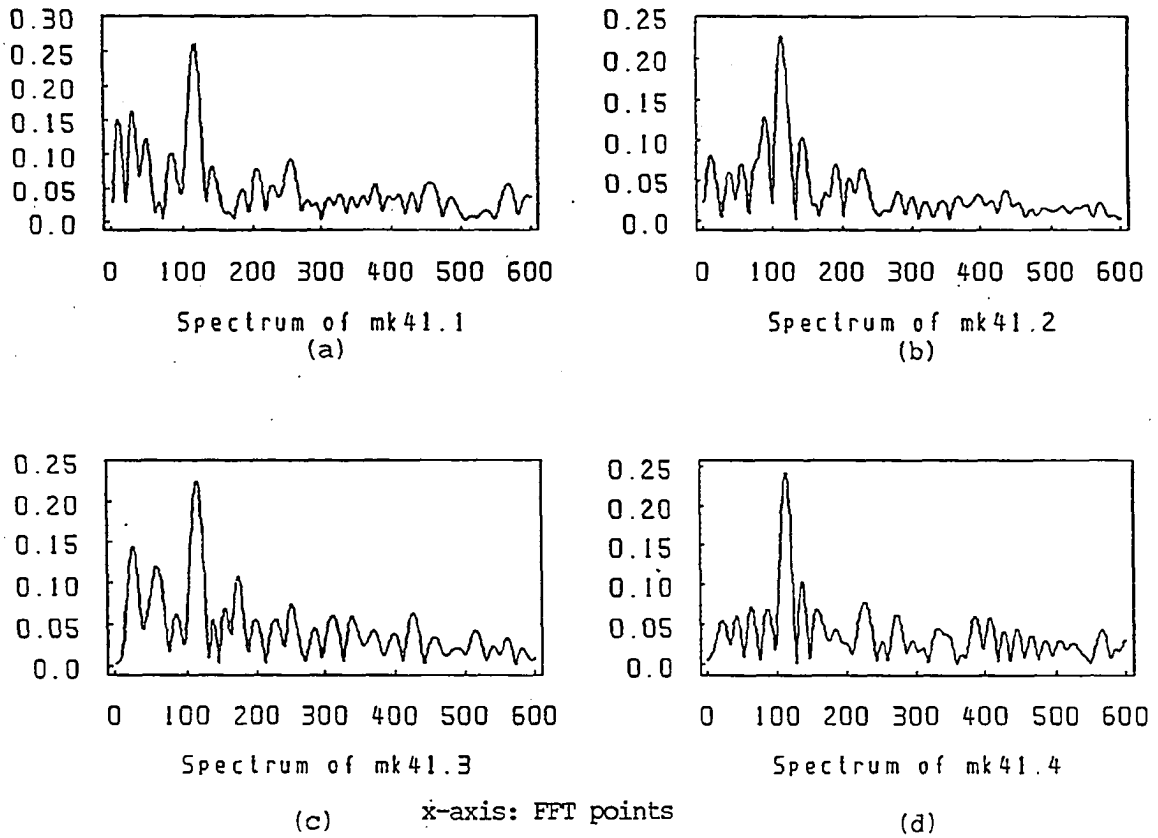

Figure 6.6: *Spectral functions of monkey 41.*

Fig.6.5 shows the spectrum from Monkey 50 who is in a free running condition. The fundamental period is 24.32 hours. All four sections show clear 2nd and 3rd harmonic structures. In data mk 50.3 and mk 50.4, the 2nd and 3rd harmonics have almost the same amplitude level. Also, low frequency components appeared in fig.6.5 (a) and (c). These frequency components show the low frequency trend included in the data.

Fig.6.6 shows the spectral function from Monkey 41 who is free running. The 2nd and 3rd harmonic structure of this data set is not clear as in the other data

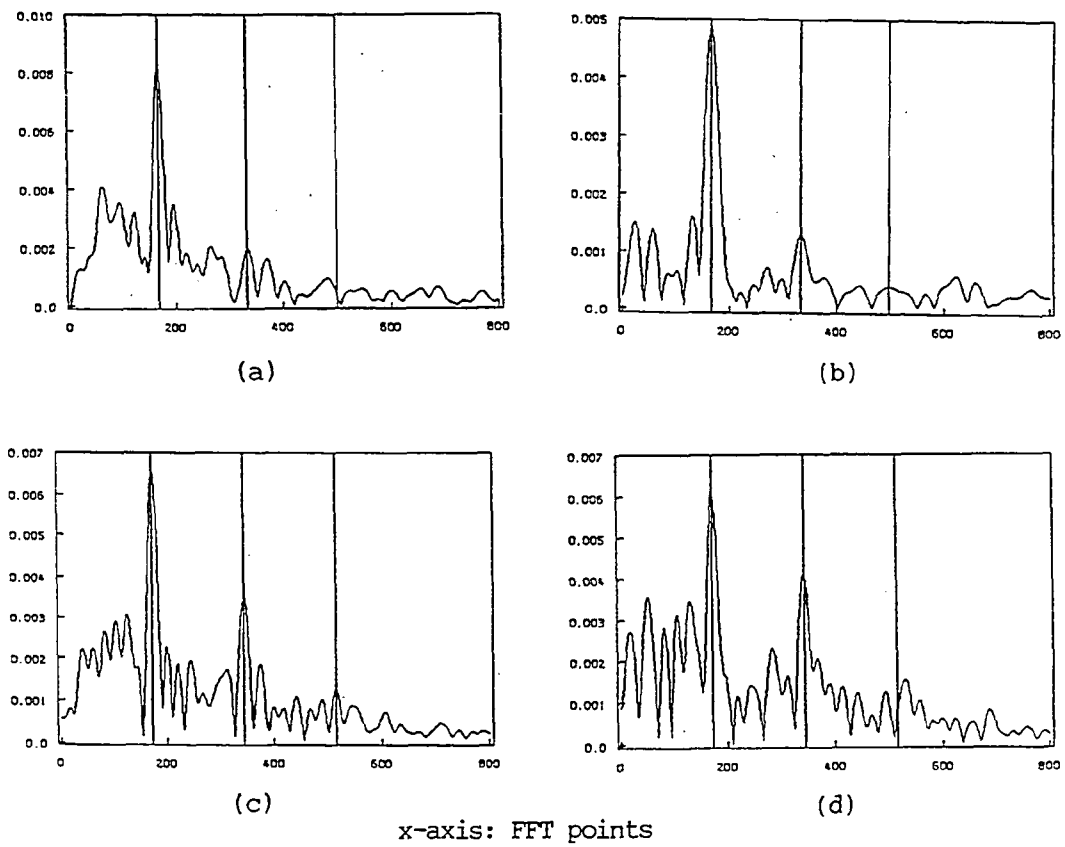

Figure 6.7: *Spectral functions of rat1.*

sets. Except for fig.6.6 (d), the other 3 spectra seem spread, and also show low frequency components with a relatively high level.

Fig.6.7 and 6.8 shows the spectra from the temperature records of two rats. The sampling frequency of these data is 4/hour. 16,384 points were used for the Fourier transform. In fig.6.7, the peak of the fundamental frequency is

$$\frac{16384}{4(166-1)} = 24.82 hours$$

Three vertical lines were drawn at exactly the estimated fundamental, 2nd and 3rd harmonic positions. All four sections of fig.6.7 show a very clear 2nd harmonic

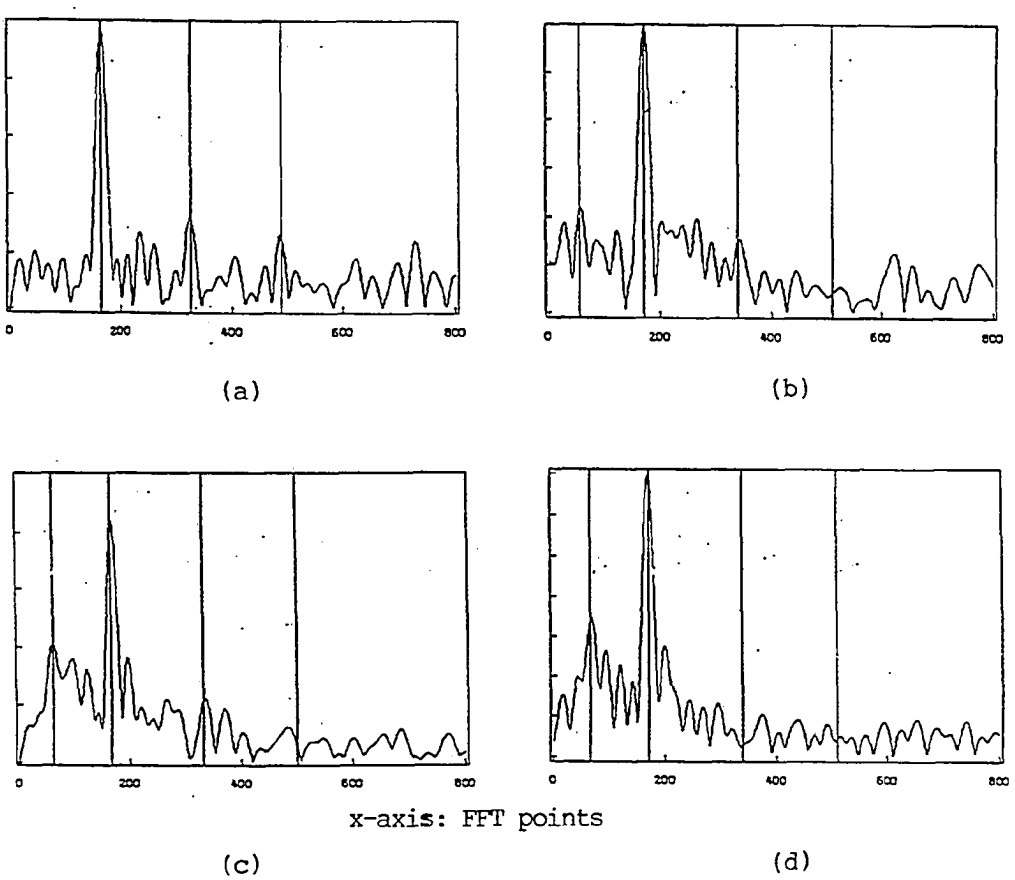

Figure 6.8: *Spectral functions of rat2.*

structure. Particularly, in (c) and (d) the level of 2nd harmonic is very high, about 2/3 that of the fundamental. The 3rd harmonics are not clear except for (c). These four figures also demonstrate the low frequency components.

Fig.6.8 shows 4 spectra from rat2. The fundamental frequency of (a) and (b) is at

$$\frac{16384}{4(166-1)} = 24.82 hours$$

while (c) and (d) is at

$$\frac{16384}{4(170-1)} = 24.23 hours$$

The 2nd harmonic of this data set is not as high as we see in rat1 (fig.6.7). Only (a) shows relatively clear 2nd and 3rd harmonics. In this data set, the frequency of the low frequency components was calculated. Their periods are respectively at

(b): $16384/(55-1)/4 = 75$ hours;

(c): $16384/(60-1)/4 = 69.42$ hours;

(d): $16384/(65-1)/4 = 64$ hours.

From examination of these experimental spectra under free running conditions, we can conclude:

1. The free running period of the circadian temperature rhythm is very near 24 hours. This is the dominant fundamental frequency in the system.
2. The 2nd, 3rd and even higher harmonics exist in the circadian rhythm. The amplitude of these harmonics vary in different subjects or at different time periods in the same subject.
3. Some low frequency components exist in the free-running spectra.

6.5 Spectral Approach in Modeling

As we mentioned at the beginning of this chapter and we have seen from the experimental data, spectral analysis is one of the important characterizations of circadian rhythms, and is also a powerful tool for comparing the model with measured data. In chapter 4, we introduced several models. If we review the frequency characteristics of these models, we can see how the models fit the experimental data in the

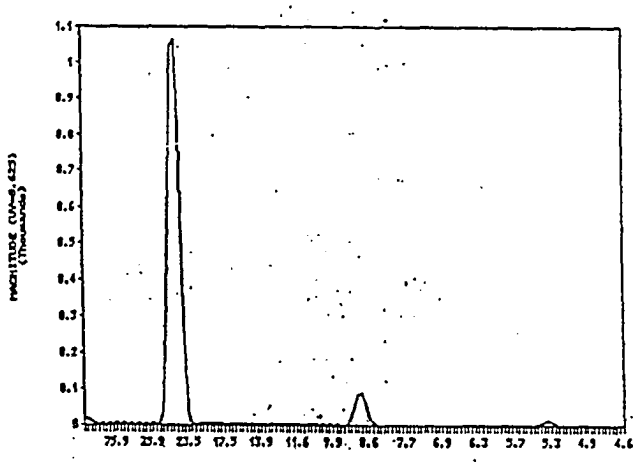

Figure 6.9: *The spectrum of single Van der Pol oscillator model.*

frequency domain.

1. The single Van der Pol oscillator model is the first model we used to simulate the circadian rhythms. Fig.6.9 shows the spectrum of this model. As we discussed in chapter 4, this model has odd harmonic frequency components, i.e., fundamental, 3rd harmonic, 5th harmonic, $\cdots$, etc. The amplitudes of the harmonics are related to the nonlinearity of the model. Therefore the level of harmonics can be adjusted by changing the degree of nonlinearity. From the spectral point of view, we can see that this simple model can be used to simulate those circadian rhythms with a small or zero level of 2nd harmonic. For subjects having high 2nd harmonic levels, this model will generate substantial errors.

2. To reflect the presence of the 2nd harmonic, we introduced the coupled Van der Pol oscillator model. The 2nd harmonic frequency component represents the bimodality of the circadian rhythm which is a very important feature

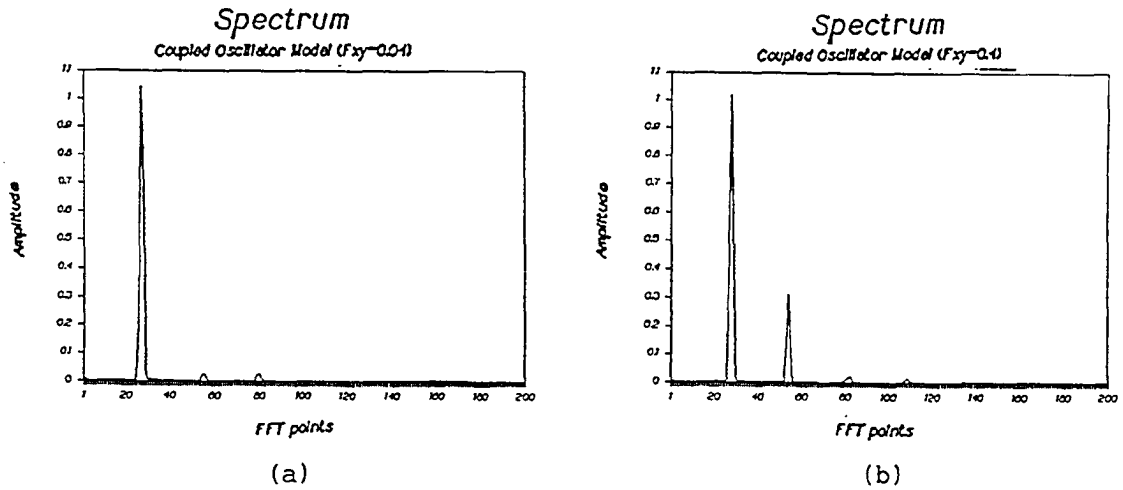

Figure 6.10: *Spectra of velocity coupled oscillator model with different coupling coefficient. a)* $F_{xy} = 0.04$, *b)* $F_{xy} = 0.4$.

of the system. In the spectral analysis of the experimental data, we have seen this frequency component in a series of spectra. We also noticed that the level of the 2nd harmonic varied with different subjects. Therefore we concluded that the 2nd harmonic component has to be inserted in the model, but its level also should be adjustable. The velocity coupled oscillator model basically meets this requirement. The coupling coefficient in the model can be adjusted to get the proper level of the 2nd harmonic. The spectrum of the velocity coupled Van der Pol oscillator model includes fundamental, 2nd, 3rd and higher harmonic frequency components. The level of the 2nd harmonic in this model can be adjusted to correspond to different experimental data. Fig.6.10 shows two spectra of velocity coupled oscillators with two different coupling coefficients.

3. The three dimensional coupled oscillator model was designed to more closely match frequency characteristics of the experimental data. The two dimen-

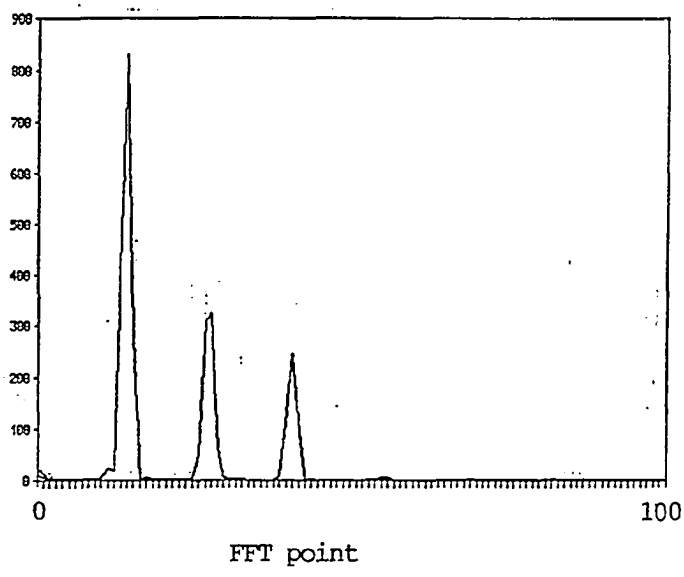

Figure 6.11: The spectrum of a 3 dimensional coupled oscillator model.

sional coupled oscillator model basically has a spectral structure similar to the experimental data, but the 3rd harmonic component is controlled by the nonlinearity of the fundamental oscillator and can therefore not be independently varied. In the experimental data, we have seen that the 3rd harmonic level is sometimes even higher than the 2nd harmonic. A three coupled oscillator model will solve this problem. The level of the three main frequency components can be adjusted independently. The frequency structure of this model introduced more higher harmonics which seemed to better approximate the real "expanded" spectrum. Fig.6.11 shows the spectrum of this model. The problem with this model is its complexity. Six coupling coefficients between the three oscillators need to be adjusted, compared to only two existing in the two dimensional coupled oscillator model. The physiological significance of this model also needs to be further explored.

The examination of spectra of other models, including the modified Van der Pol oscillator model, Kronauer et.al's coupled oscillator model and Pavlidis's biological oscillator model demonstrate differences in their frequency spectra. For example, the spectral analysis of Kronauer et al's model demonstrates that the frequency components of this model include no 2nd harmonic which we think is necessary to represent the bimodality of the system. Therefore, a mathematical model used to approximate the circadian rhythms should correspond to both time series and frequency spectrum characteristics. Spectral analysis should be one of the most important criteria used to build a model for circadian rhythms.

Chapter 7

Effects of Stimulus on Circadian Rhythms

7.1 Introduction

Circadian rhythms provide a daily "program" for physiological and behavioral processes such as sleep-wake, body temperature, and hormonal secretion. The circadian oscillator continues to oscillate in the absence of environmental input, but can be entrained by *periodic inputs*, especially light, at periods near the natural period (near 24 hr.) of the endogenous oscillator. Generally, two possible external stimuli, periodic and non-periodic, could be applied to a circadian rhythm.

In previous chapters, we have shown that a circadian system can be modeled as a self-exciting nonlinear oscillator, e.g., a Van der Pol type oscillator. We shall show here that this type of oscillator can be entrained by a driving stimulus at the appropriate frequency. During entrainment, the self-exciting oscillator adopts the period of the driving *periodic* stimulus and maintains a particular phase relation with the entraining cycle. In natural conditions, the circadian oscillator is entrained

to the 24 hr day-night cycle so that the individual's internal, biological time is set appropriately to the local time.

The periodic stimulus applied may cause the oscillator either to be entrained or to be in an "almost periodic" mode. The phenomenon of frequency entrainment occurs when a periodic force is applied to a system whose free oscillation is of the self-excited type. A typical and important case is the system governed by Van der Pol's equation with an additional "forcing" term for periodic excitation. The frequency of the self-excited oscillation falls into synchronism with the driving frequency, provided the two frequencies are not too different. If their difference is large enough, one may expect the occurrence of an almost periodic oscillation; in this mode, a beat oscillation may result. However, the entrainment of frequency still occurs when the ratio between the natural frequency of the self-excited oscillation and the driving frequency is in the neighborhood of an integer (different from unity) or a fraction of an integer. Under this condition, the natural frequency of the system is entrained by a frequency which is an integral multiple or submultiple of the driving frequency. We call such entrainments higher-harmonic and subharmonic entrainments respectively. In contrast with these types of entrainment, the phenomenon of synchronization, as mentioned earlier, will be referred to as harmonic entrainment.

A nonperiodic stimulus will cause a dynamic process. This type of stimulus acts on the oscillator transiently; therefore it will lead to a temporary change in the amplitude, frequency or the phase of the oscillator. Under certain circumstances, the circadian oscillator can be exposed to abrupt changes in the phase of the entraining stimulus. The most familiar practical example is air travel across time zones. This phase shift produced by traveling to a new local time is often

accompanied by "jet lag." Formally, the change to a new environmental time represents a *nonperiodic* stimulus to the circadian system, which can lead to temporary changes in the amplitude, frequency or the phase of the oscillator. Studies of biological processes during phase shifts have often shown complicated patterns of transient behavior. One group has suggested that these complicated patterns are indicative of the interaction of two competing processes[25], Our study shows this is substantially a frequency transient process which we will discuss in section 7.3.

In practice, the non-periodic stimulus has already been applied to human circadian rhythms adjustment. As we introduced in chapter 1, Dr.Czeisler and his team at Harvard Medical School have some successful practical examples of using light pulses to treat sleep disorders. Scientists even speculate whether long distance travelers should receive light treatments before leaving home in preparation for arrival in a new time zone. It may also be possible to equip airplanes with special lights so passengers' biological clock are reset to new time zones while they fly.[15]

We investigated the entrainment effect as well as the transient behavior of our model following various periodic and nonperiodic stimuli in order to explore the dynamics following various stimuli. In this chapter we will first discuss the effects of various types of periodic stimuli on a Van der Pol type model. Then the process of phase shift will be modeled and the mechanism of frequency transition will be explored by applying an experimentally designed nonperiodic stimulus to the model.

As we introduced in chapter 6, the spectral function is a very helpful tool in determining the characteristics of a circadian system. This is also true in the dynamic case. We used the spectral function as one of the main tools to deter-

mine the entrainment characteristics. Spectral analysis is also developed for the purpose of dynamic analysis and is combined with zero-crossing detection and frequency demodulation techniques to explore the dynamic transition process. Raster plotting, as we mentioned in chapter 5, is another useful tool for determining the entrainment quality.

7.2 Frequency Entrainment Analysis

When a linear oscillatory system is driven by an external periodic input, its response contains both frequency components. This is also, in general, true of nonlinear oscillators. However, if the external frequency is close to the characteristic frequency of the oscillator, then it is possible for the oscillator to oscillate at the external frequency only. This phenomenon is known as entrainment or synchronization.

To understand the phenomenon of entrainment, we use our single Van der Pol type circadian rhythm model as an example. With an external force acting on the system, this model is described by the following nonlinear differential equation:

$$k^2\frac{d^2X}{dt^2} + \mu(X^2 - 1)\frac{dX}{dt} + \omega^2 X = E(t) \tag{7.1}$$

Here μ is a parameter denoting the degree of *nonlinearity* of the system. k and ω are the fixed time parameter and normalized frequency parameter respectively, as we defined in Chapter 4. $E(t)$ is the external periodic stimulus or "forcing function" applied to the system which has the following form,

$$E(t) = E\cos\omega_e t \tag{7.2}$$

In Eq.7.2, E is the amplitude of the stimulus. It is assumed that the frequency difference between the natural frequency of the system and the external frequency $\Delta\omega$, i.e., $\omega_0 - \omega_e$, is considered to be relatively small.

If the nonlinear parameter μ is small, we can approximate it by the solution for $\mu \approx 0$:

$$x(t) = Asin\omega_0 t + Bcos\omega_0 t + \frac{E}{\omega_0^2 - \omega_e^2} cos\omega_e t \tag{7.3}$$

where A and B are constants depending on the initial conditions. We can see that the solution x(t) will be dominated by the $cos\omega_e t$ term if

E, the amplitude of the external stimulus is relatively high,

and / or, the frequency difference, $\Delta\omega$ is relatively small.

In the case of the nonlinear system, i.e., μ is not zero, there exists a range of E and a range of the absolute difference in frequencies $|\Delta\omega| = |\omega_0 - \omega_e|$ such that the output of the system contains only the frequency ω_e. Figure 7.1 shows a typical example of this range. Entrainment occurs in the shaded part of the plane.

If the values of E and $\Delta\omega$ are not in the entrainment range but close to that range, then there will be a variety of possible responses, usually characterized by the fact that both frequencies are present.

If ω_e is close to an integral multiple of ω_0, then it is possible to have subharmonic entrainment at the corresponding fraction of ω_e. The subharmonic entrainment is much weaker than the direct entrainment. One example of subharmonic

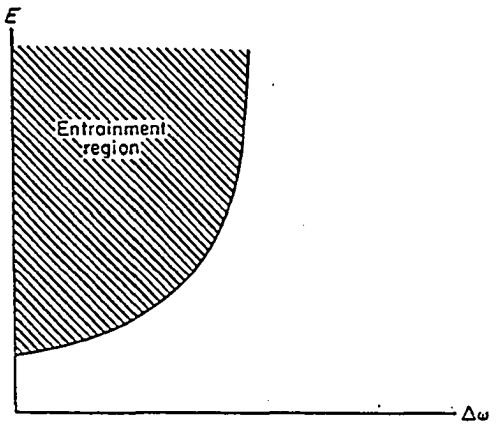

Figure 7.1: *Entrainment range in a Van der Pol oscillator (with $\mu = 0.1$)*

entrainment is shown in section 4.7 where we discussed the subharmonic entrainment effect in the two dimensional coupled oscillator model.

In the case that $\mu = 0$ and E is very small, i.e., the case of a linear system with small stimulus (Eq.7.3), the $cos\omega_e t$ term is small and therefore, the phase of the oscillation is minimally influenced by the external input. In the nonlinear system, the larger the nonlinearity, the easier the system can be entrained. Therefore the nonlinearity of the system is sometimes called the "stiffness" of the system.

The quality of the entrainment is mainly determined by three interacting properties:

1. The frequency of the periodic stimulus;
2. The amplitude of the periodic stimulus;
3. The nonlinearity of the system.

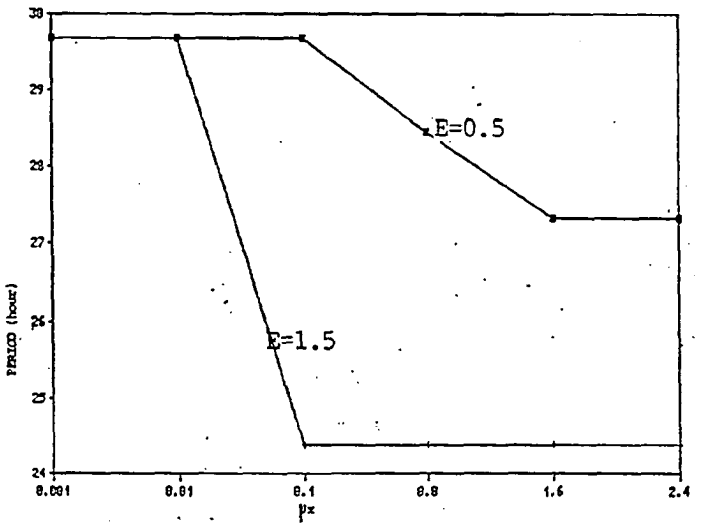

Figure 7.2: *Fundamental frequency of the system with the stimulus of two different amplitude.*

The oscillating frequencies following a periodic stimulus for different applied frequencies and amplitudes were measured on our single Van der Pol type model for different nonlinearity. Figure 7.2 shows the fundamental frequency of the system for different μ following the application of a stimulus with two different amplitudes. The results of Fig.7.2 were obtained from a series of spectra. The external force applied has the form of $Ecos\omega_e t$ where $\omega_e = 2\pi/T_e$ whose T_e is 24hr.

In this trial, the original system period is set at $T_x = 30hr$. E, the amplitude of the applied stimulus was varied from 0.5 to 1.5. It can be seen from this result that the system is never completely entrained when $E = 0.5$. Completely as defined here means that the period difference between the stimulus and system is less than one hour.

However, when E is kept at 0.5, there are some differences for different μs. The difference between the period of external stimulus and the period of the system

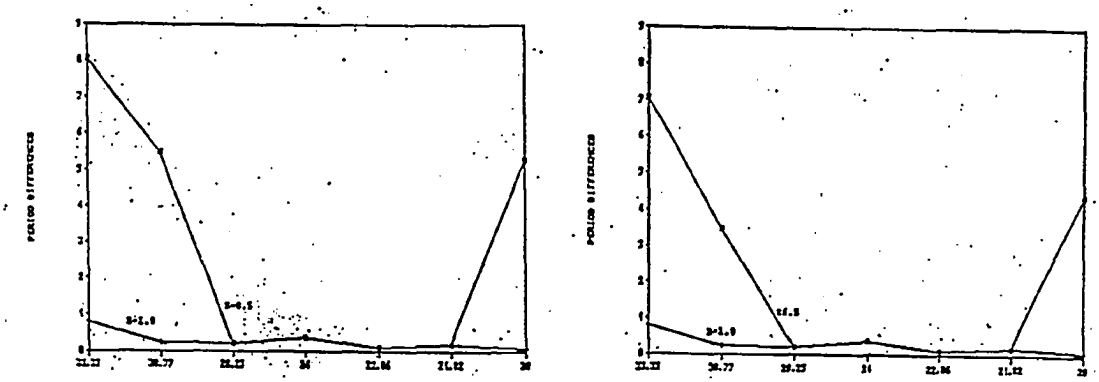

(a) (μ=0.2) (b) (μ=0.8)

x-axis: The period of the stimulus
y-axis: The period difference between
the stimulus and the model

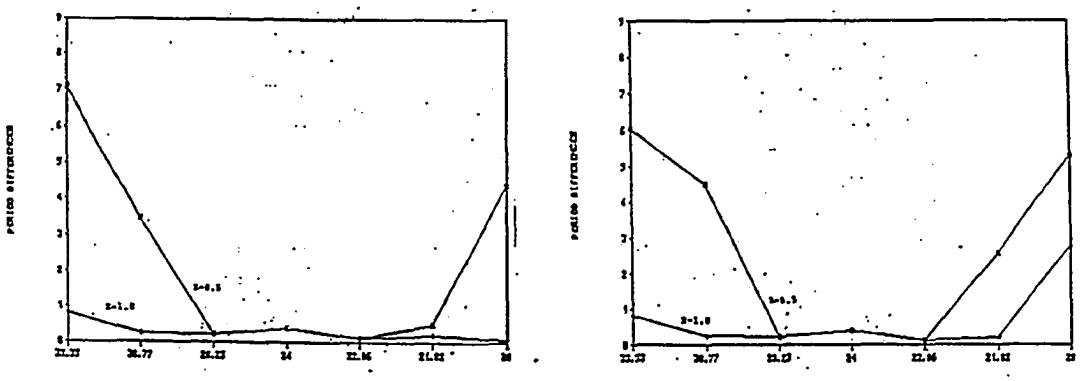

(c) (μ=1.6) (d) (μ=2.4)

Figure 7.3: *The period difference of the Van der Pol type model with the stimulus of varying frequency.*

has dropped from 5.5 hr for $\mu = 0.1$ down to 2 hr for $\mu > 1.6$;

The period of the system is entrained to 24.3 hr when $E = 1.5$ and $\mu > 0.1$. When $\mu < 0.01$, the system is unentrained and the period is 29.5 hr the same as the case of $E = 0.5$.

This result reveals there is a lower stimulus amplitude threshold level for entrainment. However, this threshold level varies with values of μ and $\Delta\omega$ as we shall show next.

In the second trial, we designed the model with free-running period of 25 hr., and the period of the stimulus varying from 33 hr to 20 hr, for a range of $\Delta\omega$ from $\Delta\omega_1 = 33 - 25 = +8hr$ to $\Delta\omega_2 = 20 - 25 = -5hr$. Fig 7.3 shows the period difference between the stimulus period and the natural period. The figure shows the cases with $\mu = 0.2$, $\mu = 0.8$, $\mu = 1.6$ and $\mu = 2.4$.

In Fig7.3 (a)-(c), with $E = 1.0$ and $\mu > 0.1$, we can see that the period difference is less than 1 hr and therefore the system is entrained in the stimulus period range from 21.82 hr to 33.33 hr.

Also In Fig7.3 (a)-(c), With $E = 0.5$, the entrainment occurs in the range of stimulus period between 21.82 hr and 28.23 hr for $\mu = 0.2$ to 1.6. Therefore in the case of $E = 0.5$, the $|\Delta\omega|$ is approximately equal to 3.2 hr for entrainment.

Again, we can see the effect of the nonlinearity parameter μ. In the case of stimulus period = 33.33 hr, the period difference is 8 hr when $\mu = 0.2$ and becomes 6hr when $\mu = 2.4$. Generally, the system will become easier to be entrained as μ increases. However, as we discussed in chapter 4, the system period increases as the nonlinearity factor μ increases. This increase should be taken in account for computing the entrainment range, e.g., fig.7.3(d) demonstrates that when $\mu = 2.4$ the entrainment range is decreased toward the low period direction. The reason is that the original system period has already changed with the increase of μ.

The effect of nonlinearity on entrainment should be always taken into account. As we discussed in chapter 4, the Van der Pol oscillator with small μ is stiff to its natural frequency, like a linear system. For large μ, the natural frequency is shifted toward the lower direction which makes the entrainment more complicated.

Spectral analysis is primarily used here to determine the entrainment quality. In the single Van der Pol type model case, the spectrum of an entrained oscillator generally has the same structure as the free-running oscillator except for the different position of the fundamental, third harmonic, etc. The spectrum becomes much different in the unentrained case, where both the natural frequency of the system and external frequency co-exist. In this case the spectrum becomes "richer" in harmonics and more complicated.

To understand the influence of nonlinearity on entrainment from the spectra, Fig.7.4 shows four spectra from the same system under the same stimulus except for different values of nonlinearity parameter μ. The system period = 30 hr, the stimulus $E = 0.5$ and period, $T_e = 24hr$.

1. When $\mu = 0.01$, the system is unentrained. Both frequency components exist in the system. This can be seen from fig.7.4(a). The two peaks are at about 30 hr and 24 hr.

2. In fig.7.4(b), when $\mu = 0.1$, the system is still unentrained but the structure undergoes some changes. The relative amplitude of the system and entraining period peaks become reversed from $\mu = 0.01$ which reveals that the system period changes toward the entraining period.

3. In fig.7.4(c), When $\mu = 0.8$, the system is basically entrained, but the main frequency component has moved to about 28 hr. The 24 hr component is still present.

4. In fig.7.4(d), when $\mu = 1.6$, the system is entrained, the main frequency peak adopts the period of 26 hr, intermediate between the original system frequency and the stimulus frequency.

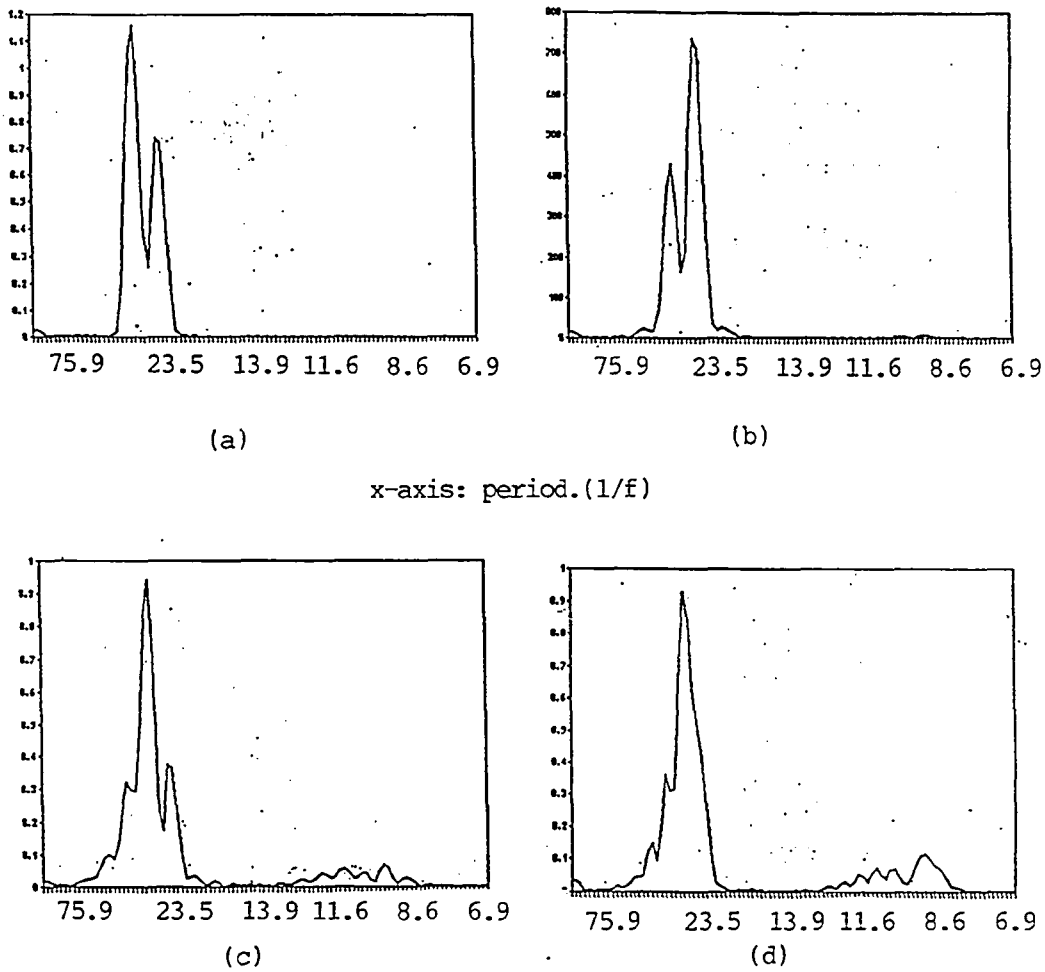

Figure 7.4: *Spectra of Van der Pol type model with different μ under external stimulus. a) $\mu = 0.01$. b) $\mu = 0.1$. c)$\mu = 0.8$. d)$\mu = 1.6$.*

The phenomenon here is similar to the phenomenon we discussed in the coupled oscillator case. In chapter 4, we discussed the spectra of direct coupled systems. In the case of 1/3 entrainment between two oscillators in the system, the spectrum becomes "clear" (only the fundamental and harmonic frequency components are present in the spectrum), while in the unentrained case, the spectrum exhibits complicated patterns as we see here in the case where a stimulus is applied but the system is not completely entrained.

7.3 Phase Shift by Nonperiodic Stimulus

Non-periodic stimuli will cause a temporary change in the amplitude, frequency or phase of the system. Light pulses are often applied to the circadian system as a effective tool for circadian phase shift. This method, which we introduced in previous chapters, has already been applied to treat sleep-disorder patients. A single light pulse can be shown to phase shift circadian rhythms; therefore we modeled the effects of a light pulse by representing a light pulse E(t) as the first time derivative of light intensity, so-called "velocity coupling." Each E(t) consisted of a positive impulse representing the change in illumination at the beginning of the light pulse and a negative impulse representing the end of the light pulse. The phase of the oscillation could be delayed or advanced depending on the amplitude, width and the timing of the pulses. The E(t) is usually determined by experiments, but there are some general rules which should be followed. According to our experience, the direction of the phase shift (whether the phase is delay shifted or advance shifted) is mainly determined by the timing of the applied pulse, while the degree of phase shift is mainly determined by the amplitude of the pulse. Usually the applied pulse is a single pulse, so we don't have to consider the frequency.

Fig.7.5 shows the time series of the single Van der Pol type models discussed previously where (a) is phase delay-shifted by E(t) in which the period is increased for one cycle following the applied pulse and (b) is phase advance-shifted by E(t) in which the period is decreased for one cycle following the applied pulse. The zero-crossing detection method was used to find the period of the above time series. Fig.7.6 shows the period of each day during 20 days detected by this method.

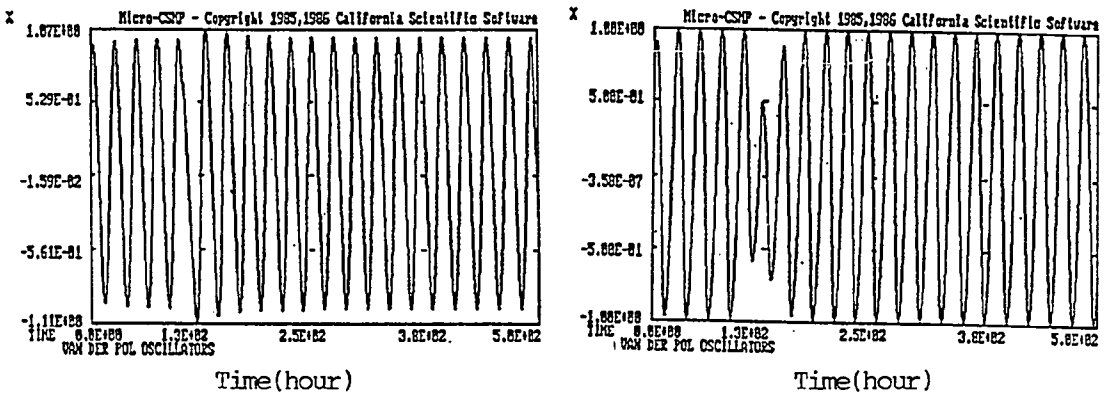

Figure 7.5: *Time series of Van der Pol type model. a) Phase delay-shifted by the stimulus. b) Phase advance-shifted by the stimulus.*

Fig.7.6(a) shows the periods with a phase delay shift and (b) shows the periods with a phase advance shift. In both cases, the phase shifts occur between day 5 and day 6. Before and following the stimulus, the period of the system is kept at very nearly 24 hours. The zero crossing detection method can not display more information due to the rapidity and complexity of the phase shift process.

Generally, the response of a system to a stimulus consists of two parts, the quasi-steady-state response and the transient response. The concept of quasi-stationary behavior of a system implies that, as long as the instantaneous frequency of the modulated signal varies *slowly* enough with time, the instantaneous amplitude and frequency at the output can be derived from the *multiplication* of instantaneous amplitude and frequency of the input by the value of the transfer function applicable to that frequency. In a quasi-stationary manner, the instantaneous frequency of the system response will be *close* to the instantaneous frequency

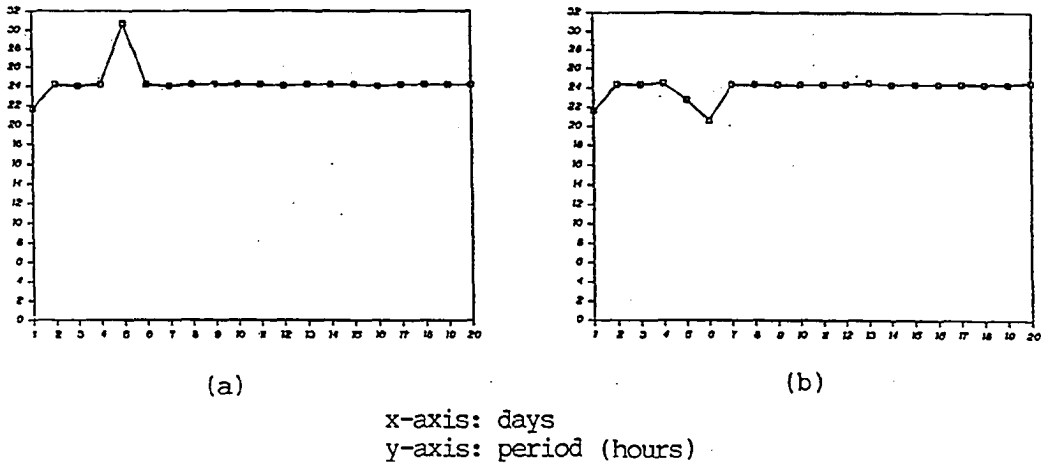

Figure 7.6: *Periods of Van der Pol type model. a) Phase delay-shifted by the stimulus. b) Phase advance-shifted by the stimulus.*

of the excitation. However, when the instantaneous frequency of the modulating signal changes abruptly so that quasi-stationary conditions are violated, as in the circadian rhythm case, the sudden temporary change in frequency corresponds to the *phase shift* produced by a change in time zone or a light pulse. In this case, the instantaneous input and output frequencies of the system may differ significantly. The problem of finding the transient response then becomes of considerable importance. In this case, the resultant output signal was shown to be composed of a *transient component* having a frequency equal to the natural frequency of the system and a *steady-state component* produced by the applied signal. These two components can be added vectorally to yield a resultant [4]. To explore this process, we can try to obtain the dynamic frequency information directly or by finding the time derivative of its phase angle indirectly. This is considered further below.

7.4 Analysis of Dynamic Process with Nonperiodic Stimulus

The transient behavior of the system with a non-periodic stimulus applied, as we discussed before, is very complicated. The zero-crossing method can be used to detect gross information of frequency variation. We analyzed this transient behavior of our model using *dynamic spectral analysis* and *frequency demodulation.*

7.4.1 Dynamic Spectral Analysis

This method uses the FFT to find the *sequential spectral functions* following the application of the excitation. The procedure is as follows:

1. Divide the time series into several segments. The first one or two segments of the time series occur just before the excitation is applied. The last segment occurs after the return of the spectrum to its original. Each segment is made to be one day (144 sample points) different from the previous segment. Therefore the time series of adjacent segments are overlapped. For example, if the first segment consists of the data from day 1 to day 5, then the second segment consists of the data from day 2 to day 6, etc. The length of the segment is mainly determined by the following consideration:

   (a) The segment should not lose the dynamic properties. In the model the stimulus is applied just in one day, and long segments will average the stimulus effect. Therefore the segment should not be too long;

   (b) The segment length should not lose the relatively low frequency components and the Fourier transform should have enough transform points.

Therefore the segment should not be too short either. In our research, the length of the segment was tested and finally determined by the experimental results. Five days (720 points) of data were used as a segment.

2. Pre-processing of each segment. This procedure is the same as we introduced for the FFT processing in chapter 6. We apply the pre-processing procedure which includes detrending, smoothing and zero padding to each segment.

3. Compute the FFT of each segment (4096 to 16384 points). Fig.7.7 shows the dynamic spectrum of a Van der Pol type model with phase shift, where (a) corresponds to the phase delay shifted case while (b) corresponds to the phase advance shifted case.

4. Analyze the sequential spectra and search for peaks of frequency components in different phases. For a short pulse stimulus, according to the zero-crossing detection results, the spectrum is expected to vary from the original to the transient process and then back to the original spectrum again. The dynamic spectrum gives us some details about this transient process.

Examining the frequency peaks in these spectra, we can see the sequential spectra start with basically one main peak and finally return to this spectrum. The other phenomenon noted was "overshoot" in the frequency components. In the phase delay-shifted case (fig.7.7(a)), it was found that the spectrum first appeared to have frequency components lower than the fundamental frequency which caused the phase delay; then it merged to have frequency components higher than the fundamental before the oscillator finally resumed its original frequency. It seems that the higher frequency component here is due to "overshoot". In the case of phase advances, the phenomenon we observed is just opposite as the case of phase

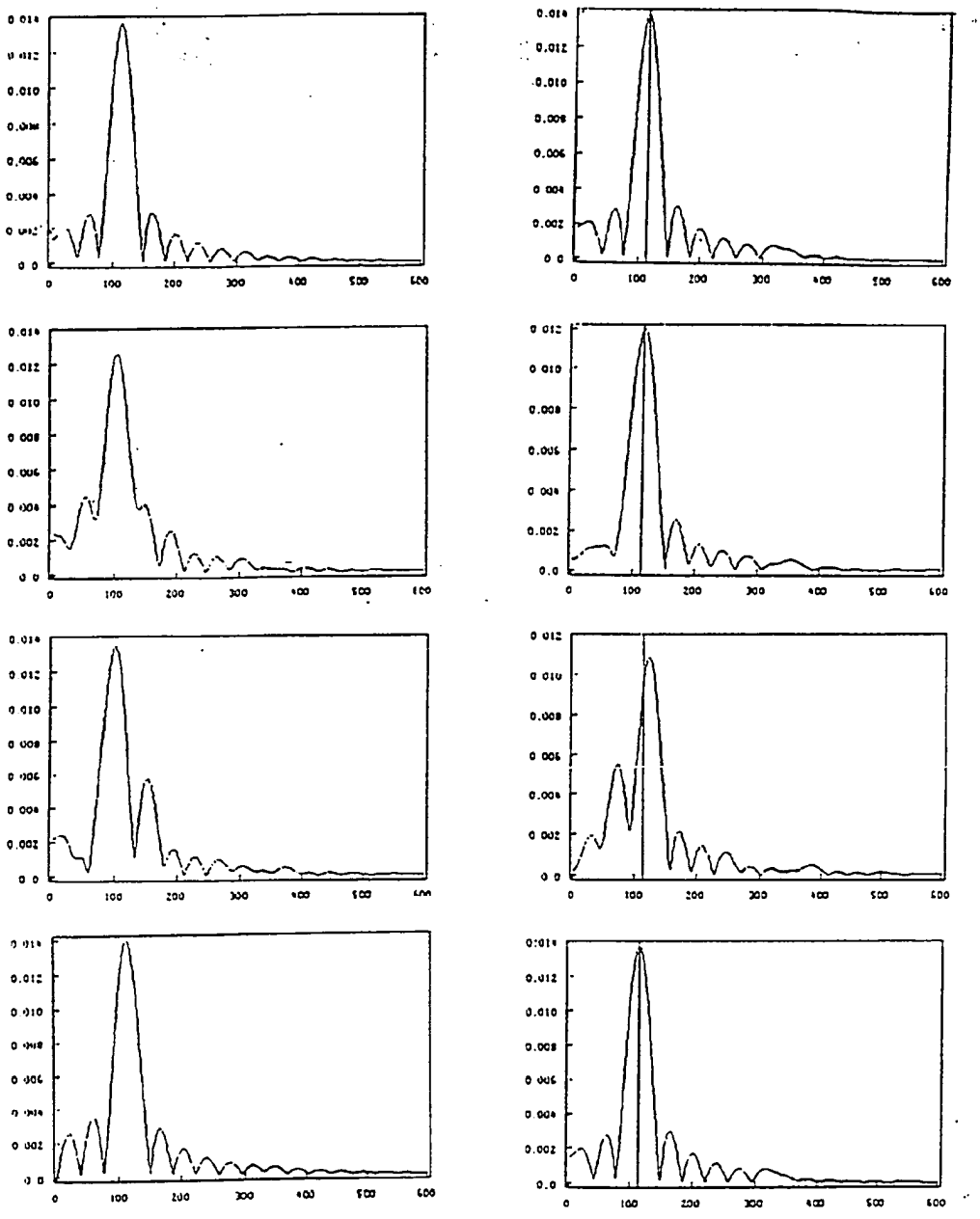

Figure 7.7: *Sequential spectra of Van der Pol type models. a) Spectra of the model with phase delay-shifted by the stimulus. b) Spectra of the model with phase advance-shifted by the stimulus.*

delay shift as we can see in fig.7.7(b). These additional frequency components and the "overshoot" give the transient response a complicated, nonmonotonic behavior.

7.4.2 Frequency Demodulation Analysis

The dynamic process of a nonlinear system following a stimulus is very complicated. We therefore used additional methods to explore its mechanism. The other method used for this purpose is frequency demodulation. Both methods reveal the dynamic transformation when a stimulus is applied.

The transient response of linear networks to FM signals, assuming an instantaneous jump in the signal frequency, has been investigated by several workers. Their work has been summarized by Weiner[44], who has carried out extensive experimental work to verify the analytical results. His results agree with the theoretical treatment and are accounted for by a simple theoretical model, originally developed by Baghdady, which explains the mechanism of the generation of FM transients in terms of the normal modes of the network.

We tried the frequency demodulation method for extracting the information in the system following an applied stimulus. The stimulated time series can be treated as a frequency modulated signal. However, there are some differences between it and a frequency modulated signal in communication systems.

1. The modulating signal for circadian phase shift is not periodic, while in communication systems, the application of the modulating signal is usually periodic or can be treated as periodic. The time interval during which the circadian modulating signal is applied is very short while it is relatively longer

in the communication system application;

2. The modulating frequency is much lower than the carrier frequency in the communication system application, while the frequency of the modulation signal applied to the circadian oscillator can be comparable with the carrier frequency.

The first method we tried was phase demodulation. If we simplify our circadian rhythms to be represented as a linear oscillation plus a phase modulation caused by the stimulus then,

$$f(t) = Acos[\omega_c t + \phi(t)]. \tag{7.4}$$

$\phi(t)$ here can be any form of phase shift caused by the stimulus. Then

$$f(t) = A[cos\omega_c t cos\phi t - sin\omega_c t sin\phi(t)] \tag{7.5}$$

If $f(t)$ is then multiplied by the carrier frequency, we obtain,

$$\begin{aligned} f(t) * cos\omega_c t &= A[cos^2\omega_c t cos\phi(t) - cos\omega_c t sin\omega_c t sin\phi(t)] \\ &= A[\frac{1}{2}(1 + cos2\omega_c t)cos\phi(t) - \frac{1}{2}(sin2\omega_c t)sin\phi(t)] \\ &= A/2[cos\phi(t) + cos2\omega_c t cos\phi(t) - sin2\omega_c t sin\phi(t)] \\ &= A/2[cos\phi(t) + cos[2\omega_c t + \phi(t)]] \end{aligned} \tag{7.6}$$

If we then use a lowpass filter to filter out the frequency component $cos[2\omega_c t + \phi(t)]$ we will have,

$$y = A/2cos\phi(t) \tag{7.7}$$

and,

$$\phi(t) = cos^{-1}(\frac{2}{A}y) \tag{7.8}$$

The problem here is $cos[\phi(t)] = cos[-\phi(t)]$, therefore the correct sign of $\phi(t)$ can not be determined.

Fig.7.8 shows the flowchart of the frequency demodulation procedure we used in this research.

The phase modulated signal $f(t)$ is defined as

$$f(t) = Acos[\omega_c t + \phi(t)] \tag{7.9}$$

The derivative of f(t) is

$$\begin{aligned} f'(t) &= Asin[\omega_c t + \phi(t)](\omega_c + \frac{d\phi(t)}{dt}) \\ &= [\omega_c + \omega_m(t)]Asin[\omega_c t + \phi(t)] \end{aligned} \tag{7.10}$$

where

$$\omega_m(t) = \frac{d\phi(t)}{dt} \tag{7.11}$$

This changes the phase modulation signal into an amplitude modulation signal.

Recall that ω_c is the carrier frequency, which is a constant while $\omega_m(t)$ is the variable modulation frequency.

The techniques for AM signal demodulation can be then applied. We let the signal then pass a "detector" which functions as a rectifier. The output signal from the detector $f_2(t)$ is,

$$f_2(t) = f'(t)S(t) \tag{7.12}$$

$S(t)$ is the switching function. By expanding $S(t)$ into its Fourier series, it can be shown that the output contains a component proportional to $\omega_m(t)$ plus higher frequency terms (sum and difference frequencies of carrier and modulating signal).[37]

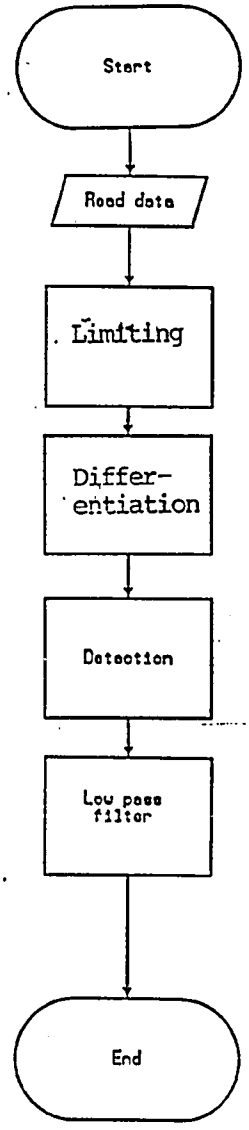

Figure 7.8: *Flowchart of frequency demodulation method.*

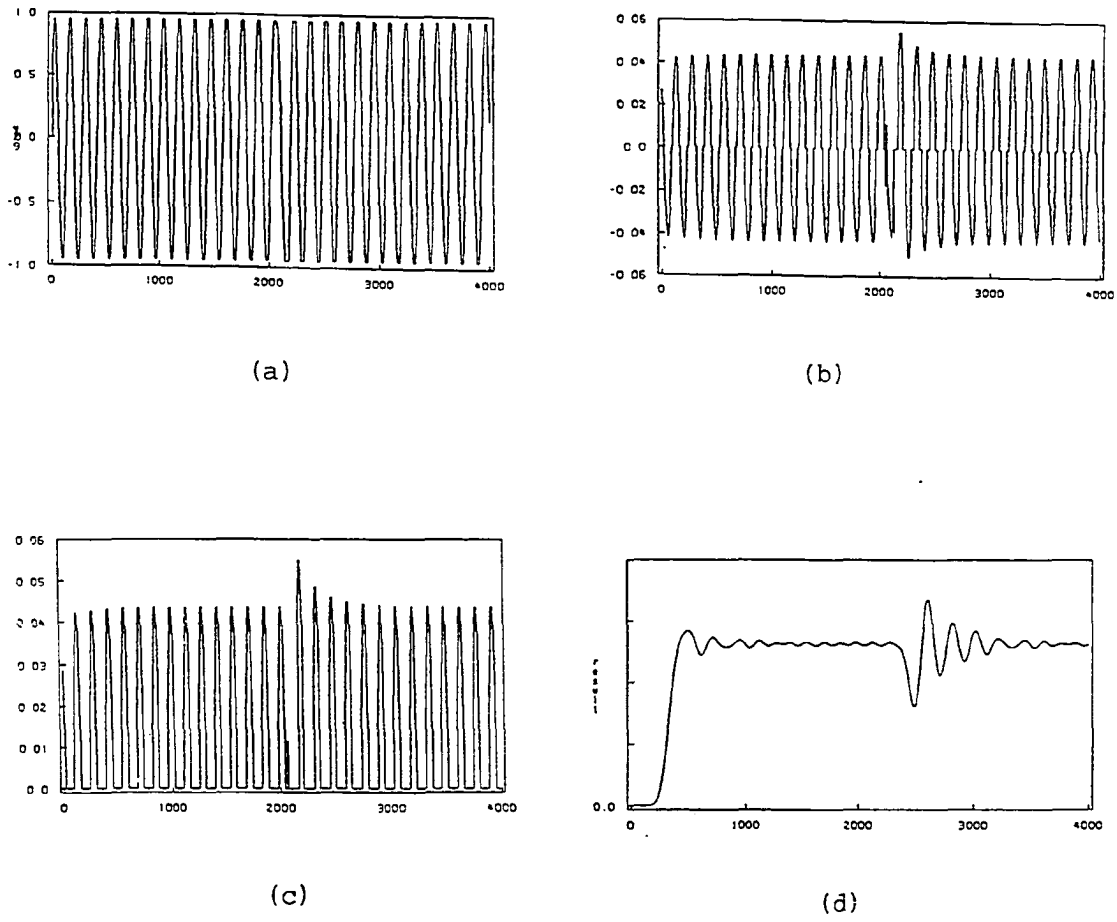

Figure 7.9: *Frequency demodulation results on a phase delay shifted model. a) After limiting. b) After differentiating. c) After detector. d) Frequency demodulation results.*

If the signal is then passed through a low–pass filter, we can get the output signal which is proportional to $\omega_m(t)$.

Fig.7.9 shows the demodulation result of the phase delay shift case. The signal of fig. 7.5(a) was first passed through the limiter to eliminate any amplitude changes (fig.7.9(a)). Then it was differentiated and low pass filtered (fig.7.9(b)). The demodulated signal is shown in Fig.7.9(d). This is the system frequency following phase delay shifting. We can see from fig.7.9(d) that the system frequency

is first reduced, then jumps to a higher a frequency and finally it resumes its original frequency. This result is consistent with the result from dynamic spectral analysis.

Nonperiodic stimuli applied to circadian rhythms produce phase shifts. This type of stimulus produced phase advances and delays that are accompanied by transients. The transients e it complicated, nonmonotonic patterns such as those described by Monk et al [25] for human biological ms following a phase-shift. He pointed out that a zig-zag recovery function for the phase shift is important in suggesting a competition between two circadian processes. However, our results from both the dynamic spectrum and frequency demodulation methods on our model show the "overshoot" process during the phase recovery which is very similar to the zig-zag phenomenon observed in practice. Our model results suggest that an nonlinear oscillator will exhibit a transient behavior when a nonperiodic stimulus is applied. This transient process is rapid and complicated . We concluded, therefore, that this transient process is sufficiently complex to account for the data and no competing processes need to be invoked.

7.5 Stopping the Oscillation in Van der Pol oscillator

A biological oscillator is very sensitive to changes in its environment. The effect of pulse stimulus on a biological system is generally modest but it can be enhanced by presenting brightness changes cyclically in resonance with the oscillator's natural period. Large phase shifts are more quickly attained by reducing the oscillation amplitude to zero. More precisely, there exists a value of the stimulus intensity I which, if applied for length of time T at a point of the limit cycle C,

will cause the state to move to or close to the singularity. In such an event, the oscillator can be stopped.

We simulated this process on different models. The stimuli applied are different for different models, but the basic idea is always to move the state toward the singularity. Following are the test results on several models:

1. Stopping the oscillation of the single Van der Pol type model.

   The Van der Pol type model is the same as we used for phase shifting research. The stimulus for stopping the oscillation should finally bring the trajectory of the system just to the singularity. Therefore the timing and amplitude of the applied pulse needs to be more precise than in the phase shift case. It is also noticed that more than one pulse should be used in this complicated case, because it is impossible to control the trajectory precisely to the singularity in one cycle (only one pulse is applied in one cycle).[22]

   E(t) was chosen to stop the oscillation by comparing the phase plane and time series results. It was noticed that a stimulus with $1\frac{1}{2}$ cycle protocol(1.5 pulses applied) when carefully designed for amplitude and phase, can bring the amplitude to zero and maintain it there, i.e., the circadian clock can be said to have been "stopped". Fig.7.10 shows the stopped time series of the oscillation in this model.

   The trigger time, amplitude and duration are three important parameters in this model which were mainly determined by experiments and which are now listed:

   The correct trigger time: 81.84851382535 hr to 81.84851382539 hr;

   The correct amplitude of the trigger pulse: 0.467954 to 0.467958;

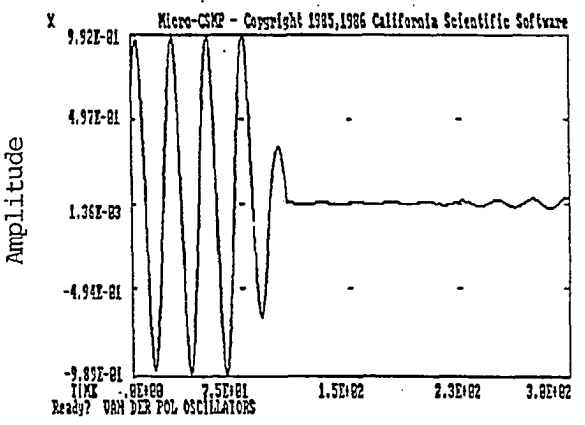

Figure 7.10: *The time series of stopped oscillation in Van der Pol oscillator model.*

The correct duration of the trigger pulse: 12 hr. (Due to the velocity coupling, a positive and a negative impulses with interval equal to 12 hr are applied to the model.)

The correct cycles to apply the stimulus: Total $1\frac{1}{2}$ cycles.

Fig.7.11 shows the phase plane trajectory of the stopped oscillation.

2. Stopping the oscillation of the biological oscillator model.

   This model, which we introduced in chapter 4, is designed based on the practical phase response curve. Its phase plane trajectory is shown in fig 5.5, where we can see that there is a section on the x-axis, where the derivative is equal to zero. Therefore a "strong" pulse applied will bring the trajectory to this zero axis and cause the oscillation to be stopped. This result is very similar to the real situation. Winfree[46] found that the system saturated very quickly to the level of light intensity, and he used the duration of the light pulse as the controlling variable. He found that exposing a rhythmic culture

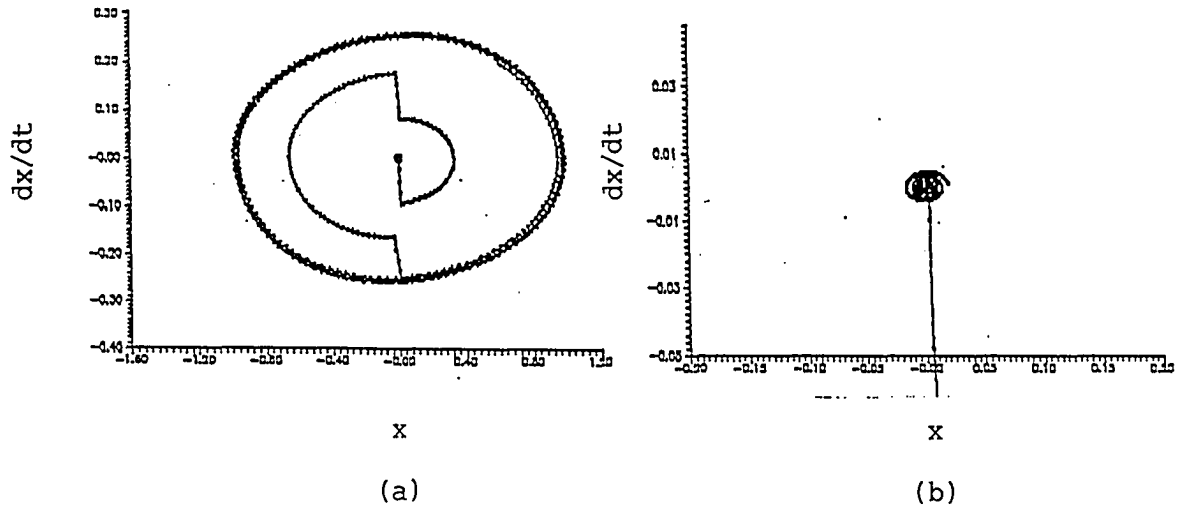

Figure 7.11: *phase plane of stopped oscillation. (a) Full plot of phase plane. (b)Detailed plot near the singularity.*

of pupae to a 50 sec strong light stimulus rapidly resulted in a complete loss of the sleep–wake rhythm. We found similar results in the simulation of this process on the biological oscillator model. Figure 7.12 shows the simulation results.

3. Stopping the oscillation of the coupled oscillator model.

   We did not succeed in stopping the coupled oscillator model. The coupled oscillator model is based on two dimensional Van der Pol oscillator equation. In the single oscillator case, the pulse series to cause the oscillator to stop has to be carefully designed. In the coupled oscillator case, if we apply the same pulse series to one of the oscillator or even to both of the oscillators, the small interference coupling from the other oscillator will cause the oscillation to resume. We tried to design several different pulse series and all of them failed. This topic has to be reconsidered from basic principles.

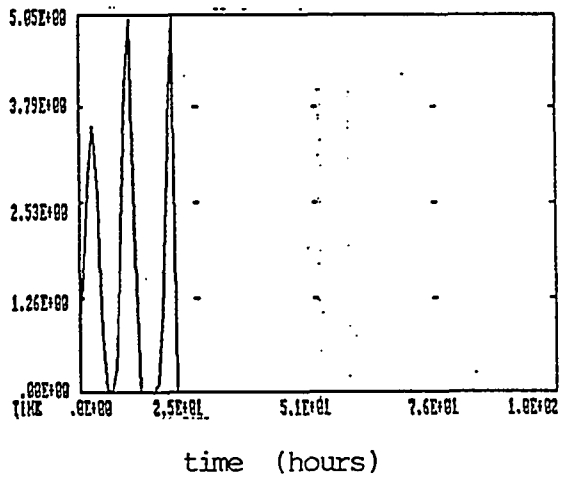

Figure 7.12: *Stopped the oscillation of the biological oscillator model.*

Stopping the biological oscillation in practice may have serious consequences. It is very difficult to simulate this in real experiments. But the knowledge of this process is very important for the physiologists. Modeling and simulation facilitates an in depth study of these potential phenomena.

Chapter 8

High Order Spectral Analysis on Circadian Rhythms

In this chapter, we will discuss the preliminary results of two high order spectrum analysis methods and their applications for further exploration of our experimental and model data. The coherence method and bispectrum method will be discussed.

8.1 Theory of Coherence Function

8.1.1 Introduction

In previous chapters we treated the concepts of Fourier analysis and the spectral functions obtained from our experimental and model data. All of them are the Fourier transform of a single channel time series. In this chapter, we are going to explore a method of analysis for two correlated time series in the frequency domain. The function obtained from this method is the **coherence** function.

In our circadian rhythm data acquisition system, as introduced in chapter 2,

the temperature and activity data were acquired simultaneously. It is interesting to find the relation between these two circadian rhythms. The relation between these two signals may possibly be explored directly from the time series or from in the frequency domain. The relation between these two time series is difficult to explore directly in the time domain, because the data acquired from either source is easily interrupted (as we mentioned in chapter 2, the interruption may be caused by noise, specious subject conditions, computers or other equipment, etc.), and this will destroy the synchronization between the signals. The frequency characteristics, on the other hand, are usually not affected by interruptions in the time domain.

Therefore, it is possible to use the coherence spectrum to explore the relations between circadian temperature and activity data in the frequency domain. Generally, the coherence spectrum is a mathematical quantity which provides a measure of correlation between circadian temperature and activity for each *frequency* and attains a very high value (i.e. near unity) at a given frequency if the phase relationship between the two channels is nearly constant over the time interval used to measure the coherence.

As we mentioned earlier, the power spectral density function of a single channel time series is the Fourier transform of the autocorrelation function. The spectral density estimate $G_x(f)$ and $G_y(f)$ of time series $x(t)$ and $y(t)$ could be computed from the Fourier transforms $X(f,T)$ and $Y(f,T)$ as follows:

$$G_x(f) = \frac{2}{T}|X(f,T)| \tag{8.1}$$

$$G_y(f) = \frac{2}{T}|Y(f,T)| \tag{8.2}$$

The cross spectral density function of a pair of time series is the Fourier transform

of the cross correlation function. Because a cross correlation function is not an even function, the cross spectral density function of two time series $x(t)$ and $y(t)$ is generally a complex, function given by

$$G_{xy}(f) = C_{xy}(f) - jQ_{xy}(f) \tag{8.3}$$

where the real part $C_{xy}(f)$ is called the coincident spectral density function (cospectrum) and the imaginary part $Q_{xy}(f)$ is called the quadrature spectral density function (quadrature spectrum). [10] The coincident spectral density function can be thought of as the average product of $x(t)$ and $y(t)$ within a narrow frequency interval between f and $f + \delta f$, divided by the frequency interval. The quadrature spectral density is the same except that either $x(t)$ or $y(t)$ is shifted in time sufficiently to produce a 90 degree phase shift at frequency f. In many practical applications, the cross spectral function may be used in normalized form, which is defined by

$$g_{xy}(f) = \frac{|G^2_{xy}(f)|}{G_x(f)G_y(f)} \tag{8.4}$$

This *normalized form of the cross spectral density function* is also called the **coherence function.**

When $g_{xy}(f) = 0$ at a particular frequency, $x(t)$ and $y(t)$ are said to be incoherent, i.e., uncorrelated, at that particular frequency. If $x(t)$ and $y(t)$ are statistically independent, then $g_{xy}(f) = 0$ at all frequencies. If $g_{xy}(f) = 1$ for all frequencies then $x(t)$ and $y(t)$ are said to be fully coherent.

There are two methods used to obtain the coherence function from time series records $x(t)$ and y(t). One method involves the calculation of autocorrelation and cross-correlation functions in the time domain to obtain the cross spectrum. The

second method involves a calculation directly from the Fourier transform to obtain the cross spectrum.

Since it is more convenient to calculate Fourier transforms with the help of the FFT algorithm, the second method has been used extensively, although variations in the technique used for smoothing (for increasing the degrees of freedom) differ depending upon processing time and memory availability.

8.1.2 Importance of Smoothing in Cross Spectrum Estimation

Smoothing is of special importance in estimation of the cross spectrum.[5] If the coherence estimate is obtained by using the unsmoothed estimate of the power spectral density function, i.e., using only two degrees of freedom, then, for the time series of length T,

$$G_{xy}(f) = \frac{2}{T}[X^*(f,T)Y(f,T)] \tag{8.5}$$

$$G_x(f) = \frac{2}{T}[X(f,T)^2] = \frac{2}{T}[X^*(f,T)X(f,T)] \tag{8.6}$$

$$G_y(f) = \frac{2}{T}[Y(f,T)^2] = \frac{2}{T}[Y^*(f,T)Y(f,T)] \tag{8.7}$$

where $X(f,T)$ and $Y(f,T)$ are the finite Fourier transforms of $x(t)$ and $y(t)$ over the record length T. According to the definition give in Eq.8.2,

$$g_{xy}(f) = \frac{|G_{xy}^2(f)|}{G_x(f)G_y(f)} = \frac{X(f,T)^*Y(f,T)X(f,T)Y(f,T)^*}{X(f,T)^*X(f,T)Y(f,T)^*Y(f,T)} = 1.0 \tag{8.8}$$

Thus with only two degrees of freedom, the coherence function estimate for the complete frequency range becomes unity even for the case of completely incoherent data. The problem here is that the coherence has an inherent bias error with only 2 degrees of freedom.

The only way to solve this problem is to increase the degrees of freedom in the spectral density estimate itself and thereby increase the reliability of the results. We can use either the segment averaging approach or the frequency smoothing approach in the calculation of auto and cross spectra. Smoothing over frequencies is performed by smoothing over a fixed number of contiguous frequency components.

Smoothing by segment averaging is performed by first computing individual estimates from a number of records $x_1(t)$, $x_2(t)$, $x_3(t)$, $\cdots$, $x_n(t)$, etc. Therefore n independent histories have been computed. The next step is to smooth n records at each frequency, i.e.,

$$G_x(f) = \frac{1}{n}[G_1(f) + G_2(f) + \cdots + G_n(f)] \tag{8.9}$$

This procedure is employed in this research by using overlapped or non-overlapped time records depending on the length of the total time series.

8.2 Computing of Coherence and Experimental Results

The algorithm we used to calculate the coherence is based on the direct method, i.e., all the calculation are in the frequency domain. The experimentally acquired temperature and activity data are first transformed into a frequency series by an overlapped fast Fourier transform technique. [12] The auto and cross power spectral density function together with the coherence are then computed. The procedure is as follows:

1. At a sampling rate of $6/hour$, the temperature and activity signals are collected and 8192 points (about 2 months) were taken from each channel.

2. The 8192 data points were segmented into 8 overlapped segments with 2048 points in each.

3. The FFT was performed on each segment, using FFT procedures introduced in chapter 6.

4. The auto spectrum and the inphase and quadrature components of the cross spectrum of each segment i were calculated point by point as follows:

$$C_{xx,k}^{(i)} = A_{x,k}A_{x,k} + B_{x,k}B_{x,k} \tag{8.10}$$

$$C_{yy,k}^{(i)} = A_{y,k}A_{y,k} + B_{y,k}B_{y,k} \tag{8.11}$$

$$C_{xy,k}^{(i)} = A_{x,k}A_{y,k} + B_{x,k}B_{y,k} \tag{8.12}$$

$$Q_{xy,k}^{(i)} = A_{y,k}B_{x,k} - A_{x,k}B_{y,k} \tag{8.13}$$

k is a point between 1 and 2048 in each segmentation.

5. The results from each segmentation were then averaged.

$$C_{xx,k} = \frac{1}{n}\sum_{i=1}^{n} C_{xx,k}^{(i)} \tag{8.14}$$

$$C_{yy,k} = \frac{1}{n}\sum_{i=1}^{n} C_{yy,k}^{(i)} \tag{8.15}$$

$$C_{xy,k} = \frac{1}{n}\sum_{i=1}^{n} C_{xy,k}^{(i)} \tag{8.16}$$

$$Q_{xy,k} = \frac{1}{n}\sum_{i=1}^{n} Q_{xy,k}^{(i)} \tag{8.17}$$

6. Coherence was finally computed by normalization.

$$coh_{xy,k}^2 = \frac{C_{xy,k}^2 + Q_{xy,k}^2}{C_{xx,k} \cdot C_{yy,k}} \tag{8.18}$$

As we mentioned in the beginning of the section, the coherence function will be used to find the relationship between two different circadian rhythms. We calculated

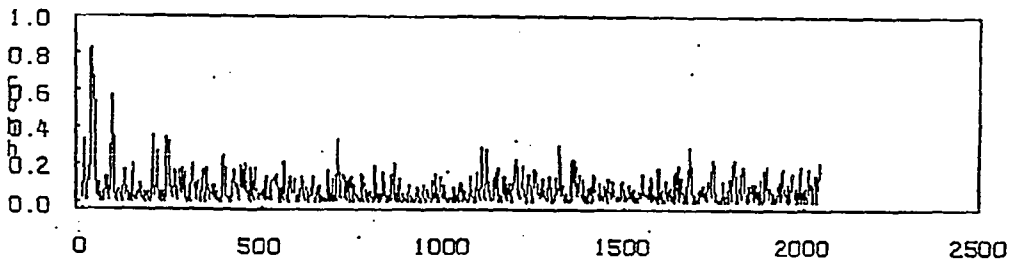

(a)

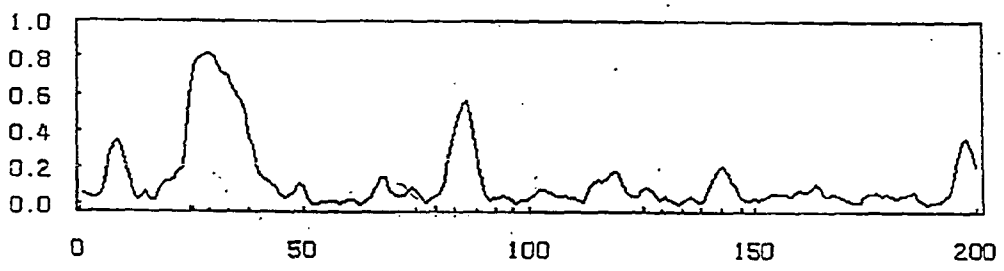

(b)

Figure 8.1: *Coherence of circadian temperature and activity of subject41. a) The coherence function between points 1 and 2048. b) The coherence function between points 1 and 200.*

the coherence function on our circadian temperature and circadian activity data of monkey 41. The algorithm was designed according to the procedures introduced above. All the computing work was implemented by two Macros Cohh1 and Cohh2 written in *S* language, which are listed in the Appendix.

Fig 8.1 show the results of the calculation. The sample rate was 6 samples/hour and a 4096 point FFT computation was applied. Fig.8.1(a) shows the full range of coherence from spectrum point 1 to 2048 while (b) shows the range from spectrum point 1 to 200. Fig.8.1(b) shows three main peaks in the range of points 1 to 200. The first high and wide peak at point 30 represents the highest

coherence near period

$$\frac{4096}{6(30-1)} = 23.54hr$$

and the adjacent range. The second peak is near point 83, and represents the period 8.03h. This frequency is the 3rd harmonic of the fundamental frequency. We see a relatively high coherence at this frequency. We can also see there is a peak in the range lower than the fundamental frequency which tells us that the two circadian rhythms have some common low frequency coherence.

Two problems arise here for further exploration:

1. What is the coherence about the second harmonic? The results from subject 41 didn't show any coherence. More experiments have to be done to determine whether this is normal. Due to the insufficient activity data, this exploration is left for further development.

2. Fig 8.1(a) shows a complete plot of the above coherence function, from point 1 to 2048. From the plot we can see there are many small peaks in the higher frequency range above point 200. It is not clear whether this is caused by the algorithm itself(e.g.,not enough smoothing) or whether there exists some information in that range which needs further analysis.

The coherence method is a useful tool for the exploration of two channel signal correlation in the frequency domain. It is especially helpful in the analysis of multi-circadian rhythm data. The test results of subject 41 show that high coherence occurs at the fundamental frequency, which does not surprise us. However, high coherence at the 3rd harmonic rather than at the 2nd harmonic is a new observation. We can not directly find this information from the spectra of either

data. As we have shown in the spectral analysis in chapter 6, the level of the 2nd harmonic varies between subjects, and even at different time episodes of the same subject, which illustrates the variation of bimodality of the subject under different conditions. This may be the reason for the low coherence at this frequency.

The coherence computation is based on the averaged FFT results. Therefore more segments of data will be helpful in smoothing the result and yield a more accurate result. Long term circadian rhythm data of other physiological variables, such as feeding, is needed for this purpose while the synchronization of these data is not strictly required, because the coherence is computed in the frequency domain.

8.3 The Bispectrum

8.3.1 Introduction

One of the most fundamental and useful tools in circadian research, as introduced in chapter 6, is the estimation of the power spectrum. In recent years, the utilization of the high order spectra has increased in the digital signal processing field.[26] Of particular importance is the bispectrum, which is the Fourier transform of the third order cumulant (TOC) sequence defined as follows:

$$B(\omega_1,\omega_2) = \sum_{m=-\infty}^{\infty} \sum_{n=-\infty}^{\infty} R(m,n) e^{j(\omega_1 m+\omega_2 n)} \tag{8.19}$$

where $R(m,n)$ is the third order cumulant defined as the expected value of the triple product,

$$R(m,n) = E[x(k)x(k+m)x(k+n)] \tag{8.20}$$

In power spectrum estimation, the process under consideration is treated as

a superposition of statistically uncorrelated harmonic components and the distribution of power among these frequency components is then estimated. As such, only linear mechanisms governing the process are investigated since phase relations between frequency components are suppressed.[34] However, there exist some practical situations where the information concerning phase relations is very important for exploring the essentials of the system. High order spectra such as the bispectrum,, defined in terms of high order cumulants of the process, do contain such information.[26]

The general motivation behind the use of high order spectra in signal processing is:

1. To extract information resulting from a deviation from Gaussianity (normality). This is based on the property that all high order spectra (order greater than two) are identically zero for Gaussian processes. Thus a nonzero higher order spectrum indicates deviation from normality. In a more practical sense, in those signal processing settings where the signal is a non–Gaussian stationary process and the additive noise process is stationary Gaussian, there might be certain advantages in estimating signal parameters in higher order spectral domains. The non–Gaussian condition is satisfied in many practical applications, since any periodic or quasi-periodic signal can be regarded as a non-Gaussian signal.

2. To estimate the phase of non-Gaussian parametric signals. The high order spectra preserve the phase information of non- Gaussian parametric signals.

3. To detect and characterize the nonlinear properties of mechanisms which generate time series via **phase relations** of their harmonic components. In

the study of circadian rhythms, we found that 2nd, 3rd and possibly higher harmonics did exist in the power spectrum with different amplitude and phase. From the viewpoint of biological oscillators, it is very important to know the details of these harmonics, especially the 2nd and 3rd harmonics.

Motivation 3 is the main purpose for us to use the bispectrum in this research. As we mentioned earlier, because of the interaction between two harmonic components of a process, there is a contribution to the power at their sum and/or difference frequencies. Such a phenomenon, which could be due to quadratic nonlinearity, gives rise to certain phase relations called quadratic phase coupling. In our study of circadian rhythms, the 2nd, 3rd and higher harmonics are nonlinear frequency components. Their relation is an essential topic to be explored.

It is important for us to know:

1. Whether the harmonics in a circadian rhythm come from the same pacemaker or, is the 3rd harmonic generated because of the interaction of the fundamental and the 2nd harmonic? This information (if correctly obtained) will be very helpful for us to understand the essentials of the circadian oscillator and will be the basis for us to build our model for circadian rhythms.

2. Are their phases correlated, especially, is the phase of third harmonic correlated with the first two frequency components?

3. If the phases are correlated, to what degree is this correlation ?

It is impossible for us to extract this information from the regular power spectrum. The bispectrum, however, is capable of detecting and quantifying phase coupling [43], and will therefore be a very helpful tool in this case.

To explore the principle of the application of the bispectrum, let us consider two stationary processes,

$$Z_1(k) = cos(\omega_1 k + \phi_1) + cos(\omega_2 k + \phi_2) + cos(\omega_3 k + \phi_3) \tag{8.21}$$

and

$$Z_2(k) = cos(\omega_1 k + \phi_1) + cos(\omega_2 k + \phi_2) + cos(\omega_3 k + (\phi_1 + \phi_2)) \tag{8.22}$$

where ϕ_1, ϕ_2 and ϕ_3 are randomly distributed in $[0, 2\pi]$ and,

$$\omega_3 = \omega_1 + \omega_2$$

i.e., $\omega_1, \omega_2, \omega_3$ are harmonically related.

In $Z_1(k)$, it is apparent that ω_3 is an independent harmonic component because ϕ_3 is an independent random phase variable. In $Z_2(k)$, $\phi_3 = \phi_1 + \phi_2$, so the frequency ω_3 is due to a quadratic phase coupling between ω_1 and ω_2.

In the bispectrum analysis, if ω_3 is indeed generated by the phase coupling between ω_1 and ω_2, a peak will appear in the bispectrum $B(\omega_1, \omega_2)$ at the location $(\omega_x = \omega_1, \omega_y = \omega_2)$. Otherwise, no peak will appear in the bispectrum.

To quantify the degree of a quadratic phase coupling, the **bicoherence** index [26] must also be computed. This index is a function of the bispectrum $B(\omega_1, \omega_2)$ and the power spectrum $P(\omega)$ defined as follows:

$$bic(\omega_1, \omega_2) = \frac{B(\omega_1, \omega_2)}{P(\omega_1)P(\omega_2)P(\omega_1 + \omega_2)} \tag{8.23}$$

It is important to note, however, that the power spectrum of both $Z_1(k)$ and $Z_2(k)$ will display three peaks at frequencies ω_1, ω_2, and ω_3 respectively, whether or not ω_3 is due to the quadratic phase coupling between ω_1 and ω_2, and consequently the power spectrum can not be used to detect the presence of phase coupling.

8.3.2 Bispectrum Computation and Smoothing

The bispectrum, by definition, is the Fourier transform of the third order cumulant sequence. Let us note that the power spectrum is, in fact, the spectrum of the second order cumulant. [26] There are two chief approaches that have been used to estimate the bispectrum, namely, the conventional and the parametric approach. We are going to discuss only the conventional method here which can be classified into two classes, indirect and direct.

For the indirect class method, the computing procedure is basically the following:

1. Segment the data into K records of M samples each.
2. Subtract the average value of each record.
3. Obtain the 3rd moment sequence $r_i(m, u)$. of each segment.
4. Average $r_i(m, u)$ over all the segments.
5. Generate the bispectrum estimate.

For the direct class method, the procedure is as follows:

1. The same as indirect class method.
2. The same as indirect class method.
3. Generate the FFT coefficients F_i of each segment, FFT points = N_0.
4. Generate the bispectrum in 2 steps:

a) Compute the bispectrum in each segmentation:

$$b_i(v_1, v_2) = \frac{1}{\Delta_0^2} F_i(v_1) \cdot F_i(v_2) \cdot F_i(v_1 + v_2) \tag{8.24}$$

where $\Delta_0 = f_s/N_0$, (f_s-sampling frequency, N_0-FFT points). The computation for each segment is over the triangular region (by using the symmetry property): $0 \leq v_2 \leq v_1, v_1 + v_2 \leq f_s/2$,

b) Average the results of K segmentations:

$$B(\omega_1, \omega_2) = \frac{1}{K} \sum_{i=1}^{K} b_i(\omega_1, \omega_2) \tag{8.25}$$

The problem encountered in practice is that usually a finite set of observation measurements is given. Therefore the data must be first segmented and the DC component subtracted in both the indirect and direct methods to increase the degrees of freedom and smooth the process. In the indirect method, the 3rd moment sequence of each segment is first computed and averaged. Finally the bispectrum is computed by transformation of the averaged 3rd moment sequence into the two dimensional spectrum. In the direct method the one dimensional spectrum is first computed for each segment and then the bispectrum is computed by computing the correlation of three frequency components: v_1, v_2 and $v_1 + v_2$. The phase relation at these three frequencies over the whole region of each segment should be continuously evaluated. Finally the results from each segment are summed and averaged. An algorithm using the direct method is employed in this research. The Macro *Bis* is listed in the Appendix.

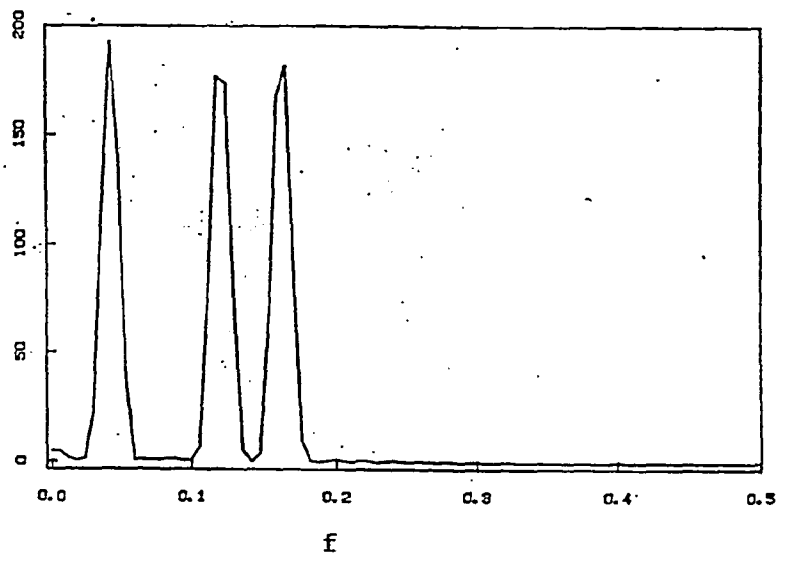

Figure 8.2: *Power spectrum of the model with 3 harmonic-related frequencies.*

8.4 Phase Coupling Detection Using Bispectrum Method

In our research, the bispectrum is used for phase coupling detection of circadian rhythm data. We first tried this calculation on a linear model including three frequency components. These three frequency components, f_1, f_2 and f_3 were harmonically related, and the phase related and phase unrelated cases were tested separately. In both cases, the power spectrum is the same as shown in Fig.8.2.

Fig.8.3 shows the three dimensional plots of the bispectrum and bicoherence functions of the phase related model. In this type of plot, the x axis represents the frequency f_x while the y axis represents the frequency f_y and the z axis represents the bispectrum or bicoherence values at the corresponding frequency f_x and f_y. There are two peaks existing in Fig.8.3(a) at $(f_x = f_1, f_y = f_2)$ and $(f_x = f_2, f_y = f_1)$. Fig.8.4 shows the bispectrum and bicoherence results of the

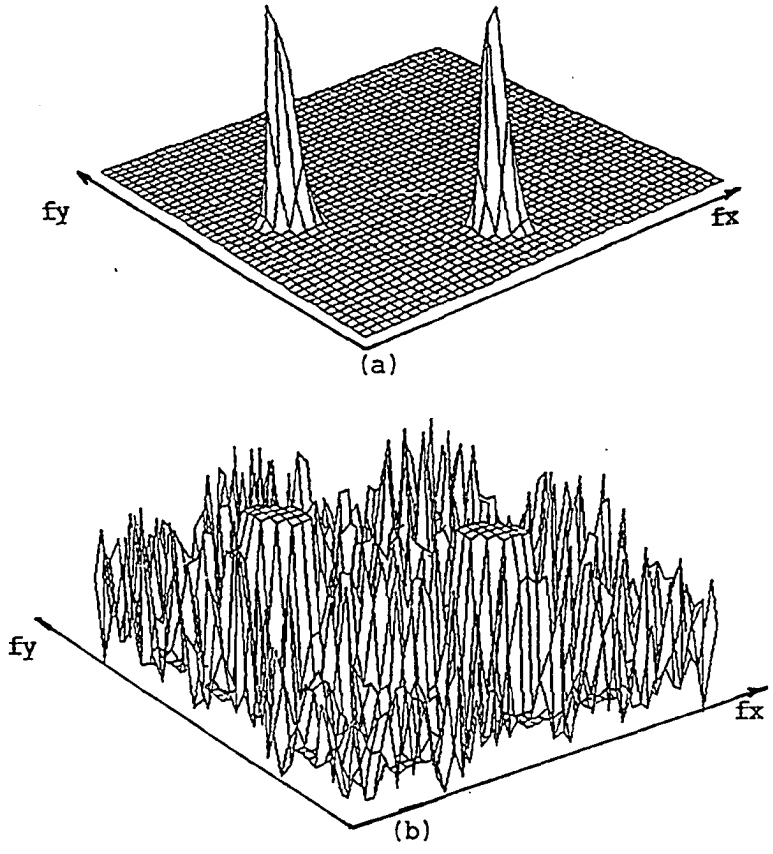

Figure 8.3: *The bispectrum and bicoherence function results of the model with related phase. a) Bispectrum. b) Bicoherence.*

model with unrelated phase.

The test result is based on 40 segmentations. The phase of three frequency components is uniformly distributed in $(0, 2\pi)$. Fig.8.3 shows the results of the model with $\phi_3 = \phi_1 + \phi_2$ while in Fig.8.4 ϕ_3 is independent of ϕ_1 and ϕ_2. The bispectrum test applied to this phase model demonstrated conclusions as follows:

1. The bispectrum computation must use a large number of segments to smooth the data in order to achieve the true results. This is because only the average

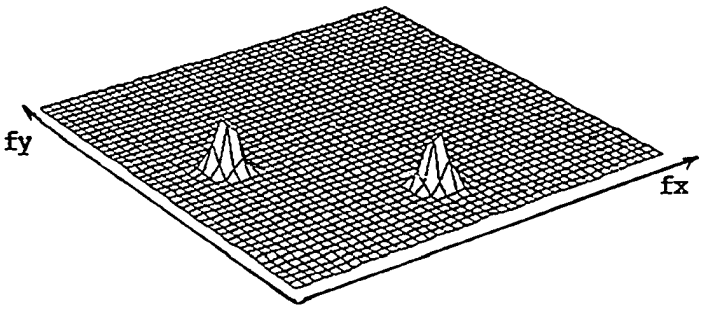

(a)

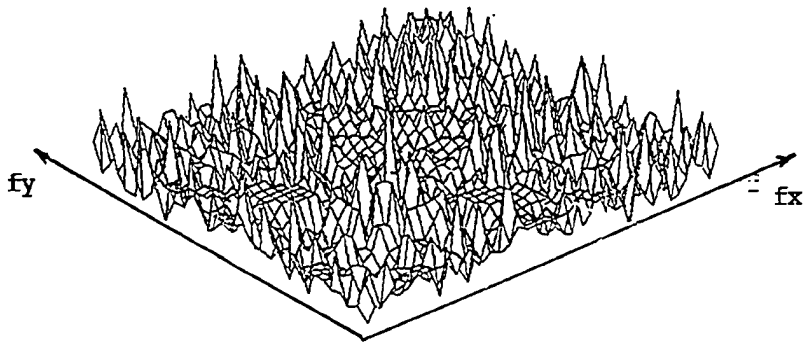

(b)

Figure 8.4: *The bispectrum and bicoherence function results of the model with unrelated phase. a) Bispectrum. b) Bicoherence.*

of a large number of segmental data can reveal the difference in the phase relations.

2. Biocoherence must accompany the bispectrum result to deduce the degree of a quadratic phase coupling. We can see the results from Fig.8.3(b) and Fig.8.4(b). In fig.8.3(a), there are two large peaks at the same position in both the bispectrum and the bicoherence function. In fig.8.4, we see two small peaks in the bispectrum but no peaks show in the bicoherence function. Therefore we can conclude that the frequency component f_3 ($f_3 = f_1 + f_2$) is phase correlated with f_1 and f_2 only if both the bispectrum and bicoherence functions show peaks at the frequency $f_x = f_1$ and $f_y = f_2$.

The bispectrum method was also tested on our experimental data. Fig.8.5 shows the spectrum, bispectrum and bicoherence functions from one of the circadian temperature data sets that we tested. The spectrum shows three main frequency components at $f_1 = 0.042, (23.43hr)$, $f_2 = 0.085(11.71hr)$, and $f_3 = 0.127(7.87hr)$. Thirty-one segmentations were used to obtain the smooth results. The bispectrum shows a peak at $f_x = f_y = 0.042, (23.43hr)$ and small peaks at $f_x = 0.085(11.71hr), f_y = 0.042(23.43hr)$. If the bicoherence function also shows high values at these locations, then we could say that the frequency components $f_x + f_y$ are phase related with f_x and f_y. However, the bicoherence function at these points shows very low values. Our test results with other circadian temperature data show similar findings. Therefore we can not say that the three main frequency components of a circadian rhythm are phase related. In other words, they seem to be derived from three independent oscillators. This conjecture needs further investigation.

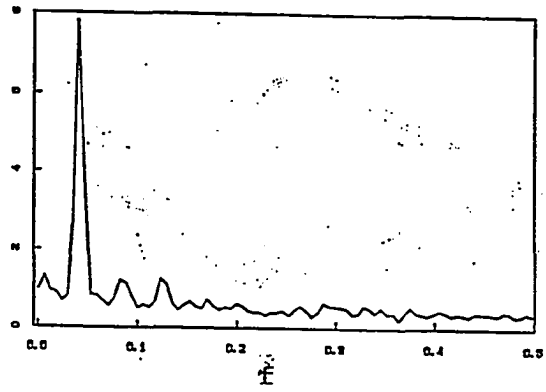

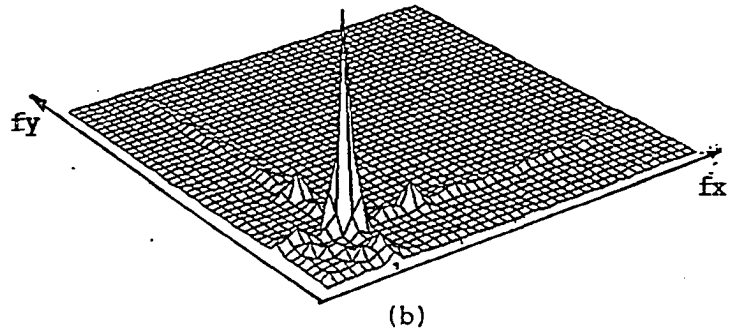

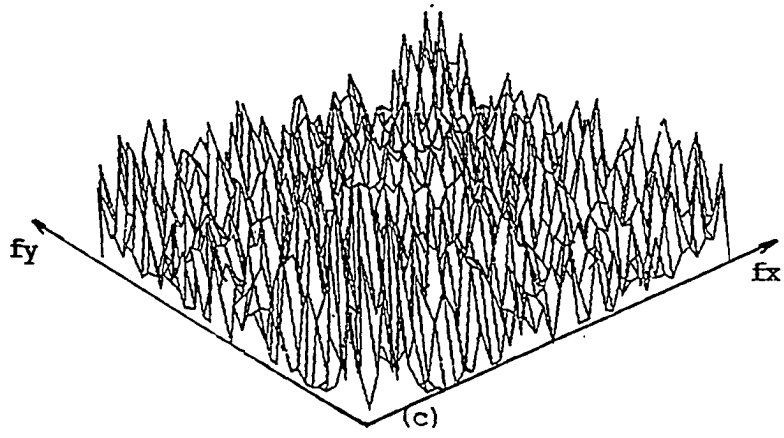

Figure 8.5: *(a)Smoothed spectrum of a experimental data. (b) Bispectrum result. (c) Bicoherence result.*

Chapter 9

Conclusions

9.1 Summary of the Research

Mathematical modeling and analysis of circadian rhythms have developed in the past 20 years. However, many existing models have not utilized both time and frequency characteristics of the circadian rhythms. In this research, we examined both time and frequency characteristics by computer modeling and explored several advanced techniques in the frequency domain. Our results revealed the relation between the bimodality observed in the time series and harmonic structure, the relation between nonlinearity and harmonic structure, the dynamic frequency process with the application of an external stimulus and the frequency coherence between two different circadian rhythms.

In this research, a reliable data acquisition system has been built to acquire high quality raw experimental circadian data. Among the circadian data we obtained, the temperature data has proved to be the most stable, best regulated circadian rhythm. This is because the temperature data is continuously monitorable and not greatly influenced by noise. For example, external high level sound may

change the activity rhythm but not the temperature rhythm of the subject. We have also developed a preprocessing procedure for raw experimental data which includes segmentation, detrending and smoothing of the data.

Based on the understanding of the experimental circadian data and the analysis of several existing models, we have developed our mathematical models for circadian rhythms. Our emphasis in modeling was to make the model approach the real circadian rhythms in **both** the time and frequency domains. The analysis of circadian rhythms in the frequency domain was rarely used in previous research.

Through frequency spectral analysis, we not only confirmed that the main frequency peak of the circadian rhythm was at approximately 24 hours but also found the existence of other frequency components which were harmonically related to the fundamental frequency.

From the physiological viewpoint the second harmonic in the spectrum of the circadian rhythm represents *bimodality characteristics*. Bimodality is a prominent feature of many circadian rhythms. We studied this phenomenon and considered it as one of the basic characteristics on which to build our model. In the spectral analysis of experimental circadian rhythm data, we found that the bimodality existed in almost all the subjects while the level of this harmonic varied in different subjects.

From the mathematical viewpoint, the harmonic frequency components in a system could possibly come from another coupled oscillator or, from the nonlinearity of the system. The circadian rhythm is a complicated nonlinear oscillation process, and it is not possible to be simulated simply by the combination of three harmonically related linear oscillators. To prove this, we simulated a linear model

with 3 harmonically related frequency components. Its frequency spectrum could be adjusted to be similar to the experimental data while the time response was far from the experimental time series. Therefore, in our model, we generated these three harmonically related frequency components by two or three coupled nonlinear oscillators which approach the experimental data well in both time and frequency domains. Following are our considerations in development of the models:

1. In the two dimensional coupled oscillator model, the frequency and amplitude of the second harmonic frequency component could be adjusted by adjusting the frequency and coupling coefficient of the coupled oscillator, and the 3rd harmonic could be adjusted by adjusting the nonlinearity of the system.

2. The mode of coupling has a direct effect on the system frequency and the structure of the spectrum. Direct coupling and velocity coupling are the two coupling methods we tested. Direct coupling has a strong effect on the system. In the case of large nonlinearity, the inserted 2nd harmonic component in the direct coupled system causes 1/3 harmonic entrainment which will cause the system frequency to jump to 1/3 of the original 2nd harmonic frequency. This is an undesirable effect, although we could examine the frequency spectrum in the transition toward the entrainment. The spectrum became "rich" and "expanded" in harmonics just before the entrainment occurred. It became "clear" again after the entrainment. The spectrum structure and time series waveform of the velocity coupled system appears closer to the experimental data. The coupling coefficient in the system could be adjusted to achieve optimum results.

3. The 3rd harmonic could be generated by the nonlinearity of the system or by

using a three dimensional coupled oscillator model. There are six coupling coefficient parameters to be adjusted in the 3 dimensional coupled oscillator model which makes the modeling complicated. In the two dimensional model, there are only two coupling coefficients to be adjusted. The two dimensional model simulates the experimental data well in most observed cases. However, in some cases, such as the harmonic structure of the rats' temperature, the three dimensional coupled oscillator model is needed to simulate the experimental data because this model gives more freedom to approximate the complex harmonic structure.

4. Dynamic spectrum analysis revealed the dynamics of frequency transition as a transient *stimulus* was applied. The dynamic process of the circadian rhythm is an important issue which we explored. Frequency analysis was performed on the model with:

   (a) Periodic stimulus applied. The system was either entrained or unentrained. The spectrum for the latter was complicated. Both original and external frequency components existed in the system and some new harmonics were generated. This was the case especially when the system was nearly "entrained". The spectrum of the entrained system has basically the same "clear" structure as its original except for a shift in frequencies.

   (b) Nonperiodic stimulus applied. Dynamic spectrum analysis showed the transition process in the case of a phase delay shift or phase advance shift. "Overshoot" frequency components were found by this method which was consistent with the results using a frequency demodulation method.

5. We computed a coherence function using the frequency information from 2 channel circadian rhythms, temperature and activity, to obtain their nor-

malized correlation. The result from one of the monkey subjects under free running conditions shows high coherence occurring at the fundamental and 3rd harmonic frequencies of circadian temperature and activity rhythms. This conclusion needs to be further proved through coherence computation on more experimental data sets. This result, however, supports our assumptions in developing a two dimensional coupled oscillator model:

(a) Two coupled oscillators contribute to one circadian rhythm;

(b) The characteristic frequency of the main oscillator is the fundamental frequency of the system while the frequency of the coupled oscillator is at the second harmonic. Therefore the second harmonic frequency component in our model is independent of the fundamental, and could be adjusted;

(c) the 3rd harmonic is generated by the nonlinearity of the oscillator. Therefore this frequency is determined by the selection of the fundamental frequency and the amplitude of this component is determined by the selection of the degree of nonlinearity.

If the temperature and activity rhythms are each controlled by such an oscillator model, then the fundamental frequencies of these two rhythms are synchronized while the second harmonic frequency components of both oscillators are desynchronized (In the model we can simulate this by adjusting the frequency of the coupled oscillator.). Coherence results similar to these experimental results could be obtained from our two dimensional coupled oscillator model.

6. We used *bispectrum* analysis in this research to find the phase relation be-

tween harmonics of a circadian rhythm. This helped us to understand the essentials of harmonic structure, i.e., whether the third harmonic was generated by the fundamental and second harmonic? We tested the bispectrum method first on a model of three frequency components with related and unrelated phases. The result of bispectrum analysis on experimental temperature data did not show a phase relation of the 3rd harmonic with the fundamental and 2nd harmonic. More analysis is needed to verify this result.

Both the coherence and bispectrum computation need large numbers of segmentations of experimental data, either overlapped or non-overlapped, from one channel (bispectrum method) or two channels (coherence method).

9.2 Summary of Nonlinearity Analysis on the Models

Nonlinearity is an important feature of circadian rhythms. We have varied the nonlinear parameters in our models. The results have given us a picture of the effects on nonlinearity of the models in both time and frequency domains.

1. In the *time series*, the nonlinearity affects the distortion of the linear oscillation waveform. The waveform of a pure linear oscillator is a sinusoid while the nonlinear oscillator produce a distorted sinusoid. In the study of a one dimensional Van der Pol oscillator model we simulated the system with different values of the nonlinear parameter μ. The simulation results show that the shapes of the time series become more and more different from a pure sinusoid as μ increases.

2. The *period* of the Van der Pol oscillator model increased with increase of the nonlinearity. Experimental results showed the period increased rapidly when $\mu > 0.8$.

3. In the *frequency domain*, the nonlinearity affected the harmonic structure. Spectral results showed that the amplitude of the harmonics increased as the nonlinearity was increased. For the single Van der Pol type model, its spectrum only includes odd harmonics, and the increase of nonlinearity causes the levels of all these odd harmonics "to increase". In our two dimensional coupled oscillator model, the increase of nonlinearity in either oscillator causes the increase of amplitude of the harmonics in the main oscillator with different effect due to the manner of coupling.

   In the two dimensional direct coupling oscillator model, as we saw in section 4.7.1, the effect of the nonlinearity became stronger during direct coupling. The increase of nonlinearity in both oscillators caused an increase in the harmonic amplitude and finally caused 1/3 harmonic entrainment. This result is the combined effect of (2) and (3).

4. In the *phase plane*, the nonlinearity of the system can be observed in the unsymmetrical shapes of the closed orbits of the oscillation.

5. In the case of application of an *external stimulus*, the system with larger nonlinearity is easier to be entrained. The mathematical background and simulation results of this phenomenon can be found in section 7.2 . In the case of a linear system (nonlinear parameter = 0) both the original frequency of the system and the frequency of the external stimulus co-exist in the system while in the nonlinear system the system frequency can be totally entrained to the applied frequency.

9.3 Conclusions

A nonlinear mathematical model can be used to describe the circadian rhythm system. The model should be built to approach the experimental data in both time and frequency domains, in both stable states and dynamic processes. Our two dimensional coupled Van der Pol oscillator model approaches the experimental data well. The difference between this model and previously existing models is that this model is the first time that two coupled oscillators are used to represent one circadian rhythm in both time and frequency domains.

The analytical method is the traditional mathematical method to obtain the solution of nonlinear systems but two reasons prevented its application in this research:

1. This method generates large errors in the case of large nonlinearity;
2. It is very difficult to use this method in the case of coupled nonlinear oscillator systems.

We used computer simulation to solve the nonlinear differential equations in our model. We could easily get outputs of all the variables in the model as well as the first or higher derivatives of all the variables. This allowed us to easily obtain the phase plane plot.

The model data and experimental data were analyzed in both the time and frequency domains. The analysis included the following major topics:

The appearance of the time series and frequency spectrum;

The effects of nonlinearity on the time and frequency characteristics;

The effects of application of periodic and nonperiodic stimuli on the system time series, spectrum, and the possibility of changing the basic properties of the system, e.g., stopping the oscillation;

The correlations in the frequency domain between circadian temperature data and activity data, especially, the frequency correlations at the fundamental frequency and low order harmonics;

The phase relations between frequency components, especially, the phase coupling between the three main frequency components of circadian rhythms.

These analyses helped us to develop and modify our models thus to further understand the essentials of circadian rhythms as follows:

First, the circadian rhythm is a complex nonlinear oscillation. The time series and frequency spectrum are similar to those derived from a nonlinear oscillator model. A one dimensional model is convenient to be used to explore the dynamic properties while two and three dimensional coupled oscillators reveal better the features of circadian rhythms. Different nonlinear parameter values could be used to reflect various type of experimental data. The analysis results showed that the time series and spectrum of the model with relatively large nonlinearity is more similar to the experimental data.

Secondly, the frequency characteristics is an important aspect of circadian rhythms. Our experimental data showed the bimodality phenomenon and our model results revealed that this phenomenon was related to the harmonic structure. We computed the coherence, i.e., the frequency correlation between two

different circadian rhythms. High values of coherence were found in the fundamental and third harmonic of the experimental data. This also indicated that the two dimensional coupled oscillator model should be used for circadian rhythms. The 3 main frequency components in the spectrum of the experimental data were harmonically related but no phase-coupling evidence was found using bispectrum analysis. The coupling mode, the range of coupling coefficients and the non-linear parameter in the two or three dimensional coupled oscillator model could be carefully selected to represent the frequency characteristics of circadian rhythms.

Investigation of circadian rhythms under different stimuli indicated that they could be entrained or phase shifted. This is another evidence of the nonlinearity of the oscillator. The entrainment of such an oscillator under periodic stimulus mainly depends on the intensity of the stimulus and the frequency difference between the stimulus and the natural frequency of the oscillator. The phase shift occurring under nonperiodic stimulus already has some clinical applications. The modeling and simulation will greatly help the practical applications.

9.4 Further Development of the Study

The study of circadian rhythms opens a totally new area in bioengineering. Although scientists have made many effects to explore the essentials of circadian rhythms during the past 20 years, there are still a lot of unknown mysteries in this field, especially in human beings. The human circadian pacemaker, which regulates the body sleep-wake, temperature and other biological cycles, if it be completely understood, could be possibly reset much like an alarm clock. This will be not only used for treatment of circadian disorder, but could also be possibly

used for controlling the human beings' moods, health and mental activities. Our further work would design new experiments and develop analysis techniques to approach this direction.

High quality experimental data is the basis for us to do further exploration, and therefore the improvement of the acquisition process should be the first consideration for further development. Temperature circadian data was mainly used in this research. Long term uninterrupted data is needed for spectral, bispectral and other analyses. For example, If we want to use 40 segmentations with 10 cycles of non-overlapped data in each segmentation for computing the bispectrum, then it means that 400 days of uninterrupted data should be acquired. This requires the modification of the current data acquisition system to improve reliability. Automation for experimental data monitoring and segmentation should be considered. To get more reliable coherence results, synchronized activity and temperature data should be acquired. We currently count the activity of the subjects by counting their physical movement. Digital video image acquisition and processing may be considered for better activity data acquisition.

The experimental subjects should include not only animals but also human beings. Therefore a data base including long term records of human circadian rhythms under different conditions must be built. Small portable devices which include transducers and recorders for circadian data acquisition should be built and tested on human subjects.

The responses of the circadian system to different types of stimuli not only help us to understand the system but also create real physiological applications on human beings. As we discussed in the previous chapters, this has already been

employed for sleep-disorder treatment. Possible applications include treatment of other circadian clock disorders such as "jet-lag". All these applications should be performed very carefully to avoid any possible harmful effects on subjects. The development of a precise model for an individual subject may be needed to assist in this application.

The relation of circadian rhythms with a human mood and health conditions is a very interesting issue. The exploration of this issue needs the cooperation of physiologists. A reliable data base and advanced analysis techniques are also necessary conditions.

The further exploration of coherence and bispectrum based on long term reliable experimental data should be contemplated. The direct method used now for coherence and bispectrum computing has certain advantages but needs large numbers of segments to get smooth results. Indirect methods, such as computing the bispectrum from complex demodulation, should be tried and compared with the direct method.

The selection of models and the parameters in the model to approach the experimental data is a complex process. As we have shown here, we have employed several techniques in both time and frequency domains to get the desired results. In recent years, AI (artificial intelligence) and neural network application have become possible with the development of advanced computer techniques. The most important feature of a neural network application is that it can "learn" the unknown system. Its possible application in the field of circadian rhythm research will open a completely new direction. This will make the model selection and parameter selection automated.

Bibliography

[1] Anderson, R. B., *The Student Edition of MathCAD,* Reading, Massachusetts: Addison-Wesley Publishing Company,Inc., 1988.

[2] Aschoff, J.,"Free running and Entrained Circadian Rhythms", Aschoff, J., Ed., *Handbook of Behavioral Neurobiology,* Vol.4: "Biological Rhythms", New York: Plenum Press, 1981,PP.86.

[3] Aschoff, J., "A Survey on Biological Rhythms", Aschoff, J., Ed.,*Handbook of Behavioral Neurobiology,* Volume 4: "Biological Rhythms", New York: Plenum Press, 1981, pp.5-6.

[4] Baghdady, E.J., Ed., *Lectures on Communication System Theory* New York: McGraw-Hill Book Company, 1960, Chap.19.

[5] Bendat, J.S. and Piersol, A.G., *Random Data: Analysis and Measurement Procedures,* John Wiley & Sons, 1971, chap.1.

[6] Bergen, M., T., Tapp, W.N. and Reisman, S., "Telemetry Recovery Antenna", *Proc. of the Sixteenth Annual Northeast Bioengineering Conference,* 1990, pp. 125-126.

[7] Borbely, A.A., "A Two Process Model of Sleep Regulation", *Human Neurobiology 1,* pp.195-204, 1982.

[8] Blackman, R.B. and Tukey, J.W., *The Measurement of Power Spectra,* New York: Dover Publications Inc., 1958.

[9] Bloomfield, P., *Fourier Analysis of Time Series: An Introduction,* John Wiley & Sons pp.151-152.

[10] Bloomfield, P., *Fourier Analysis of Time Series: An Introduction,* John Wiley & Sons, pp.214-220.

[11] Carskadon, M.A. and Dement, W.C. "Midafternoon Decline in MSLT Scores on a Constant Routine", *Sleep Res.,* 14, pp292, 1985.

[12] Carter, G.C., Knapp, C.H. and Nuttall A.H., "Estimation of the Magnitude-Squared Coherence function Via Overlapped Fast Fourier Transform Processing", *IEEE Trans.: Audio Electroacoust., Vol.AU-21, No.4* pp.337-344, Aug.1973.

[13] *China Reconstruction*, June, 1988.

[14] Czeisler, C. A., et al, "Bright Light Induction of Strong (type 0) Resetting of the Human Circadian Pacemaker", *Science*, Vol.244, 1989, pp.1328-1333.

[15] Curran, M., "Resetting the Human Circadian Pacemaker", *Research Resources Reporter*, pp.5-7, February, 1990.

[16] Davis,H.T., *The Analysis of Economic Time Series*, Bloomington, Indiana: The Principle Press,Inc., 1941, pp.87-89.

[17] DMSP, Digital Model Simulation Package.

[18] Oppenheim, A.V., Ed., *Applications of Digital Signal Processing*, Englewood Cliff, New Jersey: Prentice-Hall,Inc., 1978.

[19] Enright, Thomas, J.,"Methodology", Aschoff, J., Ed., *Handbook of Behavioral Neurobiology*, volume 4: "Biological Rhythms", New York: Plenum Press, 1981, pp.11-15.

[20] Hayashi, C., *Nonlinear Oscillations in Physical Systems*, Princeton, New Jersey: Princeton University Press, 1985.

[21] Kaplan, W., *Advanced Mathematics for Engineers*, Addison-Wesley Publishing Company, 1981.

[22] Kronauer, R. E., "The Implications of Amplitude as A Parameter In Circadian Rhythms", *Proc. of the Annual International Conference of the IEEE Engineering in Medicine and Biology Society*, 1987, pp.282-283.

[23] Kronauer R. E., et al, "Mathematical Model of the Human Circadian System with Two Interacting Oscillators", *Am.J. Physiol*, 242:R3-R17, 1982.

[24] Levin, S., *The Mathematical Structure of the Human Sleep-Wake Cycle*, New York: Springer-Verlag,1986, pp.97-99.

[25] Monk, T. H., et al, "Inducing Jet Lag in the Laboratory: Patterns of Adjustment to an Acute Shift in Routine", *Aviat. Space Environ. Med.*, Vol. 59: pp. 703-710, 1988.

[26] Nikias, C. L. and Raghuveer, M.R. "Bispectrum Estimation: A Digital Signal Processing Framework", *Proc. IEEE Trans.* Vol.75, pp.869-891, 1987.

[27] Orr, W.C. and Naitoh, P., "The Coherence Spectrum: An Extension of Correlation Analysis to Chronobiology", *International Journal of Chronobiology*, Vol.3, 1976.

[28] Panter, P. F., *Modulation, Noise, and Spectral Analysis*, New York: McGrawhill Book Company, 1965, pp.325-326.

[29] Pavlidis, T., *Biological Oscillators: Their Mathematical Analysis*, New York: Academic Press Inc, 1973.

[30] Pittendrigh, C. S., "Circadian Systems: General Perspective", Aschoff,J., Ed., *Handbook of Behavioral Neurobiology*, Volume 4: "Biological Rhythms", New York: Plenum Press, 1981, pp.57–76.

[31] Pittendrigh, C.S., "Circadian Oscillations in Cells and the Circadian Organization of Multicellular Systems", Schmitt F.O., Worden F. G., Ed., *The Neurosciences: Third Study Program*, Cambridge, Massachusetts: MIT Press, 1974, pp.437-458.

[32] Poincaré, H., "Sur Les Courbes Definies Par Une Equation Differentielles", *Journal Math.*

[33] Poincaré, H., *Oeuvres*, Paris: Gauthier-Villars, Vol.1, 1928.

[34] Raghuveer, M.R. and Nikias, C. L. "Bispectrum Estimation: A Parametric Approach", *IEEE Trans.: Acous. Speech, Sig.Proc.*, Vol.ASSP-33, pp.1213-1230, 1985.

[35] Ralph, M. R., et al, "Transplanted Suprachiasmatic Nucleus Determines Circadian Period", *Science*, Vol.247, February, 1990, pp.975–978.

[36] Roberts, S.K.F., "Circadian Activity in Cockroaches: II. Entrainment and Phase Shifting", *J. Cell.Comp. Physiol.*, Vol.59, pp.175-196, 1962.

[37] Schwartz, *Information Transmission, Modulation, and Noise*, New York: McGraw-Hill Book Company, 1970, pp.223-230.

[38] Speckhart, F. H. and Green, W. L., *CSMP-the Continuous System Modeling Program*, Englewood Cliffs, New Jersey: Prentice-Hall,Inc., 1976.

[39] Strogatz, S. H.,*The Mathematical Structure of the Human Sleep-Wake Cycle*, New York: Springer-Verlag, 1986, pp.129-130.

[40] Stanley, W. D., Dougherty G. R. and Dougherty, R., *Digital Signal Processing*, (Second Edition), Reston, Virginia: Reston Publishing Company,Inc., 1984.

[41] Tukey, J.W., "Equalization and Pulse Shaping Techniques Applied to the Determination of Initial Sense of Rayleigh Waves", *The Need for Fundamental Research on Seismology, U.S.Dept. of State Report by the Panel on Seismic Improvement*, 1959, pp.95.

[42] Urabe, M., *Numerical Study of Periodic Solutions of the Van der Pol Equation*, pp.184-192.

[43] Van Ness, J.W., "Asymptotic Normality of Bispectral Estimates", *Ann Math. Stat.*, Vol.36, pp.1257-1272, 1966.

[44] Weiner, D.D.,"Experimental Study of FM Transient and Quasistatic Response", *M.S. thesis*, Department of Electrical Engineering, MIT, 1958.

[45] Wever, R. A., *The Circadian System of Man*, New York: Springer-Verlag, 1979.

[46] Winfree, A.T., "The Effect of Light Flashes on a Circadian Rhythm in Drosophila Pseudobscura", Ph.D Thesis, Princeton Univ., 1970.

[47] Yang, S., Reisman, S. S., Tapp, W.N., and Natelson, B.H.," Modeling the Circadian Substructure: Coupled Oscillator and Entrainment", *Proc. of the Annual International Conference of the IEEE Engineering in Medicine and Biology Society,* 1988, Vol.10, pp. 1822-1823.

Appendix A

CSMP Simulation Programs

```
************************************************************
* THE FOLLOWING CSMP PROGRAM IS TO SIMULATE SINGLE VAN DER
* POL TYPE OSCILLATOR MODEL  WITH DIFFERENT NONLINEARITY.
*
************************************************************


INITIAL
    PARAMETER UY=(.2,.8,1.6,3.2)
    K=24/2/3.1416
    WY=1.0
DYNAMIC
    Y2=UY/K*(1-Y*Y)*Y1-WY*WY/K/K*Y
    Y1=INTGRL(0.2,Y2)
    Y=INTGRL(0.6,Y1)
   TERMINAL
PRINT Y
TITLE SIMULATION OF THE VAN DER POL
TIMER FINTIM =250.0, OUTDEL=.1667, PRDEL=.1667
LABEL VAN DER POL OSCILLATORS
END
STOP
ENDJOB
```

```
************************************************************
* THE FOLLOWING CSMP PROGRAM IS TO SIMULATE THE MODIFIED
* VAN DER POL TYPE OSCILLATOR MODEL.
*
************************************************************
INITIAL
    A=0.001
    UY=0.1
    K=24/2/3.1416
    WY=.9231
DYNAMIC
    Y2=0.1/K*(1-Y*Y)*Y1-WY*WY/K/K*Y-UY*Y*Y*Y
    Y1=INTGRL(0.2,Y2)
    Y=INTGRL(A,Y1)
TERMINAL
PRTPLT Y
TIMER FINTIM = 480.0, OUTDEL=0.16667,
 PRDEL=0.16667,DELMIN=0.1E-12
LABEL VAN DER POL OSCILLATORS
END
STOP
ENDJOB
************************************************************
* THE FOLLOWING CSMP PROGRAM IS TO SIMULATE THE TWO
* DIMENSIONAL COUPLED VAN DER POL TYPE OSCILLATOR MODEL
* WITH DIFFERENT NONLINEARITY.
*
************************************************************
INITIAL
    PARAMETER UY=(0.2,0.8,1.6,3.2)
    UX=UY
    K=24/2/3.1416
    WX=1.92
    WY=.923
    FYX=-0.4
    FXY=-0.4
DYNAMIC
    X2=UX/K*(1-X*X)*X1-WX*WX/K/K*X-FYX*Y1/K
    X1=INTGRL(0.2,X2)
    X=INTGRL(0.6,X1)
    Y2=UY/K*(1-Y*Y)*Y1-WY*WY/K/K*Y-FXY*X1/K
    Y1=INTGRL(0.2,Y2)
    Y=INTGRL(0.6,Y1)
TERMINAL
PRINT Y,Y1
TIMER FINTIM = 720.0, OUTDEL=.1667, PRDEL=.1667
LABEL VAN DER POL OSCILLATORS
END
STOP
```

```
ENDJOB
************************************************************
* THE FOLLOWING CSMP PROGRAM IS TO SIMULATE TWO VAN DER
* POL TYPE OSCILLATOR MODEL  WITH DIFFERENT NONLINEARITY
* AND FIND THE DIFFERENCE.
*
************************************************************
INITIAL
    UX=0.1
    UY=0.8
    K=24/2/3.1416
    WX=.923
    WY=.961
    DYNAMIC
    X2=UX/K*(1-X*X)*X1-WX*WX/K/K*X
    X1=INTGRL(0.2,X2)
    X=INTGRL(0.6,X1)
    Y2=UY/K*(1-Y*Y)*Y1-WY*WY/K/K*Y
    Y1=INTGRL(0.2,Y2)
    Y=INTGRL(0.6,Y1)
    Z=Y-X
    U=DERIV(0.0,Z)
TERMINAL
PRINT Y,X,Z,U
TIMER FINTIM = 720.0, OUTDEL=.1667, PRDEL=.1667
LABEL VAN DER POL OSCILLATORS
END
STOP
ENDJOB
```

```
*************************************************************
* THE FOLLOWING CSMP PROGRAM IS TO SIMULATE THE PROCESS
* OF DELAY ADVANCE SHIFT IN  THE VAN DER POL TYPE
* OSCILLATOR MODEL.
*************************************************************
INITIAL
    KX=24/2/3.1416
    UX=0.1
    WX=.99
DYNAMIC
    T=1.0*(STEP(100.0)-STEP(116.0))
    Z1=IMPULS(103.0,24.0)
    Z2=IMPULS(115.0,24.0)
    Z=T*(PULSE(0.2,Z1)-PULSE(0.2,Z2))
    X2=UX/KX*X1*(1-4*X*X)-1/KX/KX*WX*X+Z
    X1=INTGRL(0.2,X2)
    X=INTGRL(0.6,X1)
TERMINAL
PRINT X
TIMER FINTIM = 500.0, OUTDEL=.1667, PRDEL=.1667
LABEL VAN DER POL OSCILLATORS
END
STOP
ENDJOB
*************************************************************
* THE FOLLOWING CSMP PROGRAM IS TO SIMULATE THE PROCESS
* OF PHASE ADVANCE SHIFT IN  THE VAN DER POL TYPE
* OSCILLATOR MODEL.
*
*************************************************************
INITIAL
    KX=24/2/3.1416
    UX=0.4
    WX=.99
DYNAMIC
    T=0.8*(STEP(106.0)-STEP(121.0))
    Z1=IMPULS(108.0,24.0)
    Z2=IMPULS(120.0,24.0)
    Z=T*(PULSE(0.2,Z1)-PULSE(0.2,Z2))
    X2=UX/KX*X1*(1-4*X*X)-1/KX/KX*WX*X+Z
    X1=INTGRL(0.2,X2)
    X=INTGRL(0.6,X1)
TERMINAL
PRINT X
TIMER FINTIM = 500.0, OUTDEL=.1667, PRDEL=.1667
LABEL VAN DER POL OSCILLATORS
END
STOP
ENDJOB
```

```
************************************************************
* THE FOLLOWING CSMP PROGRAM IS TO SIMULATE TO STOP
* THE VAN DER POL TYPE OSCILLATOR MODEL.
*
************************************************************
INITIAL
    KX=24/2/3.1416
    UX=0.1
    WX=.99
DYNAMIC
    T=1.0*(STEP(340.0)-STEP(356.0))
    Z1=IMPULS(343.0,24.0)
    Z2=IMPULS(355.0,24.0)
    Z=T*(PULSE(0.2,Z1)-PULSE(0.2,Z2))
    X2=UX/KX*X1*(1-4*X*X)-1/KX/KX*WX*X+Z
    X1=INTGRL(0.2,X2)
    X=INTGRL(0.6,X1)
TERMINAL
PRINT X
TIMER FINTIM = 800.0, OUTDEL=.1667, PRDEL=.1667
LABEL VAN DER POL OSCILLATORS
END
STOP
ENDJOB
```

Appendix B

FFT and other programs

```
PROGRAM LOW.FOR

CCCCCCCCCCCCCCCCCCCCCCCCCCCCCCCCCCCCCCCCCCCCCCCCCCCCCCCCCCCCCCCCCCCC
C
C THIS PROGRAM IS USED FOR 16 ORDER BUTTERWORTH
C LOW PASS FILTER COMPLEMENTATION. THE COEFFICIENT
C WAS GENERATED BY FILTER DESIGN PROGRAM.
C
C
CCCCCCCCCCCCCCCCCCCCCCCCCCCCCCCCCCCCCCCCCCCCCCCCCCCCCCCCCCCCCCCCCCCC
       real fyy(4000), mf(4000)
       integer i,j
       a0=8102.36
       b0=-4040.70
       c0=4065.66
       a1=8102.36
       b1=-4016.223
       c1=4090.137
       a2=8102.36
       b2=-3993.165
       c2=4113.195
       a3=8102.36
       b3=-3972.412
```

```
      c3=4133.95
      a4=8102.36
      b4=-3954.77
      c4=4151.595
      a5=8102.36
      b5=-3940.89
      c5=4165.462
      a6=8102.36
      b6=-3931.354
      c6=4175.016
      a7=8102.36
      b7=-3926.48
      c7=4179.88
      open (3,file='data')
      do 30 j=1,3000
30    read(3,*) mf(j)
40    fyy(1)=mf(1)/c0
      fyy(2)=(mf(2)+2*mf(1)+a0*fyy(1))/c0
      do 50 i= 3,3000
50    fyy(i)=(mf(i)+2*mf(i-1)+mf(i-2)+a0*fyy(i-1)+\
       b0*fyy(i-2))/c0
      do 60 i=1,3000
60    mf(i)=fyy(i)
      fyy(1)=mf(1)/c1
      fyy(2)=(mf(2)+2*mf(1)+a1*fyy(1))/c1
      do 70 i= 3,3000
70    fyy(i)=(mf(i)+2*mf(i-1)+mf(i-2)+a1*fyy(i-1)+\
        b1*fyy(i-2))/c1
      do 80 i=1,3000
80      mf(i)=fyy(i)
          fyy(1)=mf(1)/c2
      fyy(2)=(mf(2)+2*mf(1)+a2*fyy(1))/c2
       do 90 i= 3,3000
90    fyy(i)=(mf(i)+2*mf(i-1)+mf(i-2)+a2*fyy(i-1)+\
        b2*fyy(i-2))/c2
      do 100 i=1,3000
100   mf(i)=fyy(i)
          fyy(1)=mf(1)/c3
      fyy(2)=(mf(2)+2*mf(1)+a3*fyy(1))/c3
      do 110 i =3,3000
110   fyy(i)=(mf(i)+2*mf(i-1)+mf(i-2)+a3*fyy(i-1)+\
        b3*fyy(i-2))/c3
      do 120 i=1,3000
120   mf(i)=fyy(i)
          fyy(1)=mf(1)/c4
      fyy(2)=(mf(2)+2*mf(1)+a4*fyy(1))/c4
       do 130 i=3,3000
130   fyy(i)=(mf(i)+2*mf(i-1)+mf(i-2)+a4*fyy(i-1)+\
        b4*fyy(i-2))/c4
      do 140 i=1,3000
```

```
140     mf(i)=fyy(i)
             fyy(1)=mf(1)/c5
        fyy(2)=(mf(2)+2*mf(1)+a5*fyy(1))/c5
          do 150 i=3,3000
150     fyy(i)=(mf(i)+2*mf(i-1)+mf(i-2)+a5*fyy(i-1)+\
          b5*fyy(i-2))/c5
        do 160 i=1,3000
160     mf(i)=fyy(i)
             fyy(1)=mf(1)/c6
        fyy(2)=(mf(2)+2*mf(1)+a6*fyy(1))/c6
        do 170 i=3,3000
170     fyy(i)=(mf(i)+2*mf(i-1)+mf(i-2)+a6*fyy(i-1)+\
          b6*fyy(i-2))/c6
        do 180 i=1,3000
180     mf(i)=fyy(i)
             fyy(1)=mf(1)/c7
        fyy(2)=(mf(2)+2*mf(1)+a7*fyy(1))/c7
        do 190 i=3,3000
190     fyy(i)=(mf(i)+2*mf(i-1)+mf(i-2)+a7*fyy(i-1)+\
          b7*fyy(i-2))/c7
        open(4,file='result')
        do 200 i=1,3000
200     write(4,*)fyy(i)
        stop
        end
```

```
Raster.C
*/
************************************************************
This program is used for ROAST PLOTTING.
************************************************************
For each day, 147 integer values are read in from DATAFILE.
The first 3 are month, day and year. Year can be 2 or 4
digits.
The rest 144 are 10-minute data values.
Every 2 consecutive 10-minute values are added to yield 72
20-minute values.
On each line, we have the plot for the current day on the
right
and the plot for the previous day on the left.
The limits and the corresponding symbols are read in from the
LIMITSFILE. The default LIMITSFILE is "limits.default".
The plot is redirected to the OUTPUTFILE.
This file is printed on a hardcopy terminal.
The horizantal pitch is set to 13.2 char/inch ( ESC[3w ).
The vertical pitch is set to 6 lines/inch ( ESC[1z ).
The horizantal pitch is reset to 10 char/inch ( ESC[1w ).

MAXDAYS determine the max. number of lines in the file OUT-
PUT.
It is currently set to 750 lines ( a little more than 2 years
of data).

*/

#include <stdio.h>
#define MARK1 "0102030405060708091011121314151617l8"
#define MARK2 "1920212223242526272829303132333435"
#define MARK3 "|||||||||||||||||||"
#define MARK4 "|||||||||||||||||||"
#define NO_INTERVALS 71
#define TRUE 1
#define MAXDAYS 750


main(argc,argv)
  int argc ;
  char *argv[] ;
  {
  if (argc == 5)
    tty20( argv[1],argv[2],argv[3],argv[4] ) ;
  else if (argc == 4)
    tty20( argv[1],argv[2],argv[3],"limits.default") ;
  else
    {
    usage() ;
```

```
    exit(1) ;
    }
  }

usage()
  {
  printf("usage:   ttyw  datafilename   datafile
 outputfile [limitsfile]\n") ;
  }

tty20(filename,datafile,outputfile,limitsfile)
  char *filename, *datafile, *outputfile, *limitsfile ;
  {
  FILE *fp1, *fp2, *fp3 ;
  char ch ;
  int value1, value2 ;
  int i, j, temp, limitcount = 0 ;
  int activity, day, month, year ;
  int daycount = 0 ;
  int  limit[20] ,              /* values of limits */
       rawdata[2*NO_INTERVALS], /* 144 values of raw data */
       data[NO_INTERVALS] ;     /* 72 values of data */
  char symbol[20],   /* symbols corresponding to limits */
       plot1[NO_INTERVALS],     /* previous-day plot */
       plot2[NO_INTERVALS] ;    /* current-day plot  */

  /* open limits file. */
  if ( (fp1 = fopen(limitsfile,"r")) == NULL )
    {
    printf("ERROR  %s: can't open for reading.
   \n",limitsfile) ;
    exit(1) ;
    }

  /* read limits & symbols from limits file. */
  while (TRUE)
    {
    if ( feof(fp1) ) break ;  /* EOF is encountered */
    fscanf(fp1,"%d %c\n", &temp, &ch) ;
    limit[limitcount] = temp ;
    symbol[limitcount++] = ch ;
    }

  fclose(fp1) ;       /* close limits file. */

  /* open data file. */
  if ( (fp2 = fopen(datafile,"r")) == NULL )
    {
    printf("ERROR  %s: can't open for reading.\n",datafile) ;
    exit(1) ;
```

```
  }

/* open output file. */
if ( (fp3 = fopen(outputfile,"w")) == NULL )
  {
  printf("ERROR  %s: can't open for
  writing.\n",outputfile) ;
  exit(1) ;
  }

/* set vertical pitch = 6 lines/inch ( ESC[1z ) */
/* fprintf(fp3,"\33\133\61\172"); */

/* form length = 66 lines (11 inches * 6 lines/inch ) */
skiplines(fp3,10) ;

/* set horizantal pitch = 8.25 char/inch ( ESC[8w ) */
/* fprintf(fp3,"\33\133\70\167"); */

/* print name of data file at the top. */
fprintf(fp3,"\n %40c filename : %s\n\n", ' ', filename) ;

/* set horizantal pitch = 13.2 char/inch ( ESC[3w ) */
/* fprintf(fp3,"\33\133\63\167"); */

/* initialize current-day plot to blanks. */
for (i=0 ; i < NO_INTERVALS ; i++ )
  *(plot2+i) = ' ' ;

while (TRUE)
  {
  if ( feof(fp2) ) break ;  /* EOF is encountered */

  if  (  daycount == MAXDAYS ) break ;  /*
 Output file is getting too fat */
  daycount++ ;

  /* read month, day and year. */
  fscanf(fp2,"%d %d %d", &month, &day, &year ) ;

  /* read 144 values of raw data. */
  for ( i = 0 ; i < 2*NO_INTERVALS ; i++)
    fscanf(fp2,"%d\n",(rawdata+i)) ;

  /* add every two consecutive values of raw data
     to yield 72 values of data.
     NA's are taken care of. */

  for ( i = 0, j = 0 ; i < NO_INTERVALS ; i++, j +=2 )
    {
```

```
      value1 = *(rawdata+j) ;
      value2 = *(rawdata+j+1) ;
      if ( value1 < 0 )
        *(data+i)  = value2 ;
      else if ( value2 < 0 )
        *(data+i)  = value1 ;
      else
        *(data+i)  = value1 + value2 ;
      }

    /* copy current-day plot into previous-day plot. */
    for (i=0 ; i < NO_INTERVALS ; i++ )
      *(plot1+i) = *(plot2+i) ;

    activity = 0 ;

    /* determine the symbol corresponding to each
   data value. */
    for ( i = 0 ; i < NO_INTERVALS ; i++ )
      {
      *(plot2+i) = ' ' ;
      temp = *(data+i) ;
      if (temp > 0)  /* add only if value is not an NA */
        activity += temp ;
      for ( j = limitcount - 1 ; j >= 0 ; j-- )
        if( temp >= *(limit+j) )
          {
          *(plot2+i) = *(symbol+j) ;
           break ;
          }
      }

    /* print date in the format dd/mm/yy */
      fprintf(fp3,"\n%d%d/%d%d/%2d
         ",month/10,month%10,day/10,day%10,year%100);

    for (i = 0 ; i < NO_INTERVALS ; i++ )   /*
      print previous-day plot */
      fprintf(fp3,"%c",*(plot1+i)) ;

    for (i = 0 ; i < NO_INTERVALS ; i++ )   /*
     print current-day plot */
      fprintf(fp3,"%c",*(plot2+i)) ;

    fprintf(fp3,"   %5d",activity) ;        /*
     print total activity */

    }  /* while */

  fclose(fp2) ;      /* close data file. */
```

```
   fprintf(fp3,"\n\n
%s%s%s%s\n",MARK3,MARK4,MARK3,MARK4) ;
  fprintf(fp3,"
%s%s%s%s\n\n\n",MARK1,MARK2,MARK1,MARK2) ;
  fprintf(fp3,"            ") ;
  for (i = 0 ; i < limitcount ; i++ )
    fprintf(fp3,"%15c  ",*(symbol+i)) ; /*
   print symbols for reference */
  fprintf(fp3,"\n            ") ;
  for (i = 0 ; i < limitcount ; i++ )
    fprintf(fp3,"%15d  ",*(limit+i))  ; /*
  print limits for reference */

  /* reset horizantal pitch to 10 char/inch ( ESC[1w ) */
  /* fprintf(fp3,"\n\33\133\61\167"); */

  /* form length = 66 lines (11 inches * 6 lines/inch ) */
  skiplines(fp3,1) ;

  fclose(fp3) ;      /* close output file. */
  }


skiplines(fp,n)
  FILE *fp ;
  int n ;
  {
  int i = 0 ;
  for (  ; i < n ; i++ )
    putc('\n',fp) ;
  }



************************************************
*
*   Symbol file: LIM
*
************************************************
0  .
8  -
16 +
24 *
32 #
```

```
PROGRAM PERIOD.FOR

CCCCCCCCCCCCCCCCCCCCCCCCCCCCCCCCCCCCCCCCCCCCCCCCCCCCCCCCCCCCCCCCCC
C
C THIS PROGRAM IS DESIGNED TO DETECT THE PERIOD
C OF A TIME SERIES BY ZERO MEANING DETECTION
C METHOD.
C
CCCCCCCCCCCCCCCCCCCCCCCCCCCCCCCCCCCCCCCCCCCCCCCCCCCCCCCCCCCCCCCCCC
C
      CHARACTER*64 FNAME, RNAMEX, RNAMEY
      INTEGER I,J,NX,NY,NU
      REAL LX,LY,LTX,LTY,TX(300),TY(100)
      DATA NX/0/,NY/0/,LX/0.1/, LY/0.1/,LTX/0.0/, LTY/0.0/
      WRITE(*,3)
3     FORMAT(' PLEASE INPUT THE NU OF DATA FILE-'\)
      READ(*,4)NU
4     FORMAT(I5)
      WRITE(*,5)
5     FORMAT(' PLEASE INPUT THE NAME OF THE DATA FILE-'\)
      READ(*,8)FNAME
8     FORMAT(A)
C     OPEN THE DATA FILE TO READ THE DATA.
C
      OPEN(3,FILE=FNAME)
      DO 60,J=1,NU
1     READ(3,15)TIME,X,Y
15    FORMAT(1X,3F10.4)
      IF((X .GE.0.0 ).AND. (LX.LT.0.0)) GOTO 20
      GOTO 25
20    TX(NX)=TIME-LTX
      LTX=TIME
      NX=NX+1
25    LX = X
      IF((Y.GE.0.0 ).AND. (LY.LT.0.0)) GOTO 40
      GOTO 50
40    TY(NY)=TIME-LTY
      LTY=TIME
      NY=NY+1
50    LY=Y
60    CONTINUE
      CLOSE (3)
      OPEN (4,FILE='TX.DAT')
      DO 80 I=6,NX
      WRITE(4,70)I-5,TX(I)
70    FORMAT(I3,F10.4)
80    CONTINUE
      CLOSE (4)
      OPEN (5,FILE='TY.DAT')
      DO 90 I=6,NY
```

```
        WRITE(5,70)I-5,TY(I)
90      CONTINUE
        CLOSE(5)
        END
```

```
PROGRAM FEXTRACT.FOR

CCCCCCCCCCCCCCCCCCCCCCCCCCCCCCCCCCCCCCCCCCCCCCCCCCCCCCCCCCCCCCCCCC
C
C
C THIS PROGRAM READ THE SIMULATION RESULTS FROM CSMP OUTPUT
C SEPERATE THEM (FOR DIFFERENT PARAMETER SIMULATION), AND
C THEN COMPUTE THE SPECTRUM AND EXTRACT THE PEAKS FROM
C THE SPECTRUM.
C
C
CCCCCCCCCCCCCCCCCCCCCCCCCCCCCCCCCCCCCCCCCCCCCCCCCCCCCCCCCCCCCCCCCC
         DIMENSION POD(40,40),YD(40,40)
         INTEGER I,NY,NU
         REAL Y(16384),W(16384),PSE(16384),YMAX,YSK
         COMPLEX YY(16384)
         CHARACTER*25 FILENAME, PSFILE
         DATA POD/1600*0.0/,YD/1600*0.0/
         PI=3.1415926
         NU=0
        OPEN(3,FILE='MODEL.OUT')
1        YMAX=1.0
        DO 4  I=1,1440
2       READ(3,15,ERR=3,END=905)TIME,YSK,Y1SKP
        GOTO 4
3       GOTO 2
4       CONTINUE
        DO 30 J=1,3000
5       READ(3,15,ERR=17,END=905)TIME,Y(J),Y1SKP
15      FORMAT(3E12.4)
16      GOTO 18
17      GOTO 5
18      IF((TIME .EQ. 0.000) .AND. (Y(J) .EQ. 0.000))GOTO 5
        IF(Y(J).GT. YMAX) YMAX=Y(J)
        IF(J .LE. 100) GOTO 30
```

```
20      IF (TIME .GE. 719.8) GOTO 40
30      CONTINUE
40      NU=NU+1
         WRITE(*,*) ' '
         WRITE(*,*) '      !!!!!!!!!!!!!!!!!!!!!!!! '
         WRITE(*,*) 'THIS PROGRAM COMPUTES THE SPECTRUM  '
         WRITE(*,*) '      !!!!!!!!!!!!!!!!!!!!!!!! '
         WRITE(*,*) ' '
C
         M=12
         NPTS=2048
         NFFT=2**M
         CALL WINDOW(W,NPTS,4)
C
C...REMOVE MEAN AND ZERO PADDING
C
         SCALE=1.0
         CALL ZOMEAN(Y,NPTS,AVE,SCALE)
C
         DO 500 K=1, NPTS
            YY(K)=CMPLX(Y(K)*W(K),0.)
500      CONTINUE
C
         DO 600 I=NPTS+1, NFFT
           YY(I)=CMPLX(0.,0.)
600      CONTINUE
         CALL NINFFT(YY,M,1)
         NY=1
         DO 610 I=1,NFFT/2+1
         PSE(I)=CABS(YY(I))
C
         IF((I .LT.4) .OR. (I .GT.200)) GOTO 610
         IF (NY.GT.6) GOTO 602
         THRE=100.0/FLOAT(NY*NY)
          GOTO 603
602      THRE=10
603         IF(PSE(I-2) .LT. THRE) GOTO 610
         D1=PSE(I-2)-PSE(I-3)
         D2=PSE(I-2)-PSE(I-1)
         D3=PSE(I-1)-PSE(I)
         DD3=PSE(I-3)/8.0
         DD1=PSE(I-1)/8.0
         DD0=PSE(I)/8.0
         IF ((D1. GT. DD3) .AND. (D2 .GT. DD1)) GOTO 604
         IF ((D1 .GT. DD3) .AND. (D3 .GT. DD0)) GOTO 605
         GOTO 610
604      POD(NU,NY)=NFFT/FLOAT(I-3)/6.0
         YD(NU,NY)=PSE(I-2)
         GOTO 608
605      IF(PSE(I-2).GT.PSE(I-1)) GOTO 604
```

```
        POD(NU,NY)=NFFT/FLOAT(I-2)/6.0
        YD(NU,NY)=PSE(I-1)
608     IF(POD(NU,NY) .EQ. POD(NU,NY-1)) THEN
        POD(NU,NY)=0.0
        YD(NU,NY)=0.0
        GOTO 610
        ENDIF
        WRITE(*,*)NU,NY
        WRITE(*,*)POD(NU,NY),YD(NU,NY)
        NY=NY+1
610     CONTINUE
CCCCCCCCCCCCCCCCCCCCCCCCCCCCCCCCCCCCCC
C
        IF(NU .EQ. 1) FILENAME='SYP1.WK1'
        IF(NU .EQ. 2) FILENAME='SYP2.WK1'
        IF(NU .EQ. 3) FILENAME='SYP3.WK1'
        IF(NU .EQ. 4) FILENAME='SYP4.WK1'
        IF(NU .EQ. 5) FILENAME='SYP5.WK1'
        IF(NU .EQ. 6) FILENAME='SYP6.WK1'
        IF(NU .EQ. 7) FILENAME='SYP7.WK1'
            OPEN(UNIT=10,FILE=FILENAME)
            DO 900 I=1, NFFT/2+1
               WRITE(10,*) PSE(I)
900       CONTINUE
            CLOSE(UNIT=10,STATUS='KEEP')
            GOTO 1
905            OPEN(UNIT=12,FILE='ANA1.WK1')
            DO 910 I=1,NU
               WRITE(12,*)POD(I,1),YD(I,1)
910        CONTINUE
            CLOSE(UNIT=12,STATUS='KEEP')
            OPEN(UNIT=12,FILE='ANA2.WK1')
            DO 920 I=1,NU
               WRITE(12,*)POD(I,2),YD(I,2)
920       CONTINUE
            CLOSE(UNIT=12,STATUS='KEEP')
            OPEN(UNIT=12,FILE='ANA3.WK1')
            DO 930 I=1,NU
               WRITE(12,*) POD(I,3),YD(I,3)
930       CONTINUE
            CLOSE(UNIT=12,STATUS='KEEP')
            OPEN(UNIT=11,FILE='ANA4.WK1')
            DO 940 I=1,NU
               WRITE(11,*) POD(I,4),YD(I,4)
940       CONTINUE
            CLOSE(UNIT=11,STATUS='KEEP')
           OPEN(UNIT=11,FILE='ANA5.WK1')
           DO 945 I=1,NU
               WRITE(11,*) POD(I,5),YD(I,5)
945       CONTINUE
```

```
            CLOSE(UNIT=11,STATUS='KEEP')
           OPEN(UNIT=11,FILE='ANA6.WK1')
           DO 948 I=1,NU
               WRITE(11,*) POD(I,6),YD(I,6)
948       CONTINUE
            CLOSE(UNIT=11,STATUS='KEEP')
950          STOP
            END

CCCCCCCCCCCCCCCCCCCCCCCCCCCCCCCCCCCCCCCCCCCCCCCCCCCCCCCCCCCCCCCCCCCC
C
C    SUBROUTINE ... WINDOW... GENERATES DIFFERENT WINDOWS
C
C    USAGE: CALL WINDOW(W,N,IDGT)
C
C    W- OUTPUT VECTOR OF DIMENSION N, WINDOW FUNCTION
C    N- WINDOW LENGTH
C    IDGT- TYPE OF WINDOWING FUNCTION
C          1: RECTANGULAR
C          2: BARTLETT
C          3: HANNING
C          4: HAMMING
C          5: BLACKMAN
C
C************************************************************
        SUBROUTINE WINDOW(W,N,IDGT)
        REAL W(N)
        PI=3.1415926
        NHAF=N/2
C
        WRITE(*,*) '  '
        IF (IDGT.EQ.1) THEN
            DO 10 I=1, N
               W(I)=1.0
  10        CONTINUE
        GOTO 99
C
        ELSEIF (IDGT.EQ.2) THEN
            DO 20 I=1, NHAF
               W(I)=2.*FLOAT(I-1)/FLOAT(N-1)
  20        CONTINUE
            DO 30 I=NHAF+1, N
               W(I)=2.-2.*FLOAT(I-1)/FLOAT(N-1)
  30        CONTINUE
        GOTO 99
C
        ELSEIF (IDGT.EQ.3) THEN
            DO 40 I=1, N
               ANG=2.*PI*FLOAT(I-1)/FLOAT(N-1)
               W(I)=0.5*(1.-COS(ANG))
```

```
 40         CONTINUE
        GOTO 99
C
        ELSEIF (IDGT.EQ.4) THEN
            DO 50 I=1, N
               ANG=2.*PI*FLOAT(I-1)/FLOAT(N-1)
               W(I)=0.54-0.46*COS(ANG)
 50         CONTINUE
        GOTO 99
C
        ELSEIF (IDGT.EQ.5) THEN
            DO 60 I=1, N
               ANG=2.*PI*FLOAT(I-1)/FLOAT(N-1)
               W(I)=0.42-0.5*COS(ANG)+0.08*COS(2.*ANG)
 60     CONTINUE
        GOTO 99
C
        ELSE
        ENDIF
 99     WRITE(*,*) '  '
        RETURN
        END
```

```
CCCCCCCCCCCCCCCCCCCCCCCCCCCCCCCCCCCCCCCCCCCCCCCCCCCCCCCCCCCCCCCCCCC
CC
CC     SUBROUTINE ZOMEAN (2/23/88)
CC
CC     USAGE: CALL ZOMEAN(X,NPTS,AVE,SCALE)
CC
CC            X- INPUT ARRAY
CC            AVE- AVERAGE OF THE INPUT ARRAY
CC            SCALE- SCALING FOR THE OUTPUT
CC
CCCCCCCCCCCCCCCCCCCCCCCCCCCCCCCCCCCCCCCCCCCCCCCCCCCCCCCCCCCCCCCCCCC
         SUBROUTINE ZOMEAN(X,NPTS,AVE,SCALE)
         REAL X(1), AVE, SCALE
         INTEGER NPTS
C
         SUM=0.0
         DO 10 I=1, NPTS
            SUM=SUM+X(I)
 10      CONTINUE
C
         AVE=SUM/FLOAT(NPTS)
         DO 20 I=1, NPTS
            X(I)=SCALE*(X(I)-AVE)
 20      CONTINUE
C
         RETURN
         END
CC
CCCCCCCCCCCCCCCCCCCCCCCCCCCCCCCCCCCCCCCCCCCCCCCCCCCCCCCCCCCCCCCCCCC
C
C        SUBROUTINE ... NINFFT ...
C
C        CALCULATES THE DISCRETE FAST FOURIAR TRANSFORM OR
C        THE INVERSE DISCRETE FAST FOURIAR TRANSFORM
C        USING DECIMATION-IN-FREQUENCY ALGORITHM
C
C        USAGE:  CALL NINFFT(X,M,SIGN)
C
C        ARGUMENTS:
C                X-COMPLEX ARRAY OF DIMENSION N
C                M-INTEGER (N=2**M)
C                SIGN=1 PERFORM FAST FOURIAR TRANSFORM
C                 SIGN=-1 PERFORM INVERSE FAST FOURIAR TRANS-
FORM
C
C        REMARKS: X(N-I+1) = C.C. OF X(I+1) FOR I:1-->N/2-1
C                 i.e., X(1)-->X(N/2+1) CORREEPONDS  0-->PI
C
C        SUBROUTINE REQUIRED : NONE
C
```

```
CCCCCCCCCCCCCCCCCCCCCCCCCCCCCCCCCCCCCCCCCCCCCCCCCCCCCCCCCCCCCCC
C
C
        SUBROUTINE NINFFT(X,M,SIGN)
        COMPLEX  X(1), U, W, T
        INTEGER LE1,LE,SIGN
        N=2**M
        PI=3.14159265358979
C...CHECK IF PERFORMING INVERSE FFT
        IF (SIGN.EQ.1) GO TO 5
        DO  1   I=1,N
           X(I)=X(I)/FLOAT(N)
  1     CONTINUE
C
  5     DO 20 L=1,M
              LE=2**(M+1-L)
              LE1=LE/2
              U=CMPLX(1.0,0.0)
          W=CMPLX(COS(PI/FLOAT(LE1)),-
SIGN*SIN(PI/FLOAT(LE1)))
              DO 20  J=1, LE1
              DO 10  I=J, N, LE
                 IP=I+LE1
                 T=X(I)+X(IP)
                 X(IP)=(X(I)-X(IP))*U
                 X(I)=T
  10         CONTINUE
             U=U*W
  20    CONTINUE
        NV2=N/2
        NM1=N-1
        J=1
        DO 30   I=1,NM1
           IF(I.GE.J) GO TO 25
           T=X(J)
           X(J)=X(I)
           X(I)=T
  25       K=NV2
  26       IF(K.GE.J) GO TO 30
           J=J-K
           K=K/2
           GO TO 26
  30    J=J+K
C
        WRITE(*,*) ' '
        WRITE(*,*) '!!! RETURN FROM SUBROUTINE NINFFT !!!'
        RETURN
        END
```

```
Program COH.FOR

CCCCCCCCCCCCCCCCCCCCCCCCCCCCCCCCCCCCCCCCCCCCCCCCCCCCCCCCCCCCCCCCCCCC
C
C THIS PROGRAM IS TO COMPUTE THE COHERENCE.
C
CCCCCCCCCCCCCCCCCCCCCCCCCCCCCCCCCCCCCCCCCCCCCCCCCCCCCCCCCCCCCCCCCCCC


      SUBROUTINE COH1(XR,XI,YR,YI,NSEG,NT,CXY,COH)
C
C
      DOUBLE TCXX(NSEG,NT),TCYY(NSEG,NT)
       DOUBLE TCXY(NSEG,NT),TQXY(NSEG,NT)
      DOUBLE CXX(NT),CYY(NT),CXY(NT),QXY(NT),NUM(NT)
      DOUBLE DEN(NT),COH(NT)
      DATA CXX(NT)/0.0,CYY(NT)/0.0,CXY(NT)/0.0,QXY(NT)/0.0
C
C
      DO 10 J=1,NSEG
      DO 10 I=1, NT
      TCXX(J,I)=XR(J,I)**2+XI(J,I)**2
      TCYY(J,I)=YR(J,I)**2+YI(J,I)**2
      TCXY(J,I)=XR(J,I)*YR(I,J)+XI(J,I)*YI(J,I)
      TQXY(J,I)=XI(J,I)*YR(I,J)-XR(J,I)*YI(J,I)
 10   CONTINUE
C
      DO 20 J=1,NSEG
      DO 20 I=1,NT
      CXX(I)=CXX(I)+TCXX(J,I)/3.0
      CYY(I)=CYY(I)+TCYY(J,I)/3.0
      CXY(I)=CXY(I)+TCXY(J,I)/3.0
      QXY(I)=QXY(I)+TQXY(J,I)/3.0
 20    CONTINUE
C
C
     DO 30 I=1,NT
     NUM(I)=CXY(I)**2+QXY(I)**2
     DEN(I)=CXX(I)*CXY(I)
     IF(DEN.EQ.0.0) THEN COH(I)=NUM(I)
      ELSE
     COH(I)=NUM(I)/DEN(I)
 30  CONTINUE
     RETURN
     END
```

```
Program BIS.FOR

CCCCCCCCCCCCCCCCCCCCCCCCCCCCCCCCCCCCCCCCCCCCCCCCCCCCCCCCCCCCCCCCCCCC
CC
CC       THIS PROGRAM IS FOR BISPECTRUM COMPUTING.
CC
CC       ESTIMATES POWER SPECTRUM, BISPECTRUM AND
CC         BICOHERENCE INDEX
CC       VIA THE CONVENTIONAL APPROACH (DIRECT METHOD)
CC
CC       SUBROUTINES REQUIRED: WINDOW, NINFFT, ZOMEAN
CC
CCCCCCCCCCCCCCCCCCCCCCCCCCCCCCCCCCCCCCCCCCCCCCCCCCCCCCCCCCCCCCCCCCCC
         REAL Y(1024),W(1024),PSE(513)
         COMPLEX YY(1024), BISP(129,129), BIJ
         INTEGER OST
         CHARACTER*1  AVG, PSEYN
         CHARACTER*25 FILENAME, INFILE, BISFILE, BICFILE,
PSFILE
         PI=3.1415926
C
         WRITE(*,*) ' '
         WRITE(*,*) '      !!!!!!!!!!!!!!!!!!!!!!!!! '
         WRITE(*,*) 'THIS PROGRAM COMPUTES THE BISPECTRUM  '
         WRITE(*,*) '  BICOHERENCE AND POWER SPECTRUM '
         WRITE(*,*) '     (VIA THE DIRECT APPROACH) '
         WRITE(*,*) '      !!!!!!!!!!!!!!!!!!!!!!!!! '
         WRITE(*,*) ' '
C
         WRITE(*,*) '>>> DATA FILE [A25] ?'
         READ(*,10) FILENAME
   10    FORMAT(A25)
         WRITE(*,*) '>>> # OF SEGMENTS OF INPUT ?'
         READ(*,*)  NSEG
         WRITE(*,*) '>>> # OF SAMPLES IN EACH SEG [MAX=1024] ?
'
         READ(*,*)  NPTS
         WRITE(*,*) '>>> SAMPLING FREQUENCY ? [Hz]:'
         READ(*,*) FSAMP
         WRITE(*,*) '>>> SCALING FACTOR ? '
         WRITE(*,*) '   (TO SCALE THE SAMPLE VALUE) '
         WRITE(*,*) '   '
         READ(*,*) SCALE
C
         WRITE(*,*) '>>> NFFT=2**M [ENTER M, MAX=10]: '
         READ(*,*) M
         NFFT=2**M
         FDIV=FSAMP/FLOAT(NFFT)
         WRITE(*,*) '  DEFAULT FREQ RESOLUTION IS ', FDIV
```

```
      WRITE(*,*) ' '
      WRITE(*,*) '>>> DESIRED FREQ RESOLUTION [HZ] ?'
      WRITE(*,*) 'NOTE:MUST BE GREATER OR EQUAL TO DEFAULT'
      WRITE(*,*) ' '
      READ(*,*) DIFF
      NSK=INT(DIFF*NFFT/FSAMP)
      WRITE(*,*) '... SKIP # --> ',NSK
      WRITE(*,*) ' '
C
      WRITE(*,*) '>>> FREQ RANGE IN X-AXIS [HZ] ?'
      READ(*,*) FX0, FX1
      NFX=INT((FX1-FX0)/DIFF)+1
      INX=INT(FX0*NFFT/FSAMP)
      WRITE(*,*) '... # OF FREQ SAMPLES --> ',NFX
CC    WRITE(*,*) '... STARTING INDEX    --> ',INX
      WRITE(*,*) ' '
C
      WRITE(*,*) '>>> FREQ RANGE IN Y-AXIS [HZ] ?'
      READ(*,*) FY0, FY1
      NFY=INT((FY1-FY0)/DIFF)+1
      INY=INT(FY0*NFFT/FSAMP)
      WRITE(*,*) '... # OF FREQ SAMPLES --> ',NFY
CC    WRITE(*,*) '... STARTING INDEX    --> ',INY
      WRITE(*,*) ' '
      NFSUM=INT((FX1+FY1)*FLOAT(NFFT)/FSAMP)
      INC=MIN0(INX,INY)
      NFEND=(NFSUM-INC)/NSK+1
C
      WRITE(*,*) '>>> EXTRA AVERAGE [Y/N: RET IF NO] ?'
      READ(*,11) AVG
 11   FORMAT(A1)
      WRITE(*,*) '>>> WINDOW FUNCTION ? '
      WRITE(*,*) ' 1: RECTANGULAR '
      WRITE(*,*) ' 2: BARTLETT '
      WRITE(*,*) ' 3: HANNING '
      WRITE(*,*) ' 4: HAMMING '
      WRITE(*,*) ' 5: BLACKMAN '
      READ(*,*) IWINDOW
      CALL WINDOW(W,NPTS,IWINDOW)
C
C...
C
      WRITE(*,*) ' '
      WRITE(*,*) '>>> GIVE FILENAME OF BISPECTRUM [A25] :'
      READ(*,10) BISFILE
C
      WRITE(*,*)  ' '
      WRITE(*,*) '>>> GIVE FILENAME OF BICOHERENCE [A25] :'
      READ(*,10) BICFILE
C
```

```
        WRITE(*,*)  ' '
        WRITE(*,*) '>>> CREATE POWER SPECTRUM
\       [Y/N: RET IF YES]
                   READ(*,11) PSEYN
        IF   (PSEYN.EQ.'Y'.OR.PSEYN.EQ.'y'.OR.
\       PSEYN.EQ.' ') THEN
           WRITE(*,*)  '>>> FILENAME OF POWER
\       SPECTRUM [A25] ?'
           READ(*,10) PSFILE
        ENDIF
C
CCCCCCCCCCCCCCCCCCCCCCCCCCCCCCCCCCCCCCCCCCCCCCCCCCCCCCC
C                                                      C
C   COMPUTE PERIODOGRAM AND TRIPLE PRODUCT             C
C                                                      C
CCCCCCCCCCCCCCCCCCCCCCCCCCCCCCCCCCCCCCCCCCCCCCCCCCCCCCC
C
        OPEN(UNIT=4,FILE=FILENAME,STATUS='OLD')
        DO 700 NS=1, NSEG
        READ(4,10) INFILE
        WRITE(*,*) '  '
        WRITE(*,*) '... READING ...', INFILE
        OPEN(UNIT=3,FILE=INFILE,STATUS='OLD')
        READ(3,*) (Y(I),I=1,NPTS)
        CLOSE(UNIT=3,STATUS='KEEP')
        WRITE(*,*) '... COMPUTING ...'
C
C...REMOVE MEAN AND ZERO PADDING
C
        CALL ZOMEAN(Y,NPTS,AVE,SCALE)
C
        DO 500 K=1, NPTS
           YY(K)=CMPLX(Y(K)*W(K),0.)
  500   CONTINUE
C
        DO 600 I=NPTS+1, NFFT
           YY(I)=CMPLX(0.,0.)
  600   CONTINUE
        CALL NINFFT(YY,M,1)
C
C...COMPUTE PERIODOGRAM
C
        DO 610 I=1, NFEND
           KI=INC+(I-1)*NSK+1
           PSE(I)=PSE(I)+CABS(YY(KI))/FLOAT(NSEG)
  610   CONTINUE
C
C...COMPUTE TRIPLE PRODUCT
C
        DO 700 I=1, NFX
```

```
          DO 700 J=1, NFY
             K1=INX+(I-1)*NSK+1
             K2=INY+(J-1)*NSK+1
             BIJ=CMPLX(0.,0.)
C
C
             IF (AVG.EQ.'Y'.OR.AVG.EQ.'y') THEN
               N0=INT(FSAMP/DIFF)
               M1=NFFT/N0
               LSIZE=(M1-1)/2
               NAVG=0
               DO 620 L1=-LSIZE, LSIZE
               DO 620 L2=-LSIZE, LSIZE
                 IF((K1+L1).GE.1.AND.(K2+L2).GE.1) THEN
                   NAVG=NAVG+1
           BIJ=BIJ+YY(K1+L1)*YY(K2+L2)*CONJG(YY(K1+L1+K2+L2-1))
                 ENDIF
  620          CONTINUE
               BIJ=BIJ/CMPLX(FLOAT(NAVG))
C
C
             ELSE
               BIJ=YY(K1)*YY(K2)*CONJG(YY(K1+K2-1))
             ENDIF
C
             BISP(I,J)=BISP(I,J)+BIJ/CMPLX(FLOAT(NSEG))
  700    CONTINUE
         CLOSE(UNIT=4,STATUS='KEEP')
C
C...CREATE POWER SPECTRUM FILE
C
         IF   (PSEYN.EQ.'Y'.OR.PSEYN.EQ.'y'.OR.
\         PSEYN.EQ.' ') THEN
             OPEN(UNIT=10,FILE=PSFILE,STATUS='NEW')
             DO 900 I=1, NFEND
                KI=INC+(I-1)*NSK
                FQ=FLOAT(KI)*FDIV
                PSEDB=20.*ALOG10(PSE(I))
                WRITE(10,*) FQ, PSEDB
  900        CONTINUE
             CLOSE(UNIT=10,STATUS='KEEP')
             NSAMP=NFEND
             WRITE(*,*)  NSAMP,'  SAMPLES
\            OF PSE (DB) --> ',PSFILE
         ENDIF
C
C...CREATE BISPECTRUM AND/OR BICOHERENCE FILES
C
         OPEN(UNIT=9,FILE=BISFILE,STATUS='NEW')
         OPEN(UNIT=8,FILE=BICFILE,STATUS='NEW')
```

```
      DO 1000 I=1, NFX
         KI=INX+(I-1)*NSK
         F1=FLOAT(KI)*FDIV
         IX=(INX-INC)/NSK+I
      DO 1000 J=1, NFY
         KJ=INY+(J-1)*NSK
         F2=FLOAT(KJ)*FDIV
         IY=(INY-INC)/NSK+J
         IXY=(INX+INY-INC)/NSK+I+J-1
C
         BISMG=CABS(BISP(I,J))
         BISPA=ATAN2(AIMAG(BISP(I,J)),REAL(BISP(I,J)))*180./PI
         WRITE(9,*) F1, F2, BISMG, BISPA
C
         BICMG=BISMG/(PSE(IX)*PSE(IY)*PSE(IXY))
         WRITE(8,*) F1, F2, BICMG, BISPA
1000  CONTINUE
C
C
      CLOSE(UNIT=8,STATUS='KEEP')
      CLOSE(UNIT=9,STATUS='KEEP')
      NSAMP=NFX*NFY
      WRITE(*,*) '  '
      WRITE(*,*) NSAMP,' SAMPLES OF BISPECTRUM --> ',BIS-
FILE
      WRITE(*,*) '  '
      WRITE(*,*)  NSAMP,'  SAMPLES OF
\       BICOHERENCE --> ', BICFILE
C
C...
C
      STOP
      END
```

Appendix C

MACRO Programs

MACRO: THE MACRO PROGRAM WRITTEN IN S LANGUAGE
AND IT CAN RUN IN S (UNDER UNIX).

CSMP PROGRAM: THE SIMULATION PROGRAM WRITTEN IN
CSMP LANGUAGE AND IT CAN BE COMPLIED
BY CSMP.

*.FOR: THE PROGRAM WRITTEN IN FORTRAN LANGUAGE.

*.C: THE PROGRAM WRITTEN IN C LANGUAGE.

MACRO: PRE

```
#####################################
# THIS MACRO IS FOR PRE-PROCESSING  OF
# EXPERIMENTAL DATA. (MK21)
#
#####################################

MACRO pre
##########
# mk21.1
##########
attach('/usr/nate0016/monkey/mk21/pdp11/swork',pos=1)
tmp21.1_array(t(op.temp.21[4:11,4:147]))
tmp21.1[na(tmp21.1)]_0
tmp21.1_tweak(tmp21.1,limits=c(330,420))
tmp21.1_tmp21.1[tmp21.1!=0]
tmp21.1l_lowess(1:len(tmp21.1),tmp21.1,f=0.6,iter=2,delta=144)$y
```

```
tmp21.1_tmp21.1-tmp21.1l
tmp21.1_?lwclean(tmp21.1)
sptmp21.1_spectrum(tmp21.1,nt=16384,nsmooth=0)
tmp21.2_array(t(op.temp.21[37:44,4:147]))
tmp21.2[na(tmp21.2)]_0
tmp21.2_tweak(tmp21.2,limits=c(330,420))
tmp21.2_tmp21.2[tmp21.2!=0]
tmp21.2l_lowess(1:len(tmp21.2),tmp21.2,f=0.6,iter=2,delta=144)$y
tmp21.2_tmp21.2-tmp21.2l
tmp21.2_?lwclean(tmp21.2)
sptmp21.2_spectrum(tmp21.2,nt=16384,nsmooth=0)
tmp21.3_array(t(op.temp.21[44:51,4:147]))
tmp21.3[na(tmp21.3)]_0
tmp21.3_tweak(tmp21.3,limits=c(330,420))
tmp21.3_tmp21.3[tmp21.3!=0]
tmp21.3l_lowess(1:len(tmp21.3),tmp21.3,f=0.6,iter=2,delta=144)$y
tmp21.3_tmp21.3-tmp21.3l
tmp21.3_?lwclean(tmp21.3)
sptmp21.3_spectrum(tmp21.3,nt=16384,nsmooth=0)
tmp21.4_array(t(op.temp.21[80:87,4:147]))
tmp21.4[na(tmp21.4)]_0
tmp21.4_tweak(tmp21.4,limits=c(330,420))
tmp21.4_tmp21.4[tmp21.4!=0]
tmp21.4l_lowess(1:len(tmp21.4),tmp21.4,f=0.6,iter=2,delta=144)$y
tmp21.4_tmp21.4-tmp21.4l
tmp21.4_?lwclean(tmp21.4)
sptmp21.4_spectrum(tmp21.4,nt=16384,nsmooth=0)
tmp21.5_array(t(op.temp.21[90:97,4:147]))
tmp21.5[na(tmp21.5)]_0
tmp21.5_tweak(tmp21.5,limits=c(330,420))
tmp21.5_tmp21.5[tmp21.5!=0]
tmp21.5l_lowess(1:len(tmp21.5),tmp21.5,f=0.6,iter=2,delta=144)$y
tmp21.5_tmp21.5-tmp21.5l
tmp21.5_?lwclean(tmp21.5)
sptmp21.5_spectrum(tmp21.5,nt=16384,nsmooth=0)
tmp21.6_array(t(op.temp.21[96:103,4:147]))
tmp21.6[na(tmp21.6)]_0
tmp21.6_tweak(tmp21.6,limits=c(330,420))
tmp21.6_tmp21.6[tmp21.6!=0]
tmp21.6l_lowess(1:len(tmp21.6),tmp21.6,f=0.6,iter=2,delta=144)$y
tmp21.6_tmp21.6-tmp21.6l
tmp21.6_?lwclean(tmp21.6)
sptmp21.6_spectrum(tmp21.6,nt=16384,nsmooth=0)
tmp21.7_array(t(op.temp.21[138:145,4:147]))
tmp21.7[na(tmp21.7)]_0
tmp21.7_tweak(tmp21.7,limits=c(330,420))
tmp21.7_tmp21.7[tmp21.7!=0]
tmp21.7l_lowess(1:len(tmp21.7),tmp21.7,f=0.6,iter=2,delta=144)$y
tmp21.7_tmp21.7-tmp21.7l
tmp21.7_?lwclean(tmp21.7)
```

```
sptmp21.7_spectrum(tmp21.7,nt=16384,nsmooth=0)
detach(pos=1)
END

MACRO Program Bistest

#########################################################
#
# THE FOLLOWING MACRO PROGRAMS ARE TO GENERATE
# PHASE RELATED DATA FOR BISPECTRUM TEST.
#
#########################################################

MACRO p0
h1_runif(50,0,2*pi)
h2_runif(50,0,2*pi)
h3_runif(50,0,2*pi)

#########################################################
MACRO p1c(y,n)
u_h1[n]+h2[n]
y_cos(2*pi/26.0*tx+h1[n])+\
  cos(2*pi/13.0*tx+h2[n])+cos(2*pi/8.67*tx+u)
write(y,"y",1)
END

#########################################################
MACRO p2
?p1(y1,1)
?p1(y2,2)
?p1(y3,3)
?p1(y4,4)
?p1(y5,5)
?p1(y6,6)
?p1(y7,7)
?p1(y8,8)
?p1(y9,9)
?p1(y10,10)
?p1(y11,11)
?p1(y12,12)
?p1(y13,13)
?p1(y14,14)
?p1(y15,15)
?p1(y16,16)
?p1(y17,17)
?p1(y18,18)
?p1(y19,19)
?p1(y20,20)
END
```